# Dissecting the molecular mechanisms of human NOP53 in nucleolar functions

**Holly Jo Sutherland**

*This thesis is submitted to the University of Sheffield in fulfilment of the requirements for the degree of Doctor of Philosophy*

August 2023

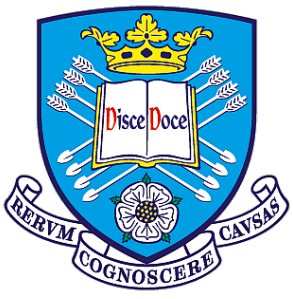


The University Of Sheffield.

Faculty of Science
School of Biosciences
Cluster of Molecular and Cell Biology

# Acknowledgements

First and foremost I would like to thank my supervisor Dr Emma Thomson. I couldn't be more grateful for your advice, support, and kindness throughout my PhD. It hasn't been an easy journey but you have helped guide me from the first day I stepped into the lab and every day since. None of this would have been possible without you. It's been a true privilege to not only be your PhD student, but your first PhD student. Thank you.

I have been extremely lucky to work alongside such incredible researchers. Special thanks to Professor Ivana Barbaric and her kind and generous lab members who were patient with me and helped me with my stem cell work. My advisor, Dr Dan Bose, thank you for all the insightful discussions, advice and the welcoming environment you helped create.

To all the wonderful members of the Thomson and Bose Labs and all I worked with during my time on E floor, you have taught me so much of what I know today. I am grateful to have worked alongside you all. Dr Monika Feigenbutz, thank you for laying the groundwork for my project and for sharing so much of your knowledge with me. To my fellow PhD students and lab members with who I shared this journey; Petra, Nicola, Katie, Pete, Ash, Laura, Archna and Vincent; your support, knowledge and friendship helped make my PhD possible.

For the most incredibly supportive friends and housemates; Nicola, Katy and Peter, thank you. You gave me the push to keep going whenever I needed it. This experience would not have been the same without you.

I would not have even considered pursuing a PhD if not for my loving parents. You have supported me through every stage of my life and have made this possible through your constant encouragement.

Finally, my incredible partner Archie, thank you for always being there for me. The last two years have been the most challenging and unpredictable time of my life and whenever I questioned if this was at all possible you never stopped believing in me. Some days that belief was all I had and all that kept me moving forward. It would not have been possible without you.

Words cannot truly express how grateful I am to every person in my life that has helped me make it here. All I can say is thank you. Thank you for your support and kindness, thank you for believing in me, I will remember it always.

Also DOGS! Thanks to all the beautiful dogs in my life who have kept me sane during this journey with their cute faces, love and waggy tails.

# Abstract

The nucleolus is the site of ribosome biogenesis, a conserved process vital for cell growth and proliferation. In higher eukaryotes, the nucleolus is also implicated in stress responses with numerous cellular stresses converging to trigger p53 stabilisation. These two nucleolar processes are linked to one another, however, the molecular mechanisms mediating their connection are not well characterised. The nucleolar protein NOP53 is an unusual factor as it is one of few directly implicated in both processes.

Current NOP53 research has limitations. The role of Nop53 in ribosome biogenesis has been characterised in *S. cerevisiae* through an interaction with Mtr4. However, yeast lack p53 and as NOP53 is implicated in RPL11-mediated p53 regulation during nucleolar stress, *Sc*Nop53 likely only plays a role in ribosome biogenesis. Additionally, mammalian studies have involved deletion/depletion of NOP53, which simultaneously removes NOP53 from both processes. Consequently, this thesis aims to overcome these limitations and elucidate the specific involvement of NOP53 in each of these two fundamental nucleolar process through generating separation of function NOP53 mutations.

To generate separation of function mutants, the interaction of NOP53 with MTR4 and with RPL11 was investigated. This confirmed the interaction between NOP53 and MTR4 in humans and the conserved AIM is required for this interaction. The NOP53 AIM mutation, D90R, abolishes the interaction with MTR4, demonstrated by complementary *in vitro* and *in vivo* approaches. CRISPR-Cas9 generated NOP53-D90R hPSC lines were produced for future phenotypic studies. The interaction between NOP53 and RPL11 was also confirmed and the NOP53 D90R mutant retained this interaction, enabling NOP53 to be studied solely in ribosome biogenesis. Both yeast-two-hybrid truncation analysis and a random mutagenetic screen of NOP53 failed to identify region(s) responsible for RPL11 binding, but the C-terminus of RPL11 was identified to mediate the interaction but requires further confirmation and study.

# Contents

# Abbreviations

| | |
|---|---|
| 3-AT | 3-Amino-1,2,4-triazole |
| AIM | Arch Interaction Motif |
| ATP | Adenosine triphosphate |
| bp | base pair |
| CRISPR | Clustered Regularly Interspaced Short Palindromic Repeats |
| crRNA | Clustered Regularly Interspaced Short Palindromic Repeats ribonucleic acid |
| DAPI | 4',6-diamidino-2-phenylindole |
| DBA | Diamond Blackfan Anaemia |
| DFC | Dense fibrillar centre |
| DNA | Deoxyribonucleic acid |
| dNTP | Deoxyribonucleotide triphosphate |
| DSB | Double strand break |
| DTT | Dithiothreitol |
| EDTA | Ethylenediaminetetraacetic acid |
| EM | Electron microscopy |
| ESC | Embryonic stem cell |
| EtOH | Ethanol |
| ETS | External transcribed spacer |
| FACS | Fluorescence-activated cell sorting |
| FC | Fibrillar centre |
| GC | Granular component |
| GSH | Glutathione |
| GST | Glutathione S-transferase |
| GTP | Guanosine triphosphate |
| $H_20$ | Water, distilled, sterile |
| HDR | Homology directed repair |
| HEPES | 4-(2-hydroxyethyl)- l -pipe razineethansulfonic acid |
| HIS | Histidine |
| hPSCs | Human pluripotent stem cells |
| IPTG | isopropyl-D-thiogalactopyranoside |
| ITS | Internal transcribed spacer |
| KOW | Kyprides, Ouzounis, Woese |
| LB | Luria Broth |
| LEU | Leucine |
| lncRNA | long non-coding ribonucleic acid |
| NEXT | nuclear exosome-targeting |
| mRNA | messenger ribonucleic acid |
| NHEJ | Non-homologous end joining |
| NOR | Nucleolar organising regions |
| NPC | Nuclear pore complex |
| OD | Optical density |
| ORF | Open reading frame |
| PAGE | Polyacrylamide gel electrophoresis |
| PAM | Protospacer adjacent motif |
| PAXT | poly(A) exosome-targeting |
| PBS | Phosphate buffered saline |
| PCR | Polymerase chain reaction |
| PEG | Polyethylene glycol |
| pre-rRNA | precursor ribosomal ribonucleic acid |

| | |
|---|---|
| qPCR | Quantitative polymerase chain reaction |
| RAF | Ribosome assembly factor |
| RNA | Ribonucleic acid |
| RNP | Ribonucleoprotein |
| RP | Ribosomal protein |
| rpm | rotations per minute |
| rRNA | ribosomal ribonucleic acid |
| SD | Synthetic drop-out |
| SDS | Sodium dodecyl sulphate |
| sgRNA | specific guide ribonucleic acid |
| siRNA | small interfering ribonucleic acid |
| snoRNA | small nucleolar ribonucleic acid |
| snoRNP | small nucleolar ribonucleoprotein |
| snRNA | small nuclear ribonucleic acid |
| SP | Sulphopropyl |
| ssODN | Single stranded oligonucleotide |
| TEMED | N, N, N', N'-tetramethylethylendiamine |
| tracrRNA | trans-activating ribonucleic acid |
| TRAMP | Trf4/5-Air1/2-Mtr4 polyadenylation |
| Tris | Tris-(hydroxymethyl) |
| tRNA | transfer ribonucleic acid |
| TRP | Tryptophan |
| UTR | Untranslated region |
| UV | Ultraviolet |
| WT | Wildtype |

# List of Figures

# List of Tables

# Chapter 1

# Introduction

## 1.1 The Nucleolus

The most prominent structure within the nucleus is the nucleolus, present in almost every eukaryotic cell type. The nucleolus is a membrane-free, phase-separated compartment. Although important in cell cycle control, viral replication and senescence, the nucleolus' primary function is ribosome biogenesis.

### 1.1.1 Nucleolar structure and organisation

It has been proposed that the nucleolus is 'an organelle formed by the act of building a ribosome' (Mélèse & Xue, 2005), because in higher eukaryotes, the stages of ribosome biogenesis and their associated machineries are compartmentalised reflecting the basic structure and organisation of the nucleolus (Hernandez-Verdun *et al.*, 2010). Additionally, when ribosome synthesis is disrupted, the nucleolus disassembles. The nucleolus is organised around repeated ribosomal DNA (rDNA) clusters to form the liquid-liquid phase separated compartment (Andersen *et al.,* 2005; Lafontaine *et al.,* 2021). Protein localisation to the nucleolus is mediated by interactions with rDNA and facilitates the initial steps of ribosome biogenesis (Frottin *et al.,* 2019; Lafontaine *et al.,* 2021).

In yeast, nucleoli have a bipartite organisation however, in humans, there are three main compartments within nucleoli as observed by electron microscopy: the fibrillar centres (FCs), the dense fibrillar component (DFC) and the granular component (GC) (Figure 1.1) (Leger-Silvestre & Gas, 1999; Scheer & Hock, 1999; Thiry & Lafontaine, 2011). There are often numerous FCs observed in human nucleoli, which are clearer areas as shown by EM, surrounded by the higher contrasted region of the DFC (Sirri *et al.,* 2008; Thiry & Goessens, 1996). The bulk of the nucleolus is made up of the GC with granules approximately 15-20 nm in diameter (Mosgoller, 2004). The tripartite structure of the nucleolus is only visible during interphase (Figure 1.1), where there is ordered dis-assembly and re-assembly of the nucleolus during cell division. Nucleolar assembly is both temporally and spatially regulated (Hernandez-Verdun, 2011a), as for the nucleolus to re-assemble at the end of the cell cycle, ribosome biogenesis machinery is needed to correctly order the dynamics of assembly (Hernandez-Verdun, 2011b). The site in the nucleolus at which specific ribosomal processes occur is debated in the field. However in general, rDNA transcription is believed to occur at the border of the FC and DFC with the GC being the site for later rRNA processing steps and pre-ribosome subunit assembly (Hernandez-Verdun, 2006).

The number of nucleoli per eukaryotic cell type, as well as their morphology and size is highly dependent on rRNA gene transcriptional activity, which in turn is dependent on cell

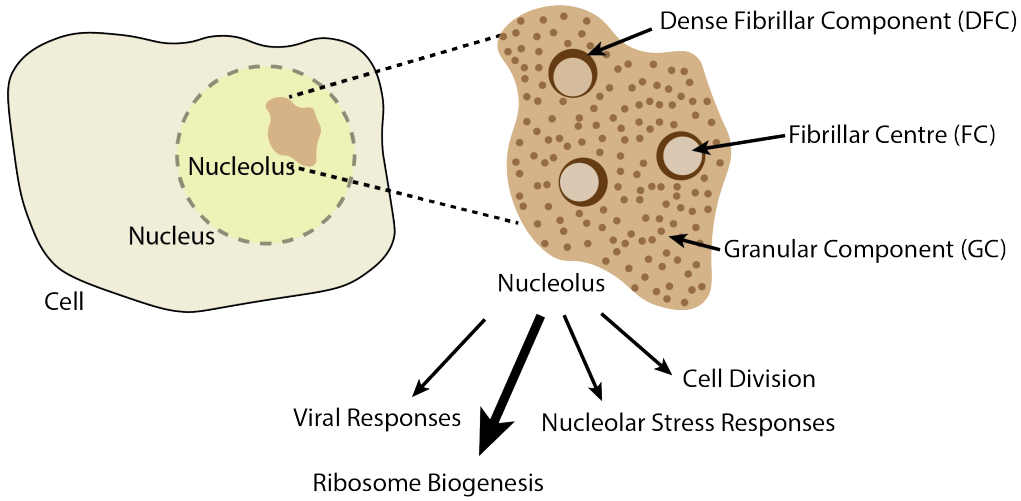


Figure 1.1: The functions of the nucleolus and its tripartite structure. When imaged by electron microscopy, the nucleolus has 3 main structures: the fibrillar centre(s) (FCs), dense fibrillar component (DFC) and the granular component (GC). The primary function of the nucleolus is ribosome biogenesis but it is also implicated in the nucleolar stress response, the cell cycle and viral responses.

growth, metabolism and developmental state. The size of nucleoli increases in proportion to the amount of synthesised rRNA (Hernandez-Verdun *et al.,* 2010). It is this feature that allows nucleolar size to be used as diagnostic marker of highly proliferative cancer cells which have high levels of rRNA transcription (Montanaro *et al.,* 2008). Structural changes in the nucleolus are also observed not only in cancer cells (Hein *et al.,* 2013) but also during early development in ESCs (reviewed in Kresoja-Rakic & Santoro, 2019). ESCs typically contain a single large nucleolus due to the hyperactive nature of ESC rDNA (Meshorer & Misteli, 2006; Gupta & Santoro, 2020; Underwood *et al.,* 2017), whereas differentiated cells tend to contain several smaller nucleoli (Hori *et al.,* 2023).

When investigating the organisation and formation of the nucleolus, emphasis has been placed on the role played by ribosome biogenesis. As both RNA polymerase I activity in the transcription of pre-rRNAs and the subsequent pre-rRNA processing are linked to compartmental organisation (Hernandez-Verdun *et al.,* 2010). However, over recent years mounting evidence supports a role for the nucleolus in additional diverse, cellular functions.

### 1.1.2 The multifunctional nucleolus

The well-established view of the nucleolus as a ribosome 'factory' has been expanded with numerous investigations describing a role for the nucleolus in other cellular processes (Figure 1.1) (Pederson & Tsai, 2009). In eukaryotes, over 500 rRNAs, RPs, snoRNAs and *trans*-acting assembly factors have been implicated in ribosome biogenesis (Nazar, 2004). However close to 1300 nucleolar proteins have been identified (Stenström *et al.,* 2020). A large proportion of which are uncharacterised and their roles in nucleolar functions remain to be studied. This may be explained if they play a role in an alternative nucleolar function aside from ribosome biogenesis, which has been the predominant focus in nucleolar protein research. For example, 36 previously uncharacterised human nucleolar proteins have recently been implicated in mitosis and suggested to play a role in protein division across daughter cells (Stenström *et al.,* 2020).

Recently, the nucleolus, has been shown to be the target for viral pathogens which induce nucleolar changes in infected cells. The nucleolus, subsequently, plays a fundamental role in several steps of the viral cycle providing the optimal environment for viral replication (Hiscox, 2002). An example of this following infection, is that the nucleolus has been shown to undergo morphological changes, aid in viral mRNA nuclear export (Boyne & Whitehouse, 2006) and inhibit host mRNA nuclear export, blocking the protein translation required for immune response (Feng *et al.,* 2020; Zhang *et al.,* 2019). Further, there is evidence that upon viral infection nucleolar proteins are redistributed to other cellular compartments and diverted from their known functions. This re-localisation has lead to reduced expression of protective pathways following infection preventing signalling cascades to initiate immune responses (Greco, 2009; Hanson *et al.,* 2019; Iarovaia *et al.,* 2021).

The nucleolus also acts as a 'stress sensor' and is responsible for maintaining low levels of p53 during homeostatic conditions (Rubbi & Milner, 2003; James *et al.,* 2014). In response to a range of cellular stresses including: UV damage, hypoxia, oxidative stress, DNA damage, nucleotide depletion and starvation, levels of p53 increase. Stabilisation of p53 then triggers cell cycle arrest and in cases of irreparable stress will initiate apoptosis. Following cell cycle arrest, ribosome biogenesis also halts as the cell is not currently growing or dividing. Inhibition of ribosome biogenesis or defects in ribosome biogenesis are also capable of triggering the nucleolar stress response. Consequently, the nucleolar stress response is closely implicated with ribosome biogenesis and will be discussed in detail later (section 1.4).

### 1.1.3 The nucleolus in disease

As the primary site of ribosome biogenesis, the nucleolus has been implicated in diseases, such as cancer and ribosomopathies. Any alterations in ribosome biogenesis or ribosome function can have severe effects on protein production and cellular function with rate of biogenesis regulating cell growth and proliferation (Stepiński, 2008). Subsequently, tumorigenic cells can often be characterised by overactive ribosome biogenesis and increased rates of protein synthesis due to their rapid cellular growth and high levels of proliferation (Derenzini *et al.,* 1998; van Sluis & McStay, 2015). Conversely, ribosomopathies are defined by defects in ribosome biogenesis leading to the production of insufficient ribosomes or altered ribosomes, capable of triggering the nucleolar stress response.

Ribosomopathies can vary, but they are typically caused by mutations in components of ribosome biogenesis. The disease only presents itself in specific cell types, despite ribosome biogenesis being a ubiquitous process across cell types. However, all cells do show an increased predisposition to cancer, in addition to the presentation of cell specific phenotypes. During embryogenesis, multiple ribosomopathies are present in tissues which are derived from neural crest cells, including the peripheral nervous system and head skeletal structures, causing developmental defects. Whilst these terminally differentiated cell types are not highly proliferative, neural crest cells are (Gerton, 2021). Many ribosomopathies also present themselves in blood cells and bone marrow which also rely on high levels of cell division. High levels of proliferation mean these cells also require high levels of ribosome biogenesis, and therefore are suggested to be particularly sensitive to defects in ribosome biogenesis (Farley-Barnes *et al.,* 2019; Khajuria *et al.,* 2018). Both ribosomopathies and cancer are tightly linked with functional ribosome biogenesis and nucleolar function and will be discussed further in chapter 6.

## 1.2 Ribosome Biogenesis

Ribosome biogenesis is a complex, energetically demanding process requiring up to 80 % of a cell's energy (Schmidt, 1999). It is unsurprising that ribosome assembly is so elaborate given that the ribosome is a large ribonucleoprotein (RNP) containing one molecule each of 80 different proteins (79 in yeast) and 4 rRNA molecules containing more than 5500 RNA bases (Perry, 2007). In mammals, the small 40S subunit contains the 18S rRNA along with 33 small ribosomal proteins (RPs), with the large 60S subunit containing 3 rRNAs; the 5S, 5.8S and 28S rRNA along with 47 ribosomal proteins (Aubert *et al.,* 2018).

The ribosome itself is structurally well conserved from prokaryotes to eukaryotes. The bacterial ribosome weights 2.3 MDa whilst that of eukaryotic ribosomes is greater at 4.3 MDa. Both share a common core (2 MDa) which is comprised of 34 proteins and 3 rRNAs. During evolution the ribosome became increasingly more complex through the incorporation of additional ribosomal proteins, the gain of an rRNA species, expansions in spacer regions and expansions in rRNA, with the 23S/28S rRNA increasing from 2843 bp in *E. coli* to 5034 bp in humans (Melnikov *et al.,* 2012).

In addition to ribosome structure being conserved, the process of ribosome biogenesis also shows conservation throughout eukaryotes (Thomson *et al.,* 2013). Ribosome biogenesis is both spatially and temporally controlled and requires the precise regulation of precursor rRNA (pre-rRNA) processing, RNA modifications and RPs binding which take place within pre-ribosomal subunits. This assembly process occurs in the nucleolus and nucleoplasm before the pre-40S and pre-60S subunits are exported into the cytoplasm (Perry 2007; Wu *et al.,* 2016). Here, it is subject to the final stages of maturation to allow the formation of the translationally competent 80S ribosome (Green & Noller, 1997) (summarised in Figure 1.2).

Understanding ribosome biogenesis has become more complex with increasing evidence of ribosome heterogeneity and specialisation (Guo, 2018). The study of ribosomal heterogeneity has expanded in recent years. Core components of the ribosome have been shown to vary, including RPs, RP modifications and rRNA modifications (Natchiar *et al.,* 2017). These variations in composition have also been implicated in ribosome function, with variations in ribosome composition contributing to the translation of subsets of mRNAs (Genuth & Barna 2018; Guo 2018; Kampen *et al.,* 2020). However, current support for a specialised function of heterogenous ribosomes in the translation of specific mRNAs is limited. Although ribosome heterogeneity and specialisation are not the focus of discussion here, it must be considered that as ribosomes differ, the described processing and assembly during ribosome biogenesis may also differ.

### 1.2.1 rRNA transcription

Eukaryotic cells typically contain over 100 copies of rRNA genes, with *S. cerevisiae* containing roughly 150 copies (Kobayashi *et al.,* 1998), and humans ever greater at 400 copies (Malinovskaya *et al.,* 2018). Although, a large number of these genes are transcriptionally silent (Nomura, 2001). These rDNA genes are arranged as arrays of repeats, and depending on the organism, are found in different genomic contexts (Sollner-Webb & Tower, 1986). In humans, rDNA arrays are present on the short arms of five acrocentric chromosomes; 13, 14, 15, 21 and 22 (Raška *et al.,* 2006), while in yeast all rDNA copies are found in a single array on chromosome XII.

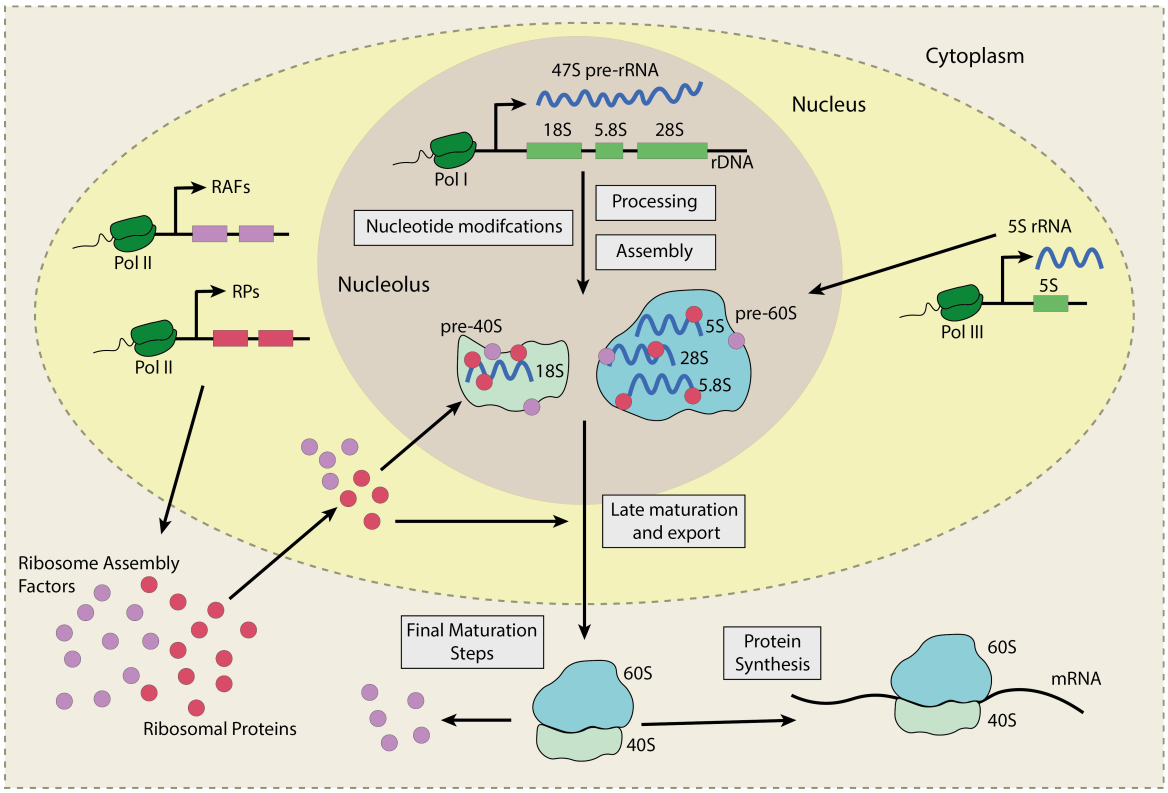


Figure 1.2: A schematic overview of ribosome biogenesis. Ribosome biogenesis is spatially and temporally regulated across cellular compartments. RNA polymerase I (PolI) transcribes the 47S rRNA containing three rRNAs with RNA polymerase III transcribing the 5S rRNA. The rRNA precursors are processed, undergo modification and are assembled with ribosomal proteins (RPs); a process that requires the activity of many ribosome assembly factors (RAFs). Maturation begins in the nucleolus before continuing in the cytoplasm where final RPs associate and RAFs dissociate forming the mature subunits. The mature 40S and 60S subunits are now competent to carry out translation. The mRNAs encoding RAFs and RPs are transcribed by RNA polymerase II.

rRNA transcription is highly active compared with average gene transcription levels to facilitate the mass production of rRNA required by the cell (Hori *et al.*, 2023). rRNA constitutes up to 80 % of total RNA in a cell (Jacob & Ghosh, 1999) and the transcription of the 47S pre-rRNA by RNA polymerase I (pol I) accounts for up to 60 % of the cell's transcriptional activity (Moss & Stefanovsky, 2002). Dysregulation of RNA polymerase I is associated with cancer (Hannan *et al.*, 2013) and its selective inhibition by small molecules leads to p53 activation and apoptosis in cancer cells (Bywater *et al.*, 2012). Whilst RNA polymerase I (pol I) is responsible for the transcription of the 47S pre-rRNA, ribosome biogenesis requires the coordinated action of all three RNA polymerases with RNA polymerase II and III responsible for the transcription of the mRNAs encoding ribosomal proteins and the 5S rRNA, respectively (Figure 1.2) (Thomson *et al.*, 2013).

The polycistronic pre-rRNA transcript encodes the 5.8S, 18S and 28S (25S in yeast) rRNA species, flanked by 5' and 3' external transcribed spacers (ETS) and two internal transcribed spacers (ITS) (Figure 1.3). The human 47S precursor rRNA is 45 kb in length and is longer than its 35S pre-rRNA yeast counterpart at 9.5 kb (Aubert *et al.*, 2018; Hori *et al.*, 2023). Whereas in *S. cerevisiae*, the 5S rRNA is located adjacent to the other three rRNA species within the tandem repeats, in humans the 5S rRNA forms independent arrays on chromosome

1. The 5S is independently transcribed from the other rRNA by RNA polymerase III.

### 1.2.2 rRNA modifications

The long precursor rRNA produced by RNA polymerase I transcription is also subject to rRNA nucleoltide modifications. In *S. cerevisiae*, over 100 rRNA residues have been shown to be covalently modified co-transcriptionally (Kos & Tollervey, 2010). This basic modification pattern is conserved but higher eukaryotes contain additional modified sites (Natchiar *et al.,* 2019; Nazar 2004; Taoka *et al.,* 2018). In humans, approximately 200 nucleotide modifications occur at specific positions within the rRNA. These positions are specified and bound by a class of small nucleolar RNAs (snoRNAs) which exist as small nucleolar RNPs (snoRNPs) (Lestrade & Weber, 2006; Mattick & Makunin, 2005). Most rRNA nucleotide modifications are pseudouridylations and 2'-*O*-ribose methylations which are guided and catalysed by two families of snoRNPs, H/ACA box or C/D box snoRNPs, respectively (Mattick & Makunin, 2005; Watkins & Bohnsack, 2012).

Typically, each modification is carried out by a specific snoRNP early in rRNA maturation, targeting nucleotides which will be found in key ribosomal regions, for example within the peptidyl transferase centre (Taoka *et al.,* 2018). The function of these rRNA modifications is not fully understood but suggests they may affect rRNA folding, reactivity or stability. Additionally, not all rRNA modifications are constitutively observed, introducing ribosome heterogeneity which may lead to translation of a subset of mRNAs depending on cell type, developmental state or pathogenicity (Henras *et al.,* 2017; Sloan *et al.,* 2017). Whilst, nucleotide modifications are a key stage of ribosome biogenesis occurring concomitantly with pre-rRNA cleavage, folding and assembly, they will not be discussed further in the context of this research.

### 1.2.3 rRNA processing and maturation

Precursor rRNA processing was first extensively characterised in *S. cerevisiae* and initially predicted to be conserved in humans. Further research on human rRNA processing has shown that this is predominantly the case, with the rRNA processing pathway largely conserved. A large number of factors which mediate rRNA processing are also conserved with a study identifying almost 30 human rRNA processing factors carry out rRNA cleavage at steps equivalent to their yeast counterparts (Tafforeau *et al.,* 2013). However, there are differences between *S. cerevisiae* and humans in both the timing and order of processing events as well as the identity of enzymes involved in particular events (Henras *et al.,* 2015; Tomecki *et al.,* 2017). Further discussion will focus on rRNA processing and maturation in humans with comparisons made to known processes, pathways and components of *S. cerevisiae* where specified.

#### 47S pre-rRNA processing

Transcription of rRNA in humans produces the long 47S rRNA precursor in the nucleolus (Wu *et al.,* 2016). Processing of the 47S rRNA involves the sequential cleavage of the pre-rRNA by numerous nucleases, eventually maturing to the 18S mature rRNA for the small ribosomal subunit and the 5.8S and 28S rRNA for the large ribosomal subunit (Figure 1.3). Whilst the sequence encoding the mature rRNAs is conserved across eukaryotes, there is a strong divergence in both length and sequence of the transcribed spacers. Despite these differences, the folding of the transcribed spacers places the endonucleolytic cleavage sites in

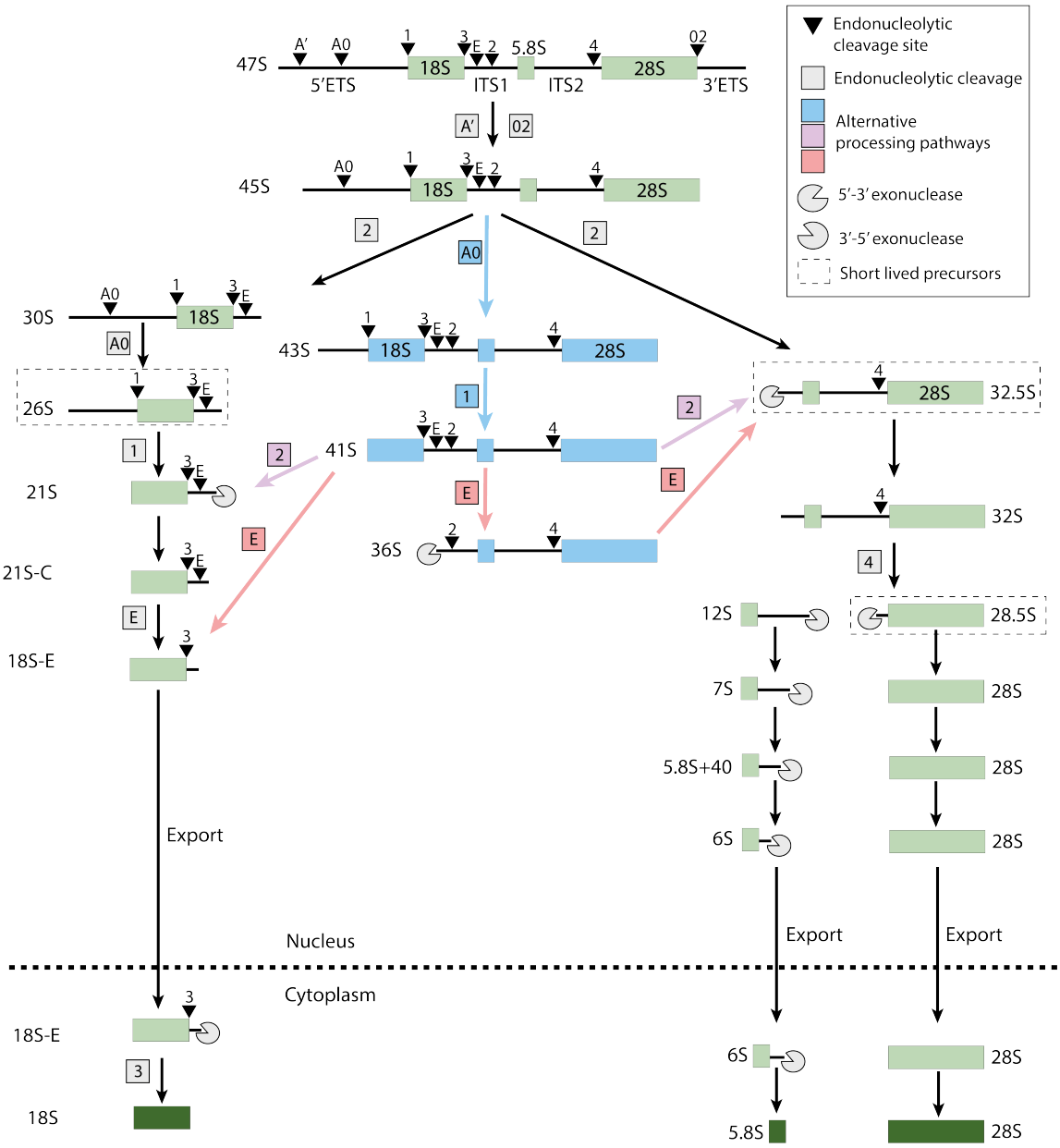


Figure 1.3: Processing of pre-ribosomal rRNA in humans. Three rRNAs are transcribed on a singular rRNA transcript, the 47S rRNA. The primary processing pathway is depicted in green with alternative processing pathways shown in alternative colours. Short lived precursors are identified by a dashed box, however the level of the precursors can vary depending on cell type and developmental state (Henras *et al.*, 2015). The 18S undergoes less extensive processing in the nucleus compared with the 5.8S and 28S. 5' to 3' exonuclease processing in humans is primarily carried out by XRN2. The exosome is known to be required for the 3' to 5' processing of the 21S, 12S, 7S and 5.8S+40 pre-rRNAs. The 5S rRNA is transcribed and processed separately.

similar secondary structure elements in both yeast and humans (Aubert *et al.,* 2018). Often in the literature, discussions on rRNA processing are described as a distinct step with no overlap in timing with the other stages of ribosome biogenesis. In yeast, rRNA processing is known to occur co-transcriptionally, but in humans rRNA cleavage primarily occurs post-transcriptionally, proceeding rRNA modification (Kos & Tollervey, 2010; Tafforeau *et al.,* 2013; Turowski & Tollervey, 2015).

For rRNA maturation in humans, transcribed spacers within the nascent pre-rRNA transcript are sequentially eliminated through a complex series of endonucleolytic and exonucleolytic cleavages (Figure 1.3). Initially cleavage occurs at the A' and 02 sites found in the 5' and 3' spacers, respectively, producing the 45S pre-rRNA. Here, the maturation pathway can diverge by further elimination of the 5' ETS with cleavage at A0 or by cleavage within the ITS1 at site 2, the main pathway. Thus, cleavage at A0 produces both 43S or 41S pre-rRNAs which are typically less abundant than the rRNA precursors in the main pathway (30S and 32S rRNA), however this alternative processing pathway reconverges on the main processing pathway (Figure 1.3).

Cleavage at site 2 within the ITS1 separates the 18S rRNA, destined for the small ribosomal subunit from the 5.8S and 28S rRNA, components of the large ribosomal subunit. In yeast, further processing of 18S rRNA precursors is achieved by a series of exclusively endonucleolytic cleavages within the 5' ETS and ITS1 sequences. However, in humans and other mammalian cells, 18S rRNA processing is carried out by a combination of both endonucleolytic and exonucleolytic processing steps in the ITS1 (Figure 1.3) (Henras *et al.,* 2015).

Following the separation of 40S and 60S precursors through cleavage in the ITS1, the 32S pre-rRNA containing the 5.8S and 28S rRNA is also produced. The 5' end of the 5.8S is processed to produce both long and short forms. The ITS2 is then cleaved at site 4 to separate the 5.8S rRNA from the 28S rRNA. The 5' end of the 28S rRNA and the 3' end of the 5.8S rRNA are processed by 5' to 3' and 3' to 5' exonucleases, respectively (Fromm *et al.,* 2017). The 12S pre-rRNA produced following ITS2 cleavage undergoes multiple stages of maturation before producing mature 5.8S rRNA which includes the 7S pre-rRNA. In *S.cerevisiae* the processing of the 7S pre-rRNA is known to be carried out by the nuclear exosome (Mitchell *et al.,* 1997) and is shown to be conserved in humans (Preti *et al.,* 2013; Tafforeau *et al.,* 2013).

Although there is some flexibility in cleavage order, certain events are hierarchical and must occur before additional processing. For example, endonucleolytic cleavage at site E within the ITS1 cannot occur until the 5' ETS has been removed by cleavage at both sites A0 and 1 (Aubert *et al.,* 2018). Since there is flexibility and variability in the rRNA processing pathways which all result in the production of mature 18S, 5.8S and 28S rRNA, the ratio of rRNA precursors can vary among different cell types and in pathological states. Interestingly cells with enhanced tumorigenicity showed a tendency for A0 cleavage producing the 43S pre-rRNA (Belin *et al.,* 2009), over cleavage at site 2, the main rRNA processing pathway. This change in preference of cleavage events may affect processing kinetics with increased rates of ribosome biogenesis and consequently enhanced cell growth and proliferation driving the tumorigenicity.

### The 5S rRNA

The 5S rRNA, unlike the other rRNAs, is transcribed by RNA polymerase III in the nucleoplasm (Figure 1.2). In humans, the 5S gene is transcribed from a separate chromosome and is the only class III gene with a type 1 promoter. Therefore, transcription initiation requires a specific regulatory factor called transcription factor IIIA (TFIIIA) (Engelke *et al.,* 1980;

Moorefield & Roeder, 1994; Dieci *et al.,* 2013). Transcription of the 5S rRNA begins directly at the 5' end, but contains a uridine rich 3' extension (Dieci *et al.,* 2013) producing the 5S precursor, 5S*. This 5S precursor associates with the La protein, which recognises other diverse RNA polymerase III transcripts by their 3' uridylates (Rinke & Steitz, 1982; Stefano, 1984). It functions as a chaperone in the maturation and stability of 5S* pre-rRNA and may also be involved in folding (Ciganda & Williams, 2011).

Processing of the 3' end of 5S RNA is carried out by a 3' to 5' exonuclease. In yeast, this was identified to be Rex1p (van Hoof, 2000) and was recently identified as REX05 in *D. melanogaster* (Gerstberger *et al.,* 2017). Whilst the exonuclease responsible for processing in humans has not been identified, the Rex1p human orthologue is conserved and found in the nucleolus suggesting a conserved role in 5S processing (Aubert *et al.,* 2018; Gerstberger *et al.,* 2017). Following this 3' processing, in both yeast and humans, the 5S rRNA associates with the ribosomal protein L5 (RPL5) and RPL11, forming the 5S RNP (Sloan *et al.,* 2013; Steitz *et al.,* 1988; Zhang *et al.,* 2007). The factors which mediate 5S RNP nucleolar import and pre-60S incorporation have not been identified in humans. However, in yeast, the association of RPL5 and RPL11 with the 5S rRNA is mediated by the symportin Syo1 which subsequently mediates 5S RNP nucleolar import (Calviño *et al.,* 2015; Kressler *et al., 2012*). Two yeast assembly factors, Rpf2 and Rrs1, are then necessary for the docking of the 5S RNP with the assembling subunit and ultimately enable 5S RNP incorporation into pre-60S particles (Zhang *et al.,* 2007).

Interestingly, a large pool of free 5S-RPL5-RPL11 RNP is found in metazoans (Steitz *et al.,* 1988) which has been shown to have a ribosome-independent function and can regulate the levels of p53 (Donati *et al.,* 2013; Sloan *et al.,* 2013). Whilst there is a relative lack of knowledge on the maturation, processing and intracellular dynamics of the 5S rRNA in human cells, its function as a regulator of p53 along with the other components of the 5S RNP, RPL5 and RPL11 have been well studied (Aubert *et al.,* 2018) and will be discussed further in section 1.4.2.

### 1.2.4 Ribosome assembly

Ribosome assembly is highly dynamic with the association of ribosomal proteins (RPs) along with the association and dissociation of ribosomal assembly factors throughout biogenesis. The main stages of assembly occur in the nucleolus, with a large number of nucleolar factors necessary for rRNA processing and modification assembling within a series of pre-ribosomal particles (Figure 1.2) (Leary & Huang, 2001; Nissan *et al.,* 2002). However, additional maturation events take place in the nucleoplasm before pre-ribosomes are actively exported to the cytoplasm to undergo the final processing events to form mature ribosomal subunits.

An intricate network of cooperative and hierarchical pre-rRNA processing and folding events (described in section 1.2.3) occur within a succession of pre-ribosomal particles with the gradual association of RPs and sequential interaction with ribosome assembly factors (Aubert *et al.,* 2018; Ferreira-Cerca *et al.,* 2005; Sanghai *et al.,* 2017). Human ribosomal proteins are necessary for subunit synthesis and the depletion of 31 out of 32 small subunit RPs prevented the maturation of the 18S rRNA (O'Donohue *et al.,* 2010). Ribosome biogenesis factors interact more dynamically, as they temporarily associate to pre-40S and pre-60S particles, playing multiple enzymatic, structural and regulatory functions. Ribosome biogenesis factors include chaperones and helicases which aid in RNA folding, nucleases and helicases for rRNA processing and methyl- or acetyltransferases to introduce nucleotide modifications. ATPases are also known assembly factors required for mechanical energy to enable

structural remodelling, GTPases act as molecular switches and further factors are needed for pre-40S and pre-60S nuclear export (Aubert *et al.,* 2018). Some of these assembly factors become associated with the pre-ribosome as multiprotein complexes whereas others interact as an individual protein (Henras *et al.,* 2008). However as pre-rRNA maturation proceeds through the nucleolus to the cytoplasm, there is a decreasing number of ribosome biogenesis factors present on the pre-ribosome (Nissan *et al.,* 2002).

There have been extensive studies into ribosome assembly in *S. cerevisiae* due to its genetic and biochemical tractability. X-ray crystallography and more recently, cryogenic electron microscopy (cryo-EM) have made use of the ease in editing the yeast genome introducing mutations and epitope tags at specific loci (Callaway, 2020; Wang & Wang, 2017). These studies have provided information on the hierarchy of ribosomal protein assembly, and on the temporal and spatial patterns of the association and dissociation of assembly factors. Detailed reviews describe the current knowledge of these dynamics, yet there is still much to be discovered (Bohnsack & Bohnsack, 2019; Kressler *et al.,* 2010; Klinge & Woolford, 2019; Oborská-Oplová *et al.,* 2022). One recent discovery is that the release of the methyltransferase Bud23, which is involved in the transformation of the SSU processome into the pre-40S intermediate, is displaced by the atypical kinase/ATPase Rio2 (Black & Johnson, 2022). In comparison with *S. cerevisiae*, relatively little is known about the assembly pathway in humans. Like with rRNA processing and transcription, the basic features of assembly are predicted to be conserved but have evolved to be more complex due to the increased size of human ribosomes and pre-ribosomes as well as increased regulatory networks that control ribosome assembly and function (Anger *et al.,* 2014; Bohnsack & Bohnsack, 2019).

Several newly emerging techniques have provided us with additional information on the dynamics and assembly required for subunit maturation. For example, inhibition of ribosome biogenesis by high-throughput drug treatments and microscopy-based screens provide information into the assembly order. As different drugs are capable of inhibiting numerous different stages of ribosome biogenesis, a wide range of rRNA processing defects has been observed (Awad *et al.,* 2019). Additionally, structural probing of pre-ribosomes has been possible through MNase tethering to numerous biogenesis factors and used to shed light on the dynamics of both formation and folding of the 40S precursor in *S. cerevisiae* (Dielforder *et al.,* 2022). However, in recent years cryo-EM has provided exceptional insight into ribosomal biogenesis across prokaryotes and eukaryotes.

Cryo-EM provides detailed structural information on both mature ribosomes and pre-ribosomes at different assembly stages. Through revealing the structure for both 60S pre-ribosomes (Barrio-Garcia *et al.,* 2016; Greber *et al.,* 2016; Leidig *et al.,* 2014; Wu *et al.,* 2016) and 40S particles (Strunk *et al.,* 2011), we gain an insight into the molecular mechanisms of ribosome assembly by visualising the ribosomal architecture and subsets of biogenesis factors present in assembly intermediates (Rabuck-Gibbons *et al.,* 2021). With over 200 ribosome biogenesis factors identified in yeast alone (Woolford & Baserga, 2013; Brüning *et al.,* 2018), dissecting the precise interactions within pre-ribosomal complexes and visualising remodeling events required to form mature ribosomal subunits will further aid the current understanding in how ribosome biogenesis is regulated.

### 1.2.5 Nuclear export and final maturation

The pre-60S subunit undergoes extensive rearrangements within the nucleolus, whilst the pre-40S subunit is more rapidly exported to the cytoplasm (Nissan *et al.,* 2002). Both pre-ribosomal subunits are exported out of the nucleus through the nuclear pore complex (NPC), with the pre-60S subunit one of the largest known cargoes to pass through the NPC (Okamura

*et al.,* 2015). More is known about the export of the pre-60S particle. The human transport receptor Crm1 is conserved from the *S. cerevisiae* transport receptor Xpo1 (Gadal *et al.,* 2001; Ruland *et al.,* 2021; Thomas & Kutay, 2003). The pre-60S is bound by Crm1/Xpo1 by the ribosome export adaptor Nmd3 with particle export mediated by the GTPase Ran (Thomas & Kutay, 2003; Trotta *et al.,* 2003). RanGTP recognises export-competent complexes and facilitates their translocation through the NPC into the cytoplasm, where GTP hydrolysis occurs, releasing the pre-60S and RanGDP (Henras *et al.,* 2008). Pre-60S export through the NPC in humans (24±4 ms), has a translocation duration in the same order or magnitude as the export of pre-60S particles through the NPC in yeast (90±50 ms) (Delavoie *et al.,* 2019; Ruland *et al.,* 2021).

In comparison, very little is known regarding pre-40S export. Leptomycin B treatment, a potent Crm1 inhibitor, which blocks nuclear export affected pre-40S particle export in addition to pre-60S export (Moy & Silver, 1999; Thomas & Kutay, 2003). However, whilst the link between Crm1 and the pre-60S is known (Nmd3), the factor linking Crm1 with the the pre-40S particle remains elusive. One candidate for the adaptor factor is the ribosomal protein RPS15 which has been shown to be an essential component of the pre-ribosomal particle to enable nuclear export (Léger-Silvestre *et al.,* 2004). Further work suggests RPS15 and several other ribosomal proteins are required for efficient pre-40S export by forming an interaction platform for the export machinery (Ferreira-Cerca *et al.,* 2007; Raska *et al.,* 2006b; Rössler *et al.,* 2022).

Once present in the cytoplasm both pre-60S and pre-40S particles must undergo final maturation steps and proofreading prior to being competent for translation initiation. Both pre-ribosomal particles are exported into the cytoplasm still bound by assembly factors. For the 60S there is sequential dissociation of assembly factors requiring cytoplasmic proteins such as ATPases and GTPases. This enables the pre-60S to bind to ribosomal proteins, interact with translation factors, induce conformational changes upon ATP/GTP hydrolysis or pair with the 40S (Henras *et al.,* 2008; Oborská-Oplová *et al.,* 2022). The exported pre-40S particle contains ribosomal biogenesis factors to prevent premature maturation and acts as a quality control mechanism.

### 1.2.6 Quality control

Ribosome biogenesis is highly complex requiring the interplay of hundreds of processes and events, it is therefore, not unlikely that a certain percentage of ribosomes are synthesised incorrectly or damaged during biogenesis. To ensure that defective ribosomal subunits do not enter the translational pool, cells have control mechanisms in place to remove these ribosomes (Sarkar *et al.,* 2017). A single defective ribosome not only produces less protein but also can inhibit functional ribosomes causing more severe effects on protein synthesis (Nazar, 2004).

Numerous mechanisms of quality control exist during ribosome biogenesis (Karbstein, 2013). These mechanisms are subdivided into three categories: (1) key structural features are recognised by assembly factors which act to mimic translation factors or RPs preventing pre-mature incorporation, (2) assembly factors bound to the pre-ribosome block translation initiation and (3) ribosomal subunits carry out functional tests mimicking the translational cycle. One of the best characterised quality control checkpoints exists for the *S. cerevisiae* pre-40S subunit, and by association the pre-60S. During the late stages of maturation the pre-40S is promoted to form 80S-like complexes by the GTPase eIF5B. There is some debate on whether it is the mature 60S particle or the pre-60S which is present in these 80S-like

complexes. Here, the binding of assembly factors, Tsr1 and Rio2, blocks the mRNA channel and initiator tRNA binding site, preventing translation. Dissociation of these two assembly factors leads to the displacement of the 60S from the 40S and the 40S is now competent for translation initiation (Lebaron *et al.,* 2009; Strunk *et al.,* 2012). Whilst, this mechanism of quality control has been well characterised in yeast, there is currently no evidence to suggest that these 80S-like complexes form in humans.

Failure of the quality control mechanisms leads to pre-ribosome degradation, but it is unclear if a surveillance mechanism exists or if particles become actively degraded if they do not undergo maturation in a certain time frame (Kressler *et al.,* 2010). This degradation of assembly intermediates is known to be carried out by the nuclear exosome, mediated by its helicase Mtr4 and the associated Trf4/5-Air1/2-Mtr4p Polyadenylation (TRAMP) complex (Holub *et al.,* 2012; Jia *et al.,* 2012; LaCava *et al.,* 2005; Lubas *et al.,* 2011; Vanácová *et al.,* 2005).

## 1.3 The Exosome

The exosome was first identified in *S. cerevisiae* as a conserved RNA processing complex containing numerous 3' to 5' exoribonuclease activities (Mitchell *et al.,* 1997). The core of the exosome in yeast and humans, composed of nine subunits, is catalytically inactive and displays little structural variability or change in subunit subcellular localisation (Table 1.1) (Chlebowski *et al.,* 2013; Schilders *et al.,* 2005; Schmid & Jensen, 2008)). In both *S. cerevisiae* and humans, six proteins with resemblance to the bacterial ribonuclease PH; Rrp45, Rrp41, Rrp42, Mtr3, Rrp43 and Rrp46, form a 'ring' structure termed the PH ring (Figure 1.4) (Van Hoof & Parker, 1999). This ring complex is unstable in the absence of Rrp4, Csl4 and Rrp40, which must bind and form the 'cap' of the exosome. This subsequent nine protein complex is then stable and forms the exosome core (often termed EXO9) (Figure 1.4). Initially, the exosome core was thought to be catalytically active, but exonuclease activity was later shown to be limited and for RNA processing/degradation, the exosome core must associate with other cofactors and complexes (Table 1.1) (Dziembowski *et al.,* 2007; LaCava *et al.,* 2005).

In eukaryotes, the exosome core associates with two nucleases, Rrp44 (Dis3) and Rrp6 (Figure 1.4) (Liu *et al.,* 2006). Rrp44 has both exo- and endo-nuclease activity, which are proposed to enable the coordinated degradation of large, structured RNAs (Schneider *et al.,* 2007; Lebreton *et al.,* 2008; Scheaffer *et al.,* 2009; Schneider *et al.,* 2009). In yeast, the exosome core constitutively associates with Rrp44 across the cell, in both the nucleus and cytoplasm, whereas, in humans, RRP44 is excluded from the nucleolus. Although in yeast, only one form of Rrp44 is present, two different human homologues have been identified to associate with the core exosome: DIS3 and DIS3L1 which are found in the nucleoplasm and cytoplasm, respectively (Figure 1.5, Table 1.1) (Sloan *et al.,* 2012; Tomecki *et al.,* 2010). Rrp6 possesses 3'-5' exonuclease activity, however, in yeast, Rrp6 is only capable of degrading unstructured rRNA substrates, whilst human RRP6 can degrade more structured RNAs (Januszyk *et al.,* 2011). Rrp6 is localised to the nucleus in yeast, however is highly concentrated to the nucleoli in humans (Tomecki *et al.,* 2010) (Figure 1.5). Therefore, as human nucleoli have significant levels of RRP6 and lack RRP44, exosome activity here is likely provided by RRP6.

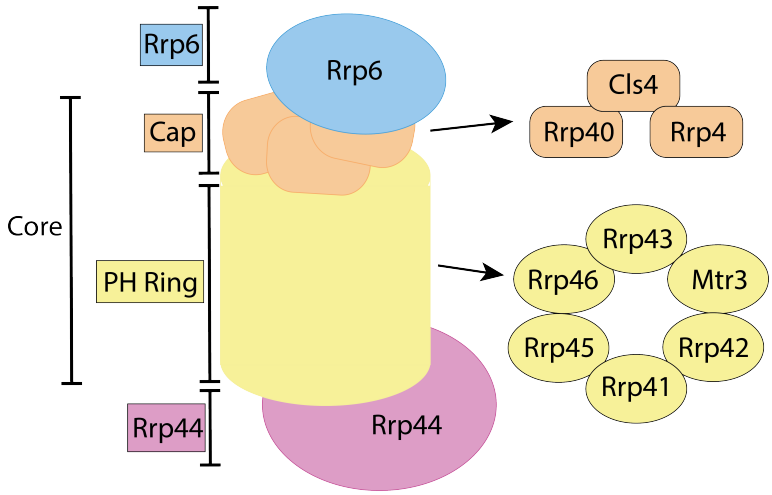


Figure 1.4: Structure of the eukaryotic RNA exosome. Schematic depicting the catalytically inactive nine subunit exosomal core comprised of the PH ring and cap which can associate with the nucleases Rrp44 and Rrp6.

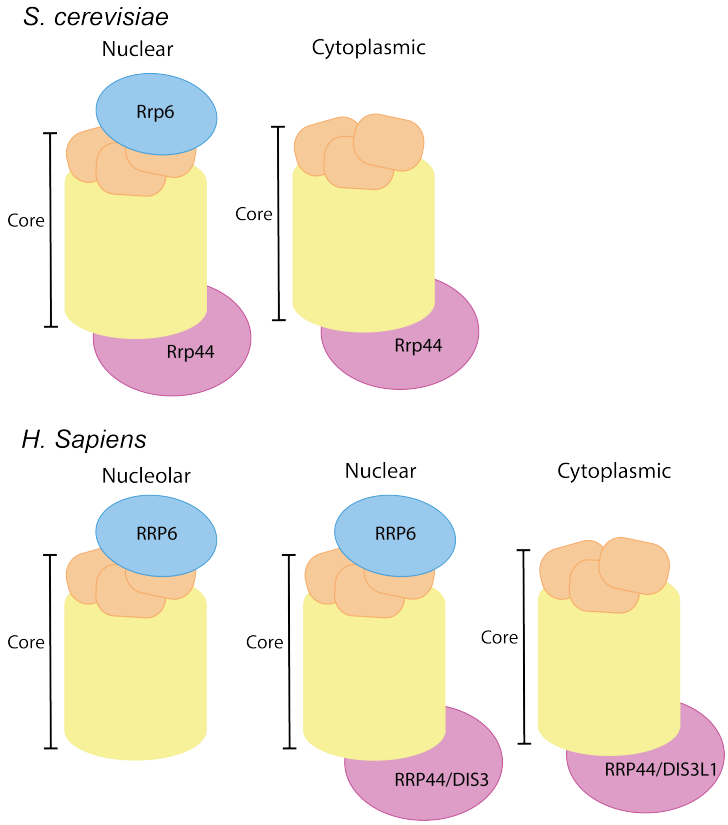


Figure 1.5: Exosome variants in different subcellular locations in *S. cerevisiae* and *H. sapiens*. In both species the nuclear variants associate with Rrp6 and Rrp44 (DIS3), with the cytoplasmic variants associating with Rrp44 (DIS3L1). *H. sapiens* have an additional nucleolar variant which associates with RRP6.

### 1.3.1 The RNA helicases and their associated complexes

In addition to variations in the nucleases associated with the exosome core depending on cellular location, the exosome also differentially associates with other cofactors and complexes (Table 1.1) (Liu *et al.,* 2006). Common to these complexes are two members of the Ski2 family of RNA helicases. In the cytoplasm, the exosome core associates with the cytoplasmic helicase Ski2, an essential component of the Ski complex (Halbach *et al.,* 2012). The nuclear exosome associates with a different member of the Ski2 family, the nuclear helicase Mtr4, which can be found within different complexes. Both Ski2 and Mtr4 are required for substrate recognition, 3'-5' unwinding of RNA duplexes and presentation of RNA to the exosome for targeted processing or degradation (de la Cruz *et al.,* 1998; Johnson & Jackson, 2013; Thoms *et al.,* 2015). Whilst the cytoplasmic exosome and Ski2 target mRNA for degradation, the nuclear exosome and Mtr4 are involved in the processing, 3'-5' degradation and surveillance of structured RNA species, including pre-rRNA, small nucleolar and small nuclear RNAs (sno/snRNAs) and transfer RNAs (tRNAs) (Allmang *et al.,* 1999; Kilchert *et al.,* 2016).

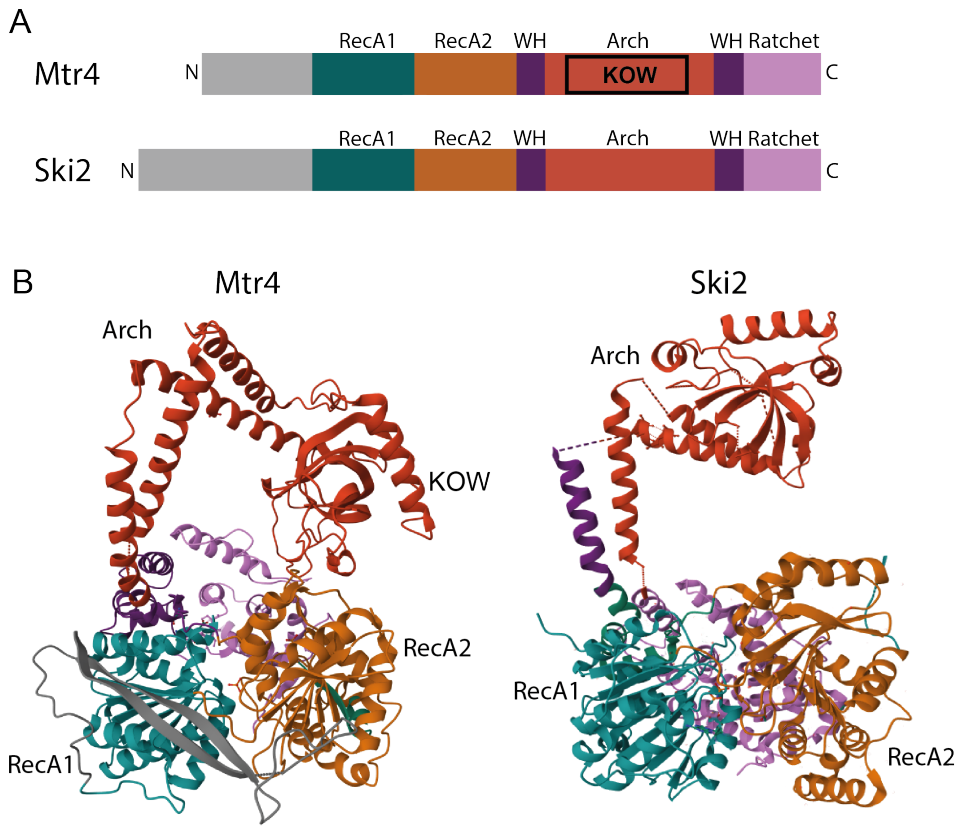


Figure 1.6: Structure of the exosome associated helicases; Ski2 and Mtr4. A) Domains found within Ski2 and Mtr4. B) Resolved structures of Ski2 (PBD 4A4Z) and Mtr4 (PBD 4QU4) with RecA1, RecA2 and the Arch domain labelled and depicted in cyan, orange and red, respectively.

Mtr4 and Ski2 were identified in *S. cerevisiae* with homologous helicases also existing in humans (Johnson & Jackson, 2013). Similar to the other members of the Ski2-like family of helicases (Brr2 and Slh1), Mtr4 and Ski2 share a common structure consisting of a DExH-box core which contains a winged helix (WH) domain, a ratchet domain and two RecA domains

Table 1.1: RNA exosome subunits, cofactors and complexes and their localisation

| | *S. cerevisiae* | | *H. sapiens* | |
|---|---|---|---|---|
| | Protein name | Localisation | Gene name | Localisation |
| Cap | Cls4<br>Rrp4<br>Rrp40 | Nucleus/<br>Cytoplasm | EXOCS1<br>EXOCS2<br>EXOCS3 | Nucleus/<br>Cytoplasm |
| PH Ring | Rrp41<br>Rrp46<br>Mtr3<br>Rrp42<br>Rrp43<br>Rrp45 | Nucleus/<br>Cytoplasm | EXOCS4<br>EXOCS5<br>EXOCS6<br>EXOCS7<br>EXOCS8<br>EXOCS9 | Nucleus/<br>Cytoplasm |
| Nucleases | Rrp6<br>Rrp44 (Dis3) | Nucleus<br>Nucleus/<br>Cytoplasm | EXOCS10<br>DIS3<br>DIS3L1 | Nucleus<br>Nucleoplasm<br>Cytoplasm |
| Cofactors | Rrp47<br>Mpp6<br>Ski7 | Nucleus<br>Nucleus<br>Cytoplasm | C1D<br>MPP6<br>HBS1L | Nucleus<br>Nucleolus<br>Cytoplasm |
| SKI complex | Ski2<br>Ski3<br>Ski8 | Cytoplasm | SKIV2L<br>TTC37<br>WDR61 | Cytoplasm |
| TRAMP complex | Mtr4 (Dob1)<br><br>Air1/2<br>Trf4/5 | Nucleus | MTR4/SKI2L2<br><br>ZCCHC7<br>PAPD5 | Nucleus<br>(MTR4)<br>Nucleolus |
| NEXT complex | N/A | N/A | MTR4/SKI2L2<br><br>ZCCHC8<br>RBM7 | Nucleus<br>(MTR4)<br>Nucleoplasm |
| PAXT complex | N/A | N/A | MTR4/SKI2L2<br><br>ZFC3H1<br>PABPN1 | Nucleus<br>(MTR4)<br>Nucleoplasm |

(He *et al.,* 2010; Weir *et al.,* 2010) (Figure 1.6). However, within the Ski2 family of helicases, only Mtr4 and Ski2 are essential components of the exosome, required for unwinding RNA in a 3' to 5' direction similar to mechanisms of other DExH helicases (Weir *et al.,* 2010).

Both Mtr4 and Ski2 contain a unique, prominent 256-266 amino acid insertion within the winged helix domain, termed the arch domain (Figure 1.6). The arch domain is formed of two pairs of anti-parallel alpha helices which terminate at a globular domain known as the fist (Johnson & Jackson, 2013). In Ski2, the fist forms a beta-barrel fold, similar to that of Mtr4, however the fist within Mtr4 contains a KOW (Kyprides, Ouzounis, Woese) motif and is referred to as a KOW domain. KOW containing proteins can bind structured RNAs (Weir *et al.,* 2010). As Ski2 lacks a KOW motif, it is less selective in RNA binding and capable of binding both structured and single stranded RNAs (Halback *et al.,* 2012), likely due to the diversity of substrates present in the cytoplasm.

#### Ski2 and the cytoplasmic exosome

Ski2 associates with the exosome as part of a multi-protein complex in the cytoplasm, know as the superkiller (Ski) complex. The Ski complex was first identified in yeast, and contains the Ski2 helicase along with two RNA-binding proteins, Ski3 and Ski8 (Table 1.1) (Schmidt *et al.,* 2016). The Ski complex is required for cytoplasmic RNA turnover and acts in several mRNA quality control pathways, including; nonsense mediated decay (NMD), no-go decay and non-stop decay (Kilchert, 2020). The interaction between the Ski complex and the core exosome is not direct and requires an additional co-factor, Ski7, which is suggested to be a a constitutive component of the cytoplasmic exosome (Kowalinski *et al.,* 2016). Homologous components of the yeast Ski complex exist in higher eukaryotes and humans (Table 1.1). The mammalian cytoplasmic SKI complex has additional functional roles in mRNA decay and has been implicated in the degradation of RNAs containing AU-rich elements (AREs), with AU binding proteins able to directly recruit the exosome (Chen *et al.,* 2001).

#### Mtr4 and the nuclear exosome

In the nucleus, the best described Mtr4-associated complex is the Trf4/5-Air1/2-Mtr4 polyadenylation (TRAMP) complex identified in *S. cerevisiae* (LaCava *et al.,* 2005). Two distinct forms of the TRAMP complex can exist depending on which poly(A) polymerase is incorporated, with TRAMP4 and TRAMP5 complexes containing Trf4 and Trf5, respectively. Both these forms also contain a zinc-knuckle protein, either Air1 or Air2, which are functionally redundant (Delan-Forino *et al.,* 2020). Both TRAMP complexes make the RNA a better substrate for exosome-mediated 3' degradation through the addition of a poly(A)-tail.

The TRAMP complex and MTR4 show functional conservation in humans where they are also required for exosome mediated degradation and processing of RNAs (Lubas *et al.,* 2011). In yeast, the TRAMP complex is nuclear, however in humans it is localised to the nucleolus (Table 1.1). In humans, two other MTR4 containing complexes not present in yeast are localised to the nucleoplasm; the Nuclear Exosome Targeting (NEXT) complex and the poly(A)tail exosome targeting (PAXT) complex (Table 1.1) (Lubas *et al.,* 2011; Meola *et al.,* 2016). The NEXT complex contains MTR4 and ZCCHC8 and the RNA-binding protein, RBM7, which is capable of binding a range of RNA substrates including sn/snoRNAs and newly synthesised RNAs for exosome targeting. (Lubas *et al.,* 2015). Whereas the PAXT complex, binds preferentially to polyadenylated RNAs via the polyA binding protein PABPN1 which is connected to MTR4 by ZFC3H1 (Meola *et al.,* 2016).

MTR4 is a key component of the nuclear exosome across several complexes in humans and in the TRAMP complex in *S. cerevisiae*, but it can also bind other co-factors which are suggested to act as bridge between MTR4 and the exosome in the nucleus, similar to the role of Ski7 in the cytoplasm. Both Rrp47 (C1D) and Mpp6 (MPP6) have been suggested to have roles in the recruitment of Mtr4 to the exosome to enable RNA degradation (Table 1.1) (Garland *et al.,* 2013; Kim *et al.,* 2016). Whilst it is important to understand and acknowledge the diversity in the exosome, it's helicases, co-factors and complexes (summarised in Table 1.1), only the nuclear exosome, and its associated helicase, Mtr4, are necessary for rRNA processing during ribosome biogenesis and therefore will be the focus for further discussion.

### 1.3.2 The nuclear exosome and Mtr4 in rRNA processing

The exosome was discovered due to a defect in rRNA maturation in *S. cerevisiae*. A mutation in one of the core proteins, *rrp4-1* caused a defect in 3' maturation of the 5.8S rRNA during pre-rRNA processing (Mitchell *et al.,* 1996). This resulted in an accumulation of 7S

pre-rRNA as the exosome is necessary for 5.8S rRNA formation by digesting the 3' extension of the 7S pre-rRNA. In a subsequent study, the same defect in 5.8S rRNA maturation was observed in addition to an accumulation of the 5' ETS fragment, when Mtr4 was either mutated or deleted (de la Cruz *et al.,* 1998; Weir *et al.,* 2010). Therefore, the conversion of the 7S precursor rRNA to the mature 5.8S rRNA, requires not only the activity of the exonucleases in the nuclear exosome but also the 3' to 5' unwinding activity of Mtr4.

Mtr4 contains a novel arch domain comprised of two anti-parallel alpha helices and a KOW domain (Figure 1.6). The KOW domain is required to bind structured RNAs and is essential for rRNA processing (Jackson *et al.,* 2010; Johnson & Jackson, 2013; Weir *et al.,* 2010). The arch domain of Mtr4 is also important for interactions with adaptor proteins containing an arch interaction motif (AIM), including *S. cerevisiae* ribosome biogenesis factors (Thoms *et al.,* 2015). Mtr4 is able to simultaneously bind an AIM-containing protein and a structured RNA at adjacent surfaces, suggesting how it can dock onto the pre-ribosome by binding to an AIM containing biogenesis factor and concurrently unwind the rRNA for processing by the exosome (Falk *et al.,* 2017).

**AIM-containing proteins**

The AIM was first identified in the *S. cerevisiae* ribosome biogenesis factors, Nop53 and Utp18 (Thoms *et al.,* 2015). The AIM in both Nop53 and Utp18 interacts with Mtr4 for exosome mediated processing of the 7S pre-rRNA and 5' ETS cleavage, respectively. The AIM found within *S. cerevisiae* Nop53 is highly conserved to higher eukaryotes and consists of a stretch of four hydrophobic amino acids with an invariable aspartate in the fifth position (LFXΦD) (Figure 1.7). The AIM in *S. cerevisiae* Utp18, shows a high level of sequence similarity to that of Nop53, however, the AIM sequence is not conserved into higher eukaryotes (Figure 1.7). This may be because an alternative adaptor has evolved in metazoans due to an additional endonucleolytic cleavage site (A'), for which MTR4 is known to be involved in (Sloan *et al.,* 2014). Alternatively, as mutations within the AIM of Utp18 showed no growth phenotype in yeast, alternative partially redundant mechanisms of 5' ETS cleavage may exist and therefore, there was no selective pressure to retain the AIM consensus sequence into higher eukaryotes (Thoms *et al.,* 2015).

Whilst, human NOP53 contains a conserved AIM (LFXΦD), the AIMs found in other human proteins typically diverge from this consensus sequence. For example, a ribosome biogenesis factor of the AAA-ATPase family, NVL, contains an amino acid sequence which had significant similarity to the NOP53 AIM sequences but was not responsible for the interaction with MTR4 (Lingaraju *et al.,* 2019). However, a few amino acids upstream, a highly conserved motif across vertebrates was shown to mediate an interaction with MTR4 and was termed, the W-AIM as it is centered around a tryptophan (Figure 1.7). A further protein ZCCHC8, a component of the NEXT complex, also contains an AIM for interacting with MTR4 that differs from both the NOP53 AIM and W-AIM, termed a C-AIM (cysteine centered) (Figure 1.7). Interestingly, whilst all these AIMs differ in length and composition, they are all required for the interaction with the arch domain of MTR4 recognising site Arg743 (Arg774 in *S. cerevisiae* Mtr4) (Lingaraju et al. 2019).

Despite the variations to the AIM found on these adaptor proteins, they have all evolved similar mechanisms to recognise MTR4 and recruit the exosome to diverse RNA targets, with MTR4 simultaneously binding an AIM and structured RNA (Falk *et al.,* 2017). It has also been shown that binding to the arch domain of MTR4 can prevent the association with specific substrates. For example, NRDE2 contains an 'AIM-like' sequence by which it interacts with MTR4 (Figure 1.7), subsequently preventing the association between Mtr4 with

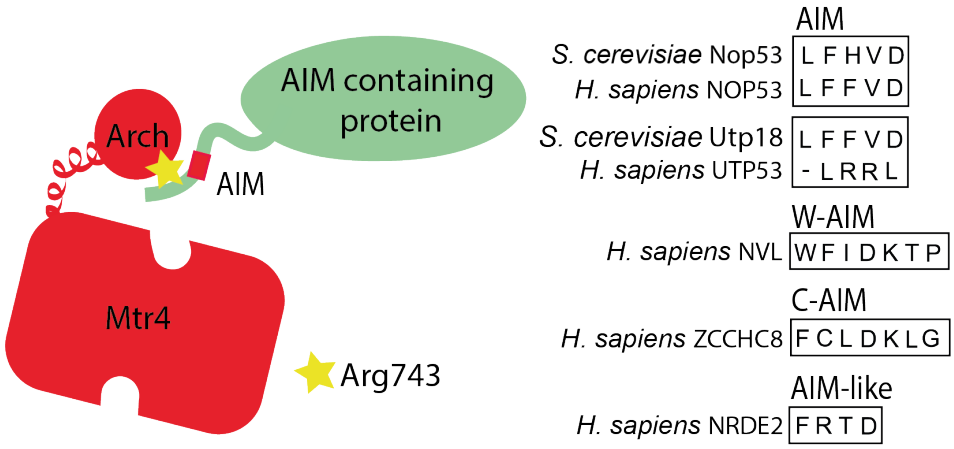


Figure 1.7: Arch interaction motif (AIM) containing proteins. AIM containing proteins interact with the Arch domain of MTR4 via a conserved arginine residue (R743 in humans, R774 in yeast). The AIM sequence is found in *S. cerevisiae* Nop53 and Utp18 (LFXΦD) is conserved in human NOP53 but not in UTP18. NVL, ZCCHC8 and NRDE2 contain AIMs which diverge from the Nop53 AIM and are termed W-AIM, C-AIM and AIM-like, respectively.

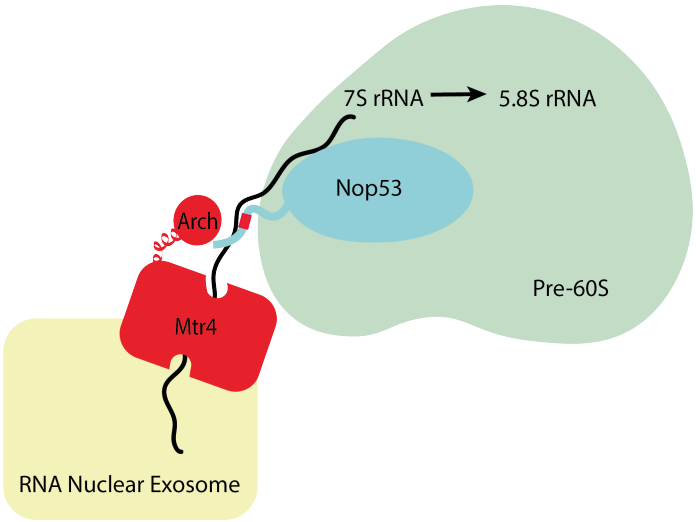


Figure 1.8: Nop53 and Mtr4 interact on the pre-60S particle to enable exosome mediated processing of the 7S pre-rRNA into mature 5.8S rRNA. Mtr4 is part of the exosomal complex and interacts with the AIM of Nop53 via its arch domain. It is unknown if Nop53, Mtr4 and the exosome associate with the pre-60S as a complex or if Nop53 is already associated with the particle prior to Mtr4 binding.

mRNAs and lncRNAs limiting exosomal degradation (Wang *et al.,* 2019). Therefore, the specific affinity that each AIM-containing protein has for MTR4, along with its expression level, results in selectivity of interaction with not only the adaptor protein, but with the RNA targeted for degradation.

### Nop53 as an Mtr4 AIM adaptor

The nucleolar protein, Nop53 (termed PICT-1 and GLTSCR2 in humans) is an AIM containing ribosome biogenesis factor identified in *S. cerevisiae*. Here, it was shown to be essential for cell viability and efficient 60S biogenesis (Granato *et al.,* 2005; Thomson & Tollervey. 2005). Nop53 is localised to the nucleolus, nucleoplasm and nuclear envelope (Thomson & Tollervey, 2005) but was not shown to transit to the cytoplasm, suggesting that Nop53 dissociates from the pre-60S subunit prior to or during export to the cytoplasm. The role of Nop53 in 60S biogenesis was first linked to that of exosome processing, since Nop53 associates with pre-ribosomal particles containing pre-rRNA exosome substrates and can activate the exosome in *in vitro* RNA degradation assays (Granato *et al.,* 2008). Subsequently, an N-terminal AIM was identified in Nop53 and shown to mediate an interaction with the arch domain of Mtr4. (Thoms *et al.,* 2015).

The interaction between the AIM of Nop53 and the arch domain of Mtr4 is responsible for targeting Mtr4 and the nuclear exosome to pre-ribosomal particles for exosome mediated rRNA processing (Figure 1.8). Mutations within the AIM of Nop53 abolish the interaction with Mtr4 resulting in an accumulation of 7S rRNA precursors (Thoms *et al.,* 2015) which is also observed following Nop53 depletion (Granato *et al.,* 2005; Thomson & Tollervey. 2005). Depletion of Mtr4 or deletion of the arch domain of Mtr4 also abolishes the Mtr4-Nop53 interaction and exhibits similar processing defects (de la Cruz *et al.,* 1998; Johnson & Jackson, 2013). Therefore, the interaction between Nop53 and Mtr4 is essential to produce mature 5.8S rRNA for 60S ribosomal subunit assembly (Figure 1.9).

This interaction has currently only been studied in *S. cerevisiae* but is believed to be conserved throughout eukaryotes to humans. There is over 50 % sequence identity between yeast and human MTR4 including the conserved arginine residue within the arch domain, suggesting a conserved interaction between NOP53 and MTR4 (LaCava *et al.,* 2005; Lubas *et al.,* 2011; Thoms *et al.,* 2015; Weir *et al.,* 2010). Additionally, as mentioned, the AIM identified in yeast Nop53 is well conserved in human NOP53 and other human AIM containing proteins are known to bind MTR4. Therefore, since both factors show high levels of conservation particularly in the regions shown to mediate the interaction, we predict that the interaction between NOP53 and MTR4 and their function in 60S biogenesis is also conserved. In addition to this proposed role in ribosome biogenesis, in humans, NOP53 has also been implicated in other nucleolar functions.

## 1.4 The Nucleolar Stress Response

A more recently identified function of the nucleolus is the nucleolar stress response. The nucleolar stress response can be triggered by a variety of cellular stresses including DNA damage, osmotic stress, nutrient stress, oncogenic stress and viral infection (Boulon *et al.,* 2010) (Figure 1.10). Further, the inhibition of RNA polymerase I, by actinomycin D treatment at low concentrations, (Iapalucci-Espinoza & Franze-Fernández, 1979) inhibits 47S pre-rRNA transcription, and, thus, prevents ribosome biogenesis and triggers the nucleolar stress response.

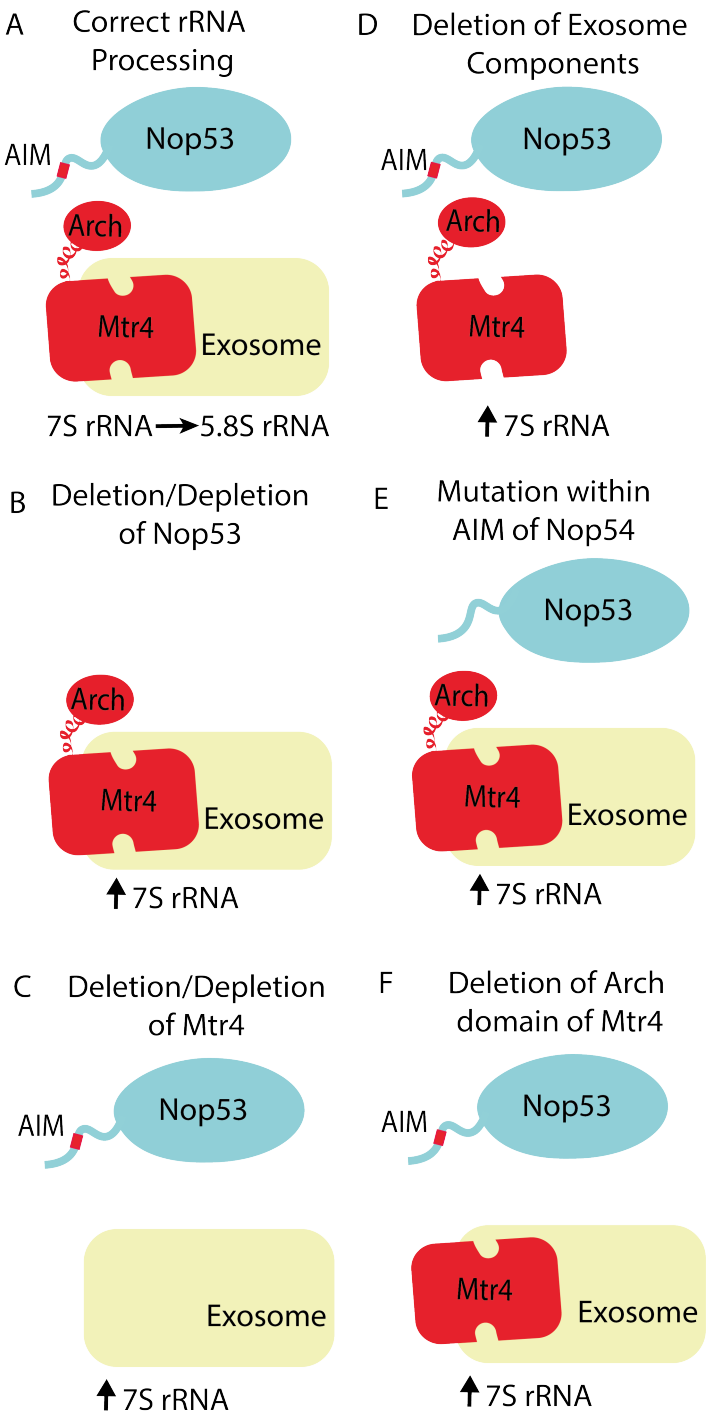


Figure 1.9: Nop53, Mtr4 and the associated nuclear exosome are required for 7S pre-rRNA processing. A) 7S rRNA undergoes correct 3' end processing into 5.8S rRNA when Nop53 and Mtr4 are capable of interacting and the exosome is present and functional. B) Deletion or depletion of Nop53 prevents Mtr4 recruitment to the pre-60S leading to 7S rRNA accumulation. C) Deletion or depletion of Mtr4 prevents exosome recruitment to the pre-60S leading to 7S rRNA accumulation. D) Mtr4 and Nop53 are capable of interacting but mutations or loss of the exosome or exosomal components prevents exonucleolytic cleavage leading to 7S rRNA accumulation. E) Mutations in the AIM of Nop53 prevents Mtr4 interaction and recruitment to the pre-60S leading to 7S rRNA accumulation. F) Deletion of the arch domain of Mtr4 prevents binding to Nop53 and therefore exosome recruitment to the pre-60S leading to 7S rRNA accumulation.

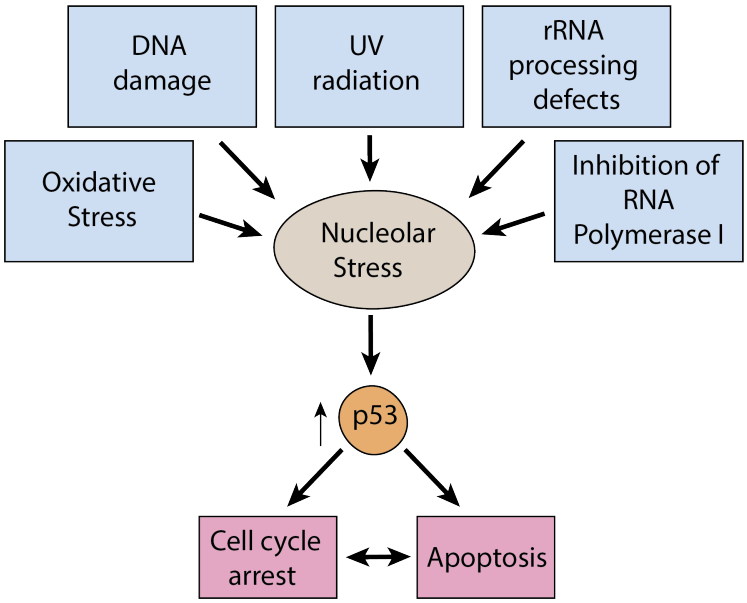


Figure 1.10: Overview of the initiation of the nucleolar stress response by different cellular triggers and the p53 mediated response. Activation of the nucleolar stress response by rRNA processing defects, UV radiation, DNA damage, RNA polymerase I inhibition and oxidative stress trigger the stabilisation and subsequent increase in p53 levels which trigger cell cycle arrest. If the stress is irreparable p53 can also trigger apoptosis or cellular senescence.

Activation of the nucleolar stress response leads to the initiation of cell-cycle arrest through p53 stabilisation and under severe irreparable stress, apoptosis (Figure 1.10) (Rubbi & Milner, 2003; Boulon *et al.,* 2010). During nucleolar stress, p53 mediates the inhibition of RNA polymerase I and III, limiting ribosome biogenesis (Budde & Grummt, 1999; Chesnokov *et al.,* 1996; Zhai & Comai, 2000). Therefore, defects in ribosome biogenesis are both a putative cause and consequence of the nucleolar stress response. Thus, there is a complex interplay between the two processes.

### 1.4.1 Degradation of p53 under homeostatic conditions

The transcription factor, p53 is a tumour suppressor and plays a key role in initiating cell cycle arrest in response to nucleolar and other cellular stresses. Under normal homeostatic cellular conditions, p53 is actively ubiquitinated by the E3 ubiquitin ligase HDM2 and targeted to the proteasome for degradation (Haupt *et al.,* 1997) (Figure 1.11 A). As most studies on the regulation of p53 have been conducted in mouse models, MDM2 was studied, however, the functional role is predicted to be conserved in its human homologue, HDM2. Alterations in both p53 and HDM2 can have profoundly negative effects on cellular function, with mutations in the gene encoding p53 found in over 50% of human cancers (Toledo & Wahl, 2006), and amplified HDM2 expression in 7% of cancers still retaining wildtype p53 (Momand *et al.,* 1998). Regulation of p53 expression by HDM2 is key to cellular survival, as deletion in mice caused early embryonic lethality which could be rescued by concomitant p53 deletion (Jones *et al.,* 1995; Montes de Oca Luna *et al.,* 1995). By actively targeting p53 for degradation HDM2 acts as a positive regulator of cell growth (Holmberg Olausson *et al.,* 2012).

### 1.4.2 RPL11-mediated p53 stabilisation under nucleolar stress

The first well characterised p53 activation pathway involves the expression of the ARF gene product (Sherr & Weber, 2000). When expressed, ARF binds to HDM2 and prevents the

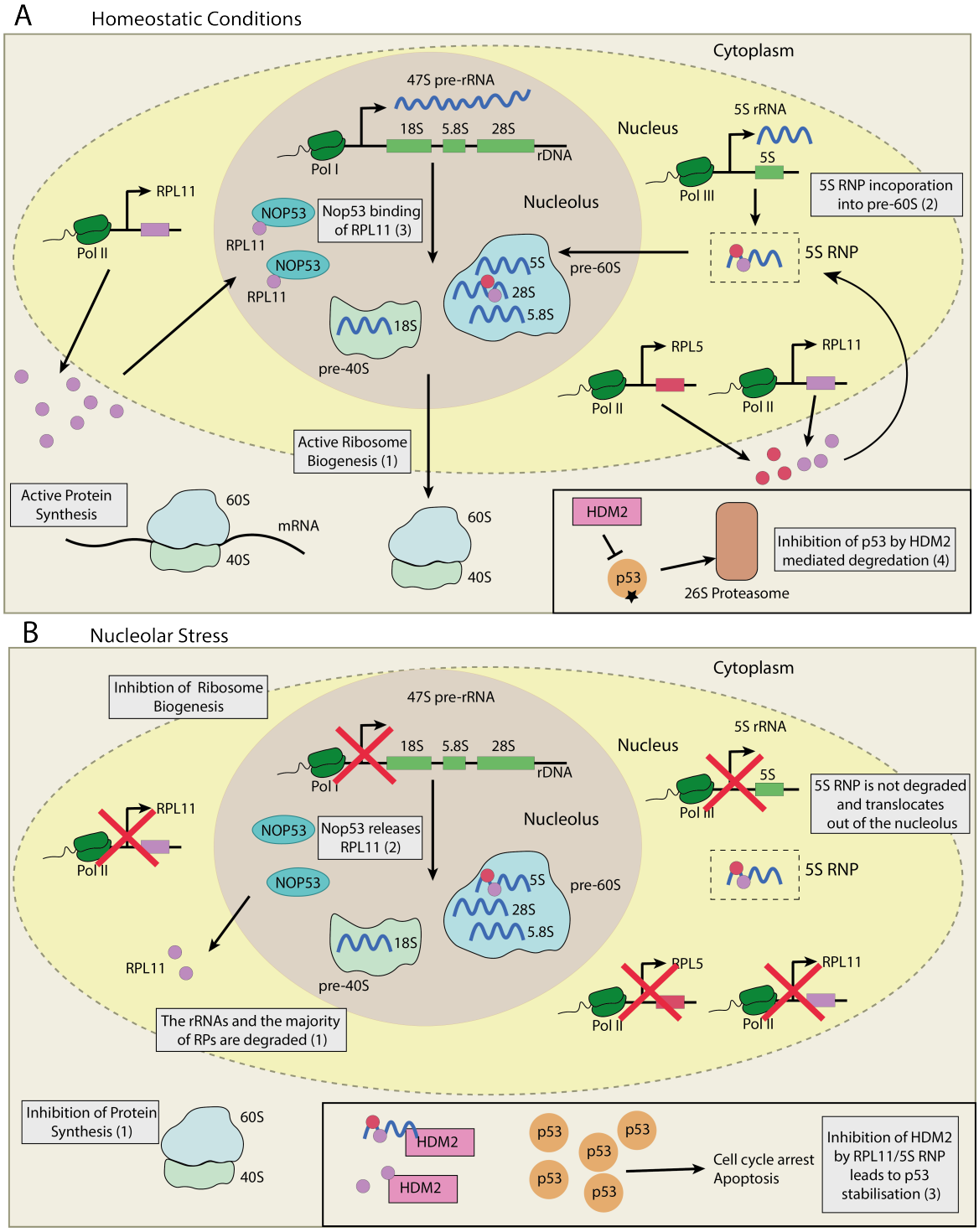


Figure 1.11: Overview of ribosome biogenesis and p53 regulation in homeostatic cellular conditions and under nucleolar stress. A) Under homeostatic conditions, ribosomes are actively synthesised (1), the 5S RNP is incorporated into pre-60S particles (2) and "free" RPL11 is sequestered in the nucleolus by NOP53 (3). The cell is actively dividing as HDM2 ubiquitinates p53, targeting it for degradation (4). B) Under nucleolar stress, ribosome biogenesis is inhibited and the majority of ribosomal proteins are degraded (1). RPL11 is released by NOP53 (2) and RPL11 and the 5S RNP bind to HDM2 preventing p53 ubiquitination (3). p53 is stabilised, triggering cell cycle arrest. It is not known whether NOP53 can interact with just free pools of RPL11 or interacts with RPL11 in the context as the 5S RNP. As no current evidence shows an interaction between NOP53 and the 5S RNP, here free pools of RPL11 are shown to bind NOP53.

association between p53 and HDM2, p53 is not ubiquitinated and levels increase triggering cell cycle arrest. p53 then activates expression of HDM2 in an autoregulatory feedback loop (Picksley & Lane, 1993). However, in response to perturbations in ribosome biogenesis an alternative parallel pathway, independent of ARF, exists to inhibit HDM2 and stabilise p53 (Macias *et al.,* 2010).

In response to cellular stresses or inhibition of ribosome biogenesis, ribosome-free RPs are degraded by the proteasome (Lam *et al.,* 2007). However, a small number of RPs that are proposed to have a dual physiological role in ribosome assembly and in p53 regulation, selectively accumulate (Zhang *et al.,* 2003). These RPs include RPL26, RPL23, RPL11, RPL5 and RPS7 and act as effectors of the nucleolar stress response. RPL11 and RPL5 are known to be particularly important in this response (Bursać *et al.,* 2012; Chakraborty *et al.,* 2009; Dai & Lu, 2004; Lohrum *et al.,* 2003; Marechal *et al.,* 1994). During nucleolar stress, RPL11/RPL5 are released from the nucleolus and translocate to the nucleoplasm where they can bind to HDM2 (Bhat *et al.,* 2004; Dai & Lu, 2004; Suzuki *et al.,* 2012). In response to RPL11 translocations, increased levels of ubiquitinated HDM2 were observed suggesting RPL11 may regulate the proteasomal degradation of HDM2 (Dai *et al.,* 2006). Inhibition of HDM2 by RPL11/RPL5 prevents ubiquitination of p53 which is consequently stabilised, thus promotes cell cycle arrest (Figure 1.11).

RPL5 and RPL11 have been shown to act cooperatively to inhibit HDM2, since HDM2 mutants which cannot bind RPL11 or RPL5 are unable to activate p53 during nucleolar stress (Lindström *et al.,* 2007). Additionally, the overexpression of either RPL11 or RPL5 was sufficient to suppress HDM2 (Horn & Vousden, 2008). Both RPL11 and RPL5 are known to interact together with the 5S rRNA to form the 5S RNP, a sub-complex of the 60S ribosomal subunit formed during ribosome biogenesis (Steitz *et al.,* 1988; Zhang *et al.,* 2007). The 5S RNP localises to the nucleolus during active ribosome biogenesis but accumulates in the nucleoplasm when biogenesis is inhibited (Donati *et al.,* 2013). There is also additional evidence to suggest that the 5S rRNA may directly contact HDM2 (Sloan *et al.,* 2013). Together, this data suggests that RPL11 and RPL5 may act in the context of the 5S RNP to inhibit HDM2 and stabilise p53 during nucleolar stress (Donati *et al.,* 2013; Sloan *et al.,* 2013). However, there is also evidence that RPL11 may act as an individual component to stabilise p53. Levels of soluble, ribosome-unbound RPL11 were shown to increase following serum starvation, indicating a release of RPL11 from the ribosomal subunits (or a failure of them to enter) (Bhat *et al.,* 2004). Moreover, only RPL11 was shown to increase levels of ubiquitinated HDM2, suggesting RPL11 may regulate HDM2 levels through a post-ubiquitination mechanism which was not observed with RPL5 (Dai *et al.,* 2006). Therefore, it cannot currently be concluded if inhibition of HDM2 (and stabilisation of p53) can be mediated by RPL11 alone, or if RPL11 regulation is always in the context of the 5S RNP.

### 1.4.3 NOP53 as an RPL11 regulator

Sometimes referred to as GLTSCR2/PICT-1, human NOP53 was first characterised as a tumour suppressor protein localised to chromosome 19 at a common site of mutation in human cancers (Smith *et al.,* 2000; Okahara *et al.,* 2006). However, recent studies provide a more complex view and suggest that NOP53 can act as both a positive and negative regulator of cancer development depending on cell and cancer type (Kim *et al.,* 2012; Moon *et al.,* 2013). While the underlying cause of this inconsistency is unclear, it may occur due to the mutational background and cell-type of the cancer. Moreover, despite levels of NOP53 being downregulated in cancer (Kim *et al.,* 2012), expression of NOP53 is essential for the survival and proliferation of embryonic stem cells, with null mutants embryonically lethal (Sasaki *et al.,* 2011).

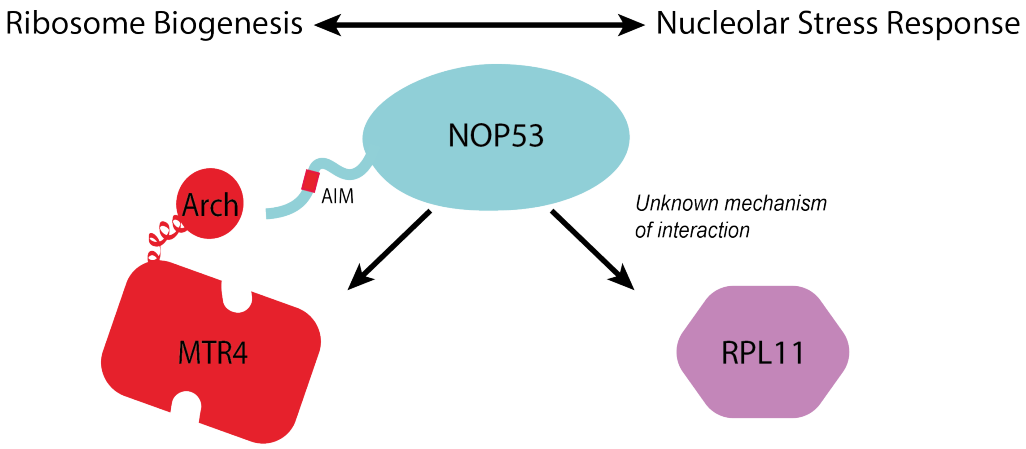


Figure 1.12: The dual functionality of NOP53 in both ribosome biogenesis and the nucleolar stress response. Nop53 is implicated in ribosome biogenesis in *S. cerevisiae* through an interaction with Mtr4 where the AIM of Nop53 binds the arch domain of Mtr4. NOP53 is implicated in nucleolar stress responses in humans through an interaction with RPL11 but the current mechanism of interaction is unknown.

As well as its identified role in recruitment of the exosome via Mtr4 during ribosome biogenesis in *S. cerevisiae*, NOP53 has also been implicated in nucleolar stress responses in humans, through a interaction with RPL11 (Figure 1.12) (Chen *et al.,* 2016; Lee *et al.,* 2012). However the nature and mechanism of this interaction is not known. During normal homeostatic conditions, NOP53 binds RPL11 sequestering it in the nucleolus, as cells depleted of NOP53 show nucleoplasmic localisation of RPL11 (Figure 1.11) (Sasaki *et al.,* 2011; Suzuki *et al.,* 2012). Upon stress, NOP53 releases RPL11, through an unclear mechanism, allowing RPL11 to associate with HDM2 resulting in p53 stabilisation. Due to this interaction with RPL11, NOP53 must be considered an important regulator of HDM2, p53 and of the nucleolar stress response. Whilst the relationship between p53 stabilisation and defects in ribosome biogenesis has been the focus of several studies (Teng *et al.,* 2013), discussion of the specific role NOP53 plays in both of these processes is limited.

It is worth noting that, to date, no study in *S. cerevisiae* suggests a direct interaction between Nop53 and Rpl11, other than both being present on the pre-60S particle. Since there are no homologs of p53 present in *S. cerevisiae*, Rpl11 regulation of p53 does not occur and therefore it is likely that Nop53 does not interact in this context with Rpl11. Therefore, in order to elucidate the connections and interplay between NOP53, the nucleolar stress and ribosome biogenesis, research into higher eukaryotes is required.

## 1.5 Aims of Thesis

NOP53 is an unusual factor as it is one of few that has been directly implicated at a molecular level in two vital nucleolar processes; ribosome biogenesis and the nucleolar stress response (Figure 1.12). These two processes are inherently linked to one another with perturbations in ribosome synthesis triggering stress responses and in turn, nucleolar stress responses inhibiting ribosome biogenesis. To date, all research conducted on human NOP53 has employed either a knockdown or depletion strategy which simultaneously removes NOP53 from both ribosome assembly and nucleolar stress pathways. Consequently, the precise role played by NOP53 in these distinct processes remains unclear. Through NOP53, we aim to dissect and

uncouple these two processes.

To do this, the molecular interactions of human NOP53 with a factor in ribosome biogenesis (MTR4) and in nucleolar stress (RPL11) will be characterised. In *S. cerevisiae*, Nop53 interacts with the exosome associated helicase Mtr4 during ribosome biogenesis, via an Arch Interaction Motif (AIM) (Thoms *et al.,* 2015). Here we look to confirm an interaction between NOP53 and MTR4 in humans and investigate if the AIM of NOP53 is conserved and required for interaction.

In parallel, the mechanism of interaction between NOP53 and RPL11 will be investigated. Whilst evidence exists of an interaction between NOP53 and RPL11, the nature of the interaction remains unclear. Following confirmation of an interaction with RPL11, the region of NOP53 mediating the interaction will be investigated, with the aim of generating a NOP53 mutant unable to bind RPL11.

Following the identification of NOP53 mutants that abolish the interaction with MTR4 and RPL11, the mutants will be assessed for binding to the other protein, i.e. the NOP53 mutant which is unable to bind MTR4 should still bind RPL11. Through the generation of these separation of function mutants, the role of NOP53 in ribosome biogenesis and nucleolar stress can be explored, allowing, in turn, the two processes to be uncoupled and the complex interplay between the two investigated.

# Chapter 2

# Materials and Methods

Unless stated otherwise all water was produced using the Purite water purification system and solutions and glassware were autoclaved at 121 °C for 20 min for sterilisation.

## 2.1 Plasmids and oligonucleotides

Table 2.1: Plasmids used in this study for mammalian expression

| **Name** | **Source** |
|---|---|
| pcDNA5 FRT TO | Invitrogen |
| pcDNA5 FRT TO CAT | Invitrogen |
| pcDNA5 FRT TO 3xFLAG 6xHis NOP53 | Holly Sutherland, University of Sheffield |
| pcDNA5 FRT TO 3xFLAG 6xHis NOP53 D90R | Holly Sutherland, University of Sheffield |
| pcDNA5 FRT TO Twin-Strep-II 3x FLAG RPL11 | Vincent WC Chan, University of Sheffield |
| pcDNA5 FRT TO Twin-Strep-II 3x FLAG RPL11 ΔC7 | Vincent WC Chan, University of Sheffield |
| pOG44 | Invitrogen |

Table 2.2: Plasmids used in this study for recombinant protein expression

| **Name** | **Source** |
|---|---|
| pET24d GST TEV NOP53 | Emma Thomson, University of Sheffield |
| pET24d GST TEV NOP53 D90R | Emma Thomson, University of Sheffield |
| pET24d GST TEV NOP53 Strep-II | Holly Sutherland, University of Sheffield |
| pET24d GST TEV NOP53 D90R Strep-II | Holly Sutherland, University of Sheffield |
| pET24d HIS TEV MTR4 | Emma Thomson, University of Sheffield |
| pET24d HIS TEV RPL11 | Emma Thomson, University of Sheffield |
| pET24d HIS TEV RPL11 ΔC7 | Holly Sutherland, University of Sheffield |

| | |
|---|---|
| pET24d Twin-Strep-II TEV NOP53 | Holly Sutherland, University of Sheffield |
| pET24d Twin-Strep-II TEV codon-opt NOP53 | Holly Sutherland, University of Sheffield |
| pET24d Twin-Strep-II TEV NOP53 D90R | Holly Sutherland, University of Sheffield |
| pET24d Twin-Strep-II TEV codon-opt NOP53 D90R | Holly Sutherland, University of Sheffield |
| pGEX GST only | Carmen Apostol, University of Sheffield |

Table 2.3: Plasmids used in this study for yeast-two-hybrid analysis

| **Name** | **Source** |
|---|---|
| pBD RPL11 | Monika Feigenbutz, University of Sheffield |
| pBD RPL11 ΔC7 | Holly Sutherland, University of Sheffield |
| pBD RPL11 ΔC5 | Hephzibah Robb, University of Sheffield |
| pBD RPL11 ΔC4 | Molly John, University of Sheffield |
| pBD RPL11 ΔC3 | Hephzibah Robb, University of Sheffield |
| pBD RPL11 ΔC2 | Molly John, University of Sheffield |
| pBD RPL11 ΔN11 | Holly Sutherland, University of Sheffield |
| pBD RPL11 II - AA | Holly Sutherland, University of Sheffield |
| pBD RPL11 II - IA | Holly Sutherland, University of Sheffield |
| pBD RPL11 II - AI | Holly Sutherland, University of Sheffield |
| pBD ScPNC1 | Ewald Hettema, University of Sheffield |
| pGAD NOP53 | Monika Feigenbutz, University of Sheffield |
| pGAD NOP53 D90R | Monika Feigenbutz, University of Sheffield |
| pGAD NOP53 ΔC91 | Holly Sutherland, University of Sheffield |
| pGAD NOP53 ΔC235 | Holly Sutherland, University of Sheffield |
| pGAD NOP53 ΔN145 | Holly Sutherland, University of Sheffield |
| pGAD NOP53 ΔN243 | Holly Sutherland, University of Sheffield |
| pGAD NOP53 1-145 | Holly Sutherland, University of Sheffield |
| pGAD NOP53 145-228 | Holly Sutherland, University of Sheffield |
| pGAD NOP53 228-387 | Holly Sutherland, University of Sheffield |
| pGAD NOP53 387-478 | Holly Sutherland, University of Sheffield |
| pGAD ScPNC1 | Ewald Hettema, University of Sheffield |

Table 2.4: Oligonucleotides used for plasmid and cDNA amplification

| **Purpose** | **5'-3' Sequence** | **Code** |
|---|---|---|
| NOP53 5' with NdeI | CGTCGACATATGGCGGCAGGAGGC AGTGGCGTT | SOET 6 |
| NOP53 3' with BamHI | CGTCGAGGATCCCTACAACTGGATC TCACGGAACGC | SOET 7 |
| NOP53 5' with BamHI | CGTCGAGGATCCGCGGCAGGAGGC AGTGGCG | SOET 86 |
| NOP53 3' with EcoRV and stop | CTTGACGATATCCTACAACTGGAT CTCACGGAAC | SOET 87 |

| | | |
|---|---|---|
| NOP53 5' ΔN145 with NdeI | CGTCGACATATGAGGCGGAAGGAG CAGCTATGGGAG | SOET 133 |
| NOP53 3' ΔC91 with BamHI and stop | CGTCGAGGATCCTTACCGCGCCAG CTCCGCCAGCC | SOET 134 |
| NOP53 5' NdeI N-terminal 723 | CGTCGAGGATCCTTAAGGCGCCAC CTCCACGGC | SOET 138 |
| NOP53 3' BamHI with stop C-terminal 711 | CGTCGAGGATCCTTAAGGCGCCACC TCCACGGC | SOET 139 |
| NOP53 5' NdeI NOP53 387 FRW | CGTCGACATATGCGGCAGAGGCGG CGGCAG | SOET 192 |
| NOP53 3' with BamHI and stop 145 REV | CGTCGAGGATCCTTAGAGCTTCTT GGCGTTGGGGACCTG | SOET 193 |
| NOP53 5' with NdeI NOP53 228 FRW | CGTCGACATATGCACACCAAGCCG TC CCAGGCACCCGC | SOET 194 |
| NOP53 3' with BamHI and stop NOP53 228 REV | CGTCGAGGATCCTTACAGGCGTGCT GGCCGCTTCACTCC | SOET 195 |
| NOP53 5' with NdeI 177 FRW | CGTCGACATATGACAAGGGCCAAGC CCGGGCCCCAGG | SOET 196 |
| NOP53 3' with BamHI and stop 305 REV | CGTCGAGGATCCTTACGACTCCTCC AGCAGCCCCTCGC | SOET 197 |
| NOP53 5' codon optimised with NdeI | CGTCGACATATGGCTGCTGGAGGG AG | SOET 290 |
| RPL11 5' with NdeI | CGTCGACATATGGCGCAGGATCAA GGTGAAA | SOET 17 |
| RPL11 3' with BamHI and stop | CGTCGAGGATCCTTATTTGCCAGGA AGGATGATC | SOET 18 |
| RPL11 5' ΔN11 with NdeI | CGTCGACATATGCGGGAACTTCGCA TCCGCAA | SOET 131 |
| RPL11 3' ΔC7 with BamHI and stop | CGTCGAGGATCCTTAATCATACTTC TGCTGGAACCA | SOET 132 |
| RPL11 3' ΔC2 with BamHI and stop | CGTCGAGGATCCTTAAGGAAGGAT GATCCCATCATA | SOET 162 |
| RPL11 3' ΔC4 with BamHI and stop | CGTCGAGGATCCTTAGATGATCCC ATCATACTTCTGCTG | SOET 163 |
| RPL11 3' ΔC3 with BamHI and stop | CGTCGAGGATCCTTAAAGGATGAT CCCATCATACTT | SOET 166 |
| RPL11 3' ΔC5 with BamHI and stop | CGTCGAGGATCCTTAGATCCCATC ATACTTCTGCTGGAA | SOET 167 |
| RPL11 3' with BamHI and stop – II to AA | CGTCGAGGATCCTTATTTGCCAGG AAGGGCGGCCCCATCATACTT | SOET 213 |
| RPL11 3' with BamHI and stop - II to AI | CGTCGAGGATCCTTATTTGCCAGG AAGGATGGCCCCATCATACTT | SOET 214 |

| | | |
|---|---|---|
| RPL11 3' with BamHI and stop - II to IA | CGTCGAGGATCCTTATTTGCCAGG AAGGGCGATCCCATCATACTT | SOET215 |
| RPL11 3' C-terminal 7xAla with BamHI and stop | CGTCGAGGATCCTTATGCCGCA GCAGCGGCGGCCGCATCATACT TCTGCTGGAACCAGCG | SOET 236 |
| Twin-Strep-II 5' with start and NcoI | AATAAATACCATGGGGATGTGGTCG | SOET 288 |
| Twin-Strep-II 3' with BamHI | CGTGCTCCAGGATCCCTATAACTGA ATCTC | SOET 289 |

Table 2.7: Oligonucleotides used for genomic amplification

| **Purpose** | **5'-3' Sequence** | **Code** |
|---|---|---|
| NOP53 D-R gRNA FRW | AGTTCTGTAAACTGCTGGGCGAAGC | SOET 218 |
| NOP53 D-R gRNA REV | ACAGGCGTGACTCACCGCAAC | SOET 219 |
| p53 exon 1 FRW | CACAGCTCTGGCTTGCAGA | SOET 258 |
| p53 exon 1 REV | AGCGATTTTCCCGAGCTGA | SOET 259 |
| p53 exon 2 FRW | AGCTGTCTCAGACACTGGCA | SOET 260 |
| p53 exon 2 REV | GAGCAGAAAGTCAGTCCCATG | SOET 261 |
| p53 exon 3+4 FRW | AGACCTATGGAAACTGTGAGTGGA | SOET 262 |
| p53 exon 3+4 REV | AGGAAGCCAAAGGGTGAAGAGG | SOET 263 |
| p53 exon 5+6 FRW | CGCTAGTGGGTTGCAGGA | SOET 264 |
| p53 exon 5+6 REV | CACTGACAACCACCCTTAAC | SOET 265 |
| p53 exon 7 FRW | AGAATGGCGTGAACCTGGGC | SOET 266 |
| p53 exon 7 REV | TCCATCTACTCCCAACCACC | SOET 267 |
| p53 exon 8+9 FRW | GTTGGGAGTAGATGGAGCCT | SOET 268 |
| p53 exon 8+9 REV | GGCATTTTGAGTGTTAGACTG | SOET 269 |
| p53 exon 10 FRW | CTCAGGTACTGTGTATATACTTAC | SOET 270 |
| p53 exon 10 REV | ATACACTGAGGCAAGAAT | SOET 271 |
| p53 exon 11 FRW | TCCCGTTGTCCCAGCCTT | SOET 272 |
| p53 exon 11 REV | TAACCCTTAACTGCAAGAACAT | SOET 273 |

Table 2.5: Oligonucleotides used for sequencing

| **Purpose** | **5'-3' Sequence** | **Code** |
|---|---|---|
| BGH seq REV | TAGAAGGCACAGTCGAGG | SOET 75 |
| CMV seq FRW | CGCAAATGGGCGGTAGGCGTG | SOET 74 |
| GalAD seq FRW | TACCACTACAATGGATGATG | SOET 135 |
| NOP53 seq +200 REV | CGTGCGCTCCTGTAGCCGC | SOET 8 |
| NOP53 seq +500 FRW | CCTTCTGCAACAAGGGCC | SOET 9 |
| NOP53 seq + 1000 FRW | GAGAAGAAGACGGAGCAG | SOET 10 |
| NOP53 seq +1000 REV | CTGCTCCGTCTTCTTCTCTGT | SOET 149 |
| RPL11 seq +200 REV | TGTGCAGTGGACAGCAATCT | SOET 148 |
| RPL11 seq +250 FRW | GAGAAGGGTCTAAAGGTGCGG | SOET 168 |
| pET24d 5' Seq ORF FRW | GCGGATAACAATTCCCCTCTA | SOET 135 |
| pET24d 3' Seq ORF REV | GCCCCAAGGGGTTATGCTAG | SOET 136 |
| T7 seq FRW | TAATACGACTCACTATAGGG | SOET 275 |

Table 2.6: Oligonucleotides used for site directed mutagenesis

| **Purpose** | **5'-3' Sequence** | **Code** |
|---|---|---|
| NOP53 FRW AIM D-R | AAACTCTTCTTCGTGCGCACTGGC TCCAAGGAA | SOET 13 |
| NOP53 REV AIM D-R | TTCCTTGGAGCCAGTGCGCACGAA GAAGAGTTT | SOET 14 |
| NOP53 codon optimised FRW AIM D-R | CGAATGAAAAGCTGTTCTTCGTAC GCACTGGCAGTAAGGAGAAGG | SOET 319 |
| NOP53 codon optimised REV AIM D-R | CCTTCTCCTTACTGCCAGTGCGTA CGAAGAACAGCTTTTCATTC | SOET 320 |

## 2.2 Bacterial strains and techniques

### 2.2.1 *E. coli* strains

Table 2.8: *E. coli* strains used in this study

| Name | Source | Genotype |
|---|---|---|
| DH5$\alpha$ | Emma Thomson, University of Sheffield | F– $\phi$80lacZ$\Delta$M15 $\Delta$(lacZYA-argF)U169 recA1 endA1 hsdR17(rK–, mK+) phoA supE44 $\lambda$–thi-1 gyrA96 relA1 |
| BL21 CodonPlus | Agilent | B F– ompT hsdS(rB– mB–) dcm+ Tetr gal $\lambda$(DE3) endA Hte [argU ileY leuW Camr] |

### 2.2.2 Making *E. coli* growth media

For *E. coli* LB broth and 2 x YT were made by dissolving 10 g tryptone for LB broth or 16 g for 2 x YT, 5 g NaCl and 10 g yeast extract in 1 L de-ionised $H_20$. Medium was mixed well using a magnetic stirrer and then autoclaved at 121 °C for 20 min to sterilise. Following sterilisation any necessary antibiotics for *E. coli* selection were added to LB or 2 x YT once the medium had cooled. Ampicillin was used at a working concentration of 100 µg/mL, kanamycin at 50 µg/mL and chloramphenical at 37 µg/mL. Agar plates are made as described above with 15 g bacto-agar also dissolved per 1 L de-ionised $H_20$ and once cooled poured into 10 cm petri dishes as required.

### 2.2.3 Growth of *E. coli*

*E. coli* from a single colony were used to inoculate 5 ml of LB broth containing an appropriate concentration of necessary antibiotic. Cultures were grown at 37 °C overnight at 200 rpm. For mini plasmid preparations this 5 ml of overnight culture was used. For midi plasmid preparations 1 ml of the overnight culture was then transferred into a 1.5 ml microcentrifuge tube and spun at 4000 g for 1 min at room temperature to pellet cells. Cells were then washed 3 times in sterilised $H_20$ and then resuspended in 1 ml fresh LB broth and diluted 1:100 in LB broth containing an appropriate concentration of necessary antibiotic before being incubated at 37 °C overnight at 200 rpm.

### 2.2.4 Cryopreservation of *E. coli*

Freshly grown *E. coli* is mixed in a 1:1 ratio with filter sterilised 30 % (v/v) glycerol and aliquoted into 1.5 ml tubes, flash frozen in liquid nitrogen and stored at -80 °C.

### 2.2.5 Production of chemically competent *E. coli*

An aliquot of the *E. coli* cells are grown overnight in a 5 ml pre-culture at 37 °C. The overnight pre-culture of cells is diluted 1:100 into pre-warmed media (1 ml cells in 100 ml media). Cells are grown at 37 °C until $OD_{600}$ reaches 0.5 and harvested by spinning at 4000 g, 5 min at 4 °C. Cells are resuspended in filter sterilised TfbI buffer (40 ml per 100 ml culture, Table 2.9) and incubated on ice for 10 min. Cells are harvested and then resuspended in 5 ml filter sterilised TfbII buffer (per 100 ml culture) and incubated on ice for 1 hr. Cells are prepared into 50 µl aliquots, flash frozen in liquid nitrogen and stored at -80 °C.

Table 2.9: Buffers and their composition for the production of chemically competent *E. coli*

| **Buffer** | **Composition** |
|---|---|
| TfbI | 100 mM RbCl<br>30 mM KOAC<br>10 mM $CaCl_2$<br>50 mM $MnCl_2$<br>15 % Glycerol<br>Adjust pH to 5.8 using 0.2 M Acetic Acid |
| TfbII | 10 mM RbCl<br>10 mM MOPS<br>75 mM $CaCl_2$<br>15 % Glycerol<br>Adjust pH to 6.5 using 0.5 M KOH |

### 2.2.6 Transformation of *E. coli*

For each chemical transformation of *E. coli* a negative control of 5 µl 1 x TE buffer (pH 8.0) was used. Chemically competent *E. coli* cells were placed on ice and allowed to thaw. Whilst the cells were thawing, up to 10 µl of DNA-ligation mix or 1-5 µl of plasmid was added to 1.5 ml microcentrifuge tubes and placed on ice. Once thawed cells were mixed and 50 µl of cells were added to the 1.5 ml tubes containing the DNA and mixed gently. Cells and DNA were then incubated on ice for 30 min. Samples were then heat shocked and placed into a 42 °C water bath for 90 s before being placed back on ice for 5 min. 950 µl LB broth was then added to each tube and the cells were incubated with shaking at 37 °C, 200 rpm for 1 hr. The samples were briefly spun at 4000 g for 1 min to pellet the cells. The supernatant was aspirated, and the cells were resuspended in 200 µl LB broth and plated onto LB-agar plates containing appropriate antibiotics. Plates were incubated in a 37 °C incubator for approximately 16 hr prior to colony selection.

### 2.2.7 Induction of recombinant protein expression in *E. coli*

BL21 *E. coli* containing the relevant pET24d construct were cultured overnight at 37 °C. 1 L of 2 x YT containing 50 µg/mL kanamycin and 37 µg/mL chloramphenicol was prepared for each induction and 10 ml of the overnight pre-culture was added to the flask and cells were incubated at 37 °C, 200 rpm until the $OD_{600}$ reached 0.4-0.5. Flasks were then transferred to a pre-cooled 18 °C incubator for 30 min. Cells were then induced with isopropyl-D-thiogalactopyranoside (IPTG) at a final concentration of 0.1 mM and incubated for the desired induction period. Cells were then pelleted by centrifugation at 4000 g, 20 min at 4 °C. The supernatant was removed, and cells were resuspended in a small volume of LB and transferred to a 50 ml tube. Cells were re-pelleted by centrifugation. The supernatant was again removed, and the pellets were dried before being frozen at – 20 °C for storage prior to recombinant protein purification.

## 2.3 Yeast strains and techniques

### 2.3.1 *S. cerevisiae* strains

Table 2.10: *S. cerevisiae* strain used in this study

| Strain | Source | Genotype |
|---|---|---|
| PJ69-4A | James *et al.*, 1996 | *MATα trp1-901 leu2-3,112 ura3-52 his3-200 gal4δ gal80δ Met2::GAL7-lacZ LYS2::GAL1 -HIS3 GAL2-ADE2* |

### 2.3.2 Making media for *S. cerevisiae* growth

For *S. cerevisiae*, YPD was made by dissolving 10 g yeast extract and 20 g peptone into 1 L deionised $H_20$. For synthetic drop-out (SD) medium, 6.9 g yeast nitrogen base (Formedium) was supplemented with 620 mg drop-out amino acids (-Leu-Trp or -Leu-Trp-His) and dissolved in 1 L $H_20$. Medium was mixed well using a magnetic stirrer and then autoclaved at 121 °C for 20 min to sterilise. Following sterilisation sterile-filtered glucose was added at a final concentration of 2 % once the medium had cooled. Agar plates are made as described above with 20 g bacto-agar also dissolved per 1 L $H_20$. Media was cooled to approximately 55 °C before the glucose was added and then poured into 10 cm petri dishes as required.

### 2.3.3 Growth of *S. cerevisiae*

*S. cerevisiae* were streaked from a slant stored at 4 °C or from glycerol stocks onto YPD plates and incubated at 30 °C for 2-3 days. Once grown, a single clone was picked and used to inoculate 20 ml of YPD which was grown overnight at 200 rpm at 30 °C. The $OD_{600}$ of the overnight culture was calculated using a spectrophotometer and then used as appropriate.

### 2.3.4 Cryopreservation of *S. cerevisiae*

Freshly grown *S. cerevisiae* is mixed in a 1:1 ratio with filter sterilised 30 % (v/v) glycerol and aliquoted into 1.5 ml tubes, flash frozen in liquid nitrogen and stored at -80 °C.

### 2.3.5 Transformation of *S. cerevisiae*

The $OD_{600}$ from the overnight culture was diluted to an OD of 0.1-0.2 in 10 ml of YPD per transformation. Cultures were grown at 30 °C until they doubled twice. Cells were then harvested at 4000 g for 5 min to pellet cells. The supernatant was removed, and the cells were washed once in TE buffer (10 mM Tris-HCl pH 7.5, 1 mM EDTA pH 8.0) and then once in LiAC buffer (10 mM Tris-HCl pH 7.5, 1 mM EDTA pH 8.0, 100 mM LiAC). Cultured cells were resuspended in 0.5 ml LiAC buffer (per 50 ml culture) and 0.1 ml of cells were aliquoted into sterile 1.5 ml tubes. Per transformation; 50 µl of LiAC buffer, 1 µg of each plasmid DNA and 50 µg carrier DNA from salmon testes (Sigma-Aldrich, D1626) were added to the 100 µl of competent cells in each 1.5 ml tube. Once all the tubes were prepared 300 µl 40 % sterile-filtered PEG in LiAC buffer was added to each tube. Tubes were mixed well and incubated at room temperature for 30 min. Following the incubation 50 µl DMSO was added per tube, mixed well and heat shocked at 42 °C for 20 min. Cells were flash spun, washed in TE buffer and then resuspended in 100 µl TE and plated onto SDC-Leu-Trp plates. Transformants were grown for 5 days at 30 °C before being replica plated onto selective SDC plates and streaked onto SDC-Leu-Trp plates.

### 2.3.6 Yeast-two-hybrid screen

Once yeast transformants had been checked by replica plating onto selective SDC plates, several selected clones per transformation were streaked onto SDC-Leu-Trp plates. Freshly growing cells were collected using a loop and resuspended in SDC-Leu-Trp liquid. A 96-well plate was used to prepare five 10-fold dilutions of cells with duplicate or triplicate sets prepared for each transformed combination. A stamp was then used to pin the prepared dilutions of cells onto control SDC-Leu-Trp plates and onto selective SDC-Leu-Trp-His plates and SDC-Leu-Trp-His containing 0.5-3 mM 3-AT (Sigma-Aldrich, A8056) plates. Plates were grown for 3-5 days at 30 °C before being analysed and imaged.

### 2.3.7 Yeast-two-hybrid mutagenic screen

Yeast were transformed as described (section 2.3.5) but the transformation was scaled up accordingly, from a singular 10 cm dish to one hundred 15 cm dishes, plating transformants onto SDC-Leu-Trp. After 5 days of growth, transformants were replica plated onto SDC-Leu-Trp-His and left to grow at 30 °C for a further 5 days. Colonies which failed to grow on SDC-Leu-Trp-His were patched onto SDC-Leu-Trp and grown for 3 days at 30 °C before being patched onto SDC-Leu-Trp-His and grown for a further 3 days at 30 °C. Any clones still failing to grow were analysed further as described (section 2.3.6). Plasmids were then extracted from validated clones using the Zymoprep Yeast Plasmid Miniprep Kit according to the manufacturer's instructions. Each extracted plasmid was then transformed into *E. coli* (section 2.2.6) and an *E. coli* mini preparation was carried out (section 2.4.1) before sending the plasmid for sequencing.

### 2.3.8 *S. cerevisiae* alkaline lysis protein extraction

In cases where a negative interaction is observed, confirmation of protein expression is required. Overnight *S. cerevisiae* culture was diluted to $OD_{600}$ 0.2 in 10 ml SDC-Leu-Trp and grown at 30 °C 200 rpm until $OD_{600}$ reached 1. Cells were then harvested at 4000 g for 5 min. The supernatant was removed, and the cells were resuspended in 500 µl ice-cold 0.2M NaOH with 0.2 % $\beta$-mercaptoethanol and incubated on ice for 10 min. Trichloroacetic acid was added to a 5 % final concentration and incubated again on ice for 10 min. Samples were then spun at 13000 g, 5 min at 4 °C. The supernatant was removed, and the cell pellet was resuspended in 10 µl 1M Tris-HCl pH 9.4 and 90 µl of 1 x SDS loading buffer was added. Samples were denatured at 90 °C for 5 min and 1 $OD_{600}$ of cells were loaded onto the SDS gel. Samples were then analysed by Western blot.

## 2.4 DNA techniques

### 2.4.1 Plasmid preparations

**Plasmid DNA mini preparation from *E. coli* using Qiagen's, QIAprep Spin Miniprep Kit '**

Saturated overnight *E. coli* culture (5 ml) was aliquoted into a 15 ml tube. Samples were centrifuged at room temperature for 5 min at 4000 g to pellet cells, then the supernatant was aspiriated. The plasmid DNA was then extracted from the cell pellet as described in the protocol from Qiagen (27106). The plasmid DNA was stored long term at -20 °C.

**Plasmid DNA midi preparation from *E. coli* using Qiagen's 'High speed plasmid Midi Kit'**

Overnight *E. coli* culture (50-200 ml) was pelleted by centrifugation for 20 min at 4000 g at 4 °C. The supernatant was decanted, and the bottle inverted to completely drain the culture medium. The plasmid DNA was then extracted from the cell pellet as described in Qiagen's Midi Kit protocol (12643). The concentration of DNA could then be measured and plasmid identity confirmed by restriction analysis and agarose gel electrophoresis with long term storage of the DNA at -20 °C.

### 2.4.2 DNA quantification

DNA preparation was analysed using the NanoDrop spectrophotometer. Samples were measured in triplicate and either 1 x TE buffer, pH 8.0 or elution buffer was blanked as the control. The concentration of the DNA was determined by measuring the $OD_{260}$.

### 2.4.3 DNA agarose gel electrophoresis

Electrophoresis-grade agarose was placed into an erlenmeyer flask along with 1 x TAE buffer with weight of agarose and volume of TAE dependent on desired size, percentage and thickness of the final gel. Serva DNA stain G (Serva Electrophoresis GMBH, 39803.01) was added to the gel just before pouring (1:50000). The gel was submerged in 1 x TAE buffer and DNA samples were mixed with 6 x DNA loading dye (ThermoScientific, R0611) and loaded in the wells alongside a GeneRuler DNA ladder (ThermoScientific, SM0311). The gel was run at 100 V and the DNA was visualised and imaged using the Geneflow G:Box gel imaging system and Syngene GeneSnap software.

### 2.4.4 Restriction enzyme digestion

For diagnostic digests to confirm plasmid identify and for plasmid/vector cleavage prior to vector insertion, the following 20 µl reactions were set up on ice:

5 µl plasmid/vector DNA
2 µl 10 x fast digest restriction enzyme buffer
1 µl Fast digest restriction enzyme (ThermoScientific)
Sterile, de-ionised $H_20$ to 20 µl

The samples were incubated at 37 °C for a period between 1-2 hrs before the DNA was separated via gel electrophoresis and visualised and imaged using the Geneflow G:Box gel imaging system and Syngene GeneSnap software.

### 2.4.5 DNA ligation with T4 DNA ligase

The following were combined in a 1.5 ml Eppendorf tube:

6 µl Insert DNA
2 µl Vector DNA (1:3 molar ration of vector:insert)
1 µl 10 x T4 DNA ligase buffer
1 µl 5 Weiss U/µl T4 DNA ligase (New England Biolabs, M0202S)
Sterile, de-ionised $H_20$ to 10 µl

The samples were mixed well and incubated at room temperature for 16 hr overnight before being used for *E. coli* transformation.

### 2.4.6 PCR using Phusion DNA polymerase for vector/insert production

The below reaction was set up on ice:

10 µl 5 x GC/HF Phusion Buffer
1 µl 10 mM dNTPs in 1 mM Tris-HCl pH 8.0
1.25 µl 10 µM Forward primer
1.25 µl 10 µM Reverse primer
0.5 µl 5 U/µl Phusion Hot Start II High Fidelity DNA polymerase (ThermoScientific, F-530L)
1 µl DNA template
Sterile $H_20$ to 50 µl

A negative control was produced using 1 x TE buffer, pH 8.0 instead of the DNA template. The reagents were mixed gently by pipetting and briefly centrifuged to collect reagents at the bottom of the tube. For NOP53 amplification the GC Phusion buffer was used and for RPL11 amplification the HF buffer was used.

Amplification of NOP53 and RPL11 using PCR was carried using a thermocycler for an initial denaturation at 98 °C for 30 s followed by 30 cycles at 98 °C denaturation for 20 s, 55 °C annealing for 30 s and extension at 72 °C for 60 s (RPL11) or 120 s (NOP53). A final extension at 72 °C for 10 min was also carried out with the sample held at 4 °C.

PCR samples were then analysed by DNA agarose gel electrophoresis and purified either from the gel using the QiaQuick gel extraction kit (Qiagen, 28704) or directly from the PCR reaction using QiaQuick PCR purification kit (Qiagen, 28104). DNA purification was carried out following the manufacturer's protocol and DNA eluted in 30 µl before being stored at -20 °C.

### 2.4.7 Site directed mutagenesis of NOP53 by PCR

Separate reactions for both the forward and reverse strand were set up on ice in PCR tubes:

10 µl 5 x GC Phusion Buffer
1 µl 10 mM dNTPs in 1 mM Tris-HCl pH 8.0
1.25 µl 20 µM primer, either forward or reverse
1 µl 5 U/µl Phusion Hot Start II High Fidelity DNA polymerase (ThermoScientific, F-530L)
5 µl plasmid template
Sterile $H_20$ to 50 µl

A negative control was produced for both the forward and reverse reaction with 1 x TE buffer, pH 8.0 used instead of the DNA template. The reagents were mixed gently by pipetting and briefly centrifuged to collect reagents at the bottom of the tube.

Amplification by PCR was carried using a thermocycler for an initial denaturation at 98 °C for 30 s followed by 30 cycles at 98 °C denaturation for 20 s, 62 °C annealing for 30 s and extension at 72 °C for 300 s. A final extension at 72 °C for 10 min was also carried out with the sample held at 4 °C. Equal volumes of the forward and reverse PCR reactions were mixed together and annealed by heating at 95 °C for 5 min, cooled down to 30 °C and incubated at 30 °C for 30 min. The annealed plasmid was digested with DpnI at 37 °C overnight to digest the methylated template DNA. Digested DNA was then transformed into DH5$\alpha$ *E. coli* (section 2.2.6).

### 2.4.8 Random mutagenesis of NOP53 by error-prone PCR

The below reaction mix was set up on ice:

75 µl 10 x Taq PCR buffer (200 mM Tris-HCl pH 8.4, 500 mM KCl)
4 µl 1 M $MgCl_2$
7.5 µl 100 µM Forward primer
7.5 µl 100 µM Reverse primer
7.5 µl 100 mM dCTP and dTTP
1.5 µl 100 mM dATP and dGTP
Sterile $H_20$ to 750 µl

From this reaction mix, 48 µl was added to tube one then 44 µl to tube 2 through to tube 16. 1 µl of plasmid DNA template was added to PCR tube 1 and placed in a thermocycler. Samples were denaturated initially for 1 min at 94 °C and held at 80 °C. To tube 1, 0.5 µl freshly prepared 50 mM $MnCl_2$ and 0.5 µl Taq DNA polymerase (Invitrogen) were added and the following amplification cycle was carried out for 4 cycles: 98 °C denaturation for 60 s, 55 °C annealing for 60 s and extension at 72 °C for 180 s. After the 4 cycles of amplification, tube 1 was removed from thermocycler and placed on ice. 5 µl of PCR reaction was then transferred from tube 1 to tube 2. Again tube 2 was place in the thermocycler, the sample was denatured for 1 min at 94 °C then held at 80 °C. To tube 2, 0.5 µl freshly prepared $MnCl_2$ and 0.5 µl Taq DNA polymerase was added proceeded by a further 4 PCR cycles as above. Tube 2 was then removed from thermocycler and placed on ice. The process was repeated for tubes 3 to 16 to create a mutagenic library by serial dilution amplification. Each PCR reaction was verified by agarose gel electrophoresis, cloned into the pAD vector by restriction digest using NdeI/BamHI restriction sites and sequenced to identify the rate of mutation in each 4-cycle sample.

### 2.4.9 Sequencing

Sanger sequencing was performed at Eurofins Genomics (Germany).

## 2.5 Mammalian cell lines and tissue culture

All mammalian cells were incubated at 37 °C with 5 % (v/v) $CO_2$ at a humidity of 95 %. Appropriate antibiotics were added to cell lines when maintained in culture. All cell culture work was carried out in a laminar flow cabinet which was sterilised using 70 % (v/v) EtOH as well as any equipment placed into the cabinet.

Table 2.11: Reagents used in this study for human cell line culture

| Name | Supplier | Product Code |
|---|---|---|
| 0.05 % Trypsin-EDTA | Gibco, Thermo Scientific | 25300-054 |
| Blasticidin S Hydrochloride | Melford Biolabs | B12150-0.1 |
| DMEM | Sigma-Aldrich | D5796-500ML |
| DMSO | Sigma-Aldrich | D2650-100 |
| Dulbecco's phosphate buffered saline (PBS) | Sigma-Aldrich | D8537-500ML |
| Fetal Bovine Serum (FBS) Tetracycline free | Biosera | FB-1001T/500 |
| Hygromycin B | Invitrogen, Thermo Scientific | 10687010 |
| Lipofectamine 2000 | Invitrogen, Thermo Scientific | 11668-027 |
| Penicillin streptomycin | Gibco, Thermo Scientific | 15070-063 |
| Tetracycline | Sigma-Aldrich | T7660 |
| Zeocin | Invitrogen, Thermo Scientific | R25001 |

Table 2.12: Human cell lines used in this study

| Cell lines | Source | Culture medium |
|---|---|---|
| HEK293T Cells | Victoria Porteous-Medley, University of Sheffield | DMEM, 10 % FBS, 1 % Penicillin-streptomycin |
| Flp-In T-REx HEK293 Cells | Invitrogen, Thermo Scientific | DMEM, 10 % FBS, 1 % Penicillin-streptomycin, 15 µg/ml blasticidin, 10 µg/ml zeocin |
| 3xFLAG-6xHis-NOP53 in Flp-In T-REx HEK293 Cells | Holly Sutherland, University of Sheffield | DMEM, 10 % FBS, 1 % Penicillin-streptomycin, 15 µg/ml blasticidin, 100 µg/ml hygromycin B |
| 3xFLAG-6xHis-NOP53 D90R in Flp-In T-REx HEK293 Cells | Holly Sutherland, University of Sheffield | DMEM, 10 % FBS, 1 % Penicillin-streptomycin, 15 µg/ml blasticidin, 100 µg/ml hygromycin B |
| Twin-StrepII-3xFLAG-RPL11 in Flp-In T-REx HEK293 Cells | Vincent WC Chan, University of Sheffield | DMEM, 10% FBS, 1 % Penicillin-streptomycin, 15 µg/ml blasticidin, 100 µg/ml hygromycin B |

### 2.5.1 Cryopreservation of mammalian cells

Cells were grown to a high confluency (approximately 95 %) in a 75 $cm^2$ flask before the media was removed and cells gently washed in 10 ml of PBS, before being treated with 0.25 % Trypsin-EDTA for 30 s and then incubated for 2 min in the incubator (37 °C, 5 % (v/v) $CO_2$, 95 % humidity). Cells were resuspended in 8 ml of 90 % (v/v) complete media containing FBS and penicillin streptomycin with 10 % (v/v) DMSO. 1 ml of cell suspension was aliquoted into the individual cryovials (8 in total) and transferred into NalGene Mr

Frosty® and placed into the -80 °C freezer. Mr Frosty® ensures that the cells freeze slowly, at a rate of 1 °C/min. After 24 hrs at -80 °C the cells were transferred into a liquid nitrogen tank for long term storage and preservation.

### 2.5.2 Revival of cells

Cryovials containing cells were removed from liquid nitrogen and incubated at 37 °C until thawed. Vials were disinfected using 70 % EtOH and cells were gently resuspended in 1 ml of pre-warmed appropriate media and then transferred into a culture flask containing 9 ml of warm appropriate media. Cells were incubated at 37 °C with 5 % (v/v) $CO_2$ at 95 % humidity and after 24 hrs media was replaced with media containing any necessary antibiotics at an appropriate concentration (Table 2.12).

### 2.5.3 Passaging of cells

Once cultured cells reached 90 % confluency their growth media was removed, and cells were gently washed in PBS and treated with 0.25 % Trypsin-EDTA for 30 s and then incubated at 37 °C with 5 % (v/v) $CO_2$ at 95 % humidity for 2 min to detach the cells from the flask. Cells were resuspended in an appropriate amount of warm media and transferred into a fresh flask to give an appropriate dilution of cells based upon initial confluency. For 75 $cm^2$ flask additional fresh warmed media was added to give a final volume of 10 ml with an appropriate concentration of antibiotics added for the maintenance of the cell line (Table 2.12). Cells were incubated at 37 °C with 5 % (v/v) $CO_2$ at 95 % humidity.

### 2.5.4 Transfection of Flp-In T-REx HEK293 cells

Cells were seeded at 70 % in 60 mm dishes to allow for adherence the day before transfection. On the day of the transfection media was removed and cells washed with PBS before fresh media was added. In 1.5 ml tubes, 18 µl Lipofectamine 2000 was diluted in 450 µl serum-free media per transfection. In additional tubes, 3.6 µg of plasmid DNA at a 9:1 ratio of the Flp-recombinase pOG44 to pcDNA5 FRT/TO-NOP53 or -CAT (positive control) was also diluted in 450 µl serum-free media. The diluted lipofectamine was then added to the DNA and incubated at room temperature for 5-10 min to allow complex formation. The DNA-lipofectamine complexes were then added to the 60 mm dish and incubated at 37 °C with 5 % (v/v) $CO_2$ at 95 % humidity for 24 hrs. After 24 hrs the transfection reagent was removed and fresh DMEM containing 10 % FBS and 1 % penicillin-streptomycin was added to the dishes and were incubated. After a further 24 hrs cells were trypsinised and split into 2 100 mm dishes with selective complete media containing 15 µg/ml blasticidin and 100 µg/ml hygromycin B and incubated under the same conditions. After 2-3 days, media was replaced to remove excess numbers of dead cells and then media was replaced every 4 days after that. After 2 weeks of culture in selective media, single colonies were visible, picked and expanded to test for tetracycline induction of protein expression. Positive clones were cryopreserved in triplicate (section 2.5.1).

### 2.5.5 Induction of NOP53 expression in Flp-In T-REx HEK293 cells

Cells were seeded in 4 ml (8 x $10^5$) DMEM, 10 % FBS, 1 % penicillin-streptomycin onto a 6-well plate and incubated at 37 °C with 5 % (v/v) $CO_2$ at 95 % humidity overnight. Freshly made 1 mg/ml tetracycline solution (from a 10 mg/ml tetracycline stock solution) was added to fresh media to give a final concentration of 0.1-1 µg/ml tetracycline. The media on the cells was removed and fresh DMEM 10 % FBS, 1 % penicillin-streptomycin containing the appropriate concentration of tetracycline was then added to the cells. The dishes were then

swirled gently before being incubated at 37 °C with 5 % (v/v) $CO_2$ at 95 % humidity for the duration of the desired time course.

### 2.5.6 Design and preparation of siRNAs for endogenous NOP53 in Flp-In T-REx HEK293 cells

siRNAs were designed *in silico* using the Horizon siDESIGN Center tool (Table 2.13). Two siRNAs were designed to the 3'UTR of NOP53 to ensure depletion of endogenous NOP53. For both siRNAs a scrambled (sc) was also designed by randomising the order of the nucleotides in the sequence. siRNAs were ordered as single stranded RNA oligonucleotides from IDT. The 5' to 3' strand and the 3' to 5' strand were then annealed together upon arrival. Equal molar amounts of each strand were mixed together, heated to 94 °C for 2 min and left to gradually cool by turning the heat block off and being allowed to cool to room temperature. Annealed siRNAs were then aliquoted and stored at - 20°C.

Table 2.13: siRNAs for depletion of endogenous NOP53

| **siRNA** | **Sequence (5'-3')** |
|---|---|
| NOP53 siRNA 1 FRW | r(GAGACUCGCCCUUCAAUAA)d(TT) |
| NOP53 siRNA 1 REV | r(UUAUUGAAGGGCGAGUCUC)d(TT) |
| NOP53 siRNA sc1 FRW | r(GCACCUUAGACGCAACAUU)d(TT) |
| NOP53 siRNA sc1 REV | r(AAUGUUGCGUCUAAGGUGC)d(TT) |
| NOP53 siRNA 2 FRW | r(AUGCCGGAGACUCGCCCUU)d(TT) |
| NOP53 siRNA 2 REV | 5'P-r(AAGGGCGAGUCUCCGGCAU)d(TT) |
| NOP53 siRNA sc2 FRW | r(GACCGCGUCGCCGAUACUU)d(TT) |
| NOP53 siRNA sc2 REV | r(AAGUAUCGGCGACGCGGUC)d(TT) |

### 2.5.7 siRNA knockdown of endogenous NOP53 expression in Flp-In T-REx HEK293 cells

Cells were seeded to aim for 70 % confluency the following day in DMEM containing 10 % (v/v) FBS. siRNAs were prepared at a working dilution of 20 µM siRNA in nuclease free buffer from 100 µM stock solutions. Lipofectamine 2000 was diluted into serum free medium, 5 µl Lipofectamine 2000 to 250 µl media per 6 x $10^5$ cells and incubated at room temperature for 5 min. siRNAs were diluted in 250 ul serum free media per 6 x $10^5$ cells and incubated at room temperature for 5 min, to make the final concentration of 5 nm. Diluted lipofectamine and diluted siRNA were mixed together in a 1:1 ratio and incubated at room temperature for 15 min. Media was removed from cells and replaced with fresh DMEM containing 10 % (v/v) FBS and 500 µl lipofectamine:siRNA complex was added per 6 x $10^5$ cells. Cells were incubated at 37 °C with 5 % (v/v) $CO_2$ at 95 % humidity for 24 hrs to allow sufficient knockdown of endogenous NOP53. After 24 hrs, the media was removed and expression of 3xFLAG-6xHIS-NOP53 was induced by tetracycline treatment for 24 hrs prior to protein extraction (section 2.8.3).

## 2.6 Human pluripotent stem cell culture and techniques

Human pluripotent stem cells were incubated at 37 °C with 5 % (v/v) $CO_2$ at a humidity of 95 %. All cell work was carried out in a laminar flow cabinet which was sterilised using 70

% (v/v) EtOH. All equipment and reagents were sterilised using 70 % (v/v) EtOH prior to being put in the laminar flow cabinet.

### 2.6.1 Human pluripotent cell lines

Table 2.14: Human pluripotent cell lines used in this study

| Cell lines | Source | Culture medium |
|---|---|---|
| MasterSheff 11 | Ivana Barbaric, University of Sheffield | Essential 8™ Medium or mTESR™ Plus Medium |
| MasterSheff 11 NOP53 $^{WT/D90R}$ | Holly Sutherland, University of Sheffield | Essential 8™ Medium or mTESR™ Plus Medium |
| MasterSheff 11 NOP53 $^{D90R/D90R}$ | Holly Sutherland, University of Sheffield | Essential 8™ Medium or mTESR™ Plus Medium |

Table 2.15: Human pluripotent stem cell culture reagents

| Name | Supplier | Product code |
|---|---|---|
| CloneR™ defined supplement | Stem Cell Technologies | 05888 |
| Essential 8™ Medium | Gibco, Thermofisher Scientific | A1517001 |
| Geltrex™ LDEV-free Reduced Growth Factor Basement Membrane Matrix | Gibco, Thermofisher Scientific | A1413201 |
| Gentamicin | Sigma | G1397 |
| mTESR™ Plus Medium | Stem Cell Technologies | 100-0276 |
| ReLeSR™ | Stem Cell Technologies | 05872 |
| STEMCELL-BANKER cryopreservation media | Amsbio | 11897 |
| TrypLE™ Express Enzyme | Gibco, Thermofisher Scientific | 12604013 |
| Vitronectin (VTN-N) Recombinant Human Protein, Truncated | Gibco, Thermofisher Scientific | A14700 |
| Y-27632 dihydrochloride (ROCK inhibitor) | Tocris Biosciences | 1254 |

### 2.6.2 Preparation of flasks for human pluripotent stem cell maintenance

Flasks were coated with vitronectin prior to the seeding or passaging of cells. Vitronectin was prepared at a concentration of 50 µg/ml in PBS and added to the flask until the culture surface was covered. The coated flask was then incubated at room temperature for a minimum of 1 hr to allow the vitronectin to polymerise prior to use. Flasks prepared in advance were stored at 4 °C for up to 1 week before use.

### 2.6.3 Cryopreservation of human pluripotent stem cells

Once stem cells reached approximately 80 % confluency their growth media was removed, cells were gently washed in PBS and treated with ReLesR for 30 s to coat the cell layer.

The ReLesR was then removed and cells incubated at room temperature for 3 min. Once cells began to detach, 1 ml DMEM was added to the flask and cells lifted by tapping against the palm of a hand. An additional volume of media was added to the flasks and cells were dissociated using a 10 ml pipette and transferred to a 15 ml tube. Cells were harvested by centrifugation for 5 min at 100 g. DMEM was then removed and the cells were resuspended at a concentration of 1 x$10^6$ cells/ml in 90 % FBS, 10 % DMSO solution or in STEM-CELL BANKER cryopreservation media. A 10 ml pipette was then used to dissociate the cells and transfer 1 ml of cells in each cryovial. cryovials were then placed into NalGene Mr Frosty® freezing container and placed into the -80 °C freezer. Mr Frosty® ensures that the cells freeze slowly, at a rate of 1 °C/min. After 24 hrs at -80 °C the cells were transferred into a liquid nitrogen tank for long term storage and preservation.

### 2.6.4 Revival of cells

One cryovial of cells was removed from liquid nitrogen and gently placed at 37 °C until almost thawed. Using a 10 ml pipette 1 ml DMEM was added drop-by-drop to the thawed cells and transferred to a 15 ml tube. Cells were centrifuged for 5 min at 100 g. During centrifugation, the vitronectin was removed from the pre-prepared flask and E8 media containing ROCK inhibitor (10 µg/ml) was then added to the flask. Medium was carefully removed from the cell pellet. The cell pellet was flicked to help with dissociation and 1 ml of E8 media containing ROCK inhibitor was then added to the pellet. Cells were resuspended using a 10 ml pipette and transferred to the flask drop-by-drop to ensure sufficient dissociation. Cells were incubated at 37 °C with 5 % (v/v) $CO_2$ at 95 % humidity for 24 hrs and then fresh E8 media was given to cells to remove the ROCK inhibitor.

### 2.6.5 Passaging of human pluripotent stem cells

Once stem cells reach approximately 80 % confluency their growth media was removed, and cells were gently washed in PBS and treated with ReLesR for 30 s to coat the cell layer. ReLesR was removed and cells incubated at room temperature for 3 min. Once cells begin to detach, they appear white. The flask was then tapped solidly twice to release cells. Cells were then resuspended in 1 ml of growth medium and tapped against the palm of a hand to lift cells. A 10 ml pipette was used to break up cells drop by drop to dissociate them into small clusters. Cells were then split at the required dilution into a vitronectin-coated flask and incubated at 37 °C with 5 % (v/v) $CO_2$ at 95 % humidity.

### 2.6.6 Seeding of human pluripotent stem cells

Once stem cells reach approximately 80 % confluency their growth media was removed, and cells were gently washed in PBS and treated with TrypLE to coat the cell layer and incubated at 37 °C for 3 min. Once cells began to detach and disassociate to form single cells, cells were resuspended in DMEM so that the TrypLE is less than 10 % (e.g. 1 ml TrypLE to 9 ml DMEM). A cell count is then taken using a haemocytometer and cells are harvested by spinning at 100 g for 5 min. Cells are then resuspended to be 1 x$10^6$ cells/ml and seeded at the required density into complete media containing ROCK inhibitor (10 µg/ml). Cells were incubated at 37 °C with 5 % (v/v) $CO_2$ at 95 % humidity.

### 2.6.7 Maintentance of human pluripotent stem cells

Following seeding or passaging, cells are left for 24 hrs to adhere. Media is then aspirated to remove dead cells and ROCK inhibitor if present, an appropriate volume dependent on flask size is then added. This is then repeated every 24 hrs to maintain cells as required. A double volume of media may be added to maintain cells for 48 hrs if required.

### 2.6.8 Karyotypic analysis of human pluripotent stem cells

For karyotypic analysis of human pluripotent clonal stem cell lines produced by CRISPR and FACs, cells were analysed by qPCR using the hPSC Genetic Analysis Kit (Stem Cell Technologies, 07550). Full karyotypic analysis of human pluripotent stem cells looking at the metaphase spread was carried out at the Sheffield Diagnostic Genetics Service part of Sheffield's Childrens Hospital.

## 2.7 Human pluripotent stem cell line generation using CRISPR-Cas9

### 2.7.1 Generation of clones using CRISPR

#### Guide design

Guides were designed *in silico* using the IDT Alt-R™ CRISPR HDR Design Tool which designs both the HDR donor templates and associated Cas9 guide RNAs for human genome editing (Table 2.16). Two gRNAs were designed to the correct region of NOP53 (Exon 2) to generate a specific cut to allow for the knock-in to occur along with the homology directed repair template to input the desired nucleotide changes. Relevant primers were designed to amplify the region for PCR using primerBLAST. Settings were altered to aim for amplified regions that were 500bp long. All primers and repair templates were ordered from IDT as DNA oligos. For the CRISPR guides, ALT-R® CRISPR-Cas9 crRNA (IDT) was ordered.

Table 2.16: gRNA and HDR sequences to introduce NOP53 D90R by CRISPR-Cas9

| **Name** | **Sequence (5'-3')** |
|---|---|
| Guide 1 | AAACTCTTCTTCGTGGACAC |
| HDR 1 | CTTGTTGTCAGAGGCCCCAAATGAAAAGCTCTTCTTCGTGCGCACT GGATCCAAGGAAAAAGGTGAGGAGAGGCTTTTGTGGT |
| Guide 2 | CTTCGTGGACACTGGCTCCA |
| HDR 2 | CTTGTTGTCAGAGGCCCCAAATGAAAAACTCTTCTTCGTGCGCACT GGATCCAAGGAAAAAGGTGAGGAGAGGCTTTTGTGGTGTGGAAT |

#### Introduction of CRISPR components via electroporation

Upon arrival, the crRNA and ALT-R® CRISPR-Cas9 tracrRNA (IDT, 1072532) were diluted to 100 µM in nuclease-free duplex buffer (IDT, 11-01-03-01), these were aliquoted and stored at -20 °C. These were then mixed in equimolar concentrations in a sterile tube and heated at 95 °C for 5 min to form the crRNA:tracrRNA duplex before being allowed to cool to room temperature. The ALT-R® S.p. HiFi Cas9 Nuclease V3 (IDT, 1081060) was diluted in Resuspension Buffer R (part of 10 µl electroporation kit, Invitrogen, MPK1025) to 36 µM and incubated at room temperature in a 50:50 mix with the crRNA:tracrRNA duplex to form the ribonucleoprotein (RNP) complex.

If using a repair template, this was resuspended similarly at 100 µM in Nuclease-Free Duplex Buffer, aliquoted and stored at -20 °C. For use in experiments stock was diluted to 10.8 µM in Resuspension Buffer R. Cells were prepared as a single cell suspension in the Resuspension Buffer R at 2.2 x $10^7$ cells/ml. For each electroporation, 1 µl of RNP complex, 9 µl cell suspension and 2 µl of repair template (replaced with R buffer if not used) were mixed and pipetted into a 10 µl Neon electroporation tip. Electroporation was carried out using the Neon Electroporation System with the following settings: 1400 V, 20 ms, 1 pulse. Cells were

transferred to a prepared and pre-warmed plate coated with vitronectin, containing E8 and Rock inhibitor. Cells were incubated at 37 °C with 5 % (v/v) $CO_2$ at 95 % humidity. Cells were fed fresh E8 media 24 hrs later and used for further experiments the following day.

**Verification of Cas9 cleavage at the target site**

DNA was isolated using Quickextract DNA extraction solution (Lucigen, QE0905) according the the manufacturer's protocol. The region of interest was amplified using 100 µg of DNA per PCR reaction with Taq DNA Polymerase (Thermofisher, 10342020) with the following cycle parameters: 94 °C for 3 min, then 30 cycles of 94 °C for 45 s, 62 °C for 30 s, 72 °C for 60 s, with a final extension at 72 °C for 10 min. T7 endonuclease I (NEB, M0302S) was used according to manufacturer's instructions. Samples were run on 1 % agarose gel at 100V for 45 min. Editing could be seen through the presence of smaller bands, indicating the nuclease had cleaved at mismatched DNA. Samples of interest were also sent for sequencing.

**PCR based screen for clones**

The HDR templates were designed to introduce both the D90R mutation and also a silent glycine to glycine mutation which introduces one extra restriction site for the enzyme BamHI (ThermoFisher, FD0054). Potential clonal DNA was extracted and amplified using Taq DNA polymerase as discussed above. 5 µl of PCR product along with the restriction enzyme and relevant buffers were incubated at 37°C for 1 hr. A sample of each product was run on a 2 % agarose gel at 100V for 45 min. Samples of interest were identified based upon band changes and sent for sequencing.

**PCR Sequencing**

PCR product was cleaned up using PCR clean up kit (Qiagen, 28104) according to manufacturer's instructions and sent to Eurofins genomics for sequencing.

**Single cell cloning of edited hPSCs**

For seeding of single hPSCs Geltrex coated plates were used. To prepare plates, Geltrex was diluted 1:100 in cold DMEM, 90 µl was then added to each well of 10 96-well plates and incubated at 37 °C for 60 min. Geltrex was removed and mTESR plus containing 10 % CloneR was added to each well and stored at 37 °C until required.

Neon transfected cells were dissociated from the plate 48 hrs after transfection (section 2.6.6). These cells were then sorted using the BD FACS Jazz to ensure a single cell was deposited in each well of the pre-prepared 96-well plate. Immediately after sorting plates were centrifuged briefly at 400 g for 60 s to aid attachment of the cells. Cells were incubated at 37 °C with 5 % (v/v) $CO_2$ at 95 % humidity for 48 hrs. An equal volume of mTESR plus containing 10 % CloneR was added to each well and cells were grown for a further 48 hrs. Media was then aspirated and replaced with fresh mTESR plus and maintained in mTESR plus on an alternate day feeding schedule for 2-3 weeks.

Once colonies were of an appropriate size they were passaged by aspirating the media and a 200 µl pipette tip containing 200 µl new media with rock inhibitor was used to scratch the colony off the plate. This was pipetted up and down to ensure all cells were captured and that colonies were of an appropriate size. 1/3 of this was transferred to the new 96-well culture dish and 2/3 sample was transferred to a 1.5 ml eppendorf for DNA extraction, PCR and restriction digest analysis.

## 2.8 Protein techniques

### 2.8.1 Human protein isolation from *E. coli* cells

Table 2.17: Solutions for protein purification

| **Buffer** | **Composition** |
|---|---|
| Buffer A | 20 mM HEPES pH 8.0<br>100 mM NaCl,<br>5 mM $MgCl_2$ |
| Buffer B | 20 mM HEPES pH 8.0<br>250 mM NaCl<br>5 mM $MgCl_2$ |
| Buffer C | 20 mM HEPES pH 8.0<br>600 mM NaCl<br>5 mM $MgCl_2$ |
| Buffer D | 20 mM HEPES pH 8.0<br>150 mM NaCl<br>5 mM $MgCl_2$ |
| Buffer E | 20 mM HEPES pH 8.0<br>150 mM NaCl<br>5 mM $MgCl_2$<br>5 % Glycerol<br>2 mM DTT |
| Buffer F | 20 mM HEPES pH 8.0,<br>350 mM NaCl,<br>5 mM $MgCl_2$ |
| Buffer G | 20 mM HEPES pH 8.0,<br>1 M NaCl,<br>5 mM $MgCl_2$ |
| No Salt Buffer | 20 mM HEPES pH 8.0<br>5 mM $MgCl_2$ |

#### NOP53 Purification

#### GST-NOP53

1 L BL21 *E. coli* cell pellets were resuspended in 25 ml of buffer A (Table 2.17) complemented with a freshly added SIGMAFAST protease inhibitor tablet and 1 mM DTT. Cells were lysed by sonication and the lysates were then cleared by centrifugation at 16000 g for 30 min at 4 °C. 5 ml of SP sepharose beads (GE healthcare), in 20 % EtOH, were transferred to a 50 ml tube and washed with buffer A. The cleared lysate was then added to the SP sepharose and incubated with rotations for 30 min at 4 °C. The beads were then transferred to a column and washed once in buffer A, washed twice in buffer B, and eluted in 5 ml buffer C. Samples were re-buffered to 150 mM NaCl using no salt buffer containing 1 mM DTT. Re-buffered samples were incubated with pre-equilibrated 1 ml GSH beads (Protino Glutathione Agarose 4B, Macherey Nagel) for 1 h at 4 °C. A sample of known percentage of beads was analysed by SDS-page to verify protein binding, with the remainder of the sample stored at 4 °C and used within 1 day for an *in vitro* binding assay.

**GST-NOP53-Strep-II and Twin-Strep-II-NOP53**

1 L BL21 *E. coli* cell pellets were resuspended in 25 ml of buffer A complemented with a freshly added SIGMAFAST protease inhibitor tablet and 1 mM DTT. Cells were lysed by sonication and the lysates were then cleared by centrifugation at 16000 g for 30 min at 4 °C. A 1 ml StrepTap HP column (Cytiva) was washed with 5 CV $H_20$ and equilibrated with buffer A. The cleared lysate was then added to the column, washed in 5 CV buffer A and eluted in 5 x 1 ml fractions using buffer D containing 2.5 mM desthiobiotin. Samples were then analysed by SDS-page to confirm protein presence. For GST-NOP53-Strep-II positive eluates were then incubated with pre-equilibrated 1 ml GSH beads (Protino Glutathione Agarose 4B, Macherey Nagel) for 1 h at 4 °C for use in an *in vitro* binding assay.

**MTR4 purification**

1 L BL21 *E. coli* cell pellets were resuspended in 20 ml of buffer F complemented with a freshly added SIGMAFAST protease inhibitor tablet. Cells were lysed by sonication and the lysates were then cleared by centrifugation at 16000 g for 30 min at 4 °C. 1 ml of protino NiNTA agarose beads (Macherey Nagel) in 20 % EtOH were transferred to a 50 ml tube and washed with buffer F. The cleared lysate was then added to the NiNTA agarose and incubated with rotations for 20 min at 4 °C. The beads were then transferred to the column and washed twice in 10 ml buffer F followed by a final wash in buffer F containing 10 mM imidazole. Proteins were then eluted in 1 ml buffer F containing 350 mM imidazole. Samples were re-buffered to 100 mM NaCl using no salt containing buffer containing 1 mM DTT and concentrated using Millipore concentrating columns to a volume slightly greater than 1 ml.

Heparin purification: The Ni eluate was then further purified using a 1 ml HiTrap Heparin HP column (GE Healthcare). Prior to use all buffers and deionised $H_20$ were chilled to 4 % and filtered. Lines A and B of the AKTA pure were washed with $H_20$. The column was attached whilst $H_20$ was actively flowing. The column was washed with a minimum of 3 column volumes (CV) $H_20$ at a flow rate of 1 ml/min so as not to exceed the pressure limit of the column (0.5 MPa). Line A was then washed in buffer A and line B washed in buffer G before equilibrating the column in a minimum of 3 CV buffer A at 1 ml/min. A 1 ml loop was attached to the AKTA and washed in 5 ml buffer A using a syringe. The sample was then manually injected into the loop using a syringe. A linear salt gradient was then applied to the column across 15 CV starting at 0 % buffer B and reaching 100 % buffer B with elution fractions of 0.5 ml collected. Peak samples corresponding to MTR4 were then analysed by SDS-PAGE and Coomassie staining. The column was then washed in 3 CV 2 M NaCl, 3 CV $H_20$ and 3 CV 20 % ethanol for storage at 4 °C.

Gel filtration: Peak samples confirmed by SDS-PAGE and Coomassie staining were dialysed overnight into buffer E. The dialysed sample was then span at 4 °C for 5 min and transferred to a fresh 1.5 ml Eppendorf tube. The samples were then purified using size-exclusion chromatography using the Superdex™ 200 increase 10/300 GL column (GE Healthcare). Lines A and B of the AKTA pure were washed with $H_20$. The column was attached whilst $H_20$ was actively flowing. The column was washed with a minimum of 1.5 CV $H_2$ 0 at a flow rate of 0.3 ml/min so as not to exceed the pressure limit of the column (3 MPa). Line A was then washed in buffer E and the column was equilbrated in a minimum of 1.5 CV buffer E at 0.15 ml/min. A 1 ml loop was attached to the AKTA and washed in 5 ml buffer E using a syringe. The sample was then manually injected into the loop using a syringe. Buffer E was then applied to the column for 1.5 CV collecting 0.5 ml sized elution fractions. Peak fractions were then analysed by SDS PAGE and Coomassie staining and MTR4 containing fractions were concentrated, flash frozen in liquid nitrogen and stored at -80 °C. The column

was washed in 3 CV 1 M NaCl, 3 CV $H_20$ and 3 CV 20 % ethanol for storage at 4 °C.

**RPL11 purification**

1 L BL21 *E. coli* cell pellets were resuspended in 20 ml of buffer D complemented with a freshly added SIGMAFAST protease inhibitor tablet and 1 mM DTT. Cells were lysed by sonication and cleared by centrifugation at 16000 g for 30 min at 4 °C. The cleared lysate was then added to 1 ml pre-equilibrated SP sepharose (GE Healthcare) and incubated with rotations for 30 min at 4 °C. The beads were then transferred to a column and washed once in buffer D, washed twice in buffer B, and eluted in 5 ml buffer C. Samples were re-buffered to 300 mM NaCl using no salt buffer. Re-buffered samples were then added to the NiNTA agarose and incubated with rotations for 30 min at 4 °C. The beads were washed twice in 10 ml buffer F followed by a final wash in buffer F containing 10 mM imidazole. Proteins were then eluted in 1 ml buffer F containing 350 mM imidazole. Samples were re-buffered to buffer E using Millipore concentrating columns to an approximate volume of 300 µl, flash frozen in liquid nitrogen and stored at -80 °C.

### 2.8.2 *In vitro* binding assay using recombinant proteins

GST pulldown assays were carried out in buffer E with 0.01 % NP-40 added fresh. Samples were prepared in 1.5 ml eppendorfs with a 2-fold molar excess of prey:bait; 95 µM GST fused bait protein on GSH agarose beads mixed with 190 µM prey protein. The total volume in the tube was always 300 µl with excess buffer added in some cases to ensure mixing. Protein samples were mixed by rotation at 4 °C for 90 min.

Following binding, samples were transferred to 1 ml columns and washed 10 times in 250 µl buffer E containing 0.01 % NP-40. 1 x SDS buffer was added to the beads and samples boiled at 95 °C for 10 min to elute protein from beads. Samples were either stored at -20 °C or analysed via SDS-PAGE.

### 2.8.3 Protein isolation from mammalian cells

One SIGMAFAST protease inhibitor cocktail tablet (Sigma-Aldrich, 88830) was added to 100 ml of ice-cold RIPA buffer (50 mM Tris·HCl, pH 8.0, 150 mM NaCl, 1 % (v/v) Triton X-100, 0.5 % (w/v) sodium deoxycholate, 0.1 % (w/v) SDS) and placed on a roller at 4 °C for 10-15 min until the tablet was completely dissolved. As the inhibitor is only stable for 24 h once dissolved, this solution was made on the day of protein isolation.

Dishes containing the cells were placed on ice and the medium was carefully aspirated, to avoid disturbing the cells, and discarded. Cells were gently washed three times in an appropriate volume of PBS. Between 100-1000 µl of ice-cold RIPA inhibitor buffer solution was then added to the dish and they were gently swirled and left to lyse on ice for 2 min. The lysis buffer was then pipetted up and back onto the dish to ensure all cells are detached and the dish placed at a 45 ° angle to collect the cells. Cells were then transferred to a 1.5 ml microcentrifuge tube and rotated for 30 min at 4 °C to allow for all lysis to occur. Protein lysates were then centrifuged at 16000 g for 30 min at 4 °C to pellet the cell debris. The supernatant was transferred to a fresh 1.5 ml microcentrifuge tube. Samples were quantified and either stored at -20 °C long-term or analysed via Western blotting.

### 2.8.4 Cryogeneic disruption of mammalian cell lines

Flp-In T-REx HEK293 3xFLAG-6xHIS-NOP53 WT and DR cells were seeded into 30 15 cm dishes per cell line. Once at 70 % confluency, tetracycline was used to induce FLAG-NOP53

expression for 24 hrs. Cells were then harvested, frozen in liquid nitrogen and ground in liquid nitrogen using the Retsch PM 100 according to the protocol published by Domanski *et al.,* 2012.

### 2.8.5 Co-immunoprecipitation from mammalian cell lines

Cell grindate was weighed into 1.5 ml tubes and resuspended in an appropriate volume of ice-cold co-IP lysis buffer (50 mM Hepes-NaOH (pH 7.5), 100 mM NaCl, 3 mM $MgCl_2$, 0.15 % NP-40, 5 % glycerol) complemented with protease inhibitor cocktail tablets (EDTA-free). The Diagenode Biorupted Pico was used to sonicate samples, 15 s on, 30 s off for 4 cycles. Samples were then centrifuged at 16000 g for 15 min at 4°C and the supernatant transferred to a clean 1.5 ml tube. Samples were then quantified and 300 mg of protein was loaded per 25 µl pre-equilibrated anti-FLAG M2 Magnetic beads (Sigma-Aldrich, M8823) in an equal volume of co-IP buffer. The beads were incubated at 4 °C with rotation for 2 hrs. Using a magnet, the protein extract was removed, and beads washed 2 times in co-IP wash buffer (50 mM Hepes-NaOH (pH 7.5), 150 mM NaCl, 3 mM $MgCl_2$, 0.15 % NP-40, 5 % glycerol) with 5 min incubations on ice. Protein was eluted from beads by adding 27.5 µl 1M Arg-HCl (pH 3.5) and mixed on ice for 2.5 min. The magnet was used to collect the beads and the eluate was transferred to a tube containing 2.5 µl Tris-HCl (pH 8.8) to neutralise. Samples were prepared for SDS-PAGE and analysed via Western blotting.

### 2.8.6 Protein quantification using the NanoDrop spectrophotometer

1 µl of the protein preparation was analysed using the NanoDrop spectrophotometer. Samples were measured in triplicate and cellular lysis buffer (i.e. RIPA) was blanked as the control. The concentration of the protein was determined by calculating absorbance at 280 nm.

### 2.8.7 SDS-PAGE for protein analysis

Gel Preparation: Pouring apparatus was set up with clean glass plates placed on the casting base and secured to prevent any leaking. A separating gel solution consisting of 30 % (w/v) acrylamide, bisacrylamide (Sigma-Aldrich, A357A), sterile de-ionised $H_20$, 1 M Tris-HCl pH 8.8, 20 % (w/v) SDS, 10 % (w/v) ammonium persulfate and TEMED were prepared in a 100 ml bottle and mixed gently by swirling. Volumes of solutions used were dependent on the number of gels being cast and the percentage of desired gels. The acrylamide solution was then pipetted between the glass plates and the separating gel was overlaid with isopropanol and left to polymerise. Once the separating gel had polymerised the isopropanol was removed, and traces rinsed off the gel using de-ionised water. The stacking gel was then prepared using the same solutions as the separating gel, but 1 M Tris-HCl pH 6.8 was used opposed to 1 M Tris-HCl pH 8.8. The stacking gel was then pipetted on top of the separating gel and combs gently inserted and left to polymerise. Once polymerised the plates were removed from the casting apparatus and inserted into the running apparatus and placed inside the gel tank. The combs were removed and 1 X SDS-PAGE running buffer (25 mM Tris, 250 mM glycine and 0.1 % SDS) was added to the upper and lower chambers of the gel tank and the wells washed by pipetting with 1 X SDS-PAGE running buffer.

Protein Sample Preparation and Loading: 50 µg of protein sample or a known percentage of sample for recombinant protein work was mixed with SDS-PAGE loading dye. Samples were incubated at 95 °C for 10 min to denature the proteins. Protein samples were then loaded into the wells of the prepared gels using gel loading pipette tips alongside 10 µl of either prestained (ThermoScientific, 26616) or unstained (ThermoScientific, 26614) PageRuler protein molecular weight marker. SDS gels were then connected to a power supply and ran

at 80 V until the samples reached the resolving gel (approx. 30 min) where voltage was increased to 120 V (approx. 90 min).

### 2.8.8 SDS gel protein staining using Coomassie Blue

After SDS-PAGE, gels were transferred to a plastic dish and submerged in an appropriate volume of 50 % methanol, 10 % acetic acid for fixation for 15-30 min. Gels were then stained in a 20 % methanol, 20 % RotiBlue solution (Carl Roth, A152.1) at room temperature overnight. Gels were then washed and destained with distilled $H_20$ and for 3-4 hrs at room temperature. Gels were then imaged using a Nikon camera over a light box.

### 2.8.9 Wet protein transfer

Preparation for wet transfer: one piece of nitrocellulose membrane plus 4 pieces of Laboratory filter paper were cut just a few millimetres larger than the areas of the SDS gel from which the proteins were being transferred from, to completely cover the gel. The membrane and filter paper were briefly soaked in 1 x transfer buffer (25 mM Tris, 190 mM glycine, 0.1 % SDS) with 20 % methanol.

Wet transfer: two pieces of the laboratory filter paper were stacked on the transfer apparatus and rolled flat to remove any air bubbles. The gel was then placed onto the filter paper (negative side of the apparatus). The membrane was then placed on top of the SDS gel ensuring coverage and a final 2 pieces of filter paper were placed on top of the membrane and were gently rolled to ensure all bubbles were removed. The membrane current machine was then used to transfer the proteins at 80 V for 2 hrs at 4 °C.

### 2.8.10 Western blotting

Nitrocellulose membranes were blocked by submersion in 1 x PBST (137 mM NaCl, 2.7 mM KCl, 10 mM $Na_2HPO_4$, 1.8 mM $KH_2PO_4$ and 1 % (v/v) Tween 20) + 5 % (w/v) skimmed dried milk powder for 30 - 60 min at room temperature on an orbital shaker. After blocking, membranes were then incubated in 1 x PBST + 5 % (w/v) skimmed dried milk powder containing an appropriate concentration of primary antibody and incubated with mixing overnight at 4 °C. Antibody concentrations used for each antibody are shown (Table 2.18). Membranes were then washed four times, 10 min each time in 1 x PBST to remove any unbound primary antibody. Membranes were then incubated in 1 x PBST + 5 % (w/v) skimmed dried milk powder containing the appropriate concentration of secondary antibody on a shaker for 1 h at room temperature. Membranes were then washed four times, 10 min each time in 1 x PBST to remove any unbound secondary antibody.

Table 2.18: Antibodies used for Western blotting

| **Name** | **Type** | **Working dilution** | **Host** | **Supplier** | **Catalogue number** |
|---|---|---|---|---|---|
| 6xHis (HRP conjugated) | Primary | 1:20000 | Mouse | Proteintech | HRP-66005 |
| c-Myc | Primary | 1:1000 | Mouse | Stuart Wilson | N/A |
| FLAG-tag | Primary | 1:1000 | Mouse | Proteintech | 66008-2-Ig |
| GAPDH | Primary | 1:10000 | Mouse | Proteintech | 6004-1-Ig |
| NOP53 | Primary | 1:1000 | Rabbit | Cell signalling technology | 73225 |
| Goat Anti-Mouse IgG (H+L) HRP conjugate | Secondary | 1:10000 | Goat | Proteintech | SA00001-1 |
| Goat Anti-Rabbit IgG (H+L) HRP conjugate | Secondary | 1:10000 | Goat | Proteintech | SA00001-2 |
| RPL11 | Primary | 1:500 | Rabbit | Abcam | ab79352 |
| SKIV2L2 polyclonal (MTR4) | Primary | 1:2500 | Rabbit | Proteintech | 12719-2-AP |

### 2.8.11 Visualisation and imaging of Western blots

Western Blots were imaged using Amersham's ECL western blotting kit (GE Healthcare, RPN2106). The solution was prepared in a 1:1 ratio according to the manufacturer's protocol in a 15 ml tube at room temperature. Nitrocellulose membranes were then mixed with solution and swirled to evenly coat the membrane at room temperature for 1 min. The membrane was then transferred to a glass plate and imaged using the Geneflow G:Box gel imaging system and Syngene GeneSnap software to produce the final image of the western blot.

### 2.8.12 Membrane stripping procedure for Western blots

To strip the membrane, membranes were placed in a plastic dish and incubated with Restore Western blot stripping buffer (ThermoScientific, 21059) according to the manufacturer's protocol. Membranes were then washed twice in 1 x PBST by shaking for 5 min. Membranes were then re-blocked and re-probed.

# Chapter 3

# NOP53 interacts with MTR4 in *H. sapiens* using a conserved amino acid identified in *S. cerevisiae*

## 3.1 Introduction

The nucleolar protein, Nop53 was first identified in *H. sapiens*, but first characterised in *S. cerevisiae*. Nop53 was shown to be essential for cell viability and for efficient 60S ribosomal subunit assembly. Depletion of Nop53 resulted in 7S pre-rRNA processing defects (Granato *et al.,* 2005; Sydorskyy *et al.,* 2005; Thomson & Tollervey, 2005); the same phenotype observed upon depletion or mutation of the nuclear exosome or exosome associated helicase, Mtr4 (de la Cruz *et al.,* 1998). Subsequent work in *S. cerevisiae* showed that Mtr4 and Nop53 directly interact with each other and that this interaction is important for efficient 7S pre-rRNA processing to produce the mature 5.8S rRNA during ribosome biogenesis (Thoms *et al.,* 2015).

Nop53 interacts with the arch domain of Mtr4 in *S. cerevisiae* via an arch interaction motif (AIM). The AIM is found on several adaptor proteins including Nop53 and Utp18 in *S. cerevisiae* and ZCCHC8 and NVL in humans (Thoms *et al.,* 2015; Lingaraju *et al.,* 2019) and mediates an interaction with Mtr4 in both species. The AIM of NOP53 is five amino acids in length; consisting of four hydrophobic amino acids with an invariable aspartate in the 5th position. Mutations made within the AIM of yeast Nop53; 5xAla or D64A, were sufficient to abolish the interaction with Mtr4 (Figure 3.1). Both mutants showed impaired 7S rRNA processing and a growth defect which was more severe in the 5xAla mutant (Thoms *et al.,* 2015).

The Nop53 AIM motif identified in *S. cerevisiae* is highly conserved across eukaryotes (Figure 3.1). Work here will look to investigate whether the interaction between NOP53 and MTR4 is conserved in humans. Using both *in vitro* and *in vivo* analyses, the regions of NOP53 responsible for MTR4 interaction will be studied.

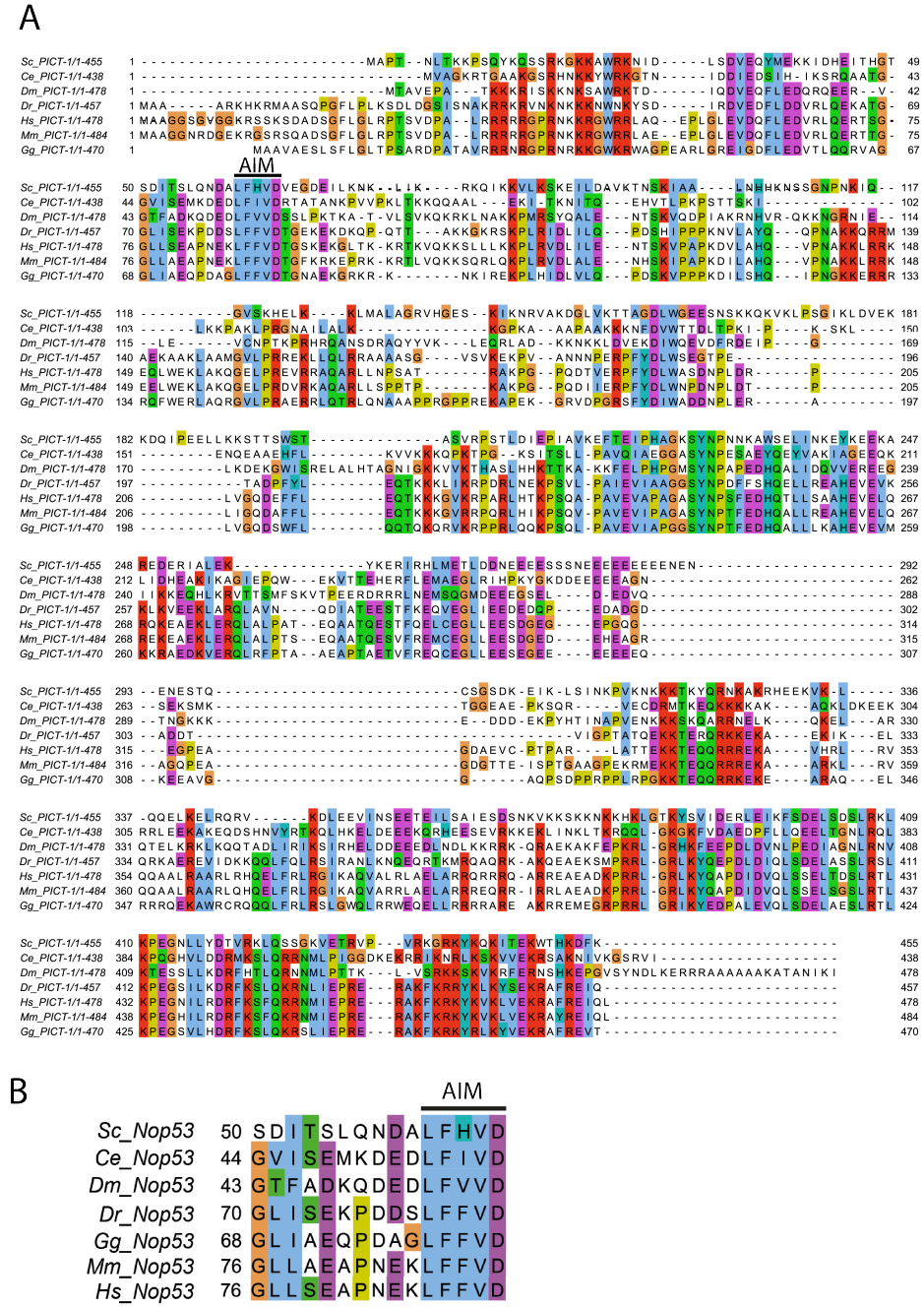


Figure 3.1: Alignment of Nop53. (A) Multiple sequence alignment of Nop53 using Clustal Omega and Jalview for the following species; *S. cerevisiae (Sc, Q6FTK4), C. elegans (Ce, Q94300), D. melanogaster (Dm, P46222), D. rerio (Dr, Q6IQI6-1), G. gallus (Gg, A0A1D5P3B1-1), M. musculus (Mm, Q9CXW4-1) and H. sapiens (Hs, P62913-1).* (B) Shorter multiple sequence alignment of the arch interaction motif (AIM) of Nop53 for the same species.

## 3.2 In *H. sapiens* a single point mutation in the AIM of NOP53 is sufficient to abolish the interaction with MTR4

### 3.2.1 Initial analysis of NOP53 and MTR4

#### Analysis using the yeast-two-Hybrid system

Initial work to explore the interaction between NOP53 and MTR4 was conducted using the yeast-two-hybrid system (Thoms *et al.,* 2015). The *S.cerevisiae* strain PJ69-4A (James *et al.,* 1996) was used for analysis using the Gal1-His3 reporter. In this system, the activation domain (AD) and the binding domain (BD) of the Gal4 transcription factor are attached to NOP53 and MTR4, respectively (Figure 3.2). If NOP53 and MTR4 interact, the AD and BD are in close enough proximity to reconstitute the Gal4 transcription factor. This allows binding at the promoter and gene activation for histidine production. Conversely, if no interaction occurs, there is no Gal4 reconstitution, promoter binding or histidine production. Therefore, by growing yeast on media lacking histidine, only those with a positive interaction between NOP53 and MTR4 are able to grow. The stringency of the interaction between NOP53 and MTR4 can be tested by the addition of 3-Amino-1,2,4-triazole (3-AT) to growth media. 3-AT competes for the histidine gene product (Chen *et al.,* 2010) meaning a stronger interaction between NOP53 and MTR4 is required for *S. cerevisiae* growth on media lacking histidine. The *S. cerevisiae* homodimer, PNC1 is used as a control in the yeast-two-hybrid system to validate that no self activation is occurring (Saryi *et al.,* 2017).

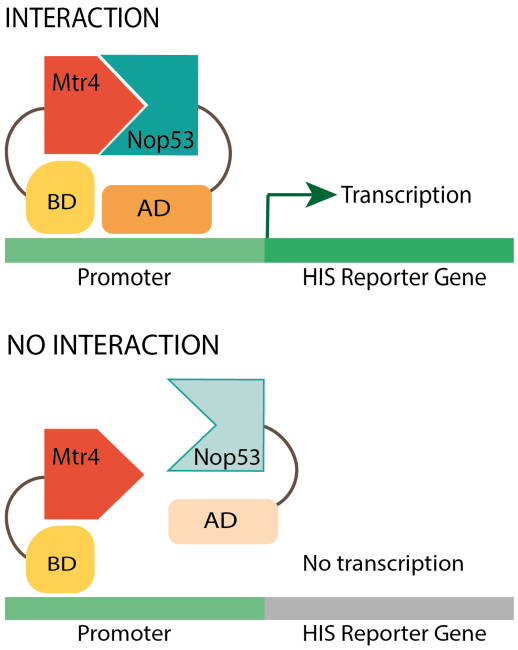


Figure 3.2: Activation of the HIS3 reporter gene in the yeast-two-hybrid system. NOP53 is fused to the activation domain (AD) of the Gal4 transcription factor and MTR4 to the binding domain (BD).

To investigate the ability of human NOP53 to bind MTR4 an equivalent reverse charge mutation (D90R) to the invariable aspartate of the AIM in *S. cerevisiae* was generated in the human NOP53 sequence (constructs and preliminary analyses performed by Monika Feigenbutz, Thomson Lab). Growth was observed with wild-type versions of NOP53 and MTR4 but not with the PNC1 control indicating that the interaction between NOP53 and MTR4 is

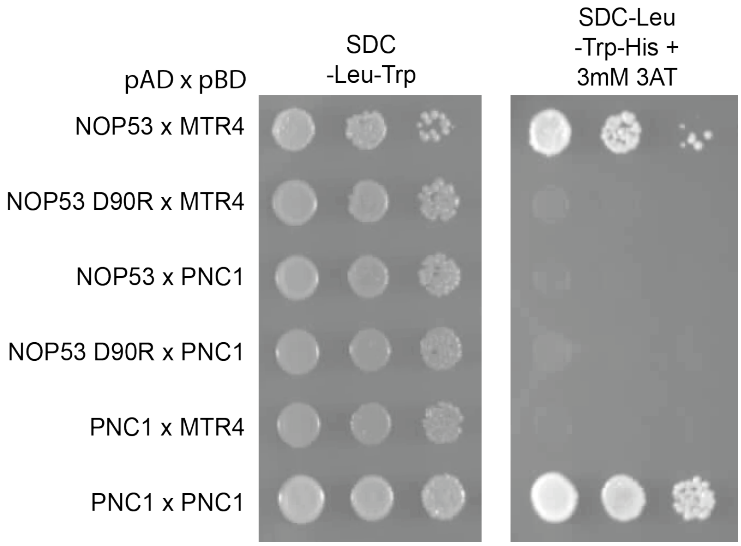


Figure 3.3: Yeast-two-hybrid analysis of NOP53 WT and D90R with MTR4. Yeast-two-hybrid dot plates for NOP53 WT or D90R transformants with MTR4 grown on SDC-Leu-Trp (SDC-L-T) and SDC–Leu-Trp-His (SDC-L-T-H) + 3 mM 3AT. The *S. cerevisiae* protein PNC1 forms a homodimer and is used as a positive control. Transformants were grown on dot plates at 30°C for 4 days.

conserved (Figure 3.3). In contrast, no growth was observed with NOP53 D90R and MTR4. indicating that mutation of the conserved, invariant, residue in the AIM identified in yeast is sufficient to abolish human NOP53 interaction with MTR4.

**Analysis using recombinant proteins for *in vitro* binding assays**

To further explore the nature of the interaction between human NOP53 and MTR4 and to confirm the observations made in the yeast-two-hybrid studies, *in vitro* binding assays using heterologously expressed recombinant NOP53 and MTR4 were carried out. MTR4 and NOP53 were cloned into variants of the pET24d vector.

For expression and purification of MTR4, a 6xHis tag was fused to the N-terminus of MTR4. Induction of MTR4 was carried out in BL21 *E .coli* and expression was observed across all time points and temperatures tested (Figure 3.4 A). An overnight (16 hour) induction at 18 °C, was selected for further inductions as it showed a high level of MTR4 expression at a cooler induction temperature which helps to minimise protein misfolding, and yield soluble protein. The purification strategy of 6xHis-MTR4 was based upon the protocol from Thoms *et al.,* 2015, for *C. thermophilum* MTR4. The three step purification consists of an initial affinity step using the 6xHis tag binding to NiNTA to pull out MTR4 (Figure 3.4 B, strategy summarised in G) and the second step utilised heparin binding of MTR4 to allow for further selectivity and isolation of MTR4 (Figure 3.4 C). These first 2 steps of purification allowed a good level of MTR4 enrichment to be achieved. The final step, size exclusion chromatography, was used to isolate MTR4 from smaller proteins and truncated MTR4 due to degradation (Figure 3.4 D). MTR4 eluted from the size exclusion column at the expected volume when compared with gel filtration standards (Figure 3.4 E, F). The purification produced 600 µM MTR4 with very few lower molecular weight bands visible following Coomassie staining, sufficient for use in a binding assay (Figure 3.4).

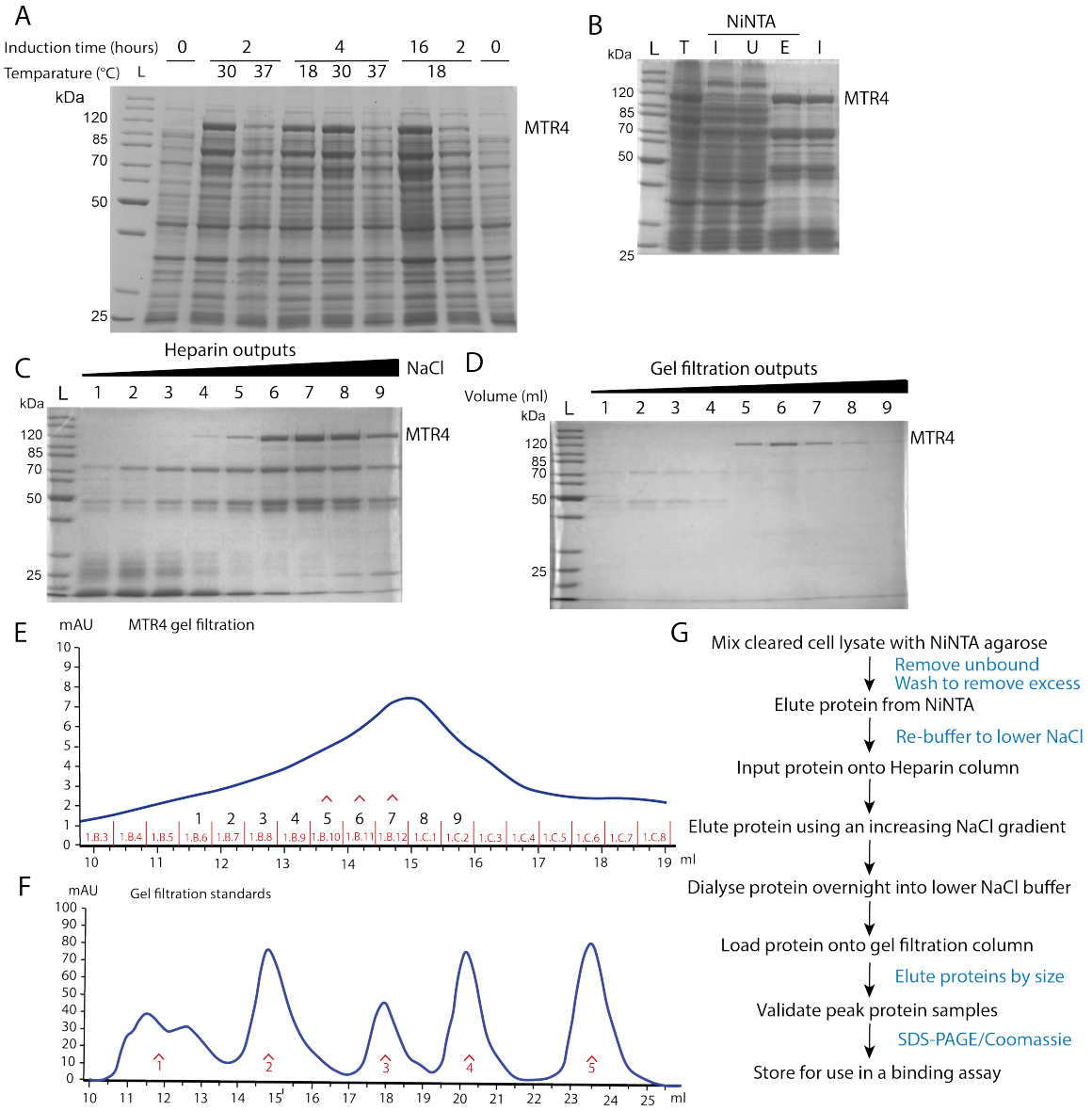


Figure 3.4: His-MTR4 recombinant expression and purification. A) Induction of His-MTR4 by 0.1 mM IPTG in BL21 *E.coli* at 3 different temperatures, 18, 30 and 37 °C for 2 and 4 hours, and overnight for 16 hours at 18 °C, with no induction at 0 hours. Total protein was loaded on a 10 % tris-glycine polyacrylamide gel. B) Purification of MTR4 by NiNTA binding. Labeling as follows; ladder (L), 0.1 % total (T), 0.1 % NiNTA input (I), 0.1 % unbound (U), 1 % eluate (E) and 1 % Heparin input (I). C) Heparin output of MTR4 (1 %) over an increased NaCl gradient. Lanes 6-8 were pooled and input on gel filtration. D) Gel filtration outputs of MTR4 (1 %). Peak MTR4 samples (lanes 5-8). E) UV trace corresponding to MTR4 gel filtration outputs using the Superdex™ 200 increase 10/300 GL column (GE Healthcare) with volume (ml) shown. Numbers 1-9 above sample fractions correspond to the lanes on panel D. Peak samples on D (lanes 5-8) containing MTR4 corresponds to fractions 1.B.10, 11, 12 and 1.C.1 eluted between 13.5 ml to 15.5 ml. F) UV trace corresponding to gel filtration standards (Bio-Rad, 1511901) using the column and conditions as panel E. Peaks 1 to 5 correspond to proteins of known molecular weight; 670 kDa, 158 kDa, 44 kDa, 17 kDa and 1.35 kDA, respectively. Peak 1 shows degradation of the 670 kDa protein. G) Flow diagram providing an overview of the stages of MTR4 purification.

For expression of NOP53, a modified pET24d construct was used which allowed an N-terminal GST tag to be added to both NOP53 WT and NOP53 D90R. Induction of expression by IPTG treatment, failed to show any change in expression levels of either GST-NOP53 WT or GST-NOP53 D90R across multiple timepoints and temperatures (Figure 3.5). Whilst no obvious expression could be seen by Coomassie staining, this was also observed for *C. thermophilum* Nop53 which was still able to be successfully purified (Thoms *et al.,* 2015). Human NOP53 has relatively high sequence similarity *C. thermophilum* Nop53, therefore, an attempt to purify human GST-Nop53 WT and D90R was carried out based up the purification protocol for *C. thermophilum* NOP53 (Thoms *et al.,* 2015). This involved cation exchange chromatography using SP sepharose, followed by an affinity purification step, utilising the GST affinity tag binding to glutathione (GSH) agarose (Figure 3.6). Despite no observed expression in the induction test for either GST-NOP53 WT or GST-NOP53 D90R (Figure 3.5), both can first be purified using SP sepharose and shown to bind GSH agarose (Figure 3.6 A, B, lane GSH B). GST-NOP53 WT could be efficiently eluted from GSH agaorse using glutathione (Figure 3.6 C). In contrast, while GST-NOP53 D90R can be immobilised on GSH agarose beads, no protein corresponding to the approximate size of GST-NOP53 D90R (85 kDa) appears to be eluted upon incubation with glutathione and remained bound to the GSH agarose (Figure 3.6 C).

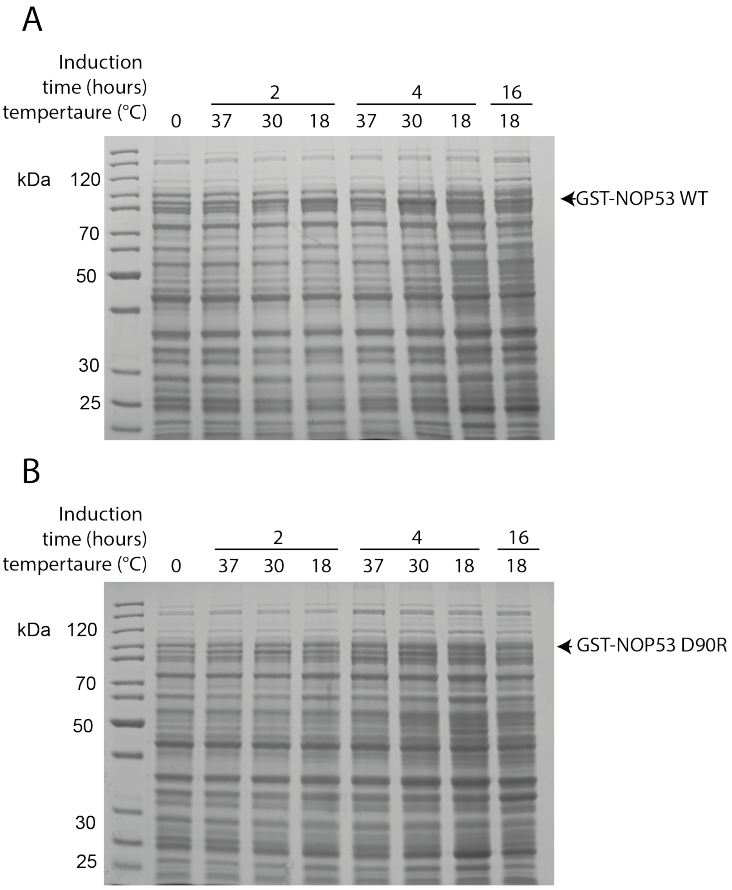


Figure 3.5: Induction of GST-NOP53 WT and GST-NOP53 D90R. A) Expression of GST-NOP53 WT was induced in BL21 *E.coli* with 0.1 mM IPTG for 2 hours and 4 hours at three different temperatures, 18, 30 and 37 °C and overnight for 16 hours at 18 °C and compared with no induction at 0 hours. B) Expression of GST-NOP53 D90R after induction at the same timepoints and temperatures as WT.

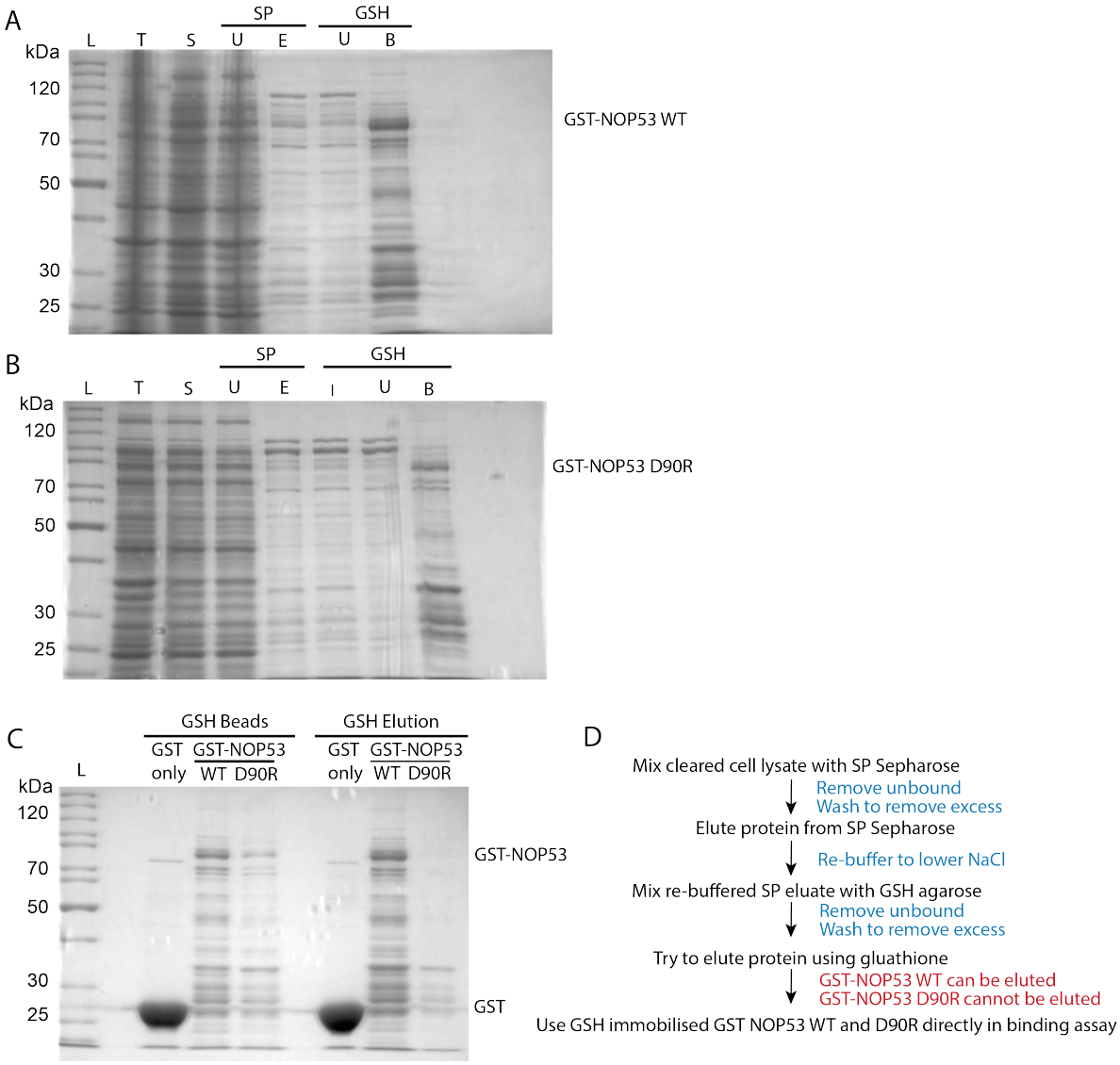


Figure 3.6: Purification of GST-NOP53 WT and GST-NOP53 D90R A) GST-NOP53 WT two-step purification. Labelling as follows; ladder (L), 0.1 % total (T), 0.1 % soluble (S), 0.1 % SP sepharose unbound (U), 1 % SP sepharose eluate (SP E), 1 % GSH unbound (U) and 1 % GSH beads (B). GST-NOP53 bound to GSH agarose was used for an *in vitro* binding assay. B) GST-NOP53 D90R two-step purification. Labeling as above with additional lane: 1 % GSH unbound (U). NOP53 within the SP eluate is in high salt (600 mM NaCl) and was diluted 1:4 in no salt buffer for GSH input. C) Test elution from GSH agarose using glutathione (20 %) and bead samples (2 %) following elution for GST-NOP53 WT (panel A, lane GSH B) and GST-NOP53 D90R (panel B, lane GSH B) with recombinant GST only used as a control for GSH binding and elution. D) Flow diagram summarising the stages of GST-NOP53 purification.

Numerous low molecular weight bands can be observed migrating under the full-length GST-NOP53 WT and D90R (approximately 85 kDa in size), likely corresponding to truncated or degraded fragments of NOP53. It is challenging to remove these, as no final gel filtration step could be carried out due to the inability to elute NOP53 D90R. An alternative purification strategy was therefore sought, and a Strep-tag was added to the GST-NOP53 constructs. The Strep-tag is minimal in length at only eight residues, it is both sensitive and selective and enables one-step purification strategies (Schmidt & Skerra, 2007). Subse-

quently, a C-terminal Strep-II tag was introduced to the GST-NOP53 constructs to produce GST-NOP53-Strep-II WT and D90R. A one-step streptactin purification was carried out and yielded a purer NOP53 for both WT and D90R, with fewer lower molecular weight (LMW) bands visible, than the previous two-step purification (Figure 3.7). However, this tag/purification strategy, yielded far less NOP53 WT than that of NOP53 D90R (Figure 3.7), but was still sufficient for use in a binding assay. GST only was also recombinantly expressed and bound to GSH agarose in a one-step purification (Figure 3.8) for use as a negative control in the binding assays (Figures 3.11, 3.12).

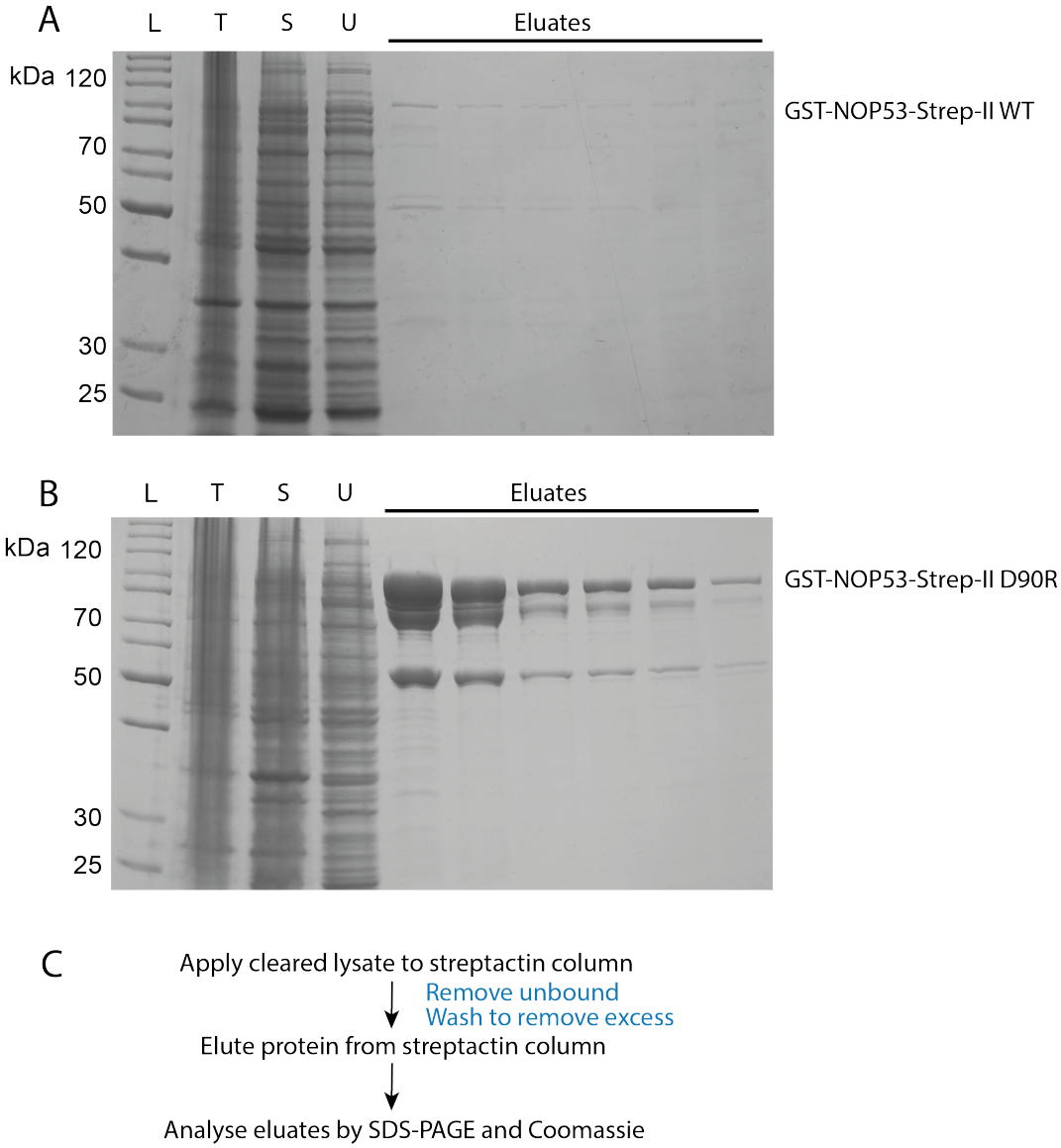


Figure 3.7: One-step purification of GST-NOP53-Strep-II WT and D90R. A) GST-NOP53-Strep-II WT purification using streptactin. Labeling as follows; Ladder (L), 0.1 % Total (T), 0.1 % Soluble (S), 0.1 % Unbound (U) and 1 % Eluates. B) GST-NOP53-Strep-II D90R purification using streptactin. C) Flow diagram summarising the stages of GST-NOP53-Strep-II purification.

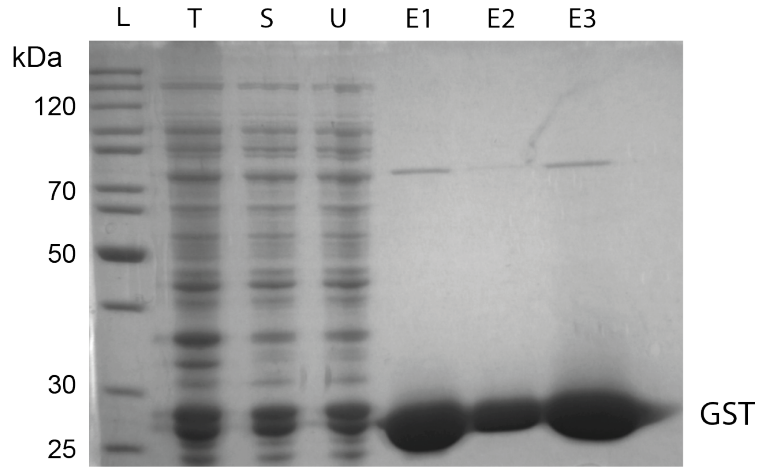


Figure 3.8: GST-only one-step purification using GSH agarose. Labelling as follows; Ladder (L), 0.1 % Total (T), 0.1 % Soluble (S) and 0.5 % Eluates (E1, E2, E3).

Recombinant NOP53 fused to a GST tag was proving problematic. GST-NOP53 D90R is unable to eluted from GSH agarose (Figure 3.6) and GST-NOP53-Strep-II failed to bind to GSH (Discussed below, Figure 3.11). Therefore, an affinity tag displaying better properties for purifications was sought. As both NOP53 WT and D90R were able to be purified via a Strep-II tag, this affinity tag was selected. However, since the GST tag was going to be removed, the Strep-II tag would be needed for both NOP53 purification and the subsequent binding assay. A Twin-Strep-II tag, consisting of two Strep-II tags connected by a linker, is compatible with magnetic streptactin beads (IBA, MagStrep XT beads) which would allow the binding assay to be carried out.

In addition to changing the affinity tag, the nucleotide sequence of human NOP53 was also codon optimised for expression in *E. coli* to improve purification yield. The *E. coli* strain used for expression, BL21 CodonPlus (Agilent), contains additional copies of genes encoding tRNAs to improve translation of the rare codons. However, the nucleotide sequence of NOP53 contains a high number of rare codons. When NOP53 was codon optimised, by changing a synonymous codon to encode the same protein sequence, sequence similarity with wild-type NOP53 was less than 75 %. The rare codons found in human NOP53 may have limited expression in *E. coli* and were optimised with the aim to improve protein production.

Subsequently, four constructs were produced; pET24d Twin-Strep-II (TSII) NOP53 WT and D90R and codon-optimised TSII-NOP53 WT and D90R. Expression was then induced by IPTG in BL21 *E. coli* and expression analysed by Coomassie staining (Figure 3.9). Both codon optimised TSII-NOP53 WT and D90R showed expression of NOP53 in induced samples (panels C and D) whereas non-codon optimised TSII-NOP53 protein expression could not be observed in induced samples by Coomassie staining (panels A and B). This was previously the case with GST-NOP53 (Figure 3.5), whilst no expression was observed following induction, the protein could still be purified. Consequently, due to the observed induction and potentially improved levels of expression, codon optimised TSII-NOP53 WT and D90R were used further. A single step streptactin purification was carried out on both WT and D90R TSII-NOP53 (Figure 3.10). Both TSII-NOP53 WT and D90R showed similar protein banding on Coomassie stained SDS gels following purification with the 'eluate' fractions showing a high level of proteins present within the 20-30 kDa range.

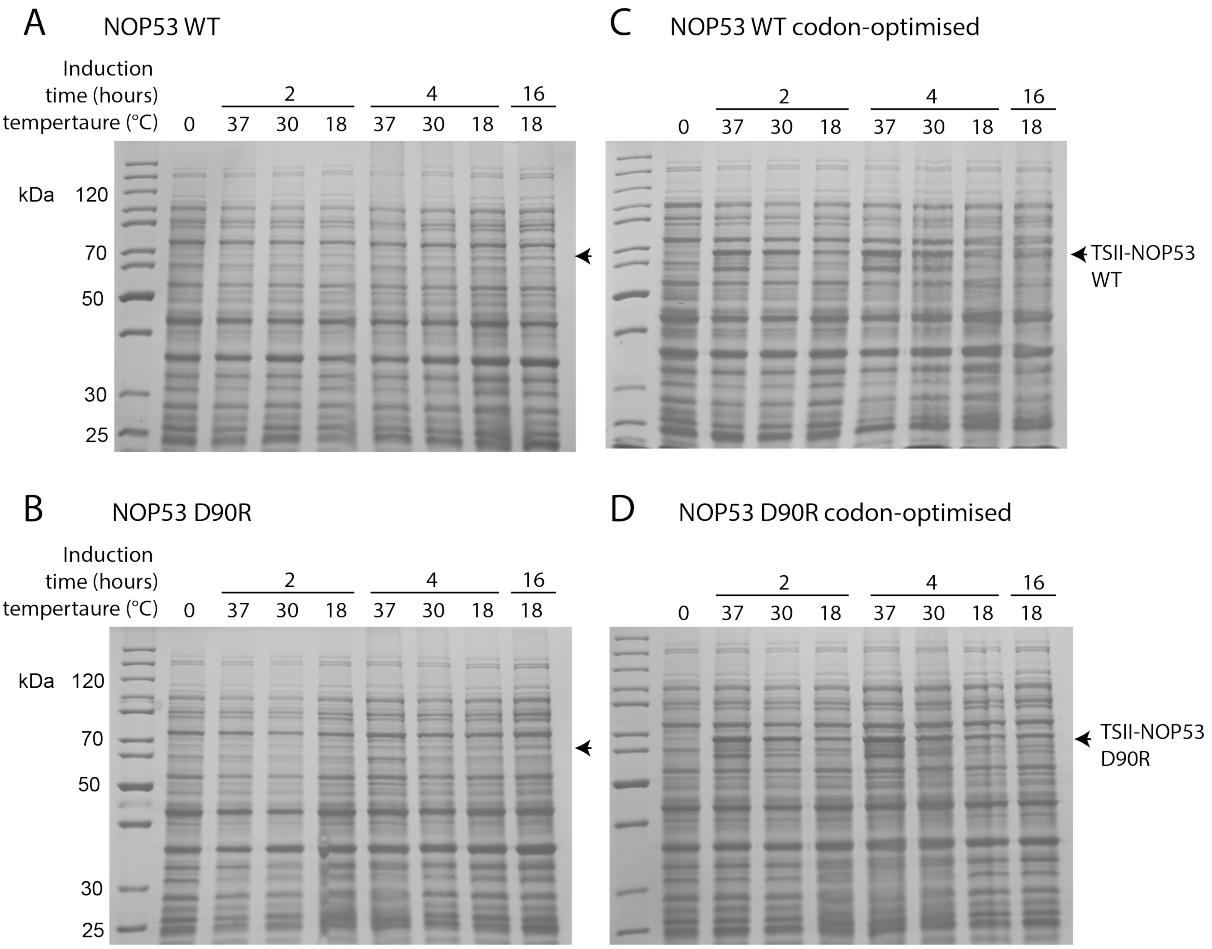


Figure 3.9: Induction of non-codon optimised Twin-Strep-II-NOP53 WT and D90R and codon optimised Twin-Strep-II-NOP53 WT and D90R. A) Expression of non-codon optimised TSII-NOP53 WT was induced using 0.1 mM IPTG at 2 hours and 4 hours at 3 different temperatures, 18, 30 and 37 °C and overnight for 16 hours at 18 °C and compared with no induction at 0 hours. B) Expression of non-codon optimised TSII-NOP53 D90R after induction. C) Expression of codon optimised TSII-NOP53 WT after induction. D) Expression of codon optimised TSII-NOP53 D90R after induction.

The aim of changing the tag on NOP53 for recombinant purifications was to improve the purity of NOP53 and enable *in vitro* binding assays to be carried out with ease, with codon optimisation to improve NOP53 expression. However, purification of codon-optimised TSII-NOP53 WT and D90R resulted in lower yields of NOP53 when compared with GST-NOP53, in addition to higher levels of LMW bands. Consequently, it was decided that GST-NOP53 would be used for further use in an *in vitro* binding assay. GST-NOP53 WT and D90R constructs were purified as described earlier for use in a binding assay.

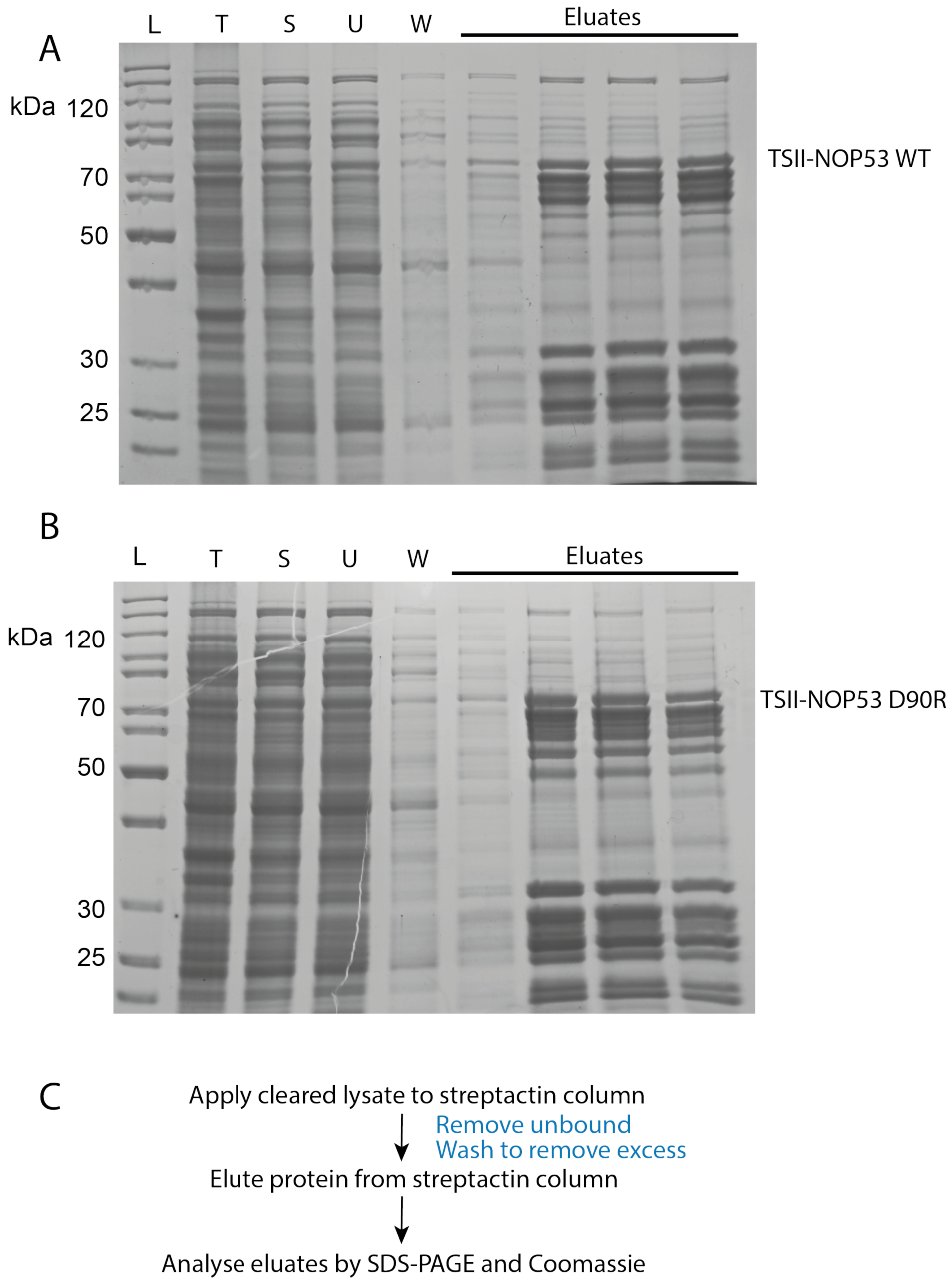


Figure 3.10: One-step purification of Twin-Strep-II-NOP53 WT and D90R. A) Twin-Strep-II-NOP53 WT purification. Labelling as follows; Ladder (L), Total (T), Soluble (S), Unbound (U), Wash (W) and Eluates. B) Twin-Strep-II-NOP53 D90R purification. C) Flow diagram summarising the stages of Twin-Strep-II NOP53 purification.

### *In vitro* binding assays

Purified GST-only (Figure 3.8), GST-NOP53-Strep-II WT and D90R were used in an *in vitro* binding assay as they had the highest level of purity and their yield was sufficient for a binding assay. GST-only, GST-NOP53-Strep-II WT and D90R (95 µM) (Figure 3.7) were mixed with His-MTR4 (190 µM) (Figure 3.4) and immobilised on GSH (Figure 3.11 A). However, neither GST-NOP53-Strep-II WT or D90R bound to the GSH agarose, with the GST-only tag being the sole protein present in the eluate (Figure 3.11 B). It is possible that the C-terminal Strep-II tag may interfere with the N-terminal GST tag preventing GSH binding, or alternatively, the GST-tag degrades and is lost from NOP53 as it is not used

during the purification process. Subsequently, as GST-NOP53-Strep-II is unable to bind to GSH, a *in vitro* binding assay using GST-NOP53 was carried out as despite the issues with eluting GST-NOP53 D90R both GST-NOP53 WT and D90R can be immobilised on GSH.

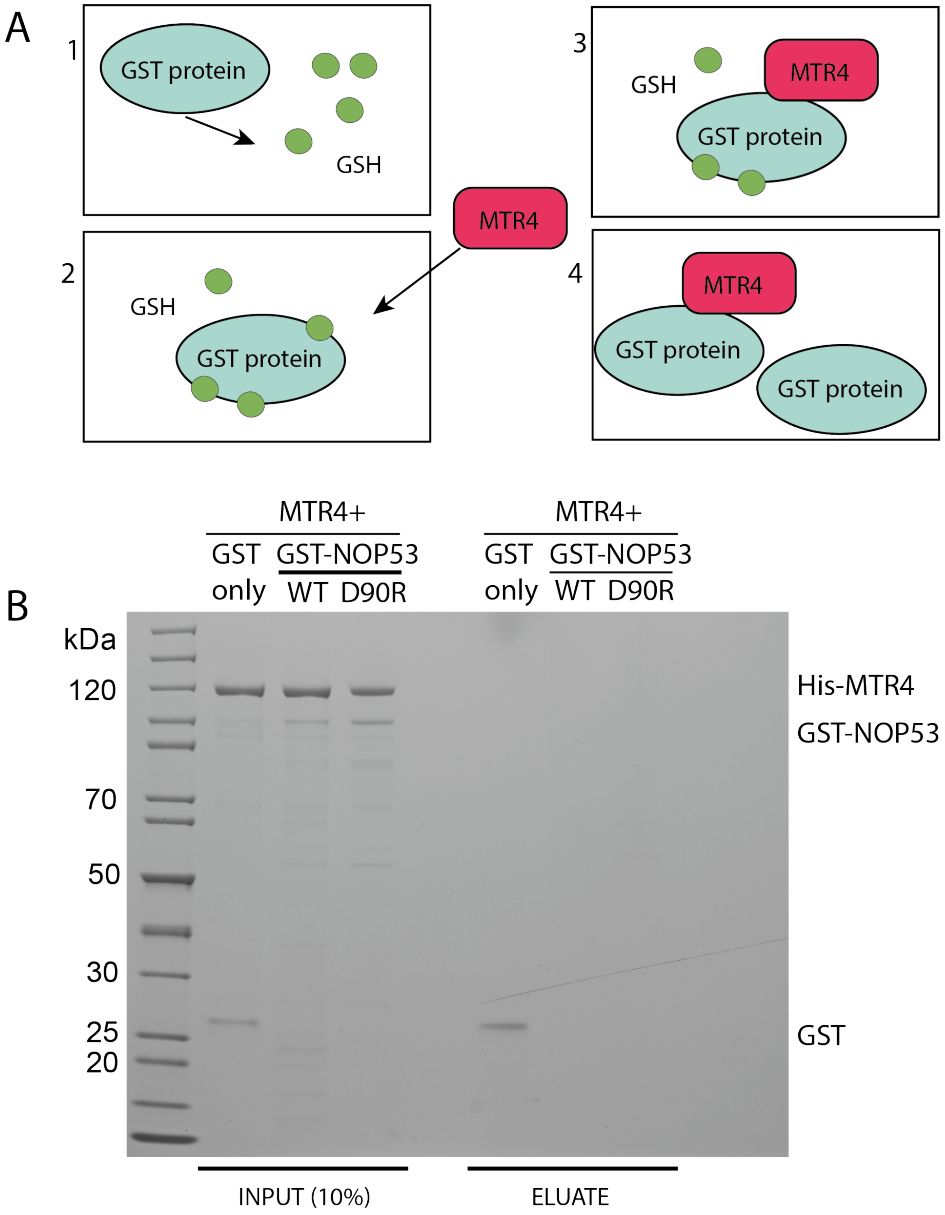


Figure 3.11: GST-NOP53-Strep-II and His-MTR4 *in vitro* binding assay. A) Schematic highlighting the steps of the binding assay (1-4). GST proteins are first incubated with purified MTR4 prior to mixing with GSH agarose. B) Coomassie stained SDS gel shows recombinantly purified His-MTR4 was mixed with either GST only, GST-NOP53-Strep-II WT or GST-NOP53-Strep-II D90R (10 % input). Each input was then bound to GSH agarose, washed and eluted to observe any MTR4 co-purification (70 % eluate).

Unlike the previous binding assay where GST-NOP53 and MTR4 are mixed prior to GSH binding, here GST-NOP53 is already bound to GSH agarose prior to the addition of MTR4 (Figure 3.12 A). GSH-immobilised GST only (Figure 3.8), GST-NOP53 WT and GST-NOP53 D90R (95 µM) (Figure 3.6) were mixed with the recombinantly purified MTR4 (190 µM) (Figure 3.4) to test binding (Figure 3.12). Consistent with the results from the yeast-two-hybrid analyses, GST-NOP53 was shown to bind to MTR4 (Figure 3.12, GST-NOP53

WT eluate). In contrast, GST-NOP53 D90R binding to MTR4 was substantially decreased, compared to WT NOP53, although residual binding can be seen (GST-NOP53 D90R eluate). This may partially be explained by residual non-specific binding as indicated by the low level of MTR4 observed in the GST only negative control (GST only eluate). Collectively, these results support those observed in yeast-two-hybrid analysis that a reverse charge mutation in the AIM of NOP53 (D90R) is sufficient to reduce the ability of NOP53 to bind to MTR4, supporting the idea that the AIM in human NOP53 mediates the interaction with MTR4.

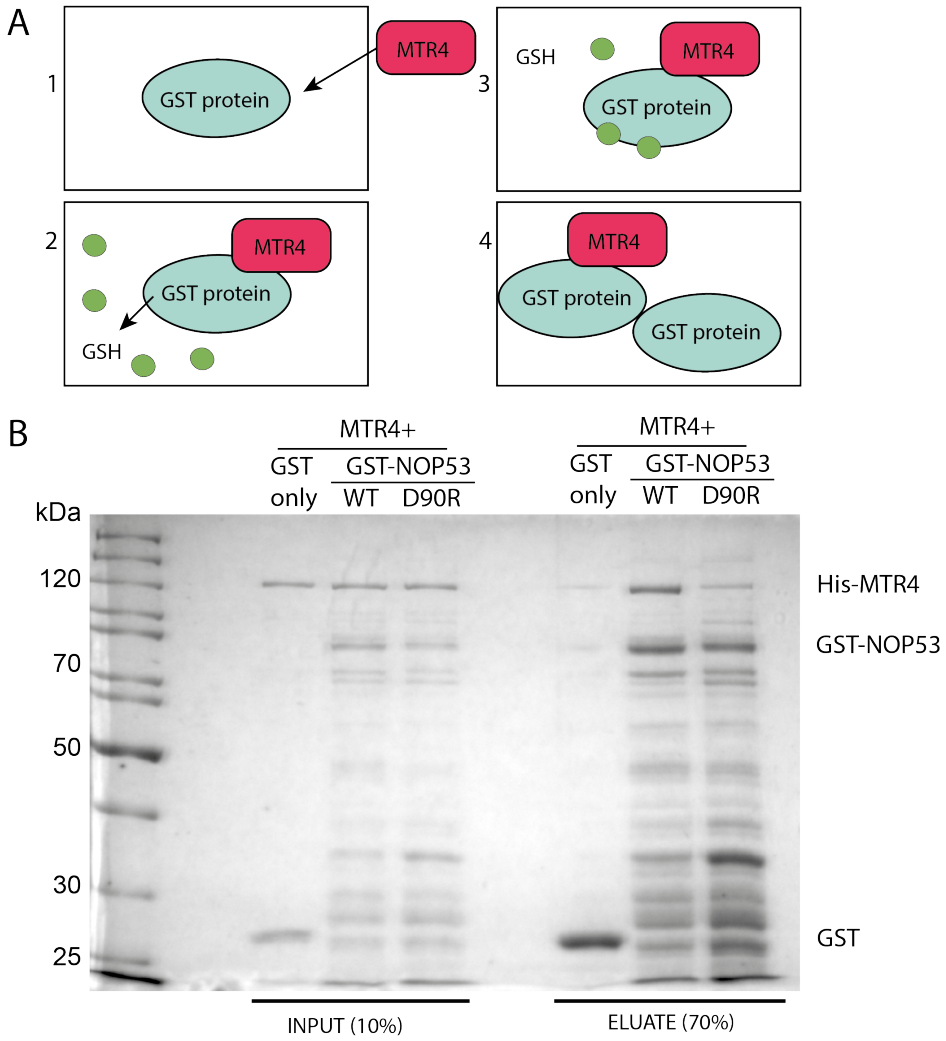


Figure 3.12: GST-NOP53 and MTR4 *in vitro* binding assay. A) Schematic highlighting the steps of the binding assay (1-4). GST proteins are immobilised prior to mixing with purified MTR4. B) Coomassie stained 4-12 % bis-tris SDS gel shows recombinantly purified His-MTR4 was mixed with either GST only, GST-NOP53 WT or GST-NOP53 D90R (10 % input). Each input was then bound to GSH agarose, washed and eluted to observe any MTR4 co-purification (70 % eluate).

### 3.2.2 *In vivo* analysis of NOP53 and MTR4

#### Generation of exogenously tagged NOP53 WT and D90R HEK293 cell lines

To determine if the interactions between MTR4 and NOP53 are observed in mammalian cells, the Flp-In T-REx system (Invitrogen) was used. Flp-In T-REx HEK293 cells were used to stably integrate 3xFLAG-6xHIS-NOP53 into the genome under the control of a tetracycline

inducible promoter that allows the expression of exogenous NOP53 to be regulated. An N-terminal tag was selected for NOP53 as previous studies in yeast had identified that while tagging of the C-termini disrupted association of NOP53 with pre-ribosomes, N-terminal tagging showed no such defects (Thoms *et al.*, 2015).

In order to generate the cell line, NOP53 and the point mutation studied *in vitro*, D90R were cloned into the pcDNA5/FRT/TO plasmid. The pcDNA5/FRT/TO plasmid additionally contains a hygromycin resistance marker and an FRT integration site. The genome of the parental Flp-In T-REx HEK293 cell line has been engineered to contain the FRT sites and when cells are co-transfected with pcDNA5/FRT/TO and the Flp recombinase (encoded by pOG44) a recombination event occurs at this FRT site which results in the integration of NOP53 into the genome (Figure 3.13).

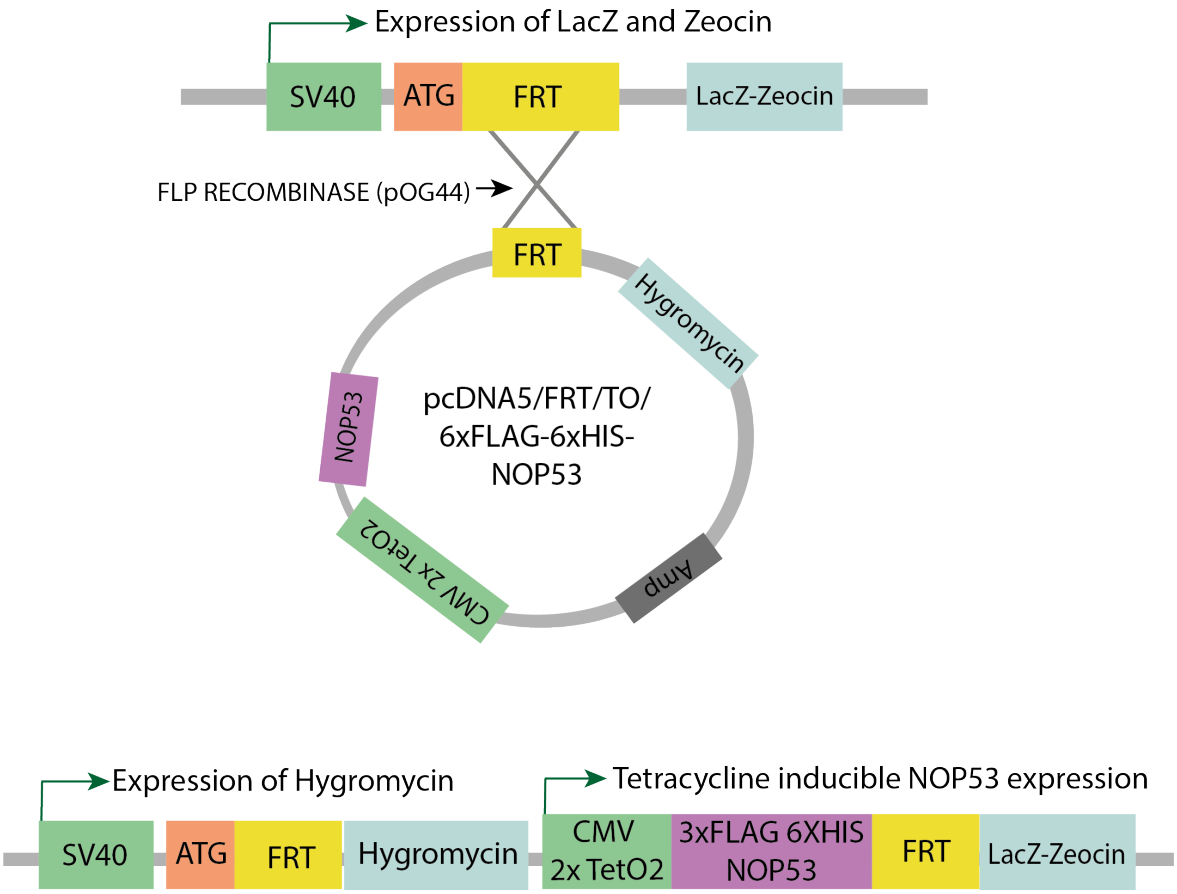


Figure 3.13: Integration of pcDNA5/FRT/TO/3xFLAG-6xHIS-NOP53 into the genome of Flp-In T-REx cell system from Invitrogen. Cell lines were generated using the FRT sites found on both the pcDNA5/FRT/TO plasmid and in the genome of the Flp-In T-REx HEK293 cell lines.

As shown in Figure 3.13, recombination results in the loss of constitutive expression of the zeocin resistance gene in the parental Flp-In T-REx HEK293 cell line and gain of hygromycin resistance when NOP53 has been successfully integrated. Subsequent hygromycin treatment leads to cellular death in cells lacking resistance and selects for cells successful in NOP53 integration. After allowing sufficient time for clonal growth, NOP53 expression can be induced by addition of tetracycline (Figure 3.14). In the absence of tetracycline there is no expression of NOP53 as tetR encoded by pcDNA6/TR, found in the parental cell line, binds

to the operator upstream of NOP53 and inhibits expression. However, when tetracycline is present, through addition to the culture medium, it binds to tetR and relieves inhibition on the operator allowing for transcription and expression of NOP53.

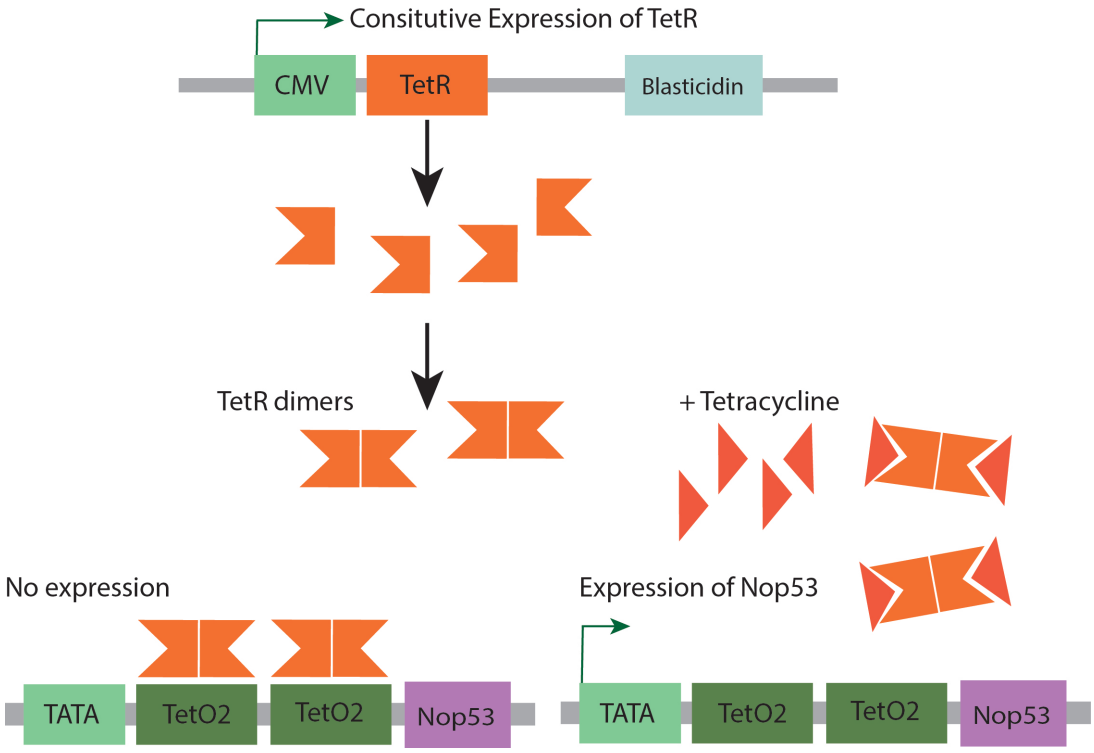


Figure 3.14: Induction of 3xFLAG-6xHIS-NOP53 expression upon addition of tetracycline. The Flp-In T-REx HEK293 cell has constitutive expression of the tetracycline repressor (TetR), which in the absence of tetracycline forms dimers and binds to the tetracycline operator (TetO2) inhibiting NOP53 expression. In the presence of tetracycline, tetracyline binds to the tetracyline repressor which inhibits binding to the operator allowing for activation of NOP53 expression.

Following hygromycin treatment, ten hygromycin resistant colonies were identified and validated for either 3xFLAG-6xHIS-NOP53 WT or D90R expression following tetracycline induction. Expression of NOP53 was observed in all twenty clones checked. Triplicate clones for both NOP53 (clones 3, 5 and 10, Figure 3.15 A, B and C, respectively) and NOP53 D90R (clones, 1, 2 and 10, Figure 3.15 D, E and F, respectively) were selected and expression was analysed varying both concentration of tetracycline used (0.5 or 1 µg/ml) and length of induction conditions (4, 8, 12 and 16 hours). Expression levels of NOP53 did not vary greatly at either concentration during the time course. Initially the aim was to titrate induction of FLAG-NOP53 to levels of expression similar to that of endogenous NOP53. However, expression of endogenous NOP53 is low and not visible for some clonal lines. Therefore, for subsequent experiments, induction conditions of 16 hours at 1 µg/ml tetracycline were selected. These conditions are convenient, the concentration is recommended by the manufacturer's protocol and induction time is within the range published for the cell line (Marin-Vinader *et al.,* 2006; Maryon *et a.,* 2007; Widberg *et al.,* 2009).

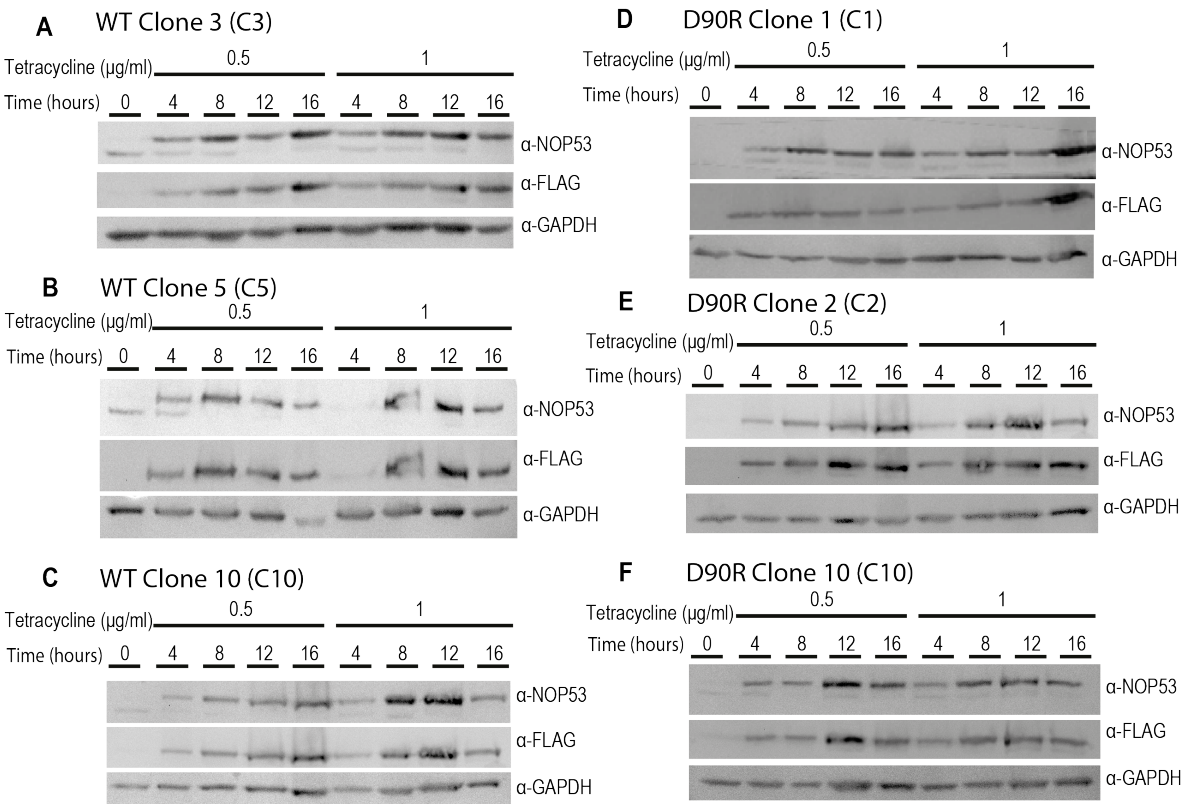


Figure 3.15: Induction 3xFLAG-6xHIS-NOP53 WT or D90R expression across triplicate cell lines. A) Expression of 3xFLAG-6xHIS-NOP53 in WT cell line clone 3 (C3) following tetracycline treatment at either 0.5 or 1 µg/ml for 4, 8, 12, or 16 hours. B) Expression of 3xFLAG-6xHIS-NOP53 in WT cell line C5. C) Expression of 3xFLAG-6xHIS-NOP53 in WT cell line C10. D) Expression of 3xFLAG-6xHIS-NOP53 D90R in DR cell line C1. E) Expression of 3xFLAG-6xHIS-NOP53 D90R in DR cell line C2. F) Expression of 3xFLAG-6xHIS-NOP53 D90R in DR cell line C10.

### NOP53 WT and D90R binding to MTR4 *in vivo*

Following the successful generation and validation of 3xFLAG-6xHIS-NOP53 WT and D90R cell lines, expression was induced using tetracycline. Co-immunoprecipitationS were subsequently carried out using the FLAG affinity tag to pull-down either NOP53 WT or NOP53 D90R. Western blot analysis of the co-immunoprecipitations showed that co-purificiation of MTR4 was reduced in the FLAG-NOP53 D90R compared to the FLAG-NOP53 wild-type (Figure 3.16). These co-immunoprecipitation results confirmed the results observed in both the yeast-two-hybrid system and binding assays and support the finding that mutation of the NOP53 AIM (D90R) is sufficient to reduce binding MTR4. The Western blot also showed that the D90R mutation had no effect on the ability of NOP53 to bind to RPL11, with both duplicate FLAG-NOP53 WT lines and duplicate FLAG-NOP53 D90R lines showing consistent levels of RPL11 present in the eluate.

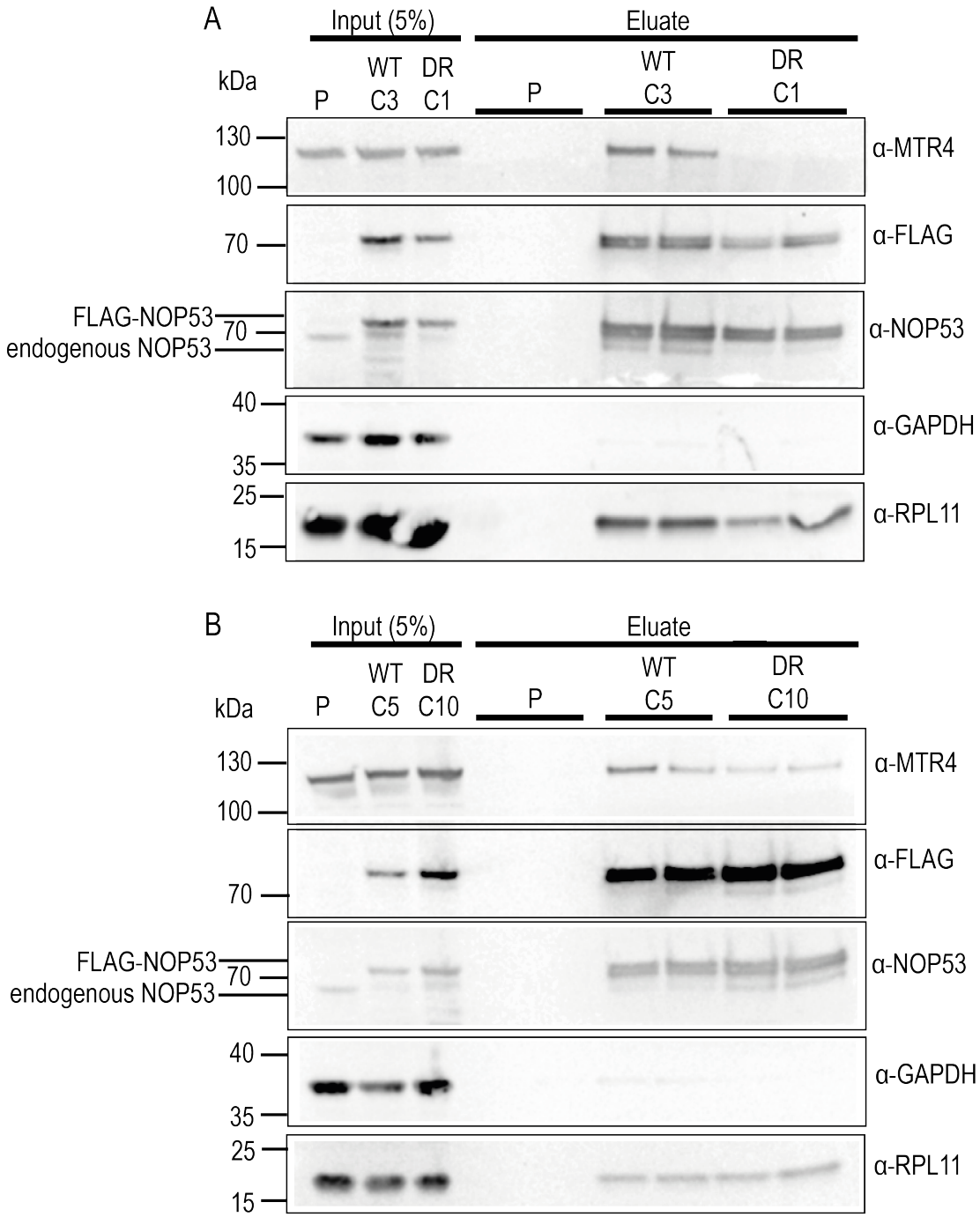


Figure 3.16: Co-immunoprecipitation from FLP-In-TREx-HEK293 patental cells and 3xFLAG-6xHIS NOP53 WT and D90R cell lines treated with 1 µg/ml tetracycline for 16 hours overnight. A) Western blot showing input (5 %) and duplicate IP samples for parental Flp-In-TREx-HEK293 cells (P), NOP53 WT clone 3 (WT C3) and NOP53 D90R clone 1 (DR C1). B) Western blot showing input (5 %) and duplicate IP samples for parental Flp-In T-REx HEK293 (P), NOP53 WT clone 5 (WT C5) and NOP53 D90R clone 10 (DR C10). The same membrane for each panel was sliced and probed with antibodies for MTR4, FLAG, NOP53, GAPDH and RPL11.

### 3.2.3 Developing a system for phenotypic analysis of NOP53 D90R using FLAG-NOP53 WT and D90R HEK293 cell lines

As the results presented show, the equivalent mutation in the AIM of human NOP53, D90R, as in *S. cerevisiae*, results in the loss of interaction with MTR4 (Thoms *et al.,* 2015). In *S. cerevisiae* this loss of interaction between NOP53 and MTR4 resulted in an accumulation of 5.8S rRNA precursors. Therefore, as the site of interaction is conserved, investigations looked to see if any defects in rRNA processing were caused by the loss of association between NOP53 D90R and MTR4, and if so, is the defect conserved.

The Flp-In T-Rex HEK293 NOP53 WT and D90R cells previously discussed, were now used to try and analyse rRNA processing following exogenous expression of FLAG-NOP53 or FLAG-NOP53 D90R. However, the endogenous copy of NOP53 present in the cell lines must first be depleted. In order to do this a strategy was developed using siRNAs to knockdown endogenous NOP53. Both the endogenous NOP53 and the inserted FLAG-NOP53 contain the same coding sequence and therefore, siRNAs could not be designed against this sequence without knocking down both endogenous and exogenous NOP53 copies. Therefore, the 3' UTR was targeted as it is only in the endogenous NOP53.

For designing the siRNAs to the 3'UTR of NOP53, the Horizon siDESIGN tool was used. The 3'UTR of NOP53 is 52 nucleotides in length (Gene ID: 29997), with the siDESIGN tool able to produce up to 50 siRNAs for this region. Two siRNAs were selected in order to limit any off-target effects and increase chances of knockdown. The siRNAs were chosen based upon their GC content with the aim being as close to 50 % as possible and also their 'score'. The score out of 100 is defined by Horizon as 'an algorithmic indicator of the likelihood of successful silencing with this siRNA design'. Therefore, the two siRNAs selected were non-overlapping to prevent both having potential off-target effects, the first had a score of 81 with GC at 42 % and the second, a score of 77 and GC at 47 %.

Each of the siRNAs for the 3'UTR of NOP53 were ordered from IDT along with scrambled (sc) versions of each siRNA where the bases were rearranged to act as a negative control. An siRNA for MTR4 (previously designed and tested by Monika Feigenbutz) was used as a positive control. MTR4 depletion should result in an rRNA processing defect due to loss of interaction with NOP53, meaning a phenotype should be observed even if the NOP53 D90R mutation is not capable of causing a defect. The two NOP53 siRNAs alongside the respective negative scrambled siRNAs and the MTR4 siRNA were transfected into duplicate FLAG-NOP53 WT (Clones 3 and 5) and duplicate FLAG-NOP53 D90R (Clones 1 and 10) HEK293 cell lines. Tetracycline treatment was then used to induce expression of FLAG-NOP53 WT or D90R in each of the cell lines, with expression and siRNA knockdown analysed by Western blot (Figure 3.17). The MTR4 siRNA used as a positive control showed partial knockdown in MTR4 expression in the cell lines tested. Exogenous FLAG-NOP53 WT or D90R was expressed following tetracycline treatment in all four cell lines with both NOP53 siRNA 1 and 2 showing reduced expression of endogenous (WT-NOP53) protein when compared with the respective scrambled siRNA (sc1/ sc2) or siRNA-untreated cells. Consequently, confirmation by Western blot of partial endogenous NOP53 knockdown and expression of FLAG-NOP53 WT or D90R, means rRNA processing can be analysed using this system.

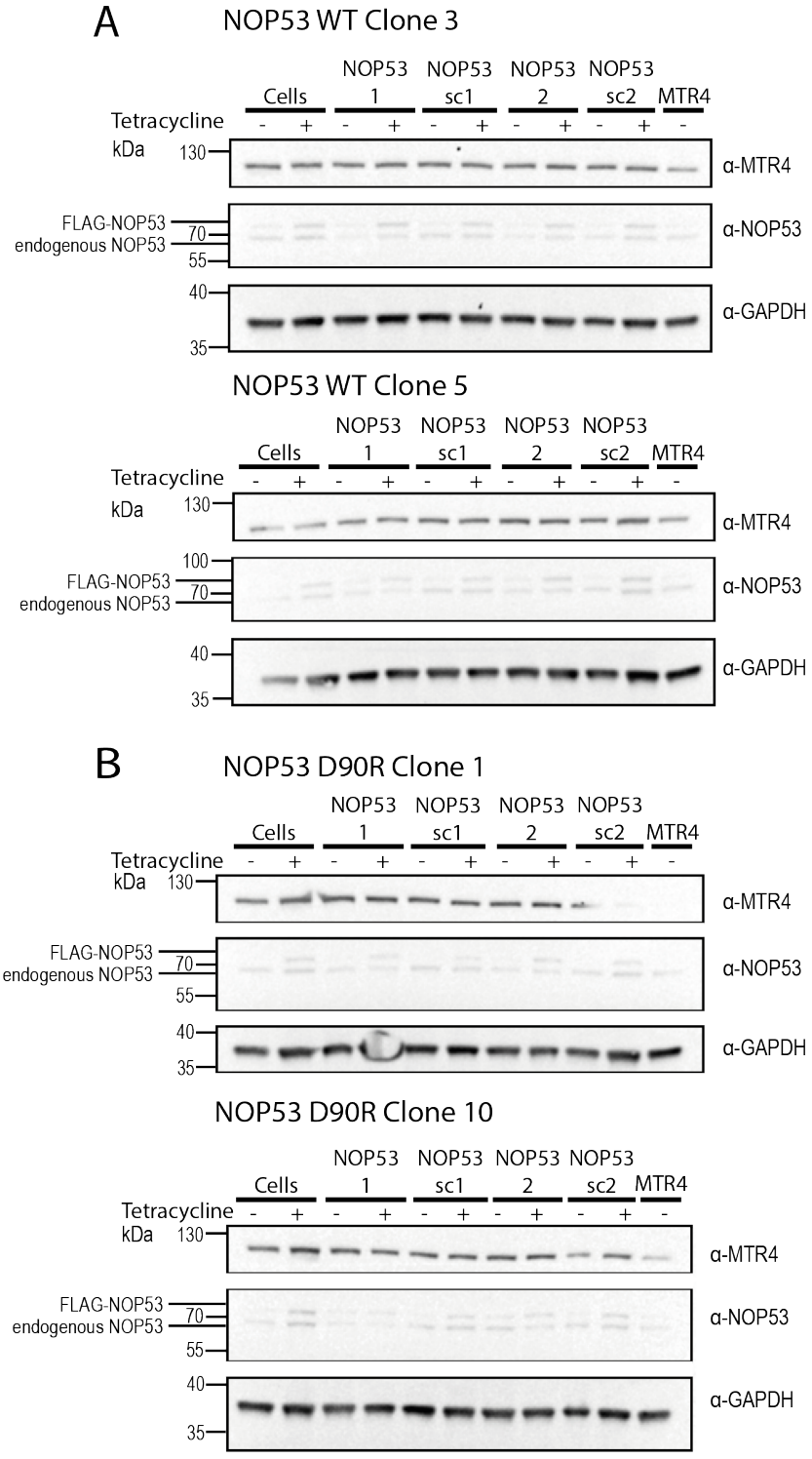


Figure 3.17: siRNA treatment of duplicate Flp-In T-REx HEK293 3xFLAG-6xHIS NOP53 WT and D90R cell lines. Western blot with and without 1 µg/ml tetracycline treatment for siRNA untreated cells and siRNA treated cells for NOP53 siRNA 1, NOP53 siRNA scrambled (sc) 1, NOP53 siRNA 2, NOP53 siRNA scrambled (sc) 2 or MTR4 siRNA without tetracycline treatment. A) Flp-In T-REx HEK293 FLAG-NOP53 WT Clone 3 B) Flp-In T-REx HEK293 FLAG-NOP53 WT Clone 5. C) Flp-In T-REx HEK293 FLAG-NOP53 D90R Clone 1. D) Flp-In T-REx HEK293 FLAG-NOP53 WT Clone 10. The same membrane was sliced and probed with antibodies for MTR4, NOP53 and GAPDH.

## 3.3 Discussion

In this chapter the interaction between NOP53 and MTR4, first studied in *S. cerevisiae*, has been characterised in humans. As well as showing a high level of sequence conservation across eukaryotes to humans, the AIM identified in *S. cerevisiae* Nop53 also mediates the interaction between human NOP53 and MTR4 where a single point mutation is able to disrupt the interaction (D90R). Three separate approaches were used to validate the interaction; yeast-two-hybrid analysis, an *in vitro* binding assay and the generation of FLAG-NOP53 inducible HEK293 cells lines.

Yeast-two-hybrid analysis was used to initially confirm an interaction between NOP53 and MTR4 and showed the interaction was disrupted following the introduction of a point mutation in the AIM (D90R). Whilst this was confirmed using recombinant proteins and an *in vitro* binding assay, residual binding of NOP53 D90R with MTR4 was observed. This may be explained due to non-specific binding between GST and MTR4, and would ideally be repeated by increasing the stringency of wash steps to remove an excess MTR4 bound to GST only.

Through the generation of FLAG-NOP53 HEK293 cell lines, the interaction between MTR4 and NOP53 was confirmed within a cellular system. Co-immunoprecipitations using FLAG-NOP53 D90R cell lines showed a loss of interaction with MTR4 when compared with FLAG-NOP53 WT cell lines. However, there was no impact on the ability of NOP53 D90R to bind to RPL11. Therefore, the NOP53 D90R mutant can be used as a separation of function mutant to study the role of NOP53 in ribosome biogenesis as it uncouples NOP53 from MTR4 whilst maintaining the interaction with RPL11. Some binding between MTR4 and NOP53 D90R could still be observed in FLAG-NOP53 D90R Clone 10, therefore, an alternative clonal line may be needed, if this limited loss of interaction between MTR4 and NOP53 D90R does not lead to a phenotype. Further work using these FLAG-NOP53 cell lines could also look to see any association between NOP53 and other exosomal components, for example RRP6, and if the D90R mutation leads to a similar loss of interaction observed with MTR4.

The findings presented here, that the AIM of NOP53 also mediates the interaction with MTR4, in humans is also supported by recently published data (Miyao *et al.,* 2022). Here, three NOP53 AIM mutants (D90A, L86A/F87A, and L86A/F87A/D90A) were transiently transfected into HEK293 cells where they showed a loss of association with MTR4 when compared to WT NOP53. An accumulation of the 12S precursor was also observed in these mutants following Northern analysis. Therefore, in addition to the mechanisms of interaction, the function of the interaction between MTR4 and NOP53 is also conserved from yeast to humans. In both cases the interaction between NOP53 and MTR4 is necessary for 3' end processing of 5.8S rRNA during 60S biogenesis.

To be able to analyse the effects of D90R mutation on ribosome assembly, we wished to deplete the endogenous NOP53 from the FLAG-NOP53 WT and D90R inducible HEK293 cell lines. The siRNAs designed for NOP53 in these cell lines, which annealed to the 3' UTR, showed limited knockdown in expression levels. Therefore, the siRNAs may require further optimisation to see a phenotype. Numerous siRNA sequences for the ORF of NOP53 have been published and shown to cause successful knockdown (Sloan *et al.,* 2013; Miyao *et al.,* 2022). However, the coding sequence for FLAG-NOP53 would need to be edited for synonymous amino acids and the Flp-In T-REx HEK293 cell lines remade to ensure only endogenous NOP53 knockdown.

Whilst HEK293 cells have been used here to first validate and characterise the interaction between NOP53 and MTR4 *in vivo* through the D90R mutation, they have limitations. HEK293 cell lines are an immortilised cell line, and like many other cell lines, have adapted to tissue culture conditions. This can involve both the gain and loss of chromosomes or chromosomal regions and gain of mutations which provide growth or survival advantages. Consequently, when studying ribosome biogenesis, a vital cellular process inherently linked to cell growth and proliferation, it is important to use a controlled cellular system displaying expected rates of cell growth and proliferation. Whilst HEK293 cells are robust and useful for biochemical analysis, when investigating cellular phenotype, alternative cell types need to be considered. HEK293 cells have high levels of constitutively active p53 (Löber *et al.,* 2002), and other commonly used cell lines have a propensity to gain p53 mutations that are strikingly similar to those observed in tumors (Berglind *et al.,* 2008). Therefore, when the aim is to uncouple ribosome biogenesis and nucleolar stress response, a system suitable for phenotypic analysis, in which NOP53 D90R can be functionally analysed is needed.

# Chapter 4

# Generation of hPSC clonal cell lines containing the NOP53 D90R mutation using CRISPR-Cas9

## 4.1 Introduction

In humans, the interaction between NOP53 and MTR4 has been shown to be mediated by the AIM of NOP53, with a singular point mutation (D90R) sufficient to substantially diminish the interaction. Whilst the methodologies and experimental systems used in chapter 3 were sufficient for validating the mechanism of interaction, they are not sufficient for investigating the phenotypic consequences of the loss of interaction between NOP53 and MTR4.

Ribosome biogenesis, and by association NOP53, are inherently linked to cell growth and proliferation. Alterations in ribosome biogenesis have significant effects on protein production and subsequent cellular function, with the increase or decrease in rate of ribosome synthesis driving and restraining cell growth and proliferation, respectively (Stepiński, 2008). Due to this property, dysregulation of ribosome biogenesis has often been used in the characterisation of tumorigenic cells (van Sluis & McStay, 2015). Over 50 % tumorigenic cells are known to contain mutations in p53 (Toledo & Wahl, 2006). In cells lacking p53 mutations, dysfunctional ribosome biogenesis triggers the nucleolar stress response, p53 stabilisation and cell cycle arrest. However, in tumorigenic cells with p53 mutations no such arrest in the cell cycle can occur, leading to uncontrolled cellular growth. As RPL11 regulates p53, and NOP53 sequesters RPL11 during homeostatic conditions, both RPL11 and NOP53 are implicated in tumorigenesis. Therefore, to fully investigate the role of NOP53 in nucleolar function, a controlled cellular system is required to study the NOP53 D90R mutant.

Stem cells are pluripotent, actively dividing, karyotypically normal cell lines (Yamanaka, 2012; Zakrzewski *et al.,* 2019), meaning they provide an excellent system in which to study NOP53 and ribosome biogenesis. Stem cells contain only two copies of each chromosome and as they are actively dividing, they are actively synthesising ribosomes. There are numerous clinical-grade stem cell lines available to use from the UK Stem Cell Bank, but the cell line MasterSheff11 is p53 positive and has been previously used to generate a point mutation by CRISPR-Cas9 (Butler *et al.,* 2022) and therefore was selected for this study.

### 4.1.1 CRISPR-Cas9 System

CRISPR-Cas9 is a two-component system developed for targeted gene editing. CRISPR has been used in a number of cell types including those which have previously been challenging to edit. Cas9 has been used widely in human stem cell research for the introduction of knockdowns and mutations (summarised in Zhang *et al.,* 2017). Cas9 is a dual endonuclease enzyme which introduces double strand breaks into DNA as directed by a specific guide RNA (sgRNA). The sgRNA enables specificity of the system to target the Cas9 to the genomic location of interest. The sgRNA is comprised of two components; a CRISPR RNA (crRNA) which is a short nucleotide sequence (17-21 nucleotides) specific to your target genomic region and a *trans*-activating RNA (tracrRNA) which serves as the scaffold for Cas9 binding to enable its nuclease activity. The sgRNA can then duplex with the Cas9 to enable targeting of the enzyme to the desired location.

Following Cas9 association with the genomic location, its nuclease activity introduces double strand breaks (DSBs) to the DNA. Within the cell there are two distinct and complementary mechanisms for DSB repair; non-homologous end joining (NHEJ) and homology directed recombination (HDR) (Khanna & Jackson, 2001). In NHEJ, proteins bind to the DNA termini at the double strand break mediating its re-ligation, whereas HDR involves the use of complementary sister chromatids as a template for repair. Of the two approaches NHEJ is more error-prone but also thought to be the pre-dominant mechanism of DSB repair in higher eukaryotes (Shrivastav *et al.,* 2008). After Cas9 cleavage, NHEJ can be used to create knockout mutations through the induction of frameshifts resulting in pre-mature stop codons, whereas HDR can be used to introduce specific mutations or tags using an exogenous template such as single-stranded oligonucleotide (ssODN). Depending on the size of the mutation required the homolgous regions, known as homology arms, found on the repair template can be as little as 30 nucleotides in length to several hundred (Schubert *et al.,* 2021).

Although Cas9 is required for the initial cleavage of the DNA, its persistence within the cell can be modified depending on the experimental set-up which may or may not be beneficial. Plasmid based systems can lead to the stable integration of the Cas9 sequence. In this instance initial editing takes longer as the Cas9 enzyme must first be transcribed and translated but also is present in the cell for longer and therefore can repeatedly cut the DNA. Conversely, RNP based systems which involve transfection of the Cas9 protein leads to faster editing, but also faster degradation, limiting the chance of re-cutting. RNPs have also been shown to have higher editing efficiency in cell types which are difficult to transfect with large plasmids (Kim *et al.,* 2015; Liang *et al.,* 2015).

Experimental setup can be used to make identification of successfully edited cells with the desired mutation easier. If any components of the system, such as the Cas9, sgRNA or HDR template, are delivered by plasmid, antibiotic selection can be used. If an insertion or deletion has been introduced, enzymes which are involved in mismatch detection from bacterial systems known as T7E1 can be used. In a T7E1 assay, DNA is separated into its component strands and re-hybridised with the aim of producing edited DNA to control DNA with T7E1 cleaving at any mismatch sites which can be visualised by gel electrophoresis (Figure 4.1). If editing has involved the introduction of an affinity tag into the gene sequence of a protein of interest the tag can be used for Western analysis of the clonal protein extracts. In cases where a small specific edit, such as a point mutation, has been introduced it may be possible to either introduce or destroy a restriction enzyme site which can then be identified by enzymatic digestion. Following all cases, the exact mutation will need to be sequenced and protein expression confirmed.

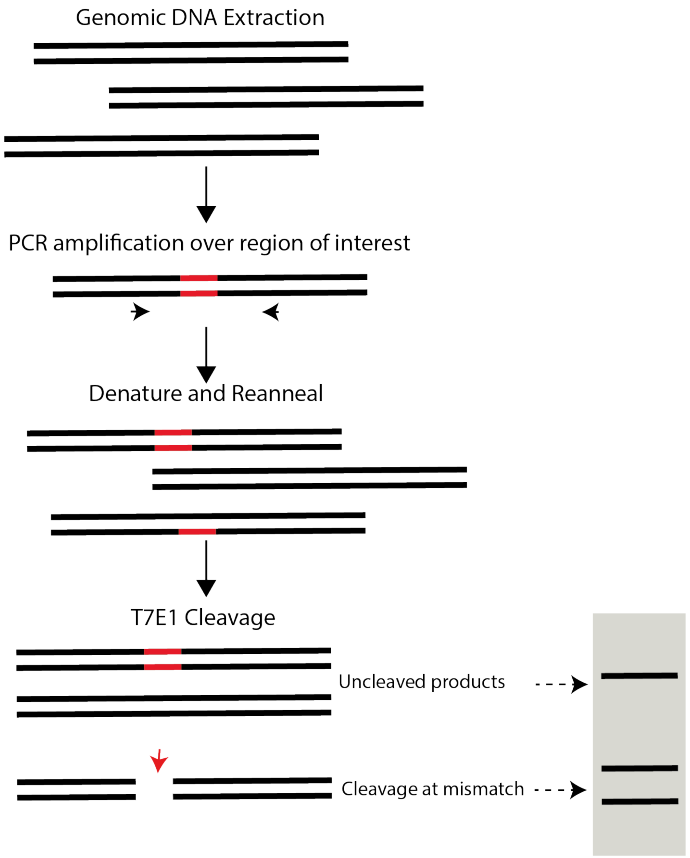


Figure 4.1: T7 Endonuclease I assay. Stages of DNA preparation prior to T7E1 cleavage. If the Cas9 has successfully cleaved the DNA at the target region, a PCR product of known size as well as smaller cleaved fragments will be visible by gel agarose electrophoresis.

As well as the desired mutation, sgRNAs may have 'off-target' effects whereby the sgRNA has some homology to other genomic regions resulting in Cas9 targeting to unintended sites. Tools exist which can predict these off-target sites meaning top hits can be checked for any off-target activity although this is subject to bias. Moreover, as stem cells are particularly prone to both the gain and loss of chromosomes and chromosomal regions during culture it is therefore essential to validate stem cells for any chromosomal aberrations following cell line generation (Andrews *et al.,* 2017; Kuijk *et al.,* 2020).

The following chapter explains the design and testing of CRISPR guides and HDR repair templates for the introduction of the D90R mutation into the NOP53 genomic sequence and the subsequent generation of clonal MasterSheff11 NOP53$^{WT/D90R}$ and NOP53$^{D90R/D90R}$ lines.

## 4.2 *In silico* design of gRNAs and repair templates

To introduce the specific mutation of D90R into NOP53 in hPSCs, CRISPR-Cas9 was selected due to its precise introduction of DSBs and specificity to allow HDR repair. To target Cas9 to the specific D90 region of NOP53 in the genome, sgRNAs were designed along with corresponding ssODNs to serve as the repair template to be used by the cells when repairing the break using the HDR pathway. Various online tools are available for the design of HDR donor templates and associated Cas9 guide RNAs, but in this instance IDT's Alt-R™ HDR Design Tool was used to identify the guides and repair templates for NOP53 editing. The

human reference genome (hg38), the *Streptococcus pyogenes* wild-type Cas9 and GLTSCR2 (NOP53, gene ID reference NM015710.4) were used as inputs for the design tool. IDT default homology arm lengths of 40bp were also utilised as part of the tool. ssODNs with 40bp homology arms have been shown to be highly efficient templates for HDR (Chen *et al.*, 2011; Davis & Maizels, 2014), and as the desired edit is only a few nucleotides, longer homology arms could decrease efficiency with longer homology arms preferred for the insertion of larger edits.

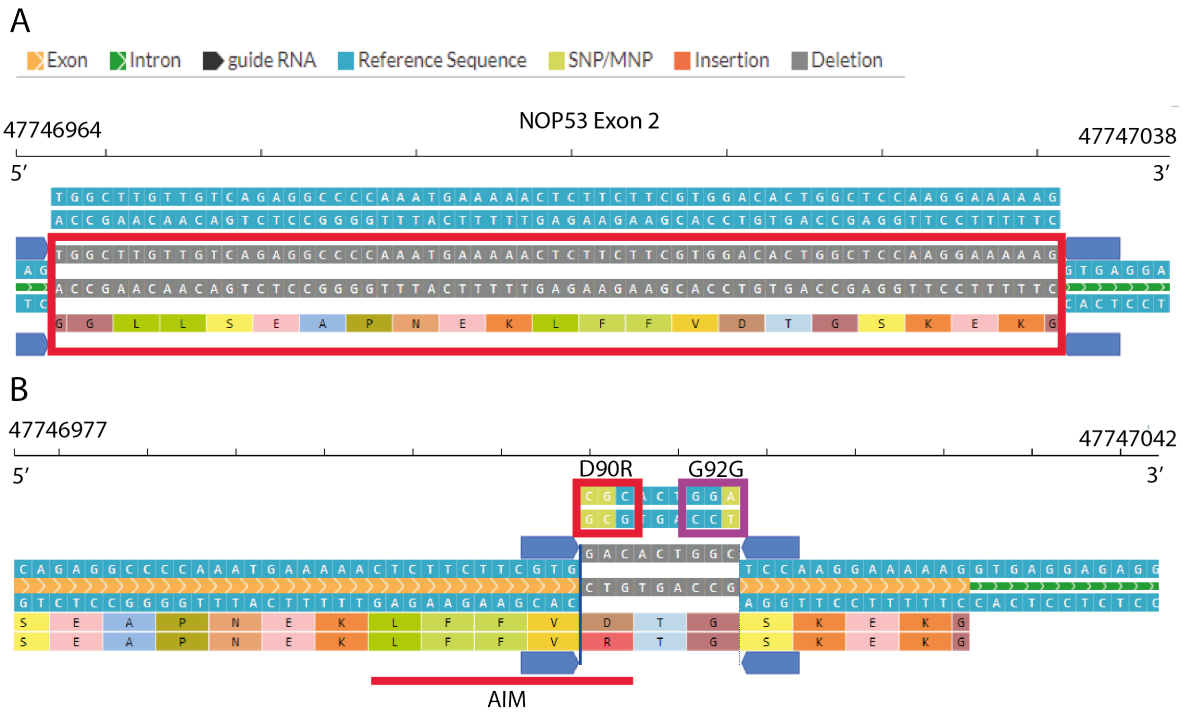


Figure 4.2: Region of exon 2 of NOP53 using the Alt-R™ HDR Design Tool from IDT. A) Expanded sequence showing exon 2 of NOP53 (NMC15710.4), both the 5' and 3' strand and the codon sequence (red box). B) Editing the region of exon 2 which encodes the AIM motif of NOP53, LFFVD (indicated by the red line). Edited bases are shown in light green with nucleotide changes to introduce the D90R mutation (red box) and the silent glycine to glycine (G92G) mutation (purple box).

The D90 codon is located within exon 2 of NOP53, therefore this region and the nucleotides required to introduce the D90R amino acid conversion were selected (Figure 4.2 A). An additional nucleotide, 7 nucleotides downstream of D90 was also selected for editing. In this instance, the mutation did not result in an amino acid change, still encoding a glycine (G92G), but at the nucleotide level the C to A transition created a BamHI restriction site. By introducing a BamHI site using a silent mutation close to the intended edit site of D90R on the same HDR template, screening of clonal lines without the need for sequencing will be possible. This is a particular advantage, since no other selection methods e.g. antibiotic, affinity tag, can be ultilised. After selecting for these 3 nucleotide changes, the software designed sgRNAs to this region and produced a corresponding HDR template (Figure 4.3 and 4.4). Guides were ranked out of 100 based upon their specificity in terms of on- and off-target effects. Two of the highest ranking guides for both on- and off-target effects (scored out of 100, with 100 being a perfect guide) near to the cut site were selected. Guide 1 scored 71 for on-target effects and 40 for off-targets (Figure 4.3 B) and guide 2 scored 60 and 49, respectively (Figure 4.4 B). A corresponding HDR template for use with each sgRNA was also designed to allow for the desired edit to take place following Cas9 cleavage.

A

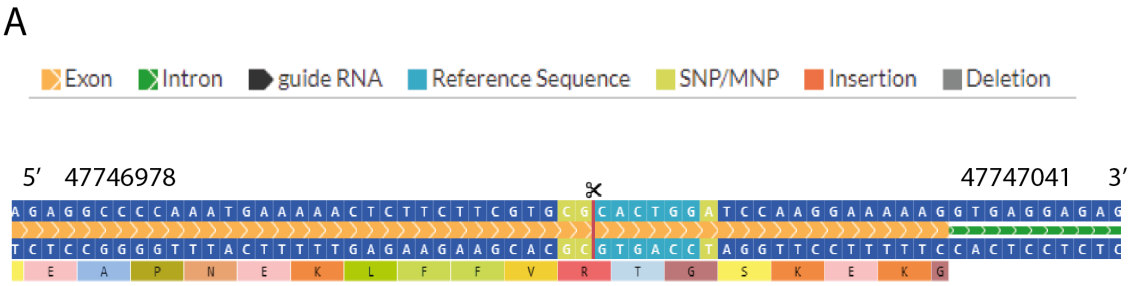


B

| Position | Strand | Sequence | PAM | Cut to mutation distance |
|---|---|---|---|---|
| 47746995 | + | AAACTCTTCTTCGTGGACAC | TGG | 0 |

Show details - | Show related products

SNP risk No SNP found
SNP location N/A
HDR Target Name Sequence 1
On-target score 71
Off-target score 40
Off-target results Demonstrates off-target hits to corresponding gRNA Design. Export to Excel | Export to CSV

C

| Target Name | Edit Start | Enzyme | Out of frame | Left arm | Right arm | Length |
|---|---|---|---|---|---|---|
| Sequence 1 | 47747010 | S.p. Cas9 | false | 40 | 40 | 89 |

Hide details - | Show related products

Transcript Accession NM_015710.4
Genome GRCh38.p11 - Human 38.p11
ref>alt GACACTGGC>CGCACTGGA
gRNA Strand +
+ Strand CTTGTTGTCAGAGGCCCCAAATGAAAAACTCTTCTTCGTGCGCACTGGATCCAAGGAAA AAGGTGAGGAGAGGCTTTTGTGGTGTGGAA
- Strand TTCCACACCACAAAAGCCTCTCCTCACCTTTTTCCTTGGATCCAGTGCGCACGAAGAAG AGTTTTTCATTTGGGGCCTCTGACAACAAG

Figure 4.3: Guide 1 and HDR design using the Alt-R™ HDR Design Tool from IDT. A) Region of exon 2 of NOP53 showing edited nucleotides in light green, the Cas9 cut site is depicted by scissors and the guide is shown in black below the sequence with the PAM site, TGG. B) The output of the IDT software tool showing the guide sequence, position and strand as well as on- and off-target scores. C) The HDR template to be used with the guide sequence in B. Sequence contains microhomology arms of 40 nucleotides either side of the edit site which introduces the GA to CG and C to A mutations.

A

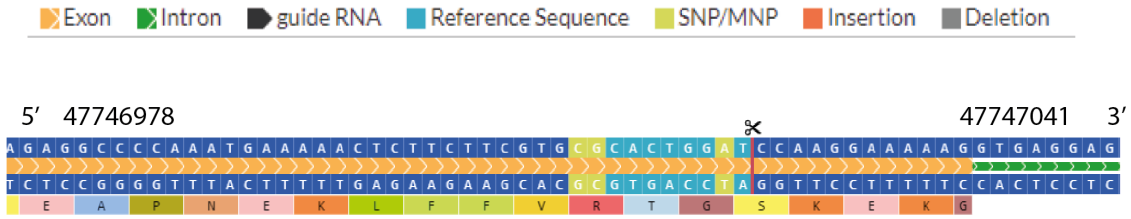


B

| Position | Strand | Sequence | PAM | Cut to mutation distance |
|---|---|---|---|---|
| 47747003 | + | CTTCGTGGACACTGGCTCCA | AGG | 1 |

Show details - | Show related products

SNP risk No SNP found
SNP location N/A
HDR Target Name Sequence 1
On-target score 60
Off-target score 49
Off-target results Demonstrates off-target hits to corresponding gRNA Design. Export to Excel | Export to CSV

C

| Target Name | Edit Start | Enzyme | Out of frame | Left arm | Right arm | Length |
|---|---|---|---|---|---|---|
| Sequence 1 | 47747010 | S.p. Cas9 | false | 40 | 40 | 90 |

Hide details - | Show related products

Transcript Accession NM_015710.4
Genome GRCh38.p11 - Human 38.p11
ref>alt GACACTGGC>CGCACTGGA
gRNA Strand +
+ Strand CTTGTTGTCAGAGGCCCCAAATGAAAAACTCTTCTTCGTGCGCACTGGATCCAAGGAAA AAGGTGAGGAGAGGCTTTTGTGGTGTGGAAT
- Strand ATTCCACACCACAAAAGCCTCTCCTCACCTTTTTCCTTGGATCCAGTGCGCACGAAGAA GAGTTTTTCATTTGGGGCCTCTGACAACAAG

Figure 4.4: Guide 2 and HDR design using the Alt-R™ HDR Design Tool from IDT. A) Region of exon 2 of NOP53 showing edited nucleotides in light green, the Cas9 cut site is depicted by scissors and the guide is shown in black below the sequence with the PAM site, AGG. B) The output of the IDT software tool showing the guide sequence, position and strand as well as on- and off-target scores. C) The HDR template to be used with the guide sequence in B. Sequence contains microhomology arms of 40 nucleotides either side of the edit site which introduces the GA to CG and C to A mutations.

As well as sgRNA and ssODN design, primers for genomic amplification by PCR were also designed. The primer sites were found in the intronic regions of NOP53, either side of exon 2 and designed to amplify a 500 bp region across exon 2, with the D90R site 200 bp from the 5' end of the PCR product and 300 bp from the 3' end.

## 4.3 Validation of gRNA efficiency and HDR

After designing both guides, their ability to recruit Cas9 to the designated D90 NOP53 genomic sequence and the efficiency of cleavage at this site was tested. Guides were ordered as separate crRNA and tracrRNA to form the sgRNA, enabling the testing of multiple guides. Recombinant Cas9 protein from IDT (Alt-R Hi-Fi Cas9) was used, forming a Cas9:sgRNA RNP prior to transfection to minimise off-target cutting (Kim *et al.*, 2014; Vakulskas *et al.*, 2018).


Figure 4.5: Assessment of D90R guide efficacy. A) T7E1 digestion of guides 1 and 2 transfected with and without Cas9. B) Guide 1 sequence analysis using Synthego ICE analysis software. The cut site is depicted with a black dashed line. The control sequence (guide only) is compared with the edited sample, guide and Cas9 (red dashed box). C) Guide 2 sequence analysis as panel B.

Previous work in the Barbaric Lab optimised electroporation for use on hPSCs, therefore the complexed RNPs were introduced into MSheff11 cell lines by this method of transfection. Both of the *in silico* designed guides were tested for the efficiency to introduce DSBs at the D90R region of NOP53 by genomic PCR, T7E1 assay, agarose gel electrophoresis and subsequent sanger sequencing and analysis (Figure 4.5). Additional smaller bands were present following T7E1 digestion in both the guide 1:Cas9 and guide 2:Cas9 samples indicating mismatches exist in the re-annealed PCR product allowing T7E1 cleavage (Figure 4.5 A). However, upon sequencing and analysis, only guide 2 showed sufficient cleavage with indel insertion at 22 % (Figure 4.5 C) with guide 1 showing no editing (Figure 4.5 B), suggesting insufficient Cas9 cleavage. Subsequently only guide 2 was used for HDR validation.

To test for HDR efficiency, Guide 2:Cas9 was transfected alongside its *in silico* designed HDR template (Figure 4.4). Sequencing analysis showed some NHEJ repair resulting in indels but also efficient HDR at 21 %, introducing both the D90R mutation and the silent G92G mutation creating a BamHI restriction site (Figure 4.6). Following the successful verification of Cas9 cleavage and HDR repair at the genomic region of interest, guide 2 was used for subsequent clonal cell line generation.

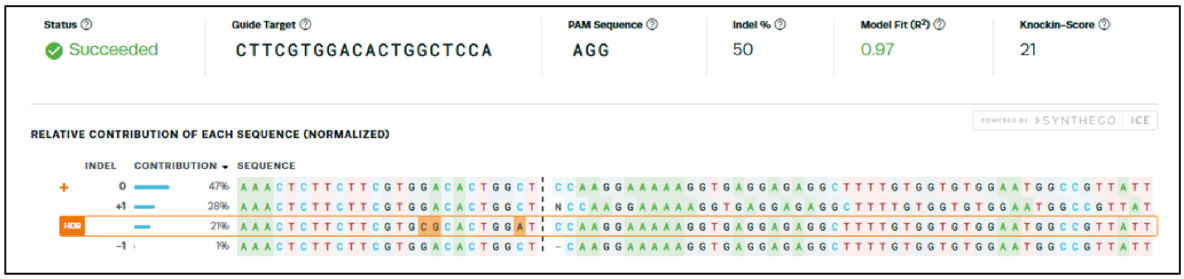


Figure 4.6: Assessment of HDR efficacy following D90R guide 2 cleavage. Guide 2 sequence analysis using Synthego ICE analysis software. The edited sample tranfected with guide 2, HDR template and Cas9 showed both indels and HDR.

## 4.4 Generation and identification of CRISPR edited MSheff 11 lines

Prior to generating CRISPR edited clonal cell lines, samples of the parental MSheff11 cell line used were sent for karyotypic analysis to ensure no chromosomal aberrations would be present in the resulting NOP53 clonal lines. Results showed the parental MSheff11 contained no chromosomal gains or losses (data not shown). Moreover, due to the propensity of hPSCs to gain dominant negative p53 mutations (Merkle *et al.,* 2017), the exons of p53 were amplified by PCR and sequenced and no mutations in the coding sequence were identified (data not shown).

Following the electroporation of Guide 2:Cas9 and the HDR template, FACs was used to individually sort 1000 cells. DAPI staining was used to select for a live population of cells to ensure each singular seeded cell had a chance of survival. Of the cells seeded, 40 % survived and proliferated producing clonal cell populations for screening (Figure 4.7 A). The BamHI restriction site, introduced by a silent single nucleotide mutation (G92G) (Figure 4.7 B), allowed screening of clonal cell lines to identify homozygotes, heterozgyotes and unedited cell lines by BamHI digestion and agarose gel electrophoresis. Analysis of the polyclonal fraction remaining after FACs showed sufficient BamHI digest (Figure 4.7 C) with 19 % HDR repair (Synthego Ice Analysis, data not shown). However following the screening of approximately

400 clonal lines (Figure 4.7 D), over 30 % of the lines produced were edited, 72 heterozygotes and 49 homozygotes. To verify the editing of the clonal lines, 5 homozygotes, 5 heterozygotes and 5 unedited cell lines were selected. Sequencing of the NOP53 locus confirmed them to be either NOP53$^{WT/WT}$, NOP53$^{WT/D90R}$ or NOP53$^{D90R/D90R}$ as the BamHI digestion suggested.

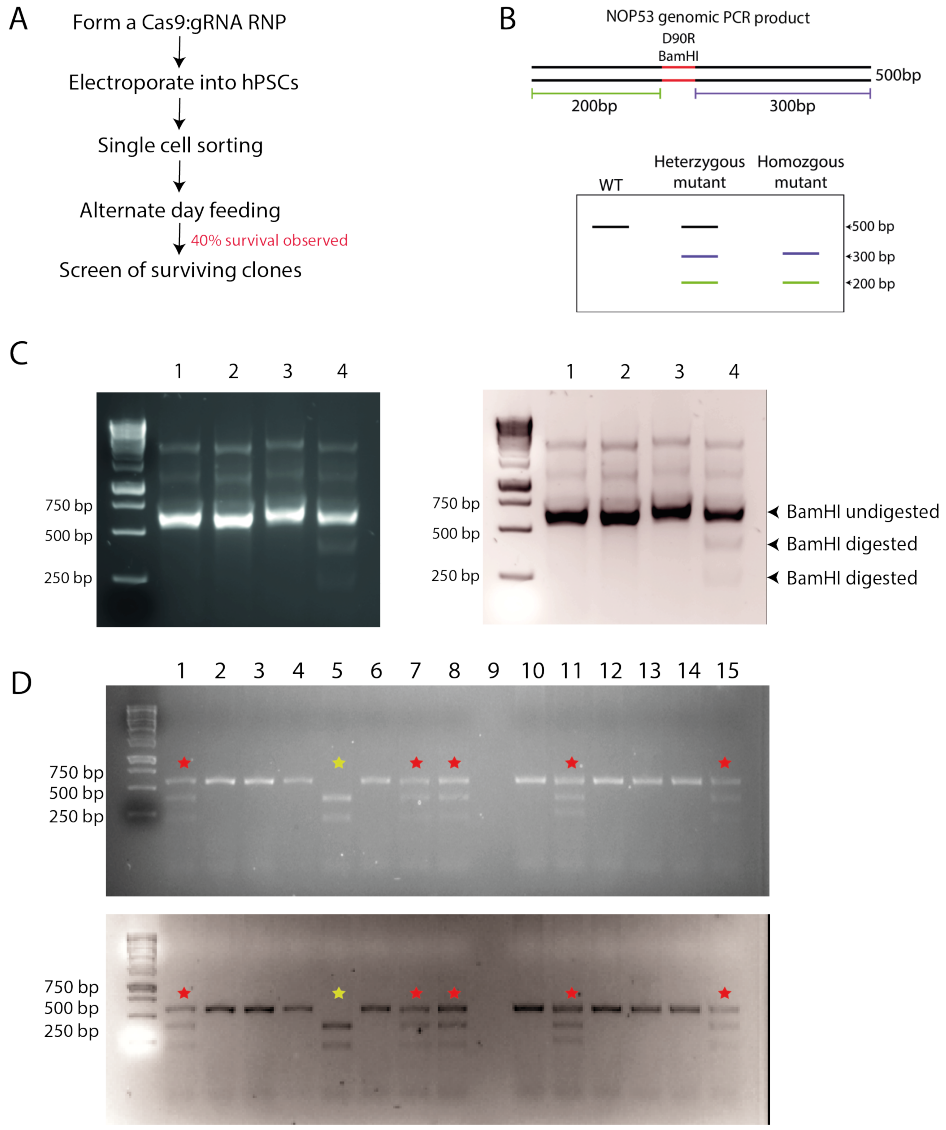


Figure 4.7: Generation of NOP53 D90R clonal lines by CRISPR-Cas9. A) Schematic showing the stages carried out for hPS clonal cell line generation. B) Schematic of the screening method for identification of clonal cell lines. The HDR template introduces a silent BamHI mutation alongside the D90R mutation. Digestion of the PCR product with BamHI can produce either a single band (WT), a double band (homozygote) or a triple band (heterozygote). C) BamHI digestion of the control lines; lane 1: Cas9 only, 2: Guide 2 only, 3: Guide 2 + Cas9, alongside the post-FACs polyclonal fraction (Guide 2 + Cas9 + HDR template) in lane 4. D) A representative example of gel electrophoresis of BamHI digested PCR product from 15 clonal cell lines (Lanes 1-15; H2, A3, B3, C3, D3, E3, F3, G3, H3, A4, B4, C4, D4 and E4). A singular homozygote is present (yellow star, lane 5) along with 5 heterozygotes (red star, lanes 1, 7, 8, 11 and 15) with the remaining clones identified as WT unedited cell lines.

## 4.5 Assessment of karyotypic identity

Following the successful identification of unedited, homozygote and heterozygote cell lines, 5 of each line were analysed by qPCR for the most common karyotypic abnormalities found in human pluripotent cell lines (Figure 4.8). Each cell should contain 2 copies of each chromosome and chromosomal region, with analysis and identification of what is classified as a chromosomal gain (>2.2) or loss (<1.8) was carried out according to published guidance (Laing *et al.,* 2019; Stem Cell Technologies, 2023). Triplicate unedited lines, 2-3, 4-3 and 5-4 were found to contain no chromosomal gains or losses in the chromosomal regions 1q, 8q, 10p, 12p 17q, 18p and 20q. However the unedited clonal line 3-2 contains a 10p chromosomal loss and 2-2 suffered a 20q loss (Figure 4.8). Only duplicate heterozygote lines, 1-3 and 3-1, showed no abnormalities, with clone 4-4 and 3-3 losing 10p and 12p, respectively. Heterozygous clone 4-2 showed several abnormalities with losses in the chromosomal arms; 8q, 10p, 12p and 20q. The homozygote lines 5-2 and 5-3 showed a loss in 17q with 5-3 also having a 20q loss. The other triplicate homozygote lines analysed, 1-2, 1-4, 2-1 appeared normal. Subsequently, duplicate cell lines for wild-type NOP53, and homozygous and heterozygous mutants of NOP53 D90R would be used in any future analysis.

## 4.6 Discussion

This chapter describes the successful generation of MSheff11 clonal lines for NOP53$^{WT/WT}$, NOP53$^{WT/D90R}$ or NOP53$^{D90R/D90R}$ by CRISPR-Cas9. Clonal cell lines were also shown to be karyotypically normal. These lines will prove useful upon further validation for investigating the role of NOP53 in ribosome biogenesis and nucleolar stress responses.

Only duplicate NOP53$^{WT/WT}$, NOP53$^{WT/D90R}$ and NOP53$^{D90R/D90R}$ clonal lines were shown to be karyotypically normal, but ideally a third clonal line would have been used. Moreover, only the second of the two gRNAs designed showed editing by sequencing analysis, despite the fact that the first guide appeared to show T7E1 cleavage. This may be explained by a low level of non-specific cleavage activity which has been observed with T7E1 (Vouillot *et al.,* 2015). Ideally two distinct guides would be used to control for off-target editing and if time was not limited an additional guide would have been designed *in silico*, verified and used to generate clonal NOP53$^{WT/WT}$, NOP53$^{WT/D90R}$ and NOP53$^{D90R/D90R}$ lines.

The hPSC lines generated using the single guide could be assessed for off-target effects of Cas9 cleavage and editing. The guide RNA (gRNA 2) used for the generation of the hPSCs had a relatively high off-target score at 49, meaning the risk of off-target editing is low. Whilst not all CRISPR generated hPSC mutant lines are analysed for off-target effects (Tu *et al.,* 2018; Xu *et al.,* 2018), as future work looks to focus on the functional roles of NOP53, it is important to validate potential off-target sites. The ALT-R HDR Design Tool from IDT which was used for the design of guides also provides a list of genomic locations, in both introns and exons, that have the highest risk of off-target Cas9 targeting. PCR amplification and sequencing over these top regions could then be carried out and analysed.

In producing NOP53$^{WT/WT}$, NOP53$^{WT/D90R}$ and NOP53$^{D90R/D90R}$ stem cell lines the role of NOP53 can be studied in a controlled cellular system. Initial work would look to conduct co-immunoprecipitations in hPSCs to validate the findings from HEK293 cells, described in chapter 3, that the NOP53 AIM mutant is unable to interact with MTR4. Whilst other mutations in the AIM of NOP53 resulted in defective rRNA processing characterised by 12S pre-rRNA accumulation (Miyao *et al.,* 2022), work was carried out transiently in

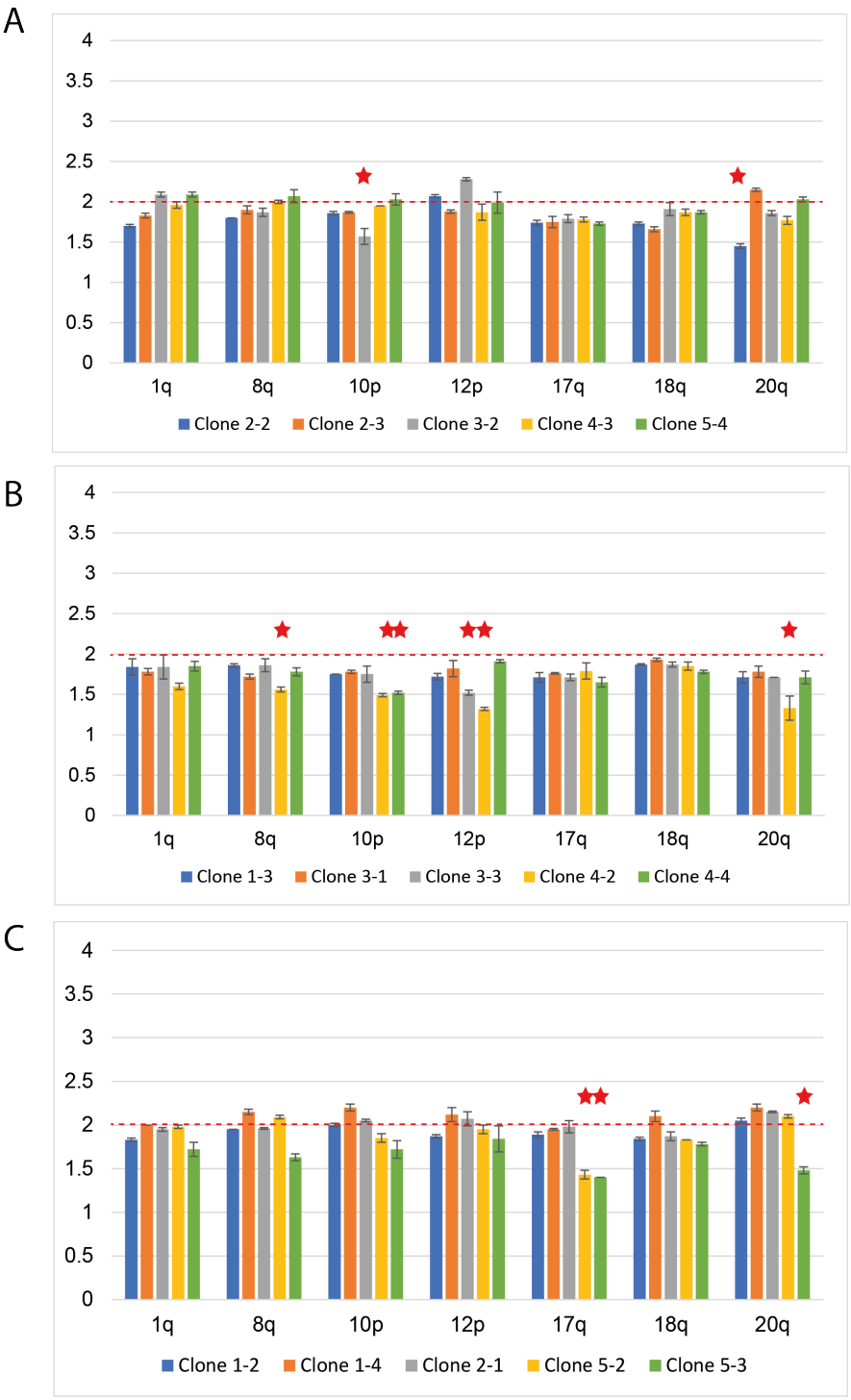


Figure 4.8: qPCR analysis of hPSC clonal lines following NOP53 D90R CRISPR-Cas9. A) Five clonal cell lines that remained unedited following CRISPR. Triplicate clonal lines are karyotypically normal containing 2 copies of each chromosomal region as indicated by the dashed red line. However two clones are abnormal as indicated by the red star. B) Five clonal cell lines that were identified as heterozygous for NOP53 D90R following CRISPR. Duplicate clonal lines appear normal with triplicate lines containing chromosomal losses (red star). C) Five clonal cell lines that were identified as homozygous for NOP53 D90R following CRISPR. Triplicate clonal lines contain 2 copies of each chromosomal region with the other two clonal lines abnormal (red stars).

HEK293 cells, to which the mutational background of the cell is unknown. The generation of clonal hPSC NOP53 lines allows for extensive phenotypic analysis to be carried out in a karyotypically normal system expressing WT p53.

Phenotypic characterisation will include the investigation of; clonal growth, proliferation, pluripotency and differentiation capacity. Pluripotency of the clonal lines would be confirmed by checking for expression of pluripotent markers such as SSEA3 (Shevinsky *et al.,* 1982) and TRA-1-81 (Badcock *et al.,* 1999). Both pluripotency and the capacity to differentiate would also be assessed through trilineage differentiation assays of the clonal lines to test that they can effectively differentiate into each of the 3 germ layers; the ectoderm, mesoderm and endoderm.

Additionally growth and proliferation assays will be conducted to compare unedited WT clones, heterozygotes and homozygotes. This will provide insight into whether the loss of the NOP53-MTR4 interaction affects cellular homeostasis. By comparing homozygotes with heterozygotes, the respective growth rate can be used to determine if the D90R mutation has a dominant negative effect as observed in *S. cerevisiae* (Thoms *et al.,* 2015). This could be further confirmed with the characterisation of RNA processing and nucleolar stress responses in heterozygotes and homozygotes.

Analysis of rRNA precursors would look to identify any processing defects in NOP53 D90R mutants. As the mechanism of interaction is conserved from *S. cerevisiae*, it is likely that the function of the interaction between NOP53 and MTR4 is also conserved. Therefore, an observed accumulation of the 12S pre-rRNA, equivalent to 7S pre-rRNA accumulation in yeast, is likely (Thoms *et al.,* 2015). rRNA analysis would also look to confirm if the D90R mutation also has no affect on the processing of the 32S rRNA which was observed with other NOP53 AIM mutants (Miyao *et al.,* 2022).

For investigating the role of NOP53 D90R in the nucleolar stress response, the interaction between NOP53 D90R and RPL11 will be validated and both p53 levels and p53 target levels e.g. p21, would be analysed. Again, in comparing homozygote D90R clones with heterozygotes, it would be interesting to see if this mutation has a dominant effect or whether a single WT copy of NOP53 is sufficient to present a phenotype like that of unedited WT clones.

Finally, the production of $NOP53^{WT/WT}$, $NOP53^{WT/D90R}$ and $NOP53^{D90R/D90R}$ stem cell lines enables the role of NOP53 to be studied in not only the pluripotent stage but also in differentiated lineages. It would be interesting to investigate the role of NOP53 in ribosome biogenesis and nucleolar stress in erythroid progenitors. In humans, the haploinsufficiency of RPL11 and other RPs is associated Diamond-Blackfan Anaemia (DBA). Primarily, the disease presents itself in erythroid progenitors. Other cell types become pre-disposed to cancer, however, most cell types appear normal despite the RP depletion. The mechanism by which this reduction in RP expression leads to the presentation of DBA in these cell types specifically is not understood. Therefore, by differentiating the NOP53 lines into erythroid progenitors in combination with RPL11 depletion, the molecular mechanisms and any subsequent phenotype may be studied.

# Chapter 5

# Characterisation of the interaction between NOP53 and RPL11

## 5.1 Introduction

In humans, NOP53 has been shown to regulate the HDM2-p53 pathway via the ribosomal protein RPL11 (Sasaki *et al.,* 2011). RPL11 interacts with RPL5 and the 5S rRNA which together comprise the 5S RNP, a sub-complex of the 60S ribosomal subunit. The 5S RNP localises to the nucleolus during ribosome biogenesis but accumulates in the nucleoplasm when biogenesis is inhibited (Donati *et al.,* 2013; Sloan *et al.,* 2013). RPL11 has been proposed to have a dual physiological role, as not only is it an essential component of the ribosome, it is also implicated in p53 regulation (Zhang *et al.,* 2003). During normal homeostatic conditions, NOP53 binds to RPL11 sequestering it in the nucleolus (Suzuki *et al.,* 2012). However, during nucleolar stress, RPL11 is released from the nucleolus and translocates to the nucleoplasm where it binds to HDM2, an E3 ubiquitin ligase. RPL11 binding prevents the association of HDM2 with the transcription factor p53, allowing for p53 stabilisation and initiation of cell cycle arrest (Bhat *et al.,* 2004). While there is evidence that supports a physical interaction between NOP53 and RPL11, with RPL11 re-localisation to the nucleoplasm upon NOP53 depletion (Sasaki *et al.,* 2011), the nature of this interaction is poorly understood. It remains unclear if these two proteins directly or indirectly contact each other. The investigation presented here aims to explore the interaction and identify key residues mediating the interaction between NOP53 and RPL11, in humans, through yeast-two-hybrid and *in vitro* reconstitution studies.

## 5.2 NOP53 binds directly to RPL11

Initial work to explore the interaction between NOP53 and RPL11 was conducted using the yeast-two-hybrid system described previously in chapter 3 (constructs and preliminary analyses performed by Monika Feigenbutz, Thomson Lab). Again, the *S.cerevisiae* strain PJ69-4A (James *et al.,* 1996) was used for analysis using the Gal1-His3 reporter. The activation domain (AD) and the binding domain (BD) of the Gal4 transcription factor are attached to NOP53 and RPL11, respectively. If NOP53 and RPL11 interact, the AD and BD are in close enough proximity to reconstitute the Gal4 transcription factor allowing histamine production and yeast growth on media lacking histidine. Conversely, if no interaction occurs, there is no Gal4 reconstitution, hstidine production or yeast growth. The *S. cerevisiae* homodimer, PNC1 is used again here as a control (Saryi *et al.,* 2017).

Growth was observed for pAD NOP53 and pBD RPL11 on SDC-Leu-Trp-His, indicating that NOP53 and RPL11 directly interact (Figure 5.1, Supplementary Figure 8.1). No

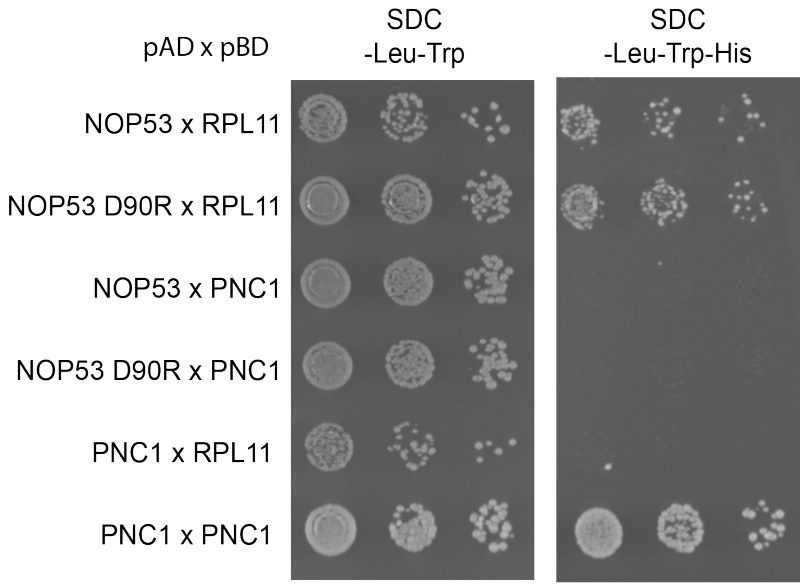


Figure 5.1: Yeast-two-hybrid analysis of NOP53 WT and D90R with RPL11. Yeast-two-hybrid dot plates for NOP53 WT or D90R transformants with RPL11 grown on SDC-Leu-Trp and SDC–Leu-Trp-His.

growth was observed on SDC-Leu-Trp-His when either NOP53 or RPL11 was grown with PNC1 confirming no self-activation of the constructs. The NOP53 AIM mutant, D90R, first described in chapter 3 was also investigated for its ability to bind to RPL11. NOP53 D90R showed growth with RPL11 on SDC-Leu-Trp-His, but no growth with PNC1. Consequently, the D90R mutation does not affect the ability of NOP53 to bind to RPL11. This observation can be further validated by the co-immunoprecipitations carried out in chapter 3 (Figure 3.16), where RPL11 binding was consistently observed across duplicated FLAG-NOP53 and FLAG-NOP53 D90R HEK293 cell lines.

## 5.3 Truncation mapping of NOP53 by yeast-two-hybrid

Having confirmed the direct interaction between NOP53 and RPL11, the residues/regions of NOP53 mediating this interaction with RPL11 were mapped. Regions of NOP53 were first tested through the generation of truncated NOP53 constructs. To identify where to place boundaries of truncations, a multiple sequence alignment of NOP53 was compiled. By looking at the conservation of amino acids across eukaryotes, regions which may mediate the NOP53-RPL11 interaction were identified through the comparison of *S. cerevisiae* with higher eukaryotes. The predicted positions of secondary structures within human NOP53 were also mapped using jnetpred (Drozdetskiy *et al.,* 2015) and added to the alignment. Human NOP53 is predicted to contain both $\beta$-sheets and $\alpha$-helices but also extensive unstructured regions (Figure 5.2). In agreement with this, the Alphafold structure prediction of NOP53, which when released became the standard for protein structure prediction, also suggests that NOP53 contains large, unstructured regions (Figure 5.3) (Jumper *et al.,* 2021; Varadi *et al.,* 2021). By predicting the structure of Nop53 and identifying the positions of secondary motifs, these regions can be avoided as generating a truncation directly through a secondary structure could cause protein destabilisation.

Based upon the predicted positions of the secondary structures within NOP53, a N-terminal and C-terminal truncated construct, NOP53 $\Delta$N145 and NOP53 $\Delta$C91, were gen-

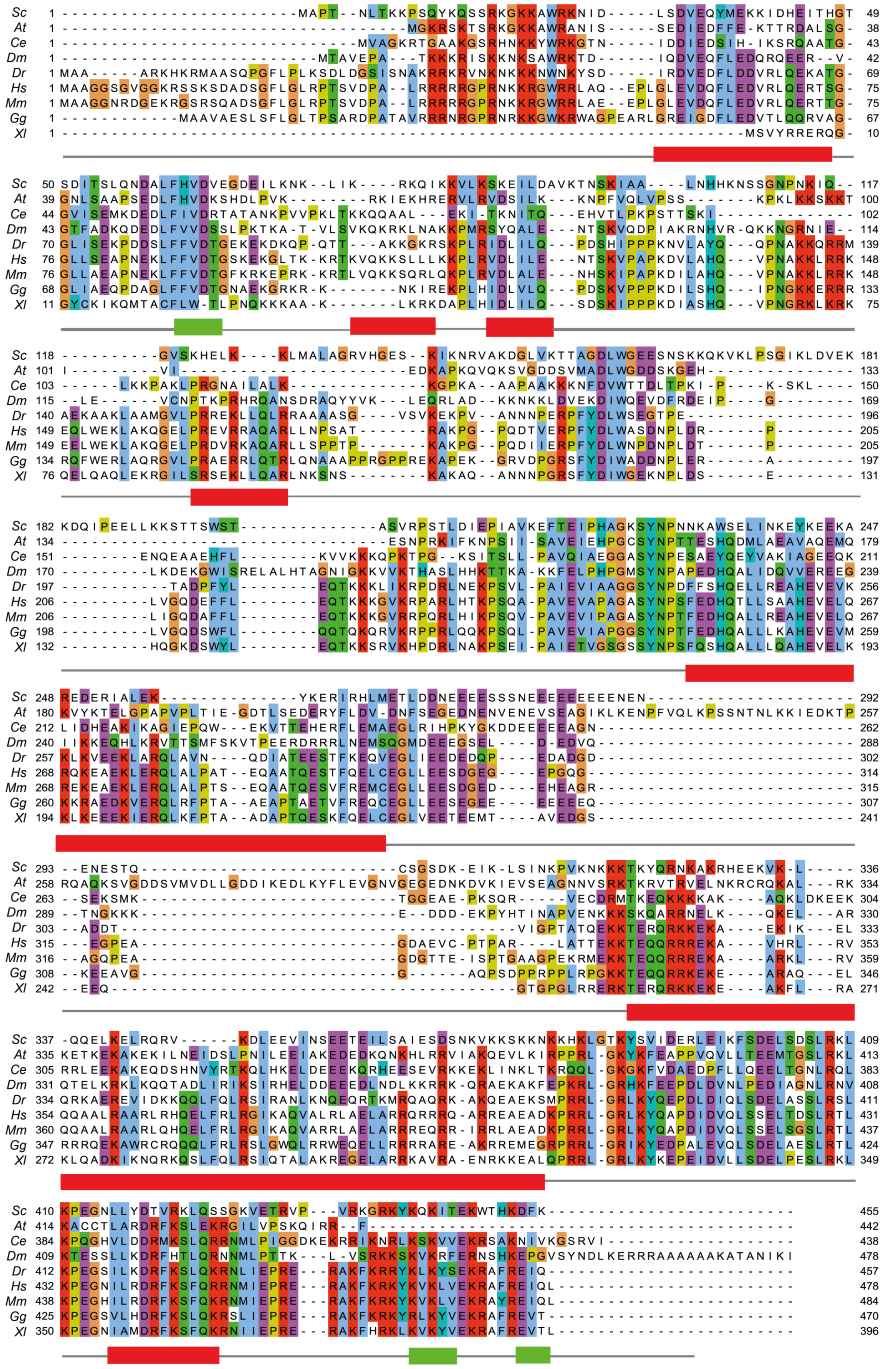

Figure 5.2: Multiple sequence alignment for NOP53 across eukaryotes with secondary structure predictions. Produced using Clustal Omega (Sievers *et al.*, 2011) and Jalview (Waterhouse *et al.*, 2009) for the following species; in *A. thaliana (At, P42794-1), S. cerevisiae (Sc, Q6FTK4), C. elegans (Ce, Q94300), D. melanogaster (Dm, P46222), X. laevis (Xl, Q66KY6-1), G. gallus (Gg, A0A1D5P3B1-1), M. musculus (Mm, Q9CXW4-1), H. sapiens (Hs, P62913-1) and D. rerio (Dr, Q6IQI6-1).* Secondary structure motifs of human NOP53 predicted using jnetpred. Predicted $\beta$-sheet secondary structures are depicted below the amino acids in green and $\alpha$-helices are displayed in red.

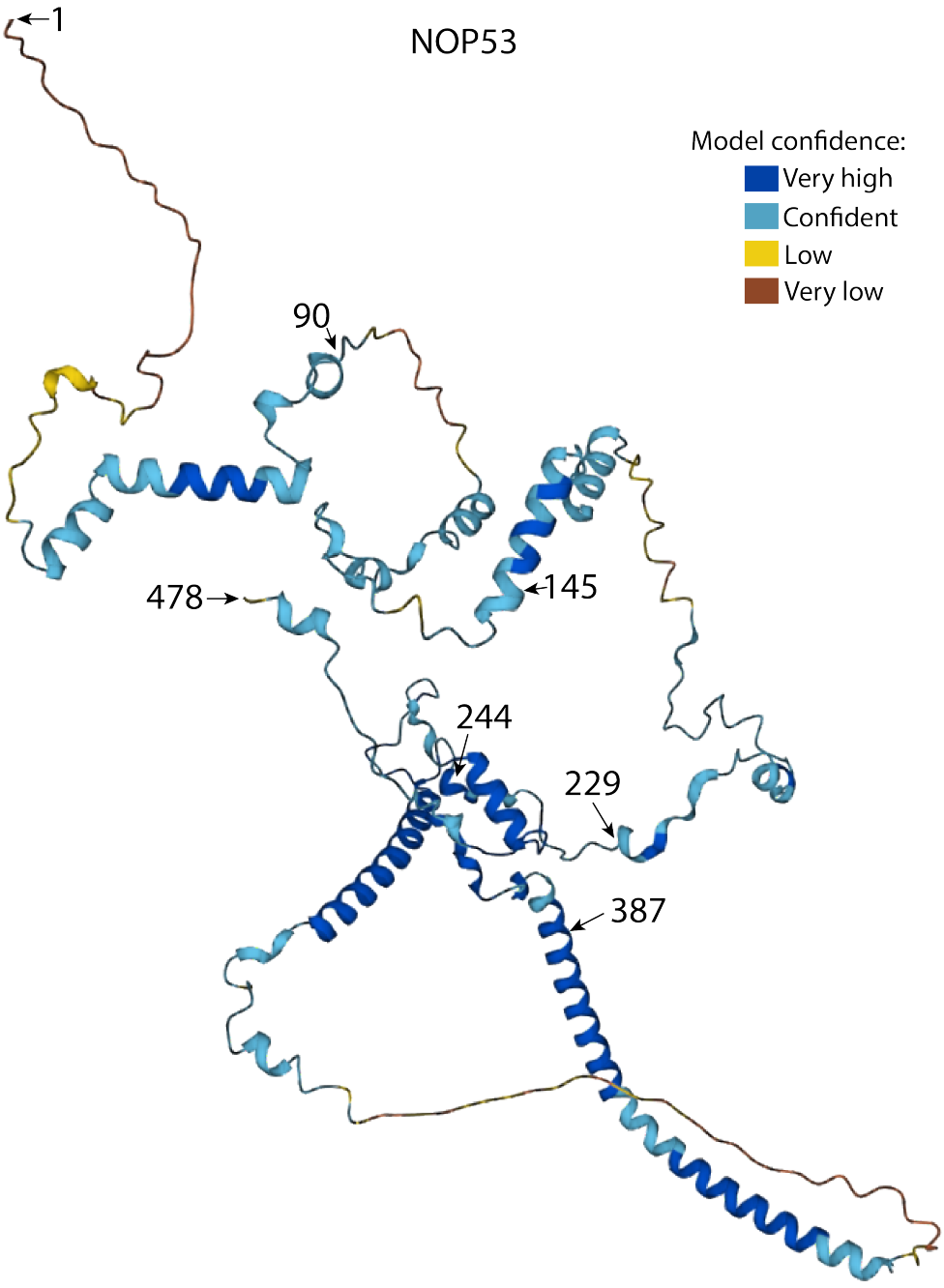


Figure 5.3: Alphafold structure prediction of NOP53. Alphafold model of NOP53 with colours indicating a a per-residue confidence score (pLDDT) between 0 and 100. This ranges from very high confidence in the model (pLDDT >90), to confident (90 >pLDDT >70), to low (70 >pLDDT >50) and then very low (pLDDT <50). Large unstructured regions of NOP53 are yellow/orange indicating low and very low confidence in the predicted structure. The N- and C-terminus of NOP53 are labelled (residues 1 and 478) along with key residues (90, 145, 229, 244 and 387) used for the generation of NOP53 truncation mutants and yeast-two-hybrid analysis.


Figure 5.4: pAD NOP53 constructs produced for yeast two hybrid analysis. The constructs NOP53 ΔN145, NOP53 ΔC91, NOP53 ΔC235, NOP53 ΔN243, NOP53 1-145, NOP53 146-228, NOP53 229-387, NOP53 387-478 were analysed by yeast-two-hybrid to investigate the interaction with RPL11.

erated (Figure 5.4). The ability of NOP53 ΔN145 and NOP53 ΔC91 to bind to RPL11 was investigated using the yeast-two-hybrid system (Figure 5.5, Supplementary Figure 8.2). NOP53 constructs were attached to the AD domain of Gal4 and the BD to RPL11 as described in section 5.2. Growth was observed on SDC-Leu-Trp-His for NOP53 ΔN145 and NOP53 ΔC91 with RPL11, suggesting both NOP53 ΔN145 and ΔC91 can interact with RPL11. No growth was observed on SDC-Leu-Trp-His for either NOP53 construct with RPL11, confirming no self activation. This suggests that neither the N-terminal 145 amino acids nor C-terminal 91 amino acids are necessary for NOP53 to bind to RPL11.

Since the loss of either N- or C- termini from NOP53 had no effect on the ability of NOP53 to interact with RPL11, NOP53 was dissected into two segments; an N-terminal (ΔC235) and C-terminal (ΔN243) segment, aiming to narrow down the region of NOP53 responsible for RPL11 binding (Figure 5.6, Supplementary Figure 8.3). For both NOP53ΔN243 and NOP53 ΔC235 growth was observed on SDC-Leu-Trp-His. However growth for NOP53ΔN243 was clearly reduced compared to both WT NOP53 and NOP53ΔC235. This suggests that the N-terminus of NOP53 (ΔC235) has a strong interaction with RPL11, compared to the C-terminus (ΔN243) which has a strongly reduced reaction. However, the expression levels of neither construct were analysed, so reduced growth may be explained by lower expression of NOP53ΔN243 in *S. cerevisiae*. The observation that both the N-terminal and the C-terminal

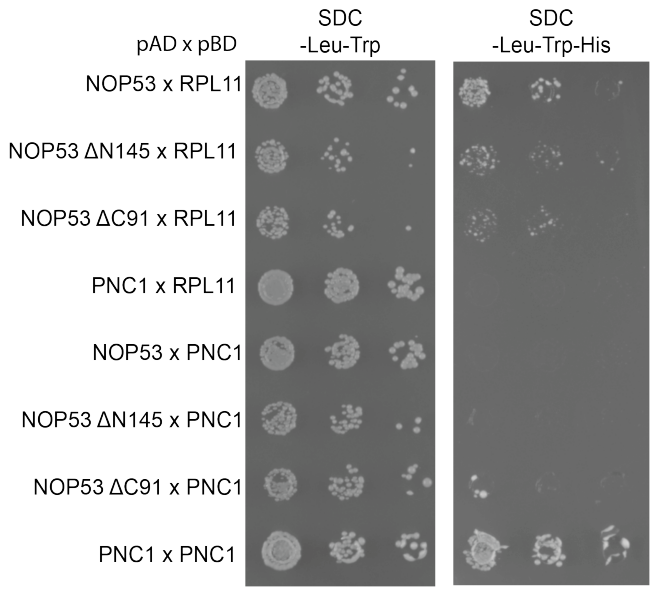


Figure 5.5: Yeast-two-hybrid analysis of NOP53 ΔN145 and NOP53 ΔC145 with RPL11. Yeast-two-hybrid dot plates for NOP53ΔN145 and NOP53 ΔC145 with RPL11 grown on SDC-Leu-Trp and SDC–Leu-Trp-His.

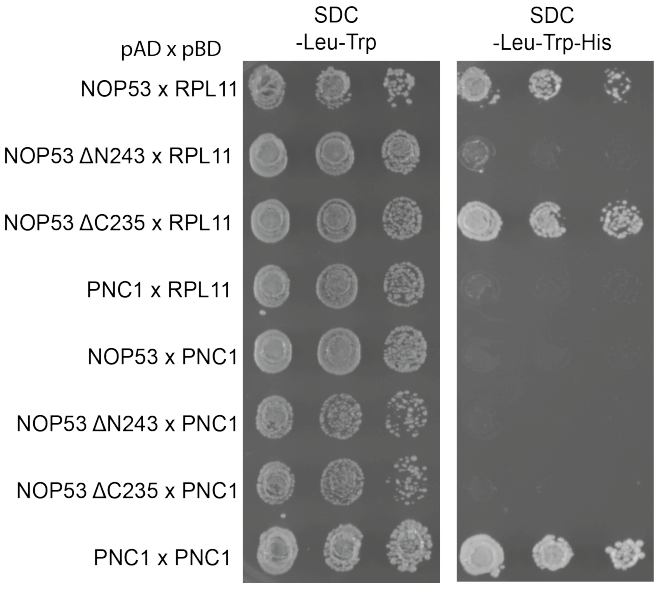


Figure 5.6: Yeast-two-hybrid analysis of NOP53 ΔN243 and NOP53 ΔC235 with RPL11. Yeast-two-hybrid dot plates for NOP53ΔN243 and NOP53 ΔC235 with RPL11 grown on SDC-Leu-Trp and SDC–Leu-Trp-His.

half of NOP53 show an interaction with RPL11, suggests there may be multiple regions of NOP53 which bind to RPL11.

These results indicate that neither of the termini are essential for interaction and each half of the protein was sufficient for interaction. Further constructs of NOP53 based upon the initial truncations were made to further analyse RPL11 binding. NOP53 was segmented into 4 fragments, 1-145, 146-228, 229-387, 388-478 all of which were shown to bind to RPL11 using yeast-two-hybrid (Figure 5.7, Supplementary Figure 8.4). The observation that all four constructs of NOP53 showed growth on SDC-Leu-Trp-His is indicative of RPL11 binding, as none of the constructs grew on SDC-Leu-Trp-His in combination with PNC1. This further suggests that multiple regions of NOP53 may interact with RPL11. Therefore, to identify the residues of NOP53 responsible for the interaction with RPL11 an alternative approach to truncation mapping is required.

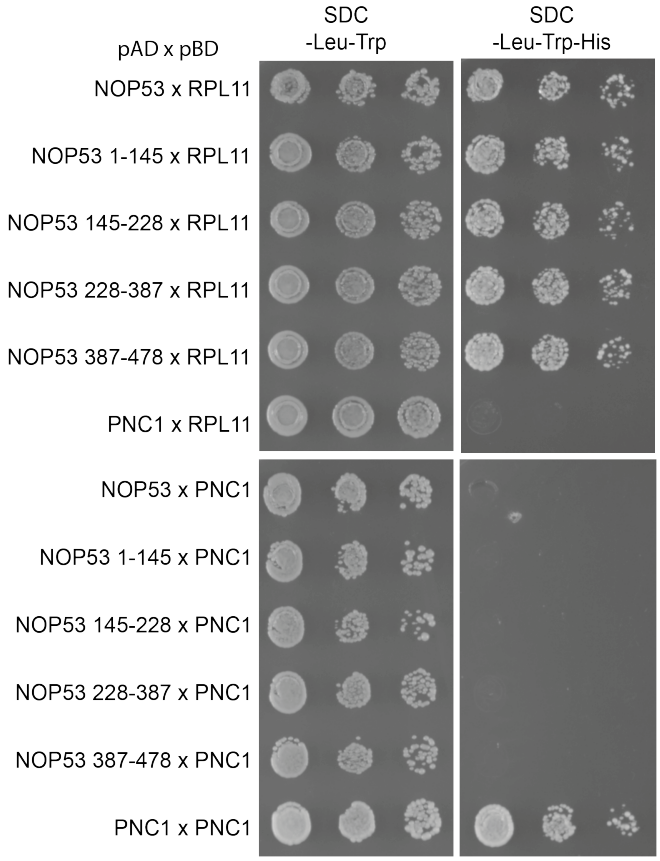


Figure 5.7: Yeast-two-hybrid analysis of NOP53 constructs; 1-145, 146-228, 229-387 and 388-478 with RPL11. Yeast-two-hybrid dot plates for NOP53 transformants; 1-145, 146-228, 229-387 and 388-478 with RPL11 grown on SDC-Leu-Trp and SDC–Leu-Trp-His.

## 5.4 Random, mutagenetic, yeast-two-hybrid screen of NOP53

An alternative approach to try and identify key residues mediating the interaction between NOP53 and RPL11, is random mutagenesis. Random mutagenesis of NOP53 was carried out by error-prone PCR. During error-prone PCR, mutations are randomly inserted in the DNA sequence under conditions which reduce Taq polymerase fidelity with increasing numbers of mutations the higher the gene duplication (Figure 5.8) (McCullum *et al.*, 2010). For NOP53, cycle conditions were optimised to only 4-6 cycles to produce PCR products containing low

single figures of mutations (between 2 and 6). Following optimisation, error-prone PCR was repeated and larger scale sequencing of 100 constructs was carried out by colony sequencing. Sequencing confirmed that no clustering of mutations was observed and mutations had been introduced across the full length of the nucleotide sequence. The average mutation rate was calculated to be 3.45 nucleotides across the length of NOP53 at 1434 nucleotides.

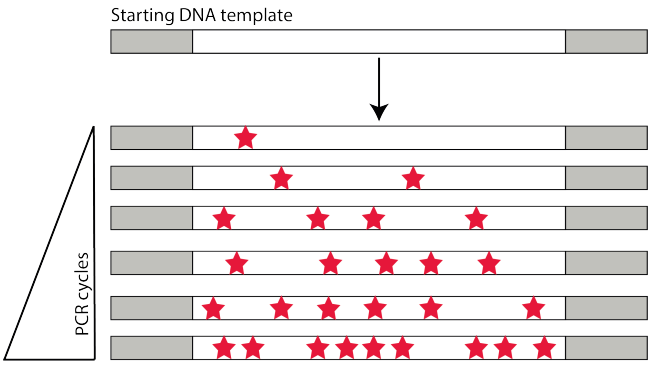


Figure 5.8: Random mutagenesis by Error-Prone PCR. Mutations (red stars) increase in number with an increasing number of PCR cycles.

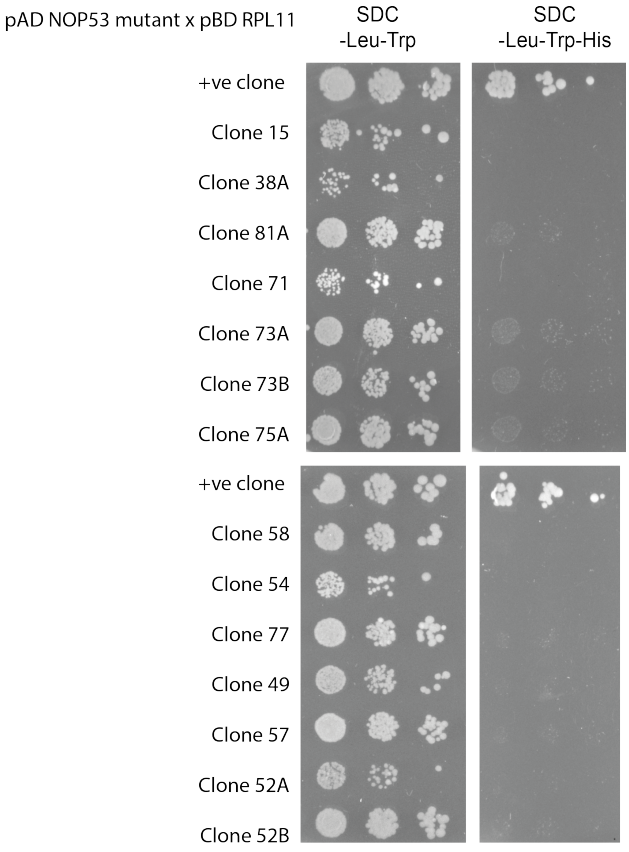


Figure 5.9: Yeast-two-hybrid analysis of negative pAD NOP53 random mutagenetic clones with RPL11. Fourteen clones identified in total; 15, 38A, 49, 52A, 52B, 54, 57, 58, 71, 73A, 73B, 75A, 77 and 81A grown alongside a positively identified clone on SDC-Leu-Trp and SDC–Leu-Trp-His.

Following this validation of mutations across the length of NOP53 constructs, a pilot yeast-two-hybrid screen was carried out. The initial transformation onto SDC-Leu-Trp produced approximately 8732 clones and following selection onto SDC-Leu-Trp-His and validation, 14 clones failed to grow on SDC-Leu-Trp-His, 0.16% of clones (Figure 5.9). The failure to grow on -His media is indicative of a failure of these clones to interact with RPL11. However, sequencing of these clones identified an inframe premature early stop codon within the first 100 amino acids. As previous results suggest multiple points of interaction on NOP53, it is statistically more likely that a mutation will introduce a premature stop codon than multiple sites of mutation to abolish the interaction with RPL11. Given this fact, the scale at which the screen would need to be carried out to generate a significant number of mutants for screening to produce mutants without early stop codons is not feasible. As the approaches discussed in this section failed to identify the region(s) of NOP53 mediating the interaction with RPL11, an alternate approach to investigate the NOP53-RPL11 interaction was needed.

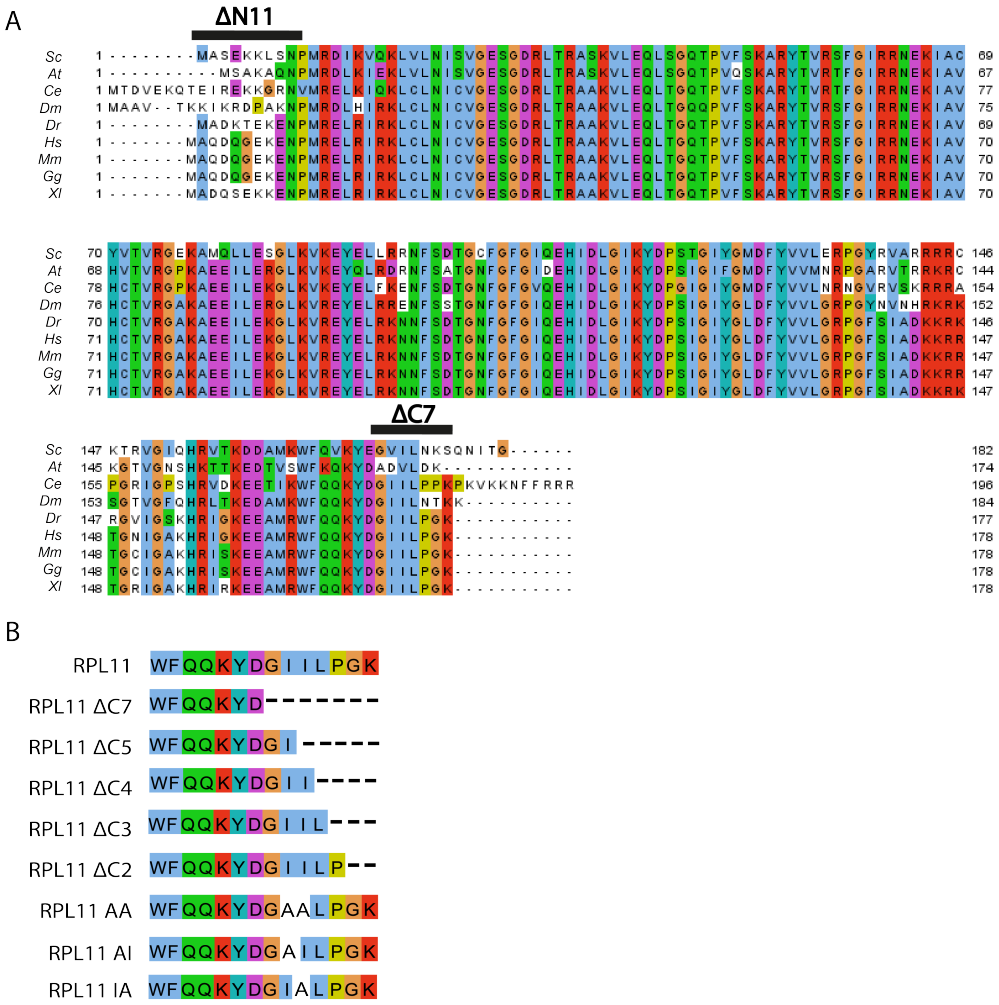


Figure 5.10: A) Multiple sequence alignment of RPL11 in p53 containing organisms alongside *S. cerevisiae* using Clustal Omega and Jalview for the following species; *A. thaliana (At, P42794-1), S. cerevisiae (Sc, Q6FTK4), C. elegans (Ce, Q94300), D. melanogaster (Dm, P46222), X. laevis (Xl, Q66KY6-1), G. gallus (Gg, A0A1D5P3B1-1), M. musculus (Mm, Q9CXW4-1), H. sapiens (Hs, P62913-1) and D. rerio (Dr, Q6IQI6-1).* B) RPL11 C-terminal mutants analysed by Yeast-two-hybrid.

## 5.5 Mapping of RPL11 by yeast-two-hybrid

In an attempt to gain further information about the NOP53-RPL11 interaction, mapping of the regions in RPL11 mediating this interaction was performed. RPL11 is a small protein, at 22 kDa, and, as with many other ribosomal proteins, very well conserved across eukaryotes. In humans and other higher eukaryotes, RPL11 has been shown to have an extraribosomal function in the regulation of p53; which in turn requires NOP53 (section 1.4.2). However, in the unicellular yeast *S. cerevisiae* no p53 exists, meaning Rpl11 does not act in p53 regulation. Consequently, it is possible that the region responsible for mediating the p53 response is absent in *S. cerevisiae*. Therefore, to identify regions of RPL11 sequence conservation observed in p53 positive organisms, not seen in *S. cerevisiae*, a multiple protein sequence alignment of RPL11 was compiled (Figure 5.10).

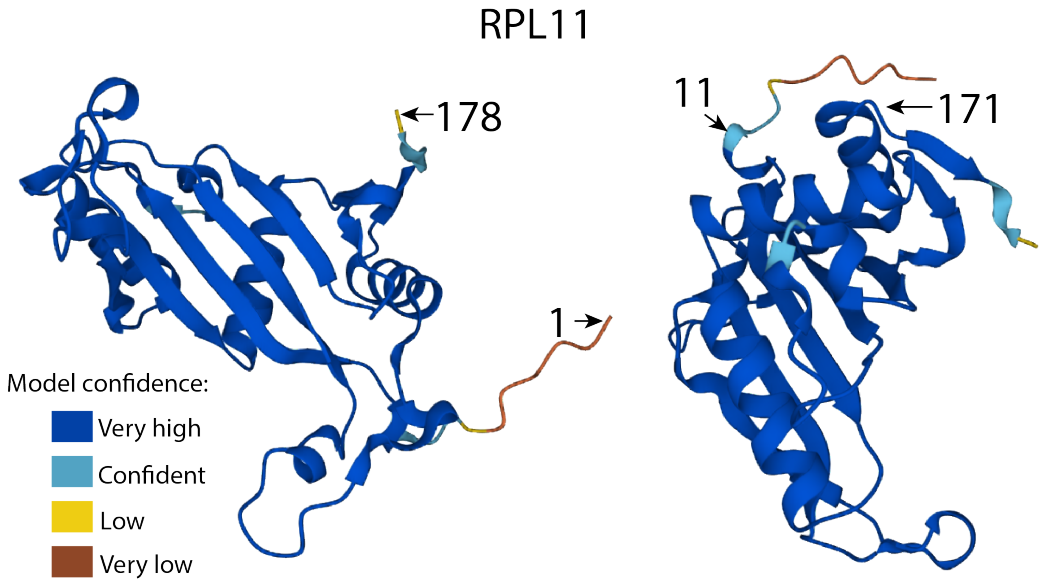


Figure 5.11: Alphafold structure prediction of RPL11. Alphafold model of RPL11 with colours indicating a a per-residue confidence score (pLDDT) between 0 and 100. This ranges from very high confidence in the model (pLDDT >90), to confident (90 >pLDDT >70), to low (70 >pLDDT >50) and then very low (pLDDT <50). The model has high confidence in the prediction except within the N- and C-terminus of RPL11. Both RPL11 termini are labelled (residues 1 and 178) along with key residues (11 and 171) used for the generation of RPL11 truncation mutants and yeast-two-hybrid analysis.

The RPL11 alignment shows a high level of conservation across all species, with yeast showing 93 % sequence similarity to human RPL11 (Figure 5.10). However, both the N-terminal and C-terminal regions of RPL11 appeared the least conserved. This is further supported by the alphafold prediction of RPL11 which shows that both termini are exposed and these regions show the lowest level of model confidence in the protein (Figure 5.11). Consequently, RPL11 ΔN11 and RPL11 ΔC7 were cloned into the pBD vector and analysed by yeast-two-hybrid (Figure 5.12, Supplementary Figure 8.5). RPL11 ΔN11 was shown to still interact with NOP53 as growth was observed on SDC-Leu-Trp-His. In contrast, RPL11 ΔC7 showed no growth suggesting the loss of interaction with NOP53 (Figure 5.12). As no growth on SDC-Leu-Trp-His may also be explained by lack of expression of RPL11 ΔC7, the expression of the RPL11 constructs were assessed by Western blot using the N-terminal

c-Myc tag found between the Gal-4 binding domain and RPL11 (Figure 5.13). This analysis showed that RPL11 ΔC7 was indeed expressed and consequently the loss of growth on SDC-Leu-Trp-His indicates the loss of NOP53 binding.

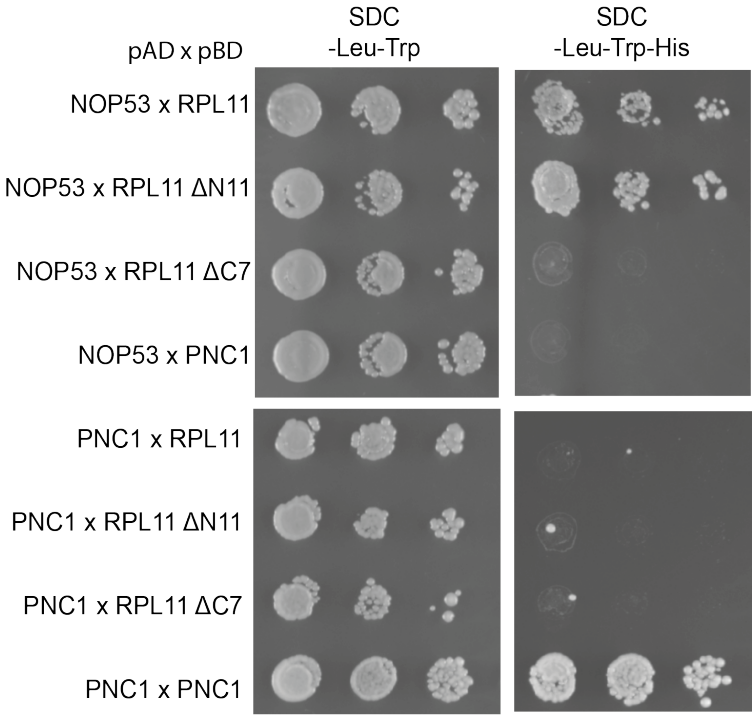


Figure 5.12: Yeast-two-hybrid analysis of NOP53 with RPL11 ΔN11 and ΔC7. Yeast-two-hybrid dot plates for NOP53 transformants with RPL11 ΔN11 and RPL11 ΔC7 grown on SDC-Leu-Trp and SDC–Leu-Trp-His.

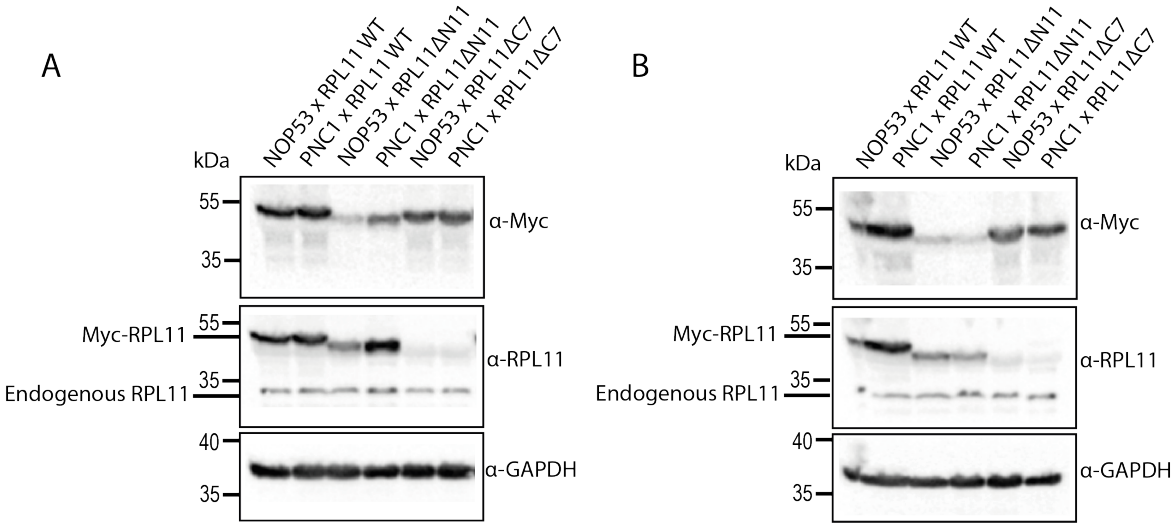


Figure 5.13: Expression of RPL11 WT, RPL11 ΔN11 and RPL11 ΔC7 with NOP53 or PNC1 in *S. cerevisiae*. Expression for RPL11 endogenous and myc-RPL11 constructs analysed using $\alpha$-RPL11 and $\alpha$-Myc. The RPL11 antibody does not recognise RPL11ΔC7 as it was produced using a short C-terminal peptide. Duplicate protein expression is shown from two separate *S. cerevisiae* clones for each construct combination.

To further explore the role of the C-terminus of RPL11 and further narrow down the point of interaction with NOP53, additional truncation mutants were produced (Figure 5.10 B). The mutants were produced by undergraduate students I supervised. RPL11 ΔC5 and RPL11 ΔC3 were generated by Hephzibah Robb and RPL11 ΔC4 and RPL11 ΔC2 were generated by Molly John. Yeast-two-hybrid analysis was carried out alongside RPL11 ΔC7 as a positive control for the loss of interaction (Figure 5.14, Supplementary Figure 8.6). All four RPL11 Δ mutants showed growth on SDC-Leu-Trp-His, indicating that these shorter RPL11 C-terminal truncations are still competent to bind to NOP53. Consequently, since these truncation mutants could still bind to NOP53, an alternative mutation approach was used.

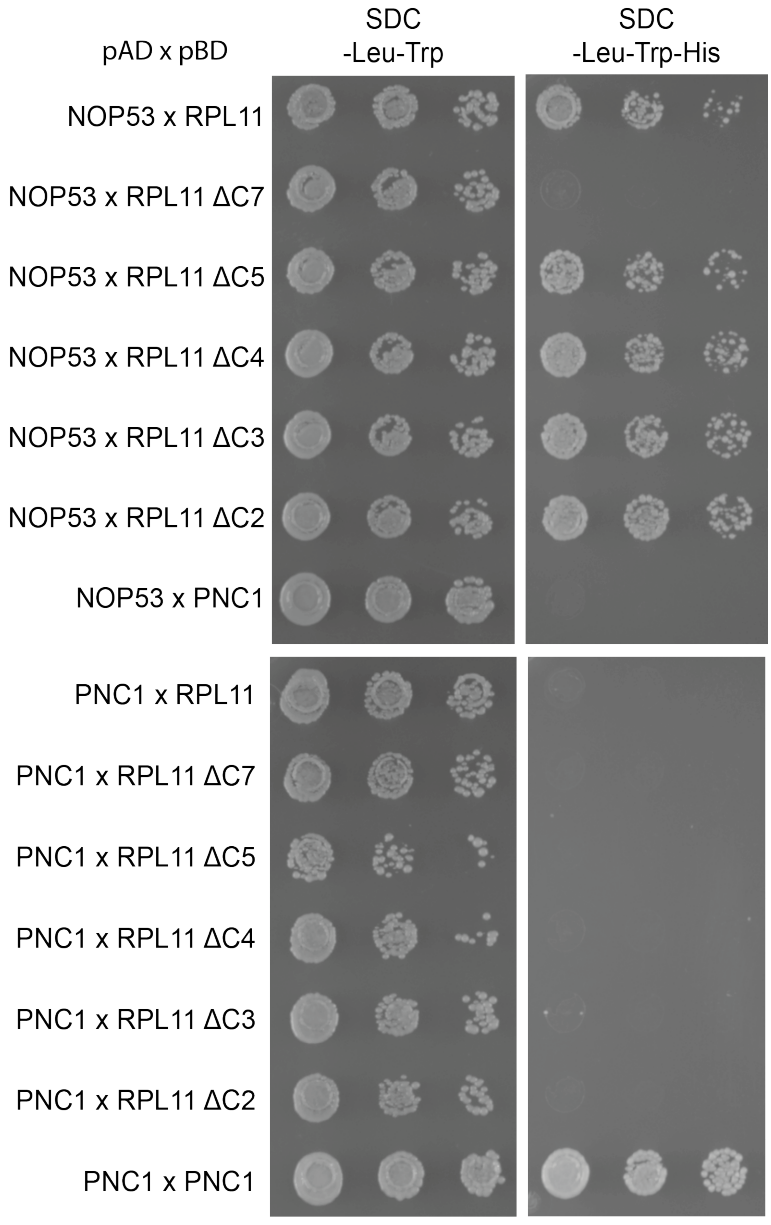


Figure 5.14: Yeast-two-hybrid analysis of NOP53 with RPL11 ΔC7, RPL11 ΔC5, RPL11 ΔC4, RPL11 ΔC3 and RPL11 ΔC2. Yeast-two-hybrid dot plates for NOP53 transformants with RPL11 ΔC7, RPL11 ΔC5, RPL11 ΔC4, RPL11 ΔC3 and RPL11 ΔC2 grown on SDC-Leu-Trp and SDC–Leu-Trp-His.

When looking at the C-terminus of RPL11 (Figure 5.10), the double isoleucine found in the final 7 amino acids is highly conserved through all p53 containing eukaryotes. Interestingly, with the ΔC5 RPL11 mutant, the isoleucine in the first position is still present on the protein, but the second isoleucine has been removed. Therefore, a double isoleucine to alanine mutation was produced alongside a single isoleucine to alanine mutation at each of the positions (RPL11 AA, RPL11 AI and RPL11 IA). Yeast-two-hybrid analysis showed that none of these alanine mutations either singular or double prevented growth on SDC-Leu-Trp-His (Figure 5.15, Supplementary Figure 8.7). RPL11 AA, RPL11 AI and RPL11 IA were still able to interact with NOP53. Subsequently, since neither the shorter truncations to the C-terminus or point mutations within the C-terminus were able to identify a shorter region of interaction, the RPL11 ΔC7 mutant would be used for further investigation.

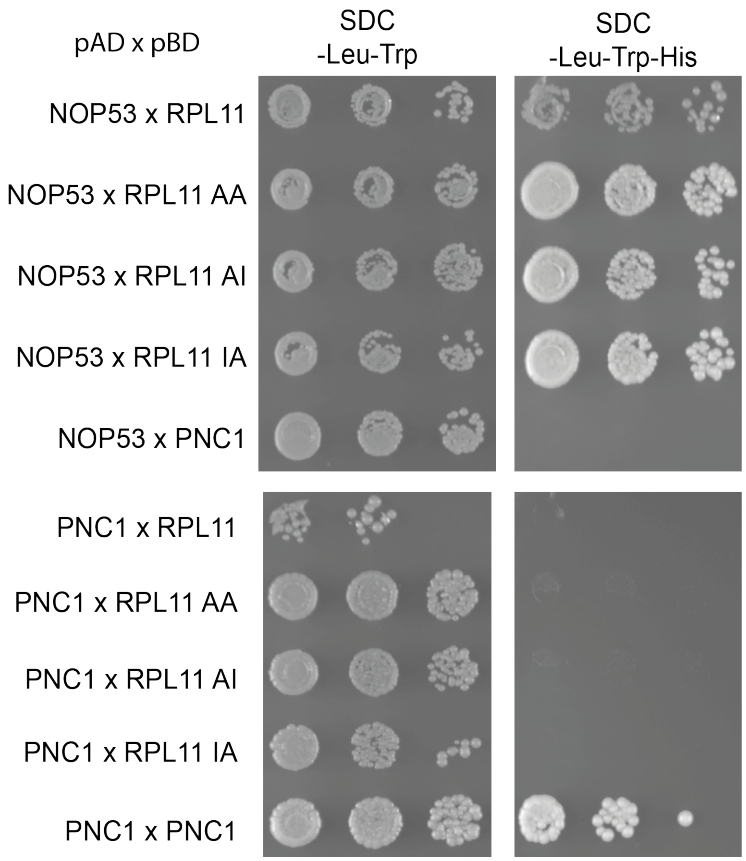


Figure 5.15: Yeast-two-hybrid analysis of NOP53 with RPL11 AA, RPL11 AI and RPL11 IA. Yeast-two-hybrid dot plates for NOP53 transformants with with RPL11 AA, RPL11 AI and RPL11 IA grown on SDC-Leu-Trp and SDC–Leu-Trp-His.

## 5.6 Purification of recombinant 6xHis-RPL11 WT and ΔC7

To complement and confirm the yeast-two-hybrid analyses, the interaction between NOP53 and RPL11 would be investigated by *in vitro* binding assays using recombinantly expressed NOP53, RPL11 WT and RPL11 ΔC7 proteins. RPL11 WT and ΔC7 were cloned into a pET24d vector containing an N-terminal 6xHis tag for induction and expression (pET24d-6xHis-RPL11 WT was produced by Emma Thomson). Induction of both 6xHis-RPL11 and 6xHis-RPL11 ΔC7 were observed and expression was successful in BL21 *E. coli* (Figure 5.16 A, C). 6xHis-RPL11 was subsequently purified using a two-step purification strategy. The

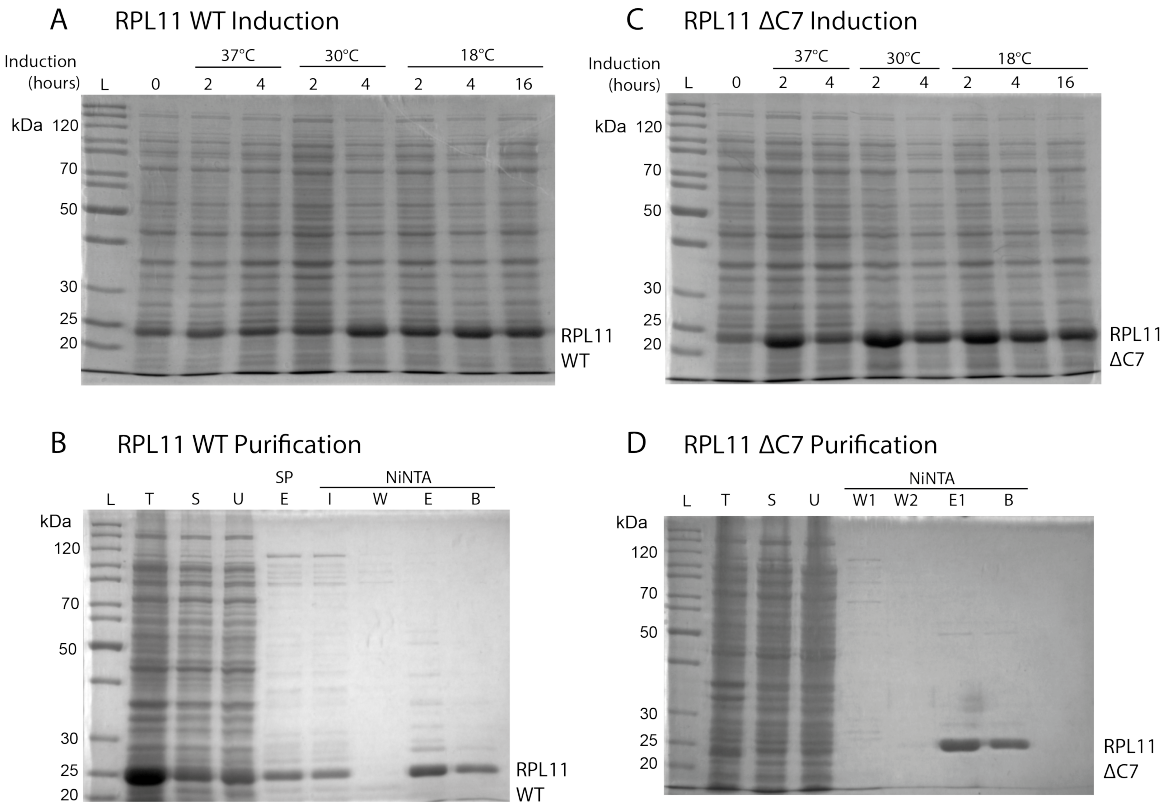


Figure 5.16: Induction and purification of recombinant 6xHis-RPL11 WT and RPL11 ΔC7. A) Induction of RPL11 WT by 0.1 mM IPTG in BL21 *E.coli* at 3 different temperatures, 18, 30 and 37 °C for 2 and 4 hours and overnight for 16 hours at 18 °C with no induction at 0 hours. B) Purification of RPL11 by SP sepharose binding followed by NiNTA binding. Labelling as follows; ladder (L), total (T), soluble (S), unbound (U), eluate (E), input (I), wash (W) and beads (B). C) Induction of RPL11 ΔC7 under the same conditions as WT (panel B). D) Purification of RPL11 ΔC7 by NiNTA binding. Purification and labelling as panel B for WT, with no SP binding and an additional NiNTA wash step.

first step utilised ion exchange chromatography, using SP sepharose followed by a second affinity step, utilising NiNTA binding via the 6xHis tag (Figure 5.16 B). However, 6xHis-RPL11 ΔC7 was unable to bind to SP sepharose likely due to the loss in charge found in the C-terminus. Therefore, a one-step NiNTA purification was carried out, producing purified 6xHis-RPL11 ΔC7 (Figure 5.16 D). Whilst successfully purified, the difficulties described previously with the purification of both NOP53 WT and D90R (section 3.2.1), precluded *in vitro* binding assays from being performed.

## 5.7 Validation and characterisation of RPL11 using Flp-In T-REx HEK293 cells

To further validate and investigate the interaction between RPL11 and NOP53 *in vivo*, the Flp-In T-REx HEK293 cellular system discussed in chapter 3 was used for the production of tetracycline inducible exogenous RPL11 cell lines. RPL11 WT and ΔC7 were cloned into the pcDNA5 vector containing an N-terminal Twin-Strep-II 3xFLAG tag (Vincent WC Chan). Although the N-terminus of RPL11 is ribosome associated (Wu *et al.,* 2016; Zhou *et al.,* 2019), there is previous precedence for N-terminal RPL11 tags being functional (Sloan *et al.,*

2013) and a C-terminal tag may affect the ability of RPL11 to bind NOP53.

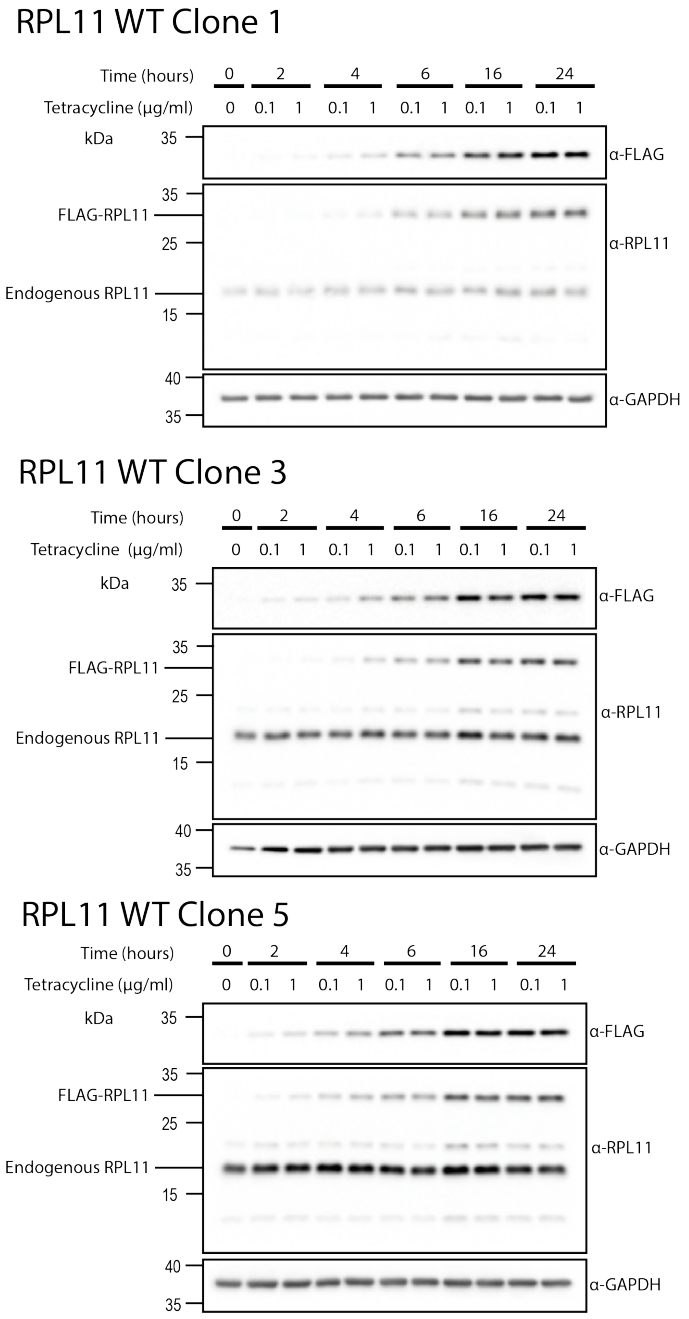


Figure 5.17: Tetracycline induction of Flp-In T-REx HEK293 Twin-Strep-II-3xFLAG RPL11 cell lines. Western blot showing RPL11 expression in triplicate clonal lines following tetracycline induction at 0, 2, 4, 6, 16 or 24 hours at 0.1 or 1 µg/ml tetracycline. The same membrane was sliced and probed with antibodies for FLAG, RPL11, and GAPDH.

A Flp-In T-REx HEK293 TSII-3xFLAG-RPL11 WT cell line was produced and validated for TSII-3xFLAG-RPL11 expression following tetracycline treatment to identify positive clones (Vincent WC Chan). Triplicate clones showing FLAG-RPL11 expression were selected (1, 3 and 5) and analysed varying both tetracycline concentration and duration of induction to optimise expression conditions (Figure 5.17). However, despite numerous attempts to generate the Flp-In T-REx HEK293 TSII-3xFLAG-RPL11 $\Delta$C7 cell line, ex-

pression of FLAG-RPL11 ΔC7 could not be observed (numerous attempts by Thomson Lab).

### RPL11 binds to NOP53 *in vivo*

Following the successful validation of exogenous RPL11 WT expression in the generated cell lines, tetracycline was used to induce the expression of Twin-Strep-II-3xFLAG-RPL11 and a co-immunoprecipitation was carried out using the FLAG affinity tag to observe any NOP53 association. Western blot analysis of the co-immunopreciptiation showed that co-purificiation of NOP53 was observed when pulling down RPL11 (Figure 5.18). These co-immunoprecipitation results confirmed the observed results in the yeast-two-hybrid system that RPL11 interacts with NOP53.

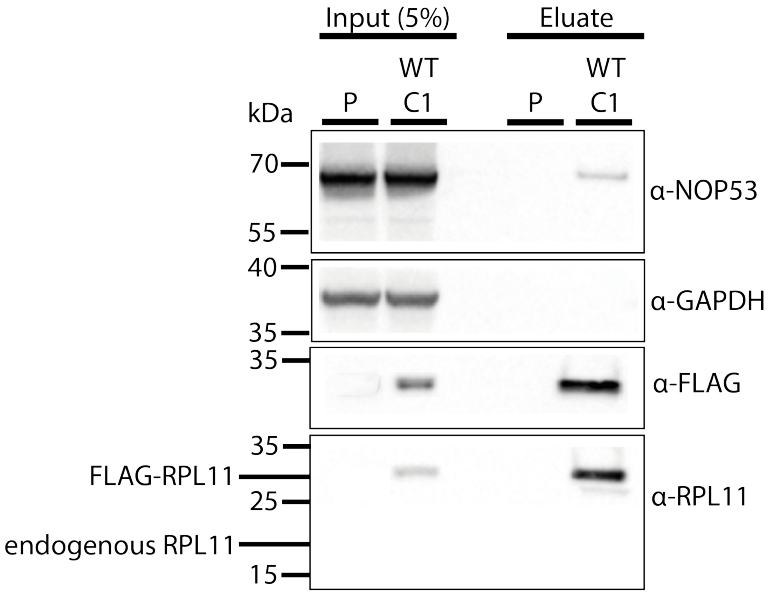


Figure 5.18: Co-immunoprecipitation from Flp-In T-REx HEK293 Twin-Strep-II-3xFLAG-RPL11 cell line. A) Western blot showing input (5 %) and IP samples for parental Flp-In T-REx HEK293 cells (P) and RPL11 WT clone 1 (WT C1). The same membrane for each panel was sliced and probed with antibodies for NOP53, GAPDH, FLAG and RPL11.

## 5.8 Discussion

There was prior evidence in the literature to suggest that NOP53 and RPL11 interact, however the nature of the interaction between NOP53 and RPL11 was poorly understood. In chapter 5, the regions of NOP53 and RPL11 responsible for this interaction have been further characterised. Through yeast-two-hybrid analyses and co-immunoprecipitations, NOP53 and RPL11 were shown to interact. Moreover the NOP53 AIM mutant, D90R, studied in chapter 3, that can no longer interact with MTR4 retained its ability to bind to RPL11. Consequently, NOP53 D90R can be used for the study of the role of NOP53 in ribosome biogenesis without directly affecting the role of NOP53 in the regulation of RPL11, p53 and nucleolar stress responses.

Identifying the regions and residues of NOP53 responsible for protein interactions has been particularly challenging. NOP53 contains limited secondary structures which may bind

to RPL11 with large regions of NOP53 unstructured (Jumper *et al.,* 2021; Varadi *et al.,* 2021; Zimmermann *et al.,* 2018). These unstructured regions are likely to be a contributing factor that has, to date, precluded the structure of NOP53 from being obtained which has proved challenging during cryo-EM analysis. Indeed, even when NOP53 was used as a bait protein, cryo-EM failed to resolve the volume (Wu *et al.,* 2016), which is likely due to a lack of structure and high flexibility. The C-terminal region of NOP53 can bind to the pre-60S particle in *S. cerevisiae* (Thoms *et al.,* 2015; Wu *et al.,* 2016) and displays a high level of sequence conservation to humans (Figure 5.2). It is likely that the function of the C-terminus is also conserved in humans, as the AIM within the N-terminus is conserved in NOP53 for MTR4 recruitment (chapter 3, Thoms *et al.,* 2015). It has been suggested that NOP53 contains two C-terminal arginine-rich nucleolar localisation sequences (Kalt *et al.,* 2012) but as nucleolar localisation of NOP53 in *S. cerevisiae* is suggested to occur due to protein-protein interactions (Granato *et al.,* 2008), these sequences may just mediate ribosomal binding which is required for nucleolar localisation.

Yeast-two-hybrid was first used to try and identify the region(s) of NOP53 responsible for the interaction with RPL11. However, all truncation mutants and NOP53 segments tested by yeast-two-hybrid were shown to retain the ability to interact with RPL11. Removal of the N-terminus (ΔN145) did not affect the ability of NOP53 to bind to RPL11 and, therefore, the N-terminal region is not necessary for the interaction. However, when the amino acids that were removed are expressed themselves (1-145), interaction with RPL11 is still seen, meaning that whilst they are not necessary for the interaction with RPL11, they are sufficient. The same conclusions can be made for the C-terminal region. The last 91 amino acids are not necessary for the interaction, as NOP53 ΔC91 is still capable of interacting, but those amino acids are sufficient for the interaction (387-478). These results suggest that there are likely multiple points of interaction on the side of NOP53. The alphafold prediction of NOP53 also supports this conclusion. The model shows an open confirmation of NOP53 which would enable potential binding of RPL11 across the length of Nop53 and the flexibility provided by the unstructured regions would allow NOP53 to encircle RPL11 creating multiple points of contact.

Random mutagenesis of NOP53 and the subsequent yeast-two-hybrid test screen showed the scale required for mutant identification was not feasible due to the high number of mutants which needed to be screened. Alternatively, alanine scanning could have been used, where the wild-type residue is systemically mutated to an alanine residue. This would avoid the issue of the introduction of pre-mature stop codons which was present following random mutagenesis. However, alanine scanning would also require large scale screening following the introduction of alanine residues due to the length of NOP53 and since there are likely multiple region(s) of interaction, the combinations of mutations to generate and investigate would be extreme.

The inability to identify the precise region of NOP53 that mediates the interaction with RPL11 lead to investigations becoming focused on the regions of RPL11 responsible for binding. Unlike NOP53, the structure of RPL11 has been shown and contains numerous secondary structures (Jumper *et al.,* 2021; Varadi *et al.,* 2021). The termini of RPL11 are exposed and show both flexibility and a lower level of sequence conservation between higher eukaryotes and *S. cerevisiae* compared with the rest of RPL11. The C-terminal sequence of RPL11 is not conserved in *S. cerevisiae*, and as yeast lack p53, there is likely no direct interaction between Nop53 and Rpl11 in the context of p53 regulation observed in higher eukaryotes, with no evidence to suggest otherwise. Upon deletion, RPL11 Δ C7 was unable to bind to NOP53 confirmed by yeast-two-hybrid analysis but evidently requires further analysis and validation.

Finally, the chapter also shows *in vivo* the successful generation of Flp-In T-Rex HEK293 Twin-Strep-II-3x-FLAG RPL11 WT cell lines. However, the RPL11 ΔC7 cell lines showed no expression despite several attempts in making the cell line. The pcDNA5 vector containing RPL11 ΔC7 was sequenced and found to harbour no mutations (Monika Feigenbutz). Therefore, it is interesting to consider why the cells may not tolerate the expression of RPL11 ΔC7. As the FLAG-RPL11 WT was successfully made and expressed and previous N-terminal RPL11 tagging strategies were successful (Sloan *et al.,* 2013), the issue with RPL11 ΔC7 is therefore unlikely to be caused by the epitope tag. However, the functionality of FLAG-RPL11 will be confirmed using gradient fraction analysis to validate successful 60S and polysome integration.

One suggestion is that tetracycline induction of RPL11 ΔC7 expression is successful, but RPL11 ΔC7 is actively degraded, so no expression can be observed by Western blot. Ribosomal proteins are known to be produced in excess of their requirements for ribosome biogenesis and actively degraded by the proteasome (Lam *et al.,* 2007; Sung *et al.,* 2016). Consequently, if FLAG-RPL11 WT is functional, overexpression would lead to excess pools of both FLAG-RPL11 and endogenous RPL11 as well as incorporation of both into the ribosome. However, if the ΔC7 mutation is non-functional and cannot be incorporated into the 60S particle, it would remain in the free pool with only endogenous RPL11 incorporated into the ribosome and subsequently, targeted for degradation. Alternatively, RPL11 ΔC7 may be toxic to cells due to the loss of interaction with NOP53. This would enable the constitutive inhibition of HDM2 and therefore stabilisation of p53, cell cycle arrest and apoptosis. This could result in apoptosis in all cells capable of expressing RPL11 ΔC7 and ultimately select for a population of cells which show limited or no RPL11 ΔC7 expression. Nevertheless, RPL11 ΔC7 requires further investigation.

# Chapter 6

# Final Discussion

The initial aim of this study was to generate separation of function mutants of human NOP53 to uncouple ribosome biogenesis and the nucleolar stress response. To do this, the sites of interaction on NOP53 with MTR4, an interaction important in ribosome biogenesis, and with RPL11, involved in the nucleolar stress response needed to be identified. Evidence presented here confirms that the mechanism of interaction between NOP53 and MTR4 is conserved from *S. cerevisiae*. A point mutation in NOP53 (D90R) is sufficient to drastically decrease the interaction with MTR4 whilst maintaining an interaction with RPL11. However, despite substantial investigations into NOP53, the region(s) responsible for the interaction with RPL11 could not be identified. To enable phenotypic analysis, p53 positive, karyotypically normal homozygous and heterozygous NOP53 D90R hPSC lines were generated. Whilst further experiments are needed to validate the lines, it would be interesting to compare the balance of NOP53 binding with MTR4 and RPL11 in the homozygous and heterozygous hPSC NOP53 D90R lines with that of the hPSC NOP53 WT (unedited) lines. These cell lines will allow the loss of NOP53 function in ribosome biogenesis to be studied without directly affecting its role in nucleolar stress. The further elucidation of the role of NOP53 in these two nucleolar processes, will aid in the understanding of the mechanisms of both cancer and ribosomopathies which will be the focus of further discussion.

## 6.1 The nucleolus, ribosome biogenesis and disease

The interplay between ribosome biogenesis and the nucleolar stress response is incredibly complex. Defects in ribosome biogenesis trigger the nucleolar stress response and activation of the nucleolar stress response inhibits ribosome biogenesis. For example, depletion of MTR4 has been shown to trigger p53 stabilisation (Miyao *et al.,* 2022), likely because of rRNA processing defects. Consequently, any disease which is associated with ribosome biogenesis and the regulation of biogenesis is inherently linked to the nucleolar stress response. This is particularly evident for ribosomopathies and cancer, as patients with mutations in ribosome biogenesis components display defective ribosome biogenesis causing tissue-specific phenotypes and have an increased risk of cancer development.

### 6.1.1 NOP53 and RPL11 in cancer

Mutations and deletions within both HMD2 and p53 have been found in a wide range of cancers. It is, therefore, no surprise that mutations or deletions within RPL5 and RPL11 which negatively regulate HDM2 and, consequently, p53 stabilisation, have also been identified in human cancer. Analysis across 49 different cancer types detected 139 RPL5 and 74 RPL11 cancer-associated mutations (Orsolic *et al.,* 2016). Mutations in both RPL5 and

RPL11 along with other RPs are often found in combination with a p53 mutation across cancer types (Ajore *et al.,* 2017). However, since NOP53 inhibits RPL11 binding to HDM2, WT p53 is found in cancers showing high levels of NOP53 transcription (Okamura *et al.,* 2014). This may be because there was no competitive pressure for p53 to overcome cell cycle arrest.

NOP53 was first identified in humans due to its position on chromosome 19q13.32 which is a common site for cancer mutations (Smith *et al.,* 2000). Later NOP53 was characterised as a tumour suppressor protein due to its stabilisation of PTEN (Kim *et al.,* 2011; Okahara *et al.,* 2006). However, the contribution of NOP53 to cancer development is more complex as it can act as both a positive and negative regulator of cancer development, depending on cell and cancer type (Böhm *et al.,* 2015; Kim *et al.,* 2012; Lee *et al.,* 2020; Moon *et al.,* 2013). While the underlying cause of this inconsistency is unclear, it may occur due to the mutational background of the cancer, e.g., if the cells are p53 +/-. Understanding the role that NOP53 plays in cancer development is made more challenging, as not only does it regulate p53 via an interaction with RPL11 (discussed in chapter 1), NOP53 is also implicated in c-Myc and PTEN regulation.

### The role and regulation of c-Myc

Whilst p53 functions as a tumour suppressor to limit cell division, the oncoprotein c-Myc, another key regulator, acts antagonistically. c-Myc can control the rate of cell growth by acting as a master regulator of ribosome biogenesis, by regulating all three RNA polymerases required for 47S rRNA, 5S rRNA and RP transcription (Oskarsson & Trumpp, 2005; Adhikary & Eilers, 2005). Subsequently, excessive expression and activity of c-Myc has been associated with variety of human cancers (Liao & Dickson, 2000; Prochownik, 2004; Teng *et al.,* 2013).

The delicate balance of cellular growth is regulated by ARF mediated degradation of both p53 and c-Myc, coupling the proteasomal degradation of two major regulators of cellular homeostasis (Dai *et al.,* 2006). Regulation of p53 and c-Myc is also coupled together through RPL11 and, in turn, NOP53. In addition to its role in the regulation of p53, RPL11 also has a novel role as a negative feedback regulator of c-Myc (Dai *et al.,* 2007). RPL11 is a transcriptional target of c-Myc via RNA polymerase II and once expressed, acts to suppress c-Myc dependent transcription of the 5S rRNA. This, in turn, inhibits c-Myc driven cell proliferation and ensures a tight coordination between c-Myc activity and ribosome biogenesis (Dai *et al.,* 2007; Dai *et al.,* 2006).

Currently, no other ribosomal proteins have been shown to be involved alongside RPL11 in regulating c-Myc activity. Therefore, the question remains as to whether RPL11, and subsequently NOP53, can act as a tumour suppressor with dual activity in stabilising p53 and inactivating c-Myc in response to nucleolar stress and perturbations in ribosome biogenesis. Additionally, as the NOP53 D90R mutation does not preclude RPL11 binding, the NOP53 D90R hPSC lines generated in this study provide a means to study the intact interplay between NOP53, RPL11 and p53 following perturbations to ribosome biogenesis. Understanding the mechanisms by which NOP53 can regulate RPL11 provides a potential target in specific cancer cases where the ARF-HDM2-p53 pathway has become inactivated as RPL11-HDM2-p53 acts independently.

#### The regulation of PTEN

NOP53 is also implicated with another key regulator of cell growth and proliferation, PTEN (Okahara *et al.,* 2004). PTEN, like p53, is a tumor suppressor and was first identified due to the high level of mutations found in the gene across multiple cancers (Li *et al.,* 1997; Steck *et al.,* 1997). Over 20 % of these mutations were found within the C-terminal region of PTEN, which was later shown to be required to interact with NOP53 (Ali *et al.,* 1999; Okahara *et al.,* 2004). NOP53 binding to PTEN mediates its phosphorylation and stabilisation.

Although, the role of NOP53 in stabilising PTEN has not been discussed previously, it is worth discussing this here in the context of NOP53 as a regulator of two key tumor suppressors, PTEN and p53. However, the role NOP53 appears to play in each of these pathways is antagonistic. Through the stabilisation of PTEN, NOP53 acts to limit cell growth. Whereas, p53 is actively degraded because NOP53 sequesters RPL11 and thus prevents p53-mediated cell cycle arrest, enabling cell growth. NOP53 is capable of both limiting and enabling cell growth, however, the mechanism by which this occurs is not understood. NOP53 may be able to bind both PTEN and RPL11 simultaneously, ensuring the tight balance of growth and proliferation is maintained. Alternatively, binding of one may preclude the binding of the other, actively driving or inhibiting cell growth. Despite attempts presented in this work, the regions of NOP53 which mediate the interaction with RPL11 could not be identified and the regions of NOP53 which bind PTEN are also not known. It would therefore, be interesting to consider if the two proteins bind to the same region of NOP53, should the interaction with RPL11 be successfully mapped. Additionally, it would be interesting to consider if the NOP53 D90R mutant is capable of interacting with PTEN and if so, by abolishing the interaction with MTR4 are the dynamics of the interaction between NOP53 and PTEN altered. NOP53 plays a complex role not only in nucleolar functions during ribosome biogenesis and the nucleolar stress response but also on cellular function as a whole through key regulators of cell growth and proliferation. Therefore, the hPSC NOP53 lines generated are invaluable in providing a cellular system capable of enabling phenotypically relevant investigations into NOP53 biology.

### 6.1.2 Ribosomopathies

Ribosomopathies are a group of human diseases, that despite being characterised by defective ribosome biogenesis, an essential, ubiquitous cellular process, display disease phenotype in specific cell types. Mutations across ribosome biogenesis components and assembly factors leads not only to tissue specific phenotypes caused by defects in ribosome biogenesis, but also a pre-disposition of all cell types to cancer development (Farley-Barnes *et al.,* 2019; Sulima *et al.,* 2019). Whilst discussion into the cause of disease has focused specifically on the impact on ribosome biogenesis, it is worth remembering that ribosomal proteins have extraribosomal functions, making the study into ribosomopathies more complex.

#### RPL11 in ribosomopathies

The extraribosomal functions of RPL11 and its regulation by NOP53 discussed throughout this work, needs to be considered in the context of ribosomopathies. Mutations within RPL11, and in other RPs including RPL5, can cause the well-studied ribosomopathy, Diamond Blackfan Anemia (DBA). These mutations are autosomal dominant and result in haploinsufficiency of RPL11. This not only leads to dysregulation of ribosome biogenesis, though either a reduction in the number of competent ribosomes or the formation of heterogenous ribosomes, but it also alters the extraribosomal function of RPL11. Therefore, regulation of p53 and c-Myc by RPL11 and RPL5 as well as other RPs may represent additional means through

which ribosomopathies present.

Individuals with DBA have reduced or absent erythroid precursors and a significant predisposition to cancer. How cells which show defective ribosome biogenesis, producing limited numbers of ribosomes that are unable to sustain growth, are capable of switching to enhanced rates of ribosome biogenesis driving cell growth and proliferation in cancer, is not well understood. The conventional idea suggested that cells were under selective pressure to gain mutations to create a cellular environment to drive increased rates of ribosome biogenesis or prevent cell cycle arrest triggered by the nucleolar stress response. For example, sporadic mutations in the p53 gene have been observed in patients with ribosomopathies (Lindsley *et al.,* 2017), which may be due to this strong selective pressure to mutate to prevent p53-mediated cell cycle arrest and enable proliferation. However, it is possible that other mechanisms for this switch in ribosomal rate and cell proliferation exist.

Perhaps changes in the balance of p53 and c-Myc as a result of the haploinsufficiency of RPL11 or other RPs may contribute to an increased risk of cancer. Alternatively, the cell may have an altered translation profile which could drive growth and proliferation. p53 activation has been shown to be coupled to translational control using ribosome profiling, with hundreds of transcripts differentially translated upon Rps6 haploinsufficiency and subsequently rescued by loss of p53 (Tiu *et al.,* 2021). Further changes in translation of specific mRNAs have also been observed in DBA models with RPL11, RPL5 and RPS19 haploinsufficiency. This includes a specific decrease in GATA1 translation, a transcription factor required for erythroid development (Horos *et al.,* 2012; Ludwig *et al.,* 2014; Sankaran *et al.,* 2012). These studies suggested that the changes in translation were as a result of the haploinsufficiency negatively impacting ribosome assembly resulting in either a limited available pool of ribosomes (Lodish, 1974; Mills & Green, 2017) or the formation of heterogenous ribosomes which have altered mRNA preference. It was not considered that the loss of regulation of p53 by RPL11, RPL5 and RPS19, prevented p53 mediated translational regulation. The importance of functional p53 control on translation and cell growth should not be dismissed due to the propensity of RP mutations concurrent with p53 mutations in cancer.

## 6.2 Concluding remarks

The molecular mechanisms coupling nucleolar processes are incredibly complex. Whilst the region of NOP53 responsible for the interaction with RPL11 could not be identified, NOP53 D90R did not interact with MTR4, but could still interact with RPL11. This will allow the hPSC NOP53 D90R cell lines generated in this study to be used as a cellular system for functional analysis to elucidate the role of NOP53 in ribosome biogenesis and study the effect of this defect on the nucleolar stress response. Both NOP53 WT and D90R hPSCs offer the potential for the investigation of ribosome biogenesis and the nucleolar stress response throughout development across a range of cell types due to their differentiation capacity. This will be of particular interest when investigating cell types in which ribosomopathies present themselves with the hope that through the molecular dissection of NOP53 we can better understand the interplay between ribosome biogenesis and the nucleolar stress response.

# Chapter 7

# References


Adhikary, S., & Eilers, M. (2005). Transcriptional regulation and transformation by Myc proteins. Nature Reviews. Molecular Cell Biology, 6(8), 635–645.

Ajore, R., Raiser, D., McConkey, M., Jöud, M., Boidol, B., Mar, B., Saksena, G., Weinstock, D. M., Armstrong, S., Ellis, S. R., Ebert, B. L., & Nilsson, B. (2017). Deletion of ribosomal protein genes is a common vulnerability in human cancer, especially in concert with TP53 mutations. EMBO Molecular Medicine, 9(4), 498–507.

Ali, I. U., Schriml, L. M., & Dean, M. (1999). Mutational spectra of PTEN/MMAC1 gene: a tumor suppressor with lipid phosphatase activity. Journal of the National Cancer Institute, 91(22), 1922–1932.

Allmang, C., Kufel, J., Chanfreau, G., Mitchell, P., Petfalski, E., & Tollervey, D. (1999). Functions of the exosome in rRNA, snoRNA and snRNA synthesis. The EMBO Journal, 18(19), 5399–5410.

Andersen, J. S., Lam, Y. W., Leung, A. K. L., Ong, S.-E., Lyon, C. E., Lamond, A. I., & Mann, M. (2005). Nucleolar proteome dynamics. Nature, 433(7021), 77–83.

Andrews, P. W., Ben-David, U., Benvenisty, N., Coffey, P., Eggan, K., Knowles, B. B., Nagy, A., Pera, M., Reubinoff, B., Rugg-Gunn, P. J., & Stacey, G. N. (2017). Assessing the Safety of Human Pluripotent Stem Cells and Their Derivatives for Clinical Applications. Stem Cell Reports, 9(1), 1–4.

Anger, A. M., Armache, J.-P., Berninghausen, O., Habeck, M., Subklewe, M., Wilson, D. N., & Beckmann, R. (2014). Structure of the human 80S ribosome. Protein Data Bank, Rutgers University.

Aubert, M., O'Donohue, M.-F., Lebaron, S., & Gleizes, P.-E. (2018). Pre-Ribosomal RNA Processing in Human Cells: From Mechanisms to Congenital Diseases. Biomolecules, 8(4).

Awad, D., Prattes, M., Kofler, L., Rössler, I., Loibl, M., Pertl, M., Zisser, G., Wolinski, H., Pertschy, B., & Bergler, H. (2019). Inhibiting eukaryotic ribosome biogenesis. BMC Biology, 17(1), 46.

Badcock, G., Pigott, C., Goepel, J., & Andrews, P. W. (1999). The human embryonal carcinoma marker antigen TRA-1-60 is a sialylated keratan sulfate proteoglycan. Cancer

Research, 59(18), 4715–4719.

Barrio-Garcia, C., Thoms, M., Flemming, D., Kater, L., Berninghausen, O., Baßler, J., Beckmann, R., & Hurt, E. (2016). Architecture of the Rix1-Rea1 checkpoint machinery during pre-60S-ribosome remodeling. Nature Structural & Molecular Biology, 23(1), 37–44.

Belin, S., Beghin, A., Solano-Gonzàlez, E., Bezin, L., Brunet-Manquat, S., Textoris, J., Prats, A.-C., Mertani, H. C., Dumontet, C., & Diaz, J.-J. (2009). Dysregulation of ribosome biogenesis and translational capacity is associated with tumor progression of human breast cancer cells. PloS One, 4(9), e7147.

Berglind, H., Pawitan, Y., Kato, S., Ishioka, C., & Soussi, T. (2008). Analysis of p53 mutation status in human cancer cell lines: a paradigm for cell line cross-contamination. Cancer Biology & Therapy, 7(5), 699–708.

Bhat, K. P., Itahana, K., Jin, A., & Zhang, Y. (2004). Essential role of ribosomal protein L11 in mediating growth inhibition-induced p53 activation. The EMBO Journal, 23(12), 2402–2412.

Black, J. J., & Johnson, A. W. (2022). Release of the ribosome biogenesis factor Bud23 from small subunit precursors in yeast. RNA , 28(3), 371–389.

Böhm, M., Reil, J.-C., Deedwania, P., Kim, J. B., & Borer, J. S. (2015). Resting heart rate: risk indicator and emerging risk factor in cardiovascular disease. The American Journal of Medicine, 128(3), 219–228.

Bohnsack, K. E., & Bohnsack, M. T. (2019). Uncovering the assembly pathway of human ribosomes and its emerging links to disease. The EMBO Journal, 38(13), e100278.

Boulon, S., Westman, B. J., Hutten, S., Boisvert, F.-M., & Lamond, A. I. (2010). The nucleolus under stress. Molecular Cell, 40(2), 216–227.

Boyne, J. R., & Whitehouse, A. (2006). Nucleolar trafficking is essential for nuclear export of intronless herpesvirus mRNA. Proceedings of the National Academy of Sciences of the United States of America, 103(41), 15190–15195.

Brüning, L., Hackert, P., Martin, R., Davila Gallesio, J., Aquino, G. R. R., Urlaub, H., Sloan, K. E., & Bohnsack, M. T. (2018). RNA helicases mediate structural transitions and compositional changes in pre-ribosomal complexes. Nature Communications, 9(1), 1–14.

Budde, A., & Grummt, I. (1999). p53 represses ribosomal gene transcription. Oncogene, 18(4), 1119–1124.

Bursać, S., Brdovčak, M. C., Pfannkuchen, M., Orsolić, I., Golomb, L., Zhu, Y., Katz, C., Daftuar, L., Grabušić, K., Vukelić, I., Filić, V., Oren, M., Prives, C., & Volarević, S. (2012). Mutual protection of ribosomal proteins L5 and L11 from degradation is essential for p53 activation upon ribosomal biogenesis stress. Proceedings of the National Academy of Sciences, 109(50), 20467–20472.

Butler, L., Adamson, K. I., Johnson, S. L., Jestice, L. H., Price, C. J., Stavish, D., Pooranachandran, N., Malicki, J. J., Tsakiridis, A., Grierson, A. J., & Barbaric, I. (2022). HDAC6 inhibition partially alleviates mitochondrial trafficking defects and restores motor

function in human motor neuron and zebrafish models of Charcot-Marie-Tooth Disease Type 2A. In bioRxiv (p. 2022.07.05.498819).

Bywater, M. J., Poortinga, G., Sanij, E., Hein, N., Peck, A., Cullinane, C., Wall, M., Cluse, L., Drygin, D., Anderes, K., Huser, N., Proffitt, C., Bliesath, J., Haddach, M., Schwaebe, M. K., Ryckman, D. M., Rice, W. G., Schmitt, C., Lowe, S. W., ... Hannan, R. D. (2012). Inhibition of RNA polymerase I as a therapeutic strategy to promote cancer-specific activation of p53. Cancer Cell, 22(1), 51–65.

Callaway, E. (2020, February 10). Revolutionary cryo-EM is taking over structural biology. Nature Publishing Group UK.

Calviño, F. R., Kharde, S., Ori, A., Hendricks, A., Wild, K., Kressler, D., Bange, G., Hurt, E., Beck, M., & Sinning, I. (2015). Symportin 1 chaperones 5S RNP assembly during ribosome biogenesis by occupying an essential rRNA-binding site. Nature Communications, 6, 6510.

Chakraborty, A., Uechi, T., Higa, S., Torihara, H., & Kenmochi, N. (2009). Loss of ribosomal protein L11 affects zebrafish embryonic development through a p53-dependent apoptotic response. PloS One, 4(1), e4152.

Chen CY, Gherzi R, Ong SE, Chan EL, Raijmakers R, Pruijn GJ, Stoecklin G, Moroni C, Mann M, Karin M. AU binding proteins recruit the exosome to degrade ARE-containing mRNAs. Cell. 2001 Nov 16;107(4):451-64.

Chen, F., Pruett-Miller, S. M., Huang, Y., Gjoka, M., Duda, K., Taunton, J., Collingwood, T. N., Frodin, M., & Davis, G. D. (2011). High-frequency genome editing using ssDNA oligonucleotides with zinc-finger nucleases. Nature Methods, 8(9), 753–755.

Chen, H., Han, L., Tsai, H., Wang, Z., Wu, Y., Duo, Y., Cao, W., Chen, L., Tan, Z., Xu, N., Huang, X., Zhuang, J., & Huang, L. (2016). PICT-1 is a key nucleolar sensor in DNA damage response signaling that regulates apoptosis through the RPL11-MDM2-p53 pathway. Oncotarget, 7(50), 83241–83257.

Chen, Y.-C., Rajagopala, S. V., Stellberger, T., & Uetz, P. (2010). Exhaustive benchmarking of the yeast two-hybrid system [Review of Exhaustive benchmarking of the yeast two-hybrid system]. Nature Methods, 7(9), 667–668; author reply 668.

Chesnokov, I., Chu, W. M., Botchan, M. R., & Schmid, C. W. (1996). p53 inhibits RNA polymerase III-directed transcription in a promoter-dependent manner. Molecular and Cellular Biology, 16(12), 7084–7088.

Chlebowski, A., Lubas, M., Jensen, T. H., & Dziembowski, A. (2013). RNA decay machines: the exosome. Biochimica et Biophysica Acta, 1829(6-7), 552–560.

Ciganda, M., & Williams, N. (2011). Eukaryotic 5S rRNA biogenesis. Wiley Interdisciplinary Reviews. RNA, 2(4), 523–533.

Dai, M.-S., Arnold, H., Sun, X.-X., Sears, R., & Lu, H. (2007). Inhibition of c-Myc activity by ribosomal protein L11. The EMBO Journal, 26(14), 3332–3345.

Dai, M.-S., Jin, Y., Gallegos, J. R., & Lu, H. (2006). Balance of Yin and Yang: Ubiquitylation-Mediated Regulation of p53 and c-Myc. Neoplasia , 8(8), 630–644.

Dai, M.-S., & Lu, H. (2004). Inhibition of MDM2-mediated p53 ubiquitination and degradation by ribosomal protein L5. The Journal of Biological Chemistry, 279(43), 44475–44482.

Dai, M.-S., Shi, D., Jin, Y., Sun, X.-X., Zhang, Y., Grossman, S. R., & Lu, H. (2006). Regulation of the MDM2-p53 pathway by ribosomal protein L11 involves a post-ubiquitination mechanism. The Journal of Biological Chemistry, 281(34), 24304–24313.

Dai, M.-S., Sun, X.-X., & Lu, H. (2010). Ribosomal protein L11 associates with c-Myc at 5 S rRNA and tRNA genes and regulates their expression. The Journal of Biological Chemistry, 285(17), 12587–12594.

Davis, L., & Maizels, N. (2014). Homology-directed repair of DNA nicks via pathways distinct from canonical double-strand break repair. Proceedings of the National Academy of Sciences, 111(10), E924–E932.

de la Cruz, J., Kressler, D., Rojo, M., Tollervey, D., & Linder, P. (1998). Spb4p, an essential putative RNA helicase, is required for a late step in the assembly of 60S ribosomal subunits in Saccharomyces cerevisiae. RNA , 4(10), 1268–1281.

Delan-Forino, C., Spanos, C., Rappsilber, J. & Tollervey, D. Substrate specificity of the TRAMP nuclear surveillance complexes. Nat Commun 11, 3122 (2020).

Delavoie, F., Soldan, V., Rinaldi, D., Dauxois, J.-Y., & Gleizes, P.-E. (2019). The path of pre-ribosomes through the nuclear pore complex revealed by electron tomography. Nature Communications, 10(1), 497.

Derenzini, M., Trerè, D., Pession, A., Montanaro, L., Sirri, V., & Ochs, R. L. (1998). Nucleolar function and size in cancer cells. The American Journal of Pathology, 152(5), 1291–1297.

Dieci, G., Conti, A., Pagano, A., & Carnevali, D. (2013). Identification of RNA polymerase III-transcribed genes in eukaryotic genomes. Biochimica et Biophysica Acta, 1829(3-4), 296–305.

Dielforder, T., Braun, C. M., Hölzgen, F., Li, S., Thiele, M., Huber, M., Ohmayer, U., & Perez-Fernandez, J. (2022). Structural Probing with MNase Tethered to Ribosome Assembly Factors Resolves Flexible RNA Regions within the Nascent Pre-Ribosomal RNA. Non-Coding RNA, 8(1).

Domanski, M., Molloy, K., Jiang, H., Chait, B. T., Rout, M. P., Jensen, T. H., & LaCava, J. (2012). Improved methodology for the affinity isolation of human protein complexes expressed at near endogenous levels. BioTechniques, 0(0), 1–6.

Donati, G., Peddigari, S., Mercer, C. A., & Thomas, G. (2013). 5S ribosomal RNA is an essential component of a nascent ribosomal precursor complex that regulates the Hdm2-p53 checkpoint. Cell Reports, 4(1), 87–98.

Drozdetskiy, A., Cole, C., Procter, J., & Barton, G. J. (2015). JPred4: a protein sec-

ondary structure prediction server. Nucleic Acids Research, 43(W1), W389–W394.

Dziembowski, A., Lorentzen, E., Conti, E., & Séraphin, B. (2007). A single subunit, Dis3, is essentially responsible for yeast exosome core activity. Nature Structural & Molecular Biology, 14(1), 15–22.

Engelke, D. R., Ng, S. Y., Shastry, B. S., & Roeder, R. G. (1980). Specific interaction of a purified transcription factor with an internal control region of 5S RNA genes. Cell, 19(3), 717–728.

Falk, S., Tants, J.-N., Basquin, J., Thoms, M., Hurt, E., Sattler, M., & Conti, E. (2017). Structural insights into the interaction of the nuclear exosome helicase Mtr4 with the preribosomal protein Nop53. RNA , 23(12), 1780–1787.

Farley-Barnes, K. I., Ogawa, L. M., & Baserga, S. J. (2019). Ribosomopathies: Old Concepts, New Controversies. Trends in Genetics: TIG, 35(10), 754–767.

Feng, H., Tian, H., Wang, Y., Zhang, Q., Lin, N., Liu, S., Yu, Y., Deng, H., & Gao, P. (2020). Molecular mechanism underlying selective inhibition of mRNA nuclear export by herpesvirus protein ORF10. Proceedings of the National Academy of Sciences, 117(43), 26719–26727.

Ferreira-Cerca, S., Pöll, G., Gleizes, P.-E., Tschochner, H., & Milkereit, P. (2005). Roles of eukaryotic ribosomal proteins in maturation and transport of pre-18S rRNA and ribosome function. Molecular Cell, 20(2), 263–275.

Ferreira-Cerca, S., Pöll, G., Kühn, H., Neueder, A., Jakob, S., Tschochner, H., & Milkereit, P. (2007). Analysis of the in vivo assembly pathway of eukaryotic 40S ribosomal proteins. Molecular Cell, 28(3), 446–457.

Fromm, L., Falk, S., Flemming, D., Schuller, J. M., Thoms, M., Conti, E., & Hurt, E. (2017). Reconstitution of the complete pathway of ITS2 processing at the pre-ribosome. Nature Communications, 8(1), 1–11.

Frottin, F., Schueder, F., Tiwary, S., Gupta, R., Körner, R., Schlichthaerle, T., Cox, J., Jungmann, R., Hartl, F. U., & Hipp, M. S. (2019). The nucleolus functions as a phase-separated protein quality control compartment. Science, 365(6451), 342–347.

Gadal, O., Strauss, D., Kessl, J., Trumpower, B., Tollervey, D., & Hurt, E. (2001). Nuclear export of 60s ribosomal subunits depends on Xpo1p and requires a nuclear export sequence-containing factor, Nmd3p, that associates with the large subunit protein Rpl10p. Molecular and Cellular Biology, 21(10), 3405–3415.

Genuth, N. R., & Barna, M. (2018). Heterogeneity and specialized functions of translation machinery: from genes to organisms. Nature Reviews. Genetics, 19(7), 431–452.

Gerstberger, S., Meyer, C., Benjamin-Hong, S., Rodriguez, J., Briskin, D., Bognanni, C., Bogardus, K., Steller, H., & Tuschl, T. (2017). The Conserved RNA Exonuclease Rexo5 Is Required for 3' End Maturation of 28S rRNA, 5S rRNA, and snoRNAs. Cell Reports, 21(3), 758–772.

Gerton, J. L. (2021). Faulty ribosome biogenesis underlies the ribosomopathy alopecia, neurological defects, endocrinopathy (ANE) syndrome. Proceedings of the National Academy of Sciences of the United States of America, 118(24).

Granato, D. C., Gonzales, F. A., Luz, J. S., Cassiola, F., Machado-Santelli, G. M., & Oliveira, C. C. (2005). Nop53p, an essential nucleolar protein that interacts with Nop17p and Nip7p, is required for pre-rRNA processing in Saccharomyces cerevisiae. The FEBS Journal, 272(17), 4450–4463.

Granato, D. C., Machado-Santelli, G. M., & Oliveira, C. C. (2008). Nop53p interacts with 5.8S rRNA co-transcriptionally, and regulates processing of pre-rRNA by the exosome. The FEBS Journal, 275(16), 4164–4178.

Greber, B. J., Gerhardy, S., Leitner, A., Leibundgut, M., Salem, M., Boehringer, D., Leulliot, N., Aebersold, R., Panse, V. G., & Ban, N. (2016). Insertion of the Biogenesis Factor Rei1 Probes the Ribosomal Tunnel during 60S Maturation. Cell, 164(1-2), 91–102.

Greco, A. (2009). Involvement of the nucleolus in replication of human viruses. Reviews in Medical Virology, 19(4), 201–214.

Green, R., & Noller, H. F. (1997). Ribosomes and translation. Annual Review of Biochemistry, 66, 679–716.

Guo, H. (2018). Specialized ribosomes and the control of translation. Biochemical Society Transactions, 46(4), 855–869.

Gupta, S., & Santoro, R. (2020). Regulation and Roles of the Nucleolus in Embryonic Stem Cells: From Ribosome Biogenesis to Genome Organization. Stem Cell Reports, 15(6), 1206–1219.

Halbach, F., Rode, M., & Conti, E. (2012). The crystal structure of S. cerevisiae Ski2, a DExH helicase associated with the cytoplasmic functions of the exosome. RNA , 18(1), 124–134.

Hannan, K. M., Sanij, E., Rothblum, L. I., Hannan, R. D., & Pearson, R. B. (2013). Dysregulation of RNA polymerase I transcription during disease. Biochimica et Biophysica Acta, 1829(3-4), 342–360.

Hanson, P. J., Hossain, A. R., Qiu, Y., Zhang, H. M., Zhao, G., Li, C., Lin, V., Sulaimon, S., Vlok, M., Fung, G., Chen, V. H., Jan, E., McManus, B. M., Granville, D. J., & Yang, D. (2019). Cleavage and Sub-Cellular Redistribution of Nuclear Pore Protein 98 by Coxsackievirus B3 Protease 2A Impairs Cardioprotection. Frontiers in Cellular and Infection Microbiology, 9, 265.

Haupt, Y., Maya, R., Kazaz, A., & Oren, M. (1997). Mdm2 promotes the rapid degradation of p53. Nature, 387(6630), 296–299.

He, Y., Andersen, G.R., and Nielsen, K.H. (2010). Structural basis for the function of DEAH helicases. EMBO Reports 11, 180–186.

Hein, N., Hannan, K. M., George, A. J., Sanij, E., & Hannan, R. D. (2013). The nucleo-

lus: an emerging target for cancer therapy. Trends in Molecular Medicine, 19(11), 643–654.

Henras, A. K., Plisson-Chastang, C., Humbert, O., Romeo, Y., & Henry, Y. (2017). Synthesis, Function, and Heterogeneity of snoRNA-Guided Posttranscriptional Nucleoside Modifications in Eukaryotic Ribosomal RNAs. The Enzymes, 41, 169–213.

Henras, A. K., Plisson-Chastang, C., O'Donohue, M.-F., Chakraborty, A., & Gleizes, P.-E. (2015). An overview of pre-ribosomal RNA processing in eukaryotes. In Wiley Interdisciplinary Reviews: RNA (Vol. 6, Issue 2, pp. 225–242).

Henras, A. K., Soudet, J., Gérus, M., Lebaron, S., Caizergues-Ferrer, M., Mougin, A., & Henry, Y. (2008). The post-transcriptional steps of eukaryotic ribosome biogenesis. Cellular and Molecular Life Sciences: CMLS, 65(15), 2334–2359.

Hernandez-Verdun, D. (2006). Nucleolus: from structure to dynamics. Histochemistry and Cell Biology, 125(1-2), 127–137.

Hernandez-Verdun, D. (2011a). Assembly and disassembly of the nucleolus during the cell cycle. Nucleus , 2(3), 189–194.

Hernandez-Verdun, D. (2011b). Structural Organization of the Nucleolus as a Consequence of the Dynamics of Ribosome Biogenesis. In The Nucleolus (pp. 3–28).

Hernandez-Verdun, D., Roussel, P., Thiry, M., Sirri, V., & Lafontaine, D. L. J. (2010). The nucleolus: structure/function relationship in RNA metabolism. Wiley Interdisciplinary Reviews. RNA, 1(3), 415–431.

Hiscox, J. A. (2002). The nucleolus–a gateway to viral infection? Archives of Virology, 147(6), 1077–1089.

Holmberg Olausson, K., Nistér, M., & Lindström, M. S. (2012). p53 -Dependent and -Independent Nucleolar Stress Responses. Cells , 1(4), 774–798.

Holub, P., Lalakova, J., Cerna, H., Pasulka, J., Sarazova, M., Hrazdilova, K., Arce, M. S., Hobor, F., Stefl, R., & Vanacova, S. (2012). Air2p is critical for the assembly and RNA-binding of the TRAMP complex and the KOW domain of Mtr4p is crucial for exosome activation. Nucleic Acids Research, 40(12), 5679–5693.

Hori, Y., Engel, C., & Kobayashi, T. (2023). Regulation of ribosomal RNA gene copy number, transcription and nucleolus organization in eukaryotes. Nature Reviews. Molecular Cell Biology.

Horn, H. F., & Vousden, K. H. (2008). Cooperation between the ribosomal proteins L5 and L11 in the p53 pathway. Oncogene, 27(44), 5774–5784.

Horos, R., Ijspeert, H., Pospisilova, D., Sendtner, R., Andrieu-Soler, C., Taskesen, E., Nieradka, A., Cmejla, R., Sendtner, M., Touw, I. P., & von Lindern, M. (2012). Ribosomal deficiencies in Diamond-Blackfan anemia impair translation of transcripts essential for differentiation of murine and human erythroblasts. Blood, 119(1), 262–272.

Iapalucci-Espinoza, S., & Franze-Fernández, M. T. (1979). Effect of protein synthesis

inhibitors and low concentrations of actinomycin D on ribosomal RNA synthesis. FEBS Letters, 107(2), 281–284.

Iarovaia, O. V., Ioudinkova, E. S., Velichko, A. K., & Razin, S. V. (2021). Manipulation of Cellular Processes via Nucleolus Hijaking in the Course of Viral Infection in Mammals. Cells , 10(7).

Jackson, R. N., Klauer, A. A., Hintze, B. J., Robinson, H., van Hoof, A., & Johnson, S. J. (2010). The crystal structure of Mtr4 reveals a novel arch domain required for rRNA processing. The EMBO Journal, 29(13), 2205–2216.

Jacob, S. T., & Ghosh, A. K. (1999). Control of RNA polymerase I-directed transcription: recent trends. Journal of Cellular Biochemistry, Suppl 32-33, 41–50.

James, A., Wang, Y., Raje, H., Rosby, R., & DiMario, P. (2014). Nucleolar stress with and without p53. Nucleus , 5(5), 402–426.

James, P., Halladay, J., & Craig, E. A. (1996). Genomic libraries and a host strain designed for highly efficient two-hybrid selection in yeast. Genetics, 144(4), 1425–1436.

Januszyk, K., Liu, Q., & Lima, C. D. (2011). Activities of human RRP6 and structure of the human RRP6 catalytic domain. RNA , 17(8), 1566–1577.

Jia, H., Wang, X., Anderson, J. T., & Jankowsky, E. (2012). RNA unwinding by the Trf4/Air2/Mtr4 polyadenylation (TRAMP) complex. Proceedings of the National Academy of Sciences of the United States of America, 109(19), 7292–7297.

Johnson, S. J., & Jackson, R. N. (2013). Ski2-like RNA helicase structures: common themes and complex assemblies. RNA Biology, 10(1), 33–43.

Jones, S. N., Roe, A. E., Donehower, L. A., & Bradley, A. (1995). Rescue of embryonic lethality in Mdm2-deficient mice by absence of p53. Nature, 378(6553), 206–208.

Jumper, J., Evans, R., Pritzel, A., Green, T., Figurnov, M., Ronneberger, O., Tunyasuvunakool, K., Bates, R., Žídek, A., Potapenko, A., Bridgland, A., Meyer, C., Kohl, S. A. A., Ballard, A. J., Cowie, A., Romera-Paredes, B., Nikolov, S., Jain, R., Adler, J., ... Hassabis, D. (2021). Highly accurate protein structure prediction with AlphaFold. Nature, 596(7873), 583–589.

Kalt, I., Levy, A., Borodianskiy-Shteinberg, T., & Sarid, R. (2012). Nucleolar localization of GLTSCR2/PICT-1 is mediated by multiple unique nucleolar localization sequences. PloS One, 7(1), e30825.

Kampen, K. R., Sulima, S. O., Vereecke, S., & De Keersmaecker, K. (2020). Hallmarks of ribosomopathies. Nucleic Acids Research, 48(3), 1013–1028.

Karbstein, K. (2013). Quality control mechanisms during ribosome maturation. Trends in Cell Biology, 23(5), 242–250.

Khajuria, R. K., Munschauer, M., Ulirsch, J. C., Fiorini, C., Ludwig, L. S., McFarland, S. K., Abdulhay, N. J., Specht, H., Keshishian, H., Mani, D. R., Jovanovic, M., Ellis, S. R.,

Fulco, C. P., Engreitz, J. M., Schütz, S., Lian, J., Gripp, K. W., Weinberg, O. K., Pinkus, G. S., ... Sankaran, V. G. (2018). Ribosome Levels Selectively Regulate Translation and Lineage Commitment in Human Hematopoiesis. Cell, 173(1), 90–103.e19.

Khanna, K. K., & Jackson, S. P. (2001). DNA double-strand breaks: signaling, repair and the cancer connection. Nature Genetics, 27(3), 247–254.

Kilchert, C. (2020). RNA Exosomes and Their Cofactors. Methods in Molecular Biology, 2062, 215–235.

Kilchert, C., Wittmann, S., & Vasiljeva, L. (2016). The regulation and functions of the nuclear RNA exosome complex. Nature Reviews. Molecular Cell Biology, 17(4), 227–239.

Kim, K., Heo, D.-H., Kim, I., Suh, J.-Y., & Kim, M. (2016). Exosome Cofactors Connect Transcription Termination to RNA Processing by Guiding Terminated Transcripts to the Appropriate Exonuclease within the Nuclear Exosome. The Journal of Biological Chemistry, 291(25), 13229–13242.

Kim, J.-Y., Park, J.-H., & Lee, S. (2012). GLTSCR2 contributes to the death resistance and invasiveness of hypoxia-selected cancer cells. FEBS Letters, 586(19), 3435–3440.

Kim, J.-Y., Seok, K.-O., Kim, Y.-J., Bae, W. K., Lee, S., & Park, J.-H. (2011). Involvement of GLTSCR2 in the DNA Damage Response. The American Journal of Pathology, 179(3), 1257–1264.

Kim, S., Kim, D., Cho, S. W., Kim, J., & Kim, J.-S. (2014). Highly efficient RNA-guided genome editing in human cells via delivery of purified Cas9 ribonucleoproteins. Genome Research, 24(6), 1012–1019.

Klinge, S., & Woolford, J. L., Jr. (2019). Ribosome assembly coming into focus. Nature Reviews. Molecular Cell Biology, 20(2), 116–131.

Kobayashi, T., Heck, D. J., Nomura, M., & Horiuchi, T. (1998). Expansion and contraction of ribosomal DNA repeats in Saccharomyces cerevisiae: requirement of replication fork blocking (Fob1) protein and the role of RNA polymerase I. In Genes & Development (Vol. 12, Issue 24, pp. 3821–3830).

Kos, M., & Tollervey, D. (2010). Yeast pre-rRNA processing and modification occur cotranscriptionally. Molecular Cell, 37(6), 809–820.

Kowalinski, E., Kögel, A., Ebert, J., Reichelt, P., Stegmann, E., Habermann, B., & Conti, E. (2016). Structure of a Cytoplasmic 11-Subunit RNA Exosome Complex. Molecular Cell, 63(1), 125–134.

Kresoja-Rakic, J., & Santoro, R. (2019). Nucleolus and rRNA Gene Chromatin in Early Embryo Development. Trends in Genetics: TIG, 35(11), 868–879.

Kressler, D., Bange, G., Ogawa, Y., Stjepanovic, G., Bradatsch, B., Pratte, D., Amlacher, S., Strauß, D., Yoneda, Y., Katahira, J., Sinning, I., & Hurt, E. (2012). Synchronizing nuclear import of ribosomal proteins with ribosome assembly. Science, 338(6107), 666–671.

Kressler, D., Hurt, E., & Bassler, J. (2010). Driving ribosome assembly. Biochimica et Biophysica Acta, 1803(6), 673–683.

Kuijk, E., Jager, M., van der Roest, B., Locati, M. D., Van Hoeck, A., Korzelius, J., Janssen, R., Besselink, N., Boymans, S., van Boxtel, R., & Cuppen, E. (2020). The mutational impact of culturing human pluripotent and adult stem cells. Nature Communications, 11(1), 2493.

LaCava, J., Houseley, J., Saveanu, C., Petfalski, E., Thompson, E., Jacquier, A., & Tollervey, D. (2005). RNA degradation by the exosome is promoted by a nuclear polyadenylation complex. Cell, 121(5), 713–724.

Lafontaine, D. L. J., Riback, J. A., Bascetin, R., & Brangwynne, C. P. (2021). The nucleolus as a multiphase liquid condensate. Nature Reviews. Molecular Cell Biology, 22(3), 165–182.

Laing, O., Halliwell, J., & Barbaric, I. (2019). Rapid PCR Assay for Detecting Common Genetic Variants Arising in Human Pluripotent Stem Cell Cultures. Current Protocols in Stem Cell Biology, 49(1), e83.

Lam, Y. W., Lamond, A. I., Mann, M., & Andersen, J. S. (2007). Analysis of nucleolar protein dynamics reveals the nuclear degradation of ribosomal proteins. Current Biology: CB, 17(9), 749–760.

Leary, D. J., & Huang, S. (2001). Regulation of ribosome biogenesis within the nucleolus. FEBS Letters, 509(2), 145–150.

Lebaron, S., Papin, C., Capeyrou, R., Chen, Y.-L., Froment, C., Monsarrat, B., Caizergues-Ferrer, M., Grigoriev, M., & Henry, Y. (2009). The ATPase and helicase activities of Prp43p are stimulated by the G-patch protein Pfa1p during yeast ribosome biogenesis. The EMBO Journal, 28(24), 3808–3819.

Lebreton, A., Tomecki, R., Dziembowski, A., & Séraphin, B. (2008). Endonucleolytic RNA cleavage by a eukaryotic exosome. Nature, 456(7224), 993–996.

Lee, S., Ahn, Y.-M., Kim, J.-Y., Cho, Y.-E., & Park, J.-H. (2020). Downregulation of NOP53 Ribosome Biogenesis Factor Leads to Abnormal Nuclear Division and Chromosomal Instability in Human Cervical Cancer Cells. Pathology Oncology Research: POR, 26(1), 453–459.

Lee, S., Kim, J.-Y., Kim, Y.-J., Seok, K.-O., Kim, J.-H., Chang, Y.-J., Kang, H.-Y., & Park, J.-H. (2012). Nucleolar protein GLTSCR2 stabilizes p53 in response to ribosomal stresses. Cell Death and Differentiation, 19(10), 1613–1622.

Leger-Silvestre, I., & Gas, N. (1999). The nucleolar ultrastructure in yeast. The Nucleolus.

Léger-Silvestre, I., Milkereit, P., Ferreira-Cerca, S., Saveanu, C., Rousselle, J.-C., Choesmel, V., Guinefoleau, C., Gas, N., & Gleizes, P.-E. (2004). The ribosomal protein Rps15p is required for nuclear exit of the 40S subunit precursors in yeast. The EMBO Journal, 23(12), 2336–2347.

Leidig, C., Thoms, M., Holdermann, I., Bradatsch, B., Berninghausen, O., Bange, G., Sinning, I., Hurt, E., & Beckmann, R. (2014). 60S ribosome biogenesis requires rotation of the 5S ribonucleoprotein particle. Nature Communications, 5, 3491.

Lestrade, L., & Weber, M. J. (2006). snoRNA-LBME-db, a comprehensive database of human H/ACA and C/D box snoRNAs. Nucleic Acids Research, 34(Database issue), D158–D162.

Li, J., Yen, C., Liaw, D., Podsypanina, K., Bose, S., Wang, S. I., Puc, J., Miliaresis, C., Rodgers, L., McCombie, R., Bigner, S. H., Giovanella, B. C., Ittmann, M., Tycko, B., Hibshoosh, H., Wigler, M. H., & Parsons, R. (1997). PTEN, a putative protein tyrosine phosphatase gene mutated in human brain, breast, and prostate cancer. Science, 275(5308), 1943–1947.

Liang, X., Potter, J., Kumar, S., Zou, Y., Quintanilla, R., Sridharan, M., Carte, J., Chen, W., Roark, N., Ranganathan, S., Ravinder, N., & Chesnut, J. D. (2015). Rapid and highly efficient mammalian cell engineering via Cas9 protein transfection. Journal of Biotechnology, 208, 44–53.

Liao, D. J., & Dickson, R. B. (2000). c-Myc in breast cancer. Endocrine-Related Cancer, 7(3), 143–164.

Lindsley, R. C., Saber, W., Mar, B. G., Redd, R., Wang, T., Haagenson, M. D., Grauman, P. V., Hu, Z.-H., Spellman, S. R., Lee, S. J., Verneris, M. R., Hsu, K., Fleischhauer, K., Cutler, C., Antin, J. H., Neuberg, D., & Ebert, B. L. (2017). Prognostic Mutations in Myelodysplastic Syndrome after Stem-Cell Transplantation. The New England Journal of Medicine, 376(6), 536–547.

Lindström, M. S., Jin, A., Deisenroth, C., White Wolf, G., & Zhang, Y. (2007). Cancer-associated mutations in the MDM2 zinc finger domain disrupt ribosomal protein interaction and attenuate MDM2-induced p53 degradation. Molecular and Cellular Biology, 27(3), 1056–1068.

Lingaraju, M., Johnsen, D., Schlundt, A., Langer, L. M., Basquin, J., Sattler, M., Heick Jensen, T., Falk, S., & Conti, E. (2019). The MTR4 helicase recruits nuclear adaptors of the human RNA exosome using distinct arch-interacting motifs. Nature Communications, 10(1), 1–11.

Liu, Q., Greimann, J. C., & Lima, C. D. (2006). Reconstitution, activities, and structure of the eukaryotic RNA exosome. Cell, 127(6), 1223–1237.

Löber C, Lenz-Stöppler C, Dobbelstein M. Adenovirus E1-transformed cells grow despite the continuous presence of transcriptionally active p53. J Gen Virol. 2002 Aug;83(Pt 8):2047-2057.

Lodish, H. F. (1974). Model for the regulation of mRNA translation applied to haemoglobin synthesis. Nature, 251(5474), 385–388.

Lohrum, M. A. E., Ludwig, R. L., Kubbutat, M. H. G., Hanlon, M., & Vousden, K. H. (2003). Regulation of HDM2 activity by the ribosomal protein L11. Cancer Cell, 3(6),

577–587.

Lubas, M., Christensen, M. S., Kristiansen, M. S., Domanski, M., Falkenby, L. G., Lykke-Andersen, S., Andersen, J. S., Dziembowski, A., & Jensen, T. H. (2011). Interaction profiling identifies the human nuclear exosome targeting complex. Molecular Cell, 43(4), 624–637.

Ludwig, L. S., Gazda, H. T., Eng, J. C., Eichhorn, S. W., Thiru, P., Ghazvinian, R., George, T. I., Gotlib, J. R., Beggs, A. H., Sieff, C. A., Lodish, H. F., Lander, E. S., & Sankaran, V. G. (2014). Altered translation of GATA1 in Diamond-Blackfan anemia. Nature Medicine, 20(7), 748–753.

Macias, E., Jin, A., Deisenroth, C., Bhat, K., Mao, H., Lindström, M. S., & Zhang, Y. (2010). An ARF-independent c-MYC-activated tumor suppression pathway mediated by ribosomal protein-Mdm2 Interaction. Cancer Cell, 18(3), 231–243.

Malinovskaya, E. M., Ershova, E. S., Golimbet, V. E., Porokhovnik, L. N., Lyapunova, N. A., Kutsev, S. I., Veiko, N. N., & Kostyuk, S. V. (2018). Copy Number of Human Ribosomal Genes With Aging: Unchanged Mean, but Narrowed Range and Decreased Variance in Elderly Group. Frontiers in Genetics, 9, 306.

Marechal, V., Elenbaas, B., Piette, J., Nicolas, J. C., & Levine, A. J. (1994). The ribosomal L5 protein is associated with mdm-2 and mdm-2-p53 complexes. Molecular and Cellular Biology, 14(11), 7414–7420.

Marin-Vinader, L., Shin, C., Onnekink, C., Manley, J. L., & Lubsen, N. H. (2006). Hsp27 enhances recovery of splicing as well as rephosphorylation of SRp38 after heat shock. Molecular Biology of the Cell, 17(2), 886–894.

Maryon, E. B., Molloy, S. A., & Kaplan, J. H. (2007). O-linked glycosylation at threonine 27 protects the copper transporter hCTR1 from proteolytic cleavage in mammalian cells. The Journal of Biological Chemistry, 282(28), 20376–20387.

Mattick, J. S., & Makunin, I. V. (2005). Small regulatory RNAs in mammals. Human Molecular Genetics, 14 Spec No 1, R121–R132.

McCullum, E. O., Williams, B. A. R., Zhang, J., & Chaput, J. C. (2010). Random mutagenesis by error-prone PCR. Methods in Molecular Biology , 634, 103–109.

Mélèse, T., & Xue, Z. (1995). The nucleolus: an organelle formed by the act of building a ribosome. Current Opinion in Cell Biology, 7(3), 319–324.

Melnikov, S., Ben-Shem, A., Garreau de Loubresse, N., Jenner, L., Yusupova, G., & Yusupov, M. (2012). One core, two shells: bacterial and eukaryotic ribosomes. Nature Structural & Molecular Biology, 19(6), 560–567.

Meola, N., Domanski, M., Karadoulama, E., Chen, Y., Gentil, C., Pultz, D., Vitting-Seerup, K., Lykke-Andersen, S., Andersen, J. S., Sandelin, A., & Jensen, T. H. (2016). Identification of a Nuclear Exosome Decay Pathway for Processed Transcripts. Molecular Cell, 64(3), 520–533.

Merkle, F. T., Ghosh, S., Kamitaki, N., Mitchell, J., Avior, Y., Mello, C., Kashin, S.,

Mekhoubad, S., Ilic, D., Charlton, M., Saphier, G., Handsaker, R. E., Genovese, G., Bar, S., Benvenisty, N., McCarroll, S. A., & Eggan, K. (2017). Human pluripotent stem cells recurrently acquire and expand dominant negative P53 mutations. Nature, 545(7653), 229–233.

Meshorer, E., & Misteli, T. (2006). Chromatin in pluripotent embryonic stem cells and differentiation. Nature Reviews. Molecular Cell Biology, 7(7), 540–546.

Mills, E. W., & Green, R. (2017). Ribosomopathies: There's strength in numbers. Science, 358(6363).

Mitchell, P., Petfalski, E., Shevchenko, A., Mann, M., & Tollervey, D. (1997). The exosome: a conserved eukaryotic RNA processing complex containing multiple 3'–¿5' exoribonucleases. Cell, 91(4), 457–466.

Mitchell, P., Petfalski, E., & Tollervey, D. (1996). The 3' end of yeast 5.8S rRNA is generated by an exonuclease processing mechanism. Genes & Development, 10(4), 502–513.

Miyao, S., Saito, K., Oshima, R., Kawahara, K., & Nagahama, M. (2022). MTR4 adaptor PICT1 functions in two distinct steps during pre-rRNA processing. Biochemical and Biophysical Research Communications, 637, 203–209.

Momand, J., Jung, D., Wilczynski, S., & Niland, J. (1998). The MDM2 gene amplification database. Nucleic Acids Research, 26(15), 3453–3459.

Montanaro, L., Treré, D., & Derenzini, M. (2008). Nucleolus, ribosomes, and cancer. The American Journal of Pathology, 173(2), 301–310.

Montes de Oca Luna, R., Wagner, D. S., & Lozano, G. (1995). Rescue of early embryonic lethality in mdm2-deficient mice by deletion of p53. Nature, 378(6553), 203–206.

Moon, A., Lim, S.-J., Jo, Y.-H., Lee, S., Kim, J.-Y., Lee, J., & Park, J.-H. (2013). Downregulation of GLTSCR2 expression is correlated with breast cancer progression. Pathology, Research and Practice, 209(11), 700–704.

Moorefield, B., & Roeder, R. G. (1994). Purification and characterization of human transcription factor IIIA. The Journal of Biological Chemistry, 269(33), 20857–20865.

Mosgoller, W. (2004). Nucleolar ultrastructure in vertebrates. In "'The Nucleolus'" (M. O. J. Olson, Ed.),. New York: Kluwer Academic/Plenum Publishers.

Moss, T., & Stefanovsky, V. Y. (2002). At the center of eukaryotic life. Cell, 109(5), 545–548.

Moy, T. I., & Silver, P. A. (1999). Nuclear export of the small ribosomal subunit requires the ran-GTPase cycle and certain nucleoporins. Genes & Development, 13(16), 2118–2133.

Natchiar, S. K., Myasnikov, A. G., Kratzat, H., Hazemann, I., & Klaholz, B. P. (2017). Visualization of chemical modifications in the human 80S ribosome structure. Nature, 551(7681), 472–477.

Natchiar, S. K., Myasnikov, A. G., Kratzat, H., Hazemann, I., & Klaholz, B. P. (2019).

High-resolution cryo-EM structure of the human 80S ribosome. Worldwide Protein Data Bank.

Nazar, R. N. (2004). Ribosomal RNA processing and ribosome biogenesis in eukaryotes. IUBMB Life, 56(8), 457–465.

Nissan, T. A., Bassler, J., Petfalski, E., Tollervey, D., & Hurt, E. (2002). 60S pre-ribosome formation viewed from assembly in the nucleolus until export to the cytoplasm. The EMBO Journal, 21(20), 5539–5547.

Nomura, M. (2001). Ribosomal RNA genes, RNA polymerases, nucleolar structures, and synthesis of rRNA in the yeast Saccharomyces cerevisiae. Cold Spring Harbor Symposia on Quantitative Biology, 66, 555–565.

O'Donohue, M.-F., Choesmel, V., Faubladier, M., Fichant, G., & Gleizes, P.-E. (2010). Functional dichotomy of ribosomal proteins during the synthesis of mammalian 40S ribosomal subunits. The Journal of Cell Biology, 190(5), 853–866.

Oborská-Oplová, M., Fischer, U., Altvater, M., & Panse, V. G. (2022). Eukaryotic Ribosome assembly and Nucleocytoplasmic Transport. Methods in Molecular Biology , 2533, 99–126.

Okahara, F., Ikawa, H., Kanaho, Y., & Maehama, T. (2004). Regulation of PTEN phosphorylation and stability by a tumor suppressor candidate protein. The Journal of Biological Chemistry, 279(44), 45300–45303.

Okahara, F., Itoh, K., Nakagawara, A., Murakami, M., Kanaho, Y., & Maehama, T. (2006). Critical role of PICT-1, a tumor suppressor candidate, in phosphatidylinositol 3,4,5-trisphosphate signals and tumorigenic transformation. Molecular Biology of the Cell, 17(11), 4888–4895.

Okamura, K., Takayama, K., Kawahara, K., Harada, T., Nishio, M., Otsubo, K., Ijichi, K., Kohno, M., Iwama, E., Fujii, A., Ota, K., Koga, T., Okamoto, T., Suzuki, A., & Nakanishi, Y. (2014). PICT1 expression is a poor prognostic factor in non-small cell lung cancer. Oncoscience, 1(5), 375–382.

Okamura, M., Inose, H., & Masuda, S. (2015). RNA Export through the NPC in Eukaryotes. Genes, 6(1), 124–149.

Orsolic, I., Jurada, D., Pullen, N., Oren, M., Eliopoulos, A. G., & Volarevic, S. (2016). The relationship between the nucleolus and cancer: Current evidence and emerging paradigms. Seminars in Cancer Biology, 37-38, 36–50.

Oskarsson, T., & Trumpp, A. (2005). The Myc trilogy: lord of RNA polymerases [Review of The Myc trilogy: lord of RNA polymerases]. Nature Cell Biology, 7(3), 215–217.

Pederson, T., & Tsai, R. Y. L. (2009). In search of nonribosomal nucleolar protein function and regulation. In Journal of Cell Biology (Vol. 184, Issue 6, pp. 771–776).

Perry, R. P. (2007). Balanced production of ribosomal proteins. Gene, 401(1-2), 1–3.

Picksley, S. M., & Lane, D. P. (1993). The p53-mdm2 autoregulatory feedback loop: a paradigm for the regulation of growth control by p53? BioEssays: News and Reviews in Molecular, Cellular and Developmental Biology, 15(10), 689–690.

Preti, M., O'Donohue, M.-F., Montel-Lehry, N., Bortolin-Cavaillé, M.-L., Choesmel, V., & Gleizes, P.-E. (2013). Gradual processing of the ITS1 from the nucleolus to the cytoplasm during synthesis of the human 18S rRNA. Nucleic Acids Research, 41(8), 4709–4723.

Prochownik, E. V. (2004). c-Myc as a therapeutic target in cancer. Expert Review of Anticancer Therapy, 4(2), 289–302.

Rabuck-Gibbons, J. N., Lyumkis, D., & Williamson, J. R. (2021). Quantitative mining of compositional heterogeneity in cryo-EM datasets of ribosome assembly intermediates. Structure.

Raška, I., Shaw, P. J., & Cmarko, D. (2006a). Structure and function of the nucleolus in the spotlight. Current Opinion in Cell Biology.

Raska, I., Shaw, P. J., & Cmarko, D. (2006b). New insights into nucleolar architecture and activity. International Review of Cytology, 255, 177–235.

Rinke, J., & Steitz, J. A. (1982). Precursor molecules of both human 5S ribosomal RNA and transfer RNAs are bound by a cellular protein reactive with anti-La lupus antibodies. Cell, 29(1), 149–159.

Rössler, I., Weigl, S., Fernández-Fernández, J., Martín-Villanueva, S., Strauss, D., Hurt, E., de la Cruz, J., & Pertschy, B. (2022). The C-terminal tail of ribosomal protein Rps15 is engaged in cytoplasmic pre-40S maturation. RNA Biology, 19(1), 560–574.

Rubbi, C. P., & Milner, J. (2003). Disruption of the nucleolus mediates stabilization of p53 in response to DNA damage and other stresses. The EMBO Journal, 22(22), 6068–6077.

Ruland, J. A., Krüger, A. M., Dörner, K., Bhatia, R., Wirths, S., Poetes, D., Kutay, U., Siebrasse, J. P., & Kubitscheck, U. (2021). Nuclear export of the pre-60S ribosomal subunit through single nuclear pores observed in real time. Nature Communications, 12(1), 6211.

Sanghai, Z. A., Miller, L., Molloy, K. R., Barandun, J., Hunziker, M., Chaker-Margot, M., Wang, J., Chait, B. T., & Klinge, S. (2018). Modular assembly of the nucleolar pre-60S ribosomal subunit. Nature, 556(7699), 126–129.

Sankaran, V. G., Ghazvinian, R., Do, R., Thiru, P., Vergilio, J.-A., Beggs, A. H., Sieff, C. A., Orkin, S. H., Nathan, D. G., Lander, E. S., & Gazda, H. T. (2012). Exome sequencing identifies GATA1 mutations resulting in Diamond-Blackfan anemia. The Journal of Clinical Investigation, 122(7), 2439–2443.

Sarkar, A., Thoms, M., Barrio-Garcia, C., Thomson, E., Flemming, D., Beckmann, R., & Hurt, E. (2017). Preribosomes escaping from the nucleus are caught during translation by cytoplasmic quality control. Nature Structural & Molecular Biology, 24(12), 1107–1115.

Saryi, N. A. A., Hutchinson, J. D., Al-Hejjaj, M. Y., Sedelnikova, S., Baker, P., & Hettema, E. H. (2017). Pnc1 piggy-back import into peroxisomes relies on Gpd1 homodimerisa-

tion. Scientific Reports, 7, 42579.

Sasaki, M., Kawahara, K., Nishio, M., Mimori, K., Kogo, R., Hamada, K., Itoh, B., Wang, J., Komatsu, Y., Yang, Y. R., Hikasa, H., Horie, Y., Yamashita, T., Kamijo, T., Zhang, Y., Zhu, Y., Prives, C., Nakano, T., Mak, T. W., ... Suzuki, A. (2011). Regulation of the MDM2-P53 pathway and tumor growth by PICT1 via nucleolar RPL11. Nature Medicine, 17(8), 944–951.

Schaeffer, D., Tsanova, B., Barbas, A., Reis, F. P., Dastidar, E. G., Sanchez-Rotunno, M., Arraiano, C. M., & van Hoof, A. (2009). The exosome contains domains with specific endoribonuclease, exoribonuclease and cytoplasmic mRNA decay activities. Nature Structural & Molecular Biology, 16(1), 56–62.

Scheer, U., & Hock, R. (1999). Structure and function of the nucleolus. Current Opinion in Cell Biology, 11(3), 385–390.

Schilders, G., Raijmakers, R., Raats, J. M. H., & Pruijn, G. J. M. (2005). MPP6 is an exosome-associated RNA-binding protein involved in 5.8S rRNA maturation. Nucleic Acids Research, 33(21), 6795–6804.

Schmid, M., & Jensen, T. H. (2008). The exosome: a multipurpose RNA-decay machine. Trends in Biochemical Sciences, 33(10), 501–510.

Schmidt, C., Kowalinski, E., Shanmuganathan, V., Defenouillère, Q., Braunger, K., Heuer, A., Pech, M., Namane, A., Berninghausen, O., Fromont-Racine, M., Jacquier, A., Conti, E., Becker, T., & Beckmann, R. (2016). The cryo-EM structure of a ribosome–Ski2-Ski3-Ski8 helicase complex. Science, 354(6318), 1431–1433.

Schmidt, E. V. (1999). The role of c-myc in cellular growth control. Oncogene, 18(19), 2988–2996.

Schmidt, T. G. M., & Skerra, A. (2007). The Strep-tag system for one-step purification and high-affinity detection or capturing of proteins. Nature Protocols, 2(6), 1528–1535.

Schneider, C., Anderson, J. T., & Tollervey, D. (2007). The exosome subunit Rrp44 plays a direct role in RNA substrate recognition. Molecular Cell, 27(2), 324–331.

Schneider, C., Leung, E., Brown, J., & Tollervey, D. (2009). The N-terminal PIN domain of the exosome subunit Rrp44 harbors endonuclease activity and tethers Rrp44 to the yeast core exosome. Nucleic Acids Research, 37(4), 1127–1140.

Schubert, M. S., Thommandru, B., Woodley, J., Turk, R., Yan, S., Kurgan, G., McNeill, M. S., & Rettig, G. R. (2021). Optimized design parameters for CRISPR Cas9 and Cas12a homology-directed repair. Scientific Reports, 11(1), 1–15.

Sherr, C. J., & Weber, J. D. (2000). The ARF/p53 pathway. Current Opinion in Genetics & Development, 10(1), 94–99.

Shevinsky, L. H., Knowles, B. B., Damjanov, I., & Solter, D. (1982). Monoclonal antibody to murine embryos defines a stage-specific embryonic antigen expressed on mouse embryos and human teratocarcinoma cells. Cell, 30(3), 697–705.

Shrivastav, M., De Haro, L. P., & Nickoloff, J. A. (2008). Regulation of DNA double-strand break repair pathway choice. In Cell Research (Vol. 18, Issue 1, pp. 134–147).

Sievers, F., Wilm, A., Dineen, D., Gibson, T. J., Karplus, K., Li, W., Lopez, R., McWilliam, H., Remmert, M., Söding, J., Thompson, J. D., & Higgins, D. G. (2011). Fast, scalable generation of high-quality protein multiple sequence alignments using Clustal Omega. Molecular Systems Biology, 7, 539.

Sirri, V., Urcuqui-Inchima, S., Roussel, P., & Hernandez-Verdun, D. (2008). Nucleolus: the fascinating nuclear body. Histochemistry and Cell Biology, 129(1), 13–31.

Sloan, K. E., Bohnsack, M. T., Schneider, C., & Watkins, N. J. (2014). The roles of SSU processome components and surveillance factors in the initial processing of human ribosomal RNA. RNA , 20(4), 540–550.

Sloan, K. E., Bohnsack, M. T., & Watkins, N. J. (2013). The 5S RNP couples p53 homeostasis to ribosome biogenesis and nucleolar stress. Cell Reports, 5(1), 237–247.

Sloan, K. E., Schneider, C., & Watkins, N. J. (2012). Comparison of the yeast and human nuclear exosome complexes. Biochemical Society Transactions, 40(4), 850–855.

Sloan, K. E., Warda, A. S., Sharma, S., Entian, K.-D., Lafontaine, D. L. J., & Bohnsack, M. T. (2017). Tuning the ribosome: The influence of rRNA modification on eukaryotic ribosome biogenesis and function. RNA Biology, 14(9), 1138–1152.

Smith, J. S., Tachibana, I., Pohl, U., Lee, H. K., Thanarajasingam, U., Portier, B. P., Ueki, K., Ramaswamy, S., Billings, S. J., Mohrenweiser, H. W., Louis, D. N., & Jenkins, R. B. (2000). A transcript map of the chromosome 19q-arm glioma tumor suppressor region. Genomics, 64(1), 44–50.

Sollner-Webb, B., & Tower, J. (1986). Transcription of cloned eukaryotic ribosomal RNA genes. Annual Review of Biochemistry, 55, 801–830.

Steck, P. A., Pershouse, M. A., Jasser, S. A., Yung, W. K., Lin, H., Ligon, A. H., Langford, L. A., Baumgard, M. L., Hattier, T., Davis, T., Frye, C., Hu, R., Swedlund, B., Teng, D. H., & Tavtigian, S. V. (1997). Identification of a candidate tumour suppressor gene, MMAC1, at chromosome 10q23.3 that is mutated in multiple advanced cancers. Nature Genetics, 15(4), 356–362.

Stefano, J. E. (1984). Purified lupus antigen La recognizes an oligouridylate stretch common to the 3' termini of RNA polymerase III transcripts. Cell, 36(1), 145–154.

Steitz, J. A., Berg, C., Hendrick, J. P., La Branche-Chabot, H., Metspalu, A., Rinke, J., & Yario, T. (1988). A 5S rRNA/L5 complex is a precursor to ribosome assembly in mammalian cells. The Journal of Cell Biology, 106(3), 545–556.

Stem Cell Technologies. (2023) Human Pluripotent Stem Cell (PSC) Genetic Analysis Kit. Retrieved March 1, 2023, from https://www.stemcell.com/products/hpsc-genetic-analysis-kit.html

Stenström, L., Mahdessian, D., Gnann, C., Cesnik, A. J., Ouyang, W., Leonetti, M. D., Uhlén, M., Cuylen-Haering, S., Thul, P. J., & Lundberg, E. (2020). Mapping the nucleolar proteome reveals a spatiotemporal organization related to intrinsic protein disorder. Molecular Systems Biology, 16(8), e9469.

Stepiński, D. (2018). The nucleolus, an ally, and an enemy of cancer cells. Histochemistry and Cell Biology, 150(6), 607–629.

Strunk, B. S., Loucks, C. R., Su, M., Vashisth, H., Cheng, S., Schilling, J., Brooks, C. L., 3rd, Karbstein, K., & Skiniotis, G. (2011). Ribosome assembly factors prevent premature translation initiation by 40S assembly intermediates. Science, 333(6048), 1449–1453.

Strunk, B. S., Novak, M. N., Young, C. L., & Karbstein, K. (2012). A translation-like cycle is a quality control checkpoint for maturing 40S ribosome subunits. Cell, 150(1), 111–121.

Sulima, S. O., Kampen, K. R., & De Keersmaecker, K. (2019). Cancer Biogenesis in Ribosomopathies. Cells , 8(3).

Sung, M.-K., Reitsma, J. M., Sweredoski, M. J., Hess, S., & Deshaies, R. J. (2016). Ribosomal proteins produced in excess are degraded by the ubiquitin-proteasome system. Molecular Biology of the Cell, 27(17), 2642–2652.

Suzuki, A., Kogo, R., Kawahara, K., Sasaki, M., Nishio, M., Maehama, T., Sasaki, T., Mimori, K., & Mori, M. (2012). A new PICTure of nucleolar stress. Cancer Science, 103(4), 632–637.

Sydorskyy, Y., Dilworth, D. J., Halloran, B., Yi, E. C., Makhnevych, T., Wozniak, R. W., & Aitchison, J. D. (2005). Nop53p is a novel nucleolar 60S ribosomal subunit biogenesis protein. Biochemical Journal, 388(Pt 3), 819–826.

Tafforeau, L., Zorbas, C., Langhendries, J.-L., Mullineux, S.-T., Stamatopoulou, V., Mullier, R., Wacheul, L., & Lafontaine, D. L. J. (2013). The complexity of human ribosome biogenesis revealed by systematic nucleolar screening of Pre-rRNA processing factors. Molecular Cell, 51(4), 539–551.

Taoka, M., Nobe, Y., Yamaki, Y., Sato, K., Ishikawa, H., Izumikawa, K., Yamauchi, Y., Hirota, K., Nakayama, H., Takahashi, N., & Isobe, T. (2018). Landscape of the complete RNA chemical modifications in the human 80S ribosome. Nucleic Acids Research, 46(18), 9289–9298.

Teng, T., Thomas, G., & Mercer, C. A. (2013). Growth control and ribosomopathies. Current Opinion in Genetics & Development, 23(1), 63–71.

Thiry, M., & Goessens, G. (1996). The nucleolus during the cell cycle. In Landes RG, ed. Molecular Biology Intelligence Unit, Heidelberg, Springer-Verlag, 1–144.

Thiry, M., Lamaye, F., & Lafontaine, D. L. J. (2011). The nucleolus: When 2 became 3. Nucleus , 2(4), 289–293.

Thomas, F., & Kutay, U. (2003). Biogenesis and nuclear export of ribosomal subunits in higher eukaryotes depend on the CRM1 export pathway. Journal of Cell Science, 116(Pt 12),

2409–2419.

Thoms, M., Thomson, E., Baßler, J., Gnädig, M., Griesel, S., & Hurt, E. (2015). The Exosome Is Recruited to RNA Substrates through Specific Adaptor Proteins. Cell, 162(5), 1029–1038.

Thomson, E., Ferreira-Cerca, S., & Hurt, E. (2013). Eukaryotic ribosome biogenesis at a glance. Journal of Cell Science, 126(Pt 21), 4815–4821.

Thomson, E., & Tollervey, D. (2005). Nop53p is required for late 60S ribosome subunit maturation and nuclear export in yeast. RNA , 11(8), 1215–1224.

Tiu, G. C., Kerr, C. H., Forester, C. M., Krishnarao, P. S., Rosenblatt, H. D., Raj, N., Lantz, T. C., Zhulyn, O., Bowen, M. E., Shokat, L., Attardi, L. D., Ruggero, D., & Barna, M. (2021). A p53-dependent translational program directs tissue-selective phenotypes in a model of ribosomopathies. Developmental Cell, 56(14), 2089–2102.e11.

Toledo, F., & Wahl, G. M. (2006). Regulating the p53 pathway: in vitro hypotheses, in vivo veritas. Nature Reviews. Cancer, 6(12), 909–923.

Tomecki, R., Kristiansen, M. S., Lykke-Andersen, S., Chlebowski, A., Larsen, K. M., Szczesny, R. J., Drazkowska, K., Pastula, A., Andersen, J. S., Stepien, P. P., Dziembowski, A., & Jensen, T. H. (2010). The human core exosome interacts with differentially localized processive RNases: hDIS3 and hDIS3L. The EMBO Journal, 29(14), 2342–2357.

Tomecki, R., Sikorski, P. J., & Zakrzewska-Placzek, M. (2017). Comparison of preribosomal RNA processing pathways in yeast, plant and human cells - focus on coordinated action of endo- and exoribonucleases. FEBS Letters, 591(13), 1801–1850.

Trotta, C. R., Lund, E., Kahan, L., Johnson, A. W., & Dahlberg, J. E. (2003). Coordinated nuclear export of 60S ribosomal subunits and NMD3 in vertebrates. The EMBO Journal, 22(11), 2841–2851.

Tu, J., Huo, Z., Liu, M., Wang, D., Xu, A., Zhou, R., Zhu, D., Gingold, J., Shen, J., Zhao, R., & Lee, D.-F. (2018). Generation of human embryonic stem cell line with heterozygous RB1 deletion by CRIPSR/Cas9 nickase. Stem Cell Research, 28, 29–32.

Turowski, T. W., & Tollervey, D. (2015). Cotranscriptional events in eukaryotic ribosome synthesis. Wiley Interdisciplinary Reviews. RNA, 6(1), 129–139.

Underwood, J. M., Becker, K. A., Stein, G. S., & Nickerson, J. A. (2017). The Ultrastructural Signature of Human Embryonic Stem Cells. Journal of Cellular Biochemistry, 118(4), 764–774.

Vakulskas, C. A., Dever, D. P., Rettig, G. R., Turk, R., Jacobi, A. M., Collingwood, M. A., Bode, N. M., McNeill, M. S., Yan, S., Camarena, J., Lee, C. M., Park, S. H., Wiebking, V., Bak, R. O., Gomez-Ospina, N., Pavel-Dinu, M., Sun, W., Bao, G., Porteus, M. H., & Behlke, M. A. (2018). A high-fidelity Cas9 mutant delivered as a ribonucleoprotein complex enables efficient gene editing in human hematopoietic stem and progenitor cells. Nature Medicine, 24(8), 1216–1224.

van Hoof, A. (2000). Three conserved members of the RNase D family have unique and overlapping functions in the processing of 5S, 5.8S, U4, U5, RNase MRP and RNase P RNAs in yeast. In The EMBO Journal (Vol. 19, Issue 6, pp. 1357–1365).

van Hoof A, Parker R. The exosome: a proteasome for RNA? Cell. 1999 Nov 12;99(4):347-50.

van Sluis, M., & McStay, B. (2015). A localized nucleolar DNA damage response facilitates recruitment of the homology-directed repair machinery independent of cell cycle stage. Genes & Development, 29(11), 1151–1163.

Vanácová, S., Wolf, J., Martin, G., Blank, D., Dettwiler, S., Friedlein, A., Langen, H., Keith, G., & Keller, W. (2005). A new yeast poly(A) polymerase complex involved in RNA quality control. PLoS Biology, 3(6), e189.

Varadi, M., Anyango, S., Deshpande, M., Nair, S., Natassia, C., Yordanova, G., Yuan, D., Stroe, O., Wood, G., Laydon, A., Žídek, A., Green, T., Tunyasuvunakool, K., Petersen, S., Jumper, J., Clancy, E., Green, R., Vora, A., Lutfi, M., ... Velankar, S. (2021). AlphaFold Protein Structure Database: massively expanding the structural coverage of protein-sequence space with high-accuracy models. Nucleic Acids Research, 50(D1), D439–D444.

Vouillot, L., Thélie, A., & Pollet, N. (2015). Comparison of T7E1 and surveyor mismatch cleavage assays to detect mutations triggered by engineered nucleases. G3 , 5(3), 407–415.

Wang, H.-W., & Wang, J.-W. (2017). How cryo-electron microscopy and X-ray crystallography complement each other. Protein Science: A Publication of the Protein Society, 26(1), 32–39.

Wang, J., Chen, J., Wu, G., Zhang, H., Du, X., Chen, S., Zhang, L., Wang, K., Fan, J., Gao, S., Wu, X., Zhang, S., Kuai, B., Zhao, P., Chi, B., Wang, L., Li, G., Wong, C. C. L., Zhou, Y., ... Cheng, H. (2019). NRDE2 negatively regulates exosome functions by inhibiting MTR4 recruitment and exosome interaction. Genes & Development, 33(9-10), 536–549.

Waterhouse, A. M., Procter, J. B., Martin, D. M. A., Clamp, M., & Barton, G. J. (2009). Jalview Version 2–a multiple sequence alignment editor and analysis workbench. Bioinformatics , 25(9), 1189–1191.

Watkins, N. J., & Bohnsack, M. T. (2012). The box C/D and H/ACA snoRNPs: key players in the modification, processing and the dynamic folding of ribosomal RNA. Wiley Interdisciplinary Reviews. RNA, 3(3), 397–414.

Weir, J. R., Bonneau, F., Hentschel, J., & Conti, E. (2010). Structural analysis reveals the characteristic features of Mtr4, a DExH helicase involved in nuclear RNA processing and surveillance. Proceedings of the National Academy of Sciences of the United States of America, 107(27), 12139–12144.

Widberg, C. H., Newell, F. S., Bachmann, A. W., Ramnoruth, S. N., Spelta, M. C., Whitehead, J. P., Hutley, L. J., & Prins, J. B. (2009). Fibroblast growth factor receptor 1 is a key regulator of early adipogenic events in human preadipocytes. American Journal of Physiology. Endocrinology and Metabolism, 296(1), E121–E131.

Woolford, J. L., Jr, & Baserga, S. J. (2013). Ribosome biogenesis in the yeast Saccharomyces cerevisiae. Genetics, 195(3), 643–681.

Wu, S., Tutuncuoglu, B., Yan, K., Brown, H., Zhang, Y., Tan, D., Gamalinda, M., Yuan, Y., Li, Z., Jakovljevic, J., Ma, C., Lei, J., Dong, M.-Q., Woolford, J. L., Jr, & Gao, N. (2016). Diverse roles of assembly factors revealed by structures of late nuclear pre-60S ribosomes. Nature, 534(7605), 133–137.

Xu, A., Zhou, R., Tu, J., Huo, Z., Zhu, D., Wang, D., Gingold, J. A., Mata, H., Rao, P. H., Liu, M., Mohamed, A. M. T., Kong, C. S. L., Jewell, B. E., Xia, W., Zhao, R., Hung, M.-C., & Lee, D.-F. (2018). Establishment of a human embryonic stem cell line with homozygous TP53 R248W mutant by TALEN mediated gene editing. Stem Cell Research, 29, 215–219.

Yamanaka, S. (2012). Induced pluripotent stem cells: past, present, and future. Cell Stem Cell, 10(6), 678–684.

Zaccara, S., Tebaldi, T., Pederiva, C., Ciribilli, Y., Bisio, A., & Inga, A. (2014). p53-directed translational control can shape and expand the universe of p53 target genes. In Cell Death & Differentiation (Vol. 21, Issue 10, pp. 1522–1534).

Zakrzewski, W., Dobrzyński, M., Szymonowicz, M., & Rybak, Z. (2019). Stem cells: past, present, and future. Stem Cell Research & Therapy, 10(1), 68.

Zhai, W., & Comai, L. (2000). Repression of RNA polymerase I transcription by the tumor suppressor p53. Molecular and Cellular Biology, 20(16), 5930–5938.

Zhang, J., Harnpicharnchai, P., Jakovljevic, J., Tang, L., Guo, Y., Oeffinger, M., Rout, M. P., Hiley, S. L., Hughes, T., & Woolford, J. L., Jr. (2007). Assembly factors Rpf2 and Rrs1 recruit 5S rRNA and ribosomal proteins rpL5 and rpL11 into nascent ribosomes. Genes & Development, 21(20), 2580–2592.

Zhang, K., Xie, Y., Muñoz-Moreno, R., Wang, J., Zhang, L., Esparza, M., García-Sastre, A., Fontoura, B. M. A., & Ren, Y. (2019). Structural basis for influenza virus NS1 protein block of mRNA nuclear export. Nature Microbiology, 4(10), 1671–1679.

Zhang, Y., Wolf, G. W., Bhat, K., Jin, A., Allio, T., Burkhart, W. A., & Xiong, Y. (2003). Ribosomal protein L11 negatively regulates oncoprotein MDM2 and mediates a p53-dependent ribosomal-stress checkpoint pathway. Molecular and Cellular Biology, 23(23), 8902–8912.

Zhang, Z., Zhang, Y., Gao, F., Han, S., Cheah, K. S., Tse, H.-F., & Lian, Q. (2017). CRISPR/Cas9 Genome-Editing System in Human Stem Cells: Current Status and Future Prospects. Molecular Therapy. Nucleic Acids, 9, 230–241.

Zhou, D., Zhu, X., Zheng, S., Tan, D., Dong, M.-Q., & Ye, K. (2019). Cryo-EM structure of an early precursor of large ribosomal subunit reveals a half-assembled intermediate. Protein & Cell, 10(2), 120–130.

Zimmermann, L., Stephens, A., Nam, S.-Z., Rau, D., Kübler, J., Lozajic, M., Gabler, F., Söding, J., Lupas, A. N., & Alva, V. (2018). A Completely Reimplemented MPI Bioinfor-

matics Toolkit with a New HHpred Server at its Core. Journal of Molecular Biology, 430(15), 2237–2243.

# Chapter 8

# Appendix

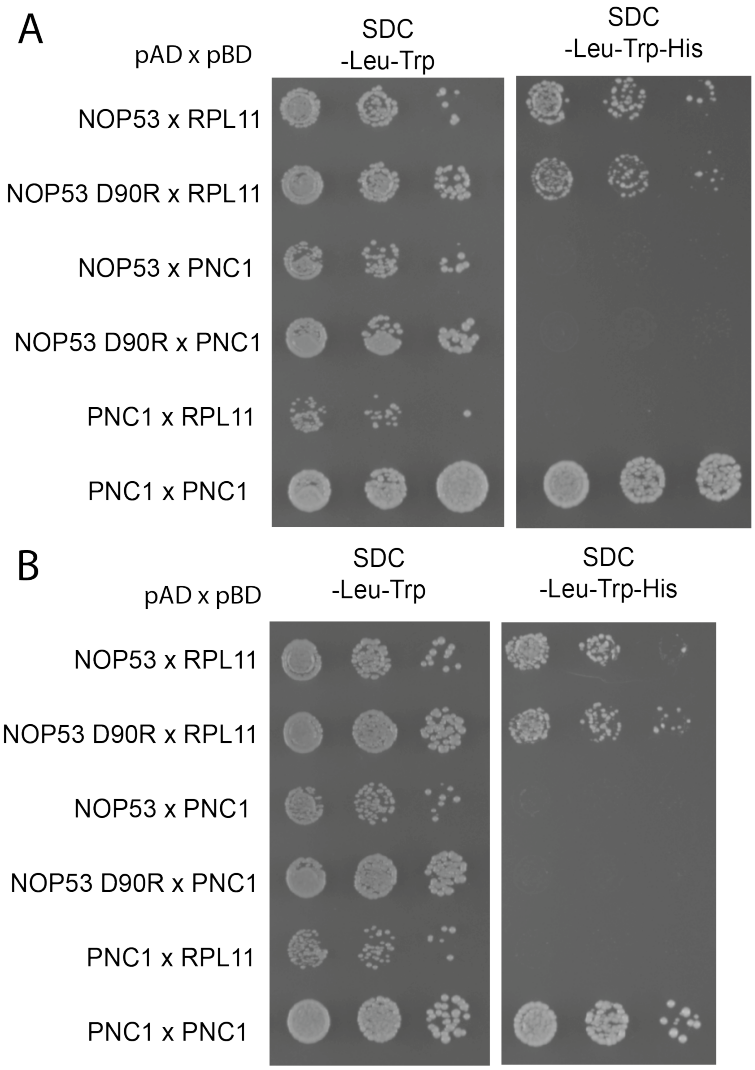


Figure 8.1: Yeast-two-hybrid analysis of NOP53 WT and D90R with RPL11. Yeast-two-hybrid dot plates for duplicate NOP53 WT or DR transformants with RPL11 grown on SDC-Leu-Trp and SDC–Leu-Trp-His.

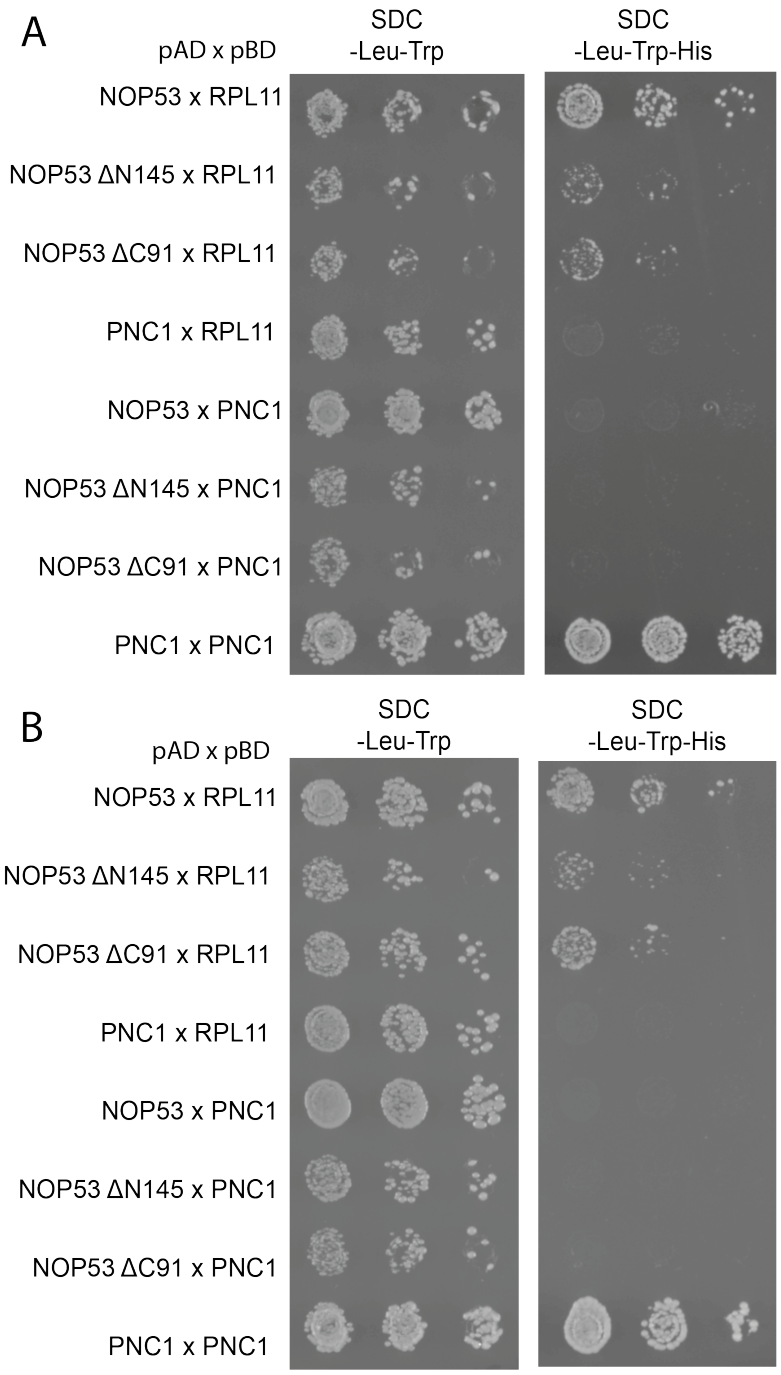


Figure 8.2: Yeast-two-hybrid analysis of NOP53 ΔN145 and NOP53 ΔC91 with RPL11. Yeast-two-hybrid dot plates for duplicate NOP53ΔN145 and NOP53 ΔC91 with RPL11 grown on SDC-Leu-Trp and SDC–Leu-Trp-His.

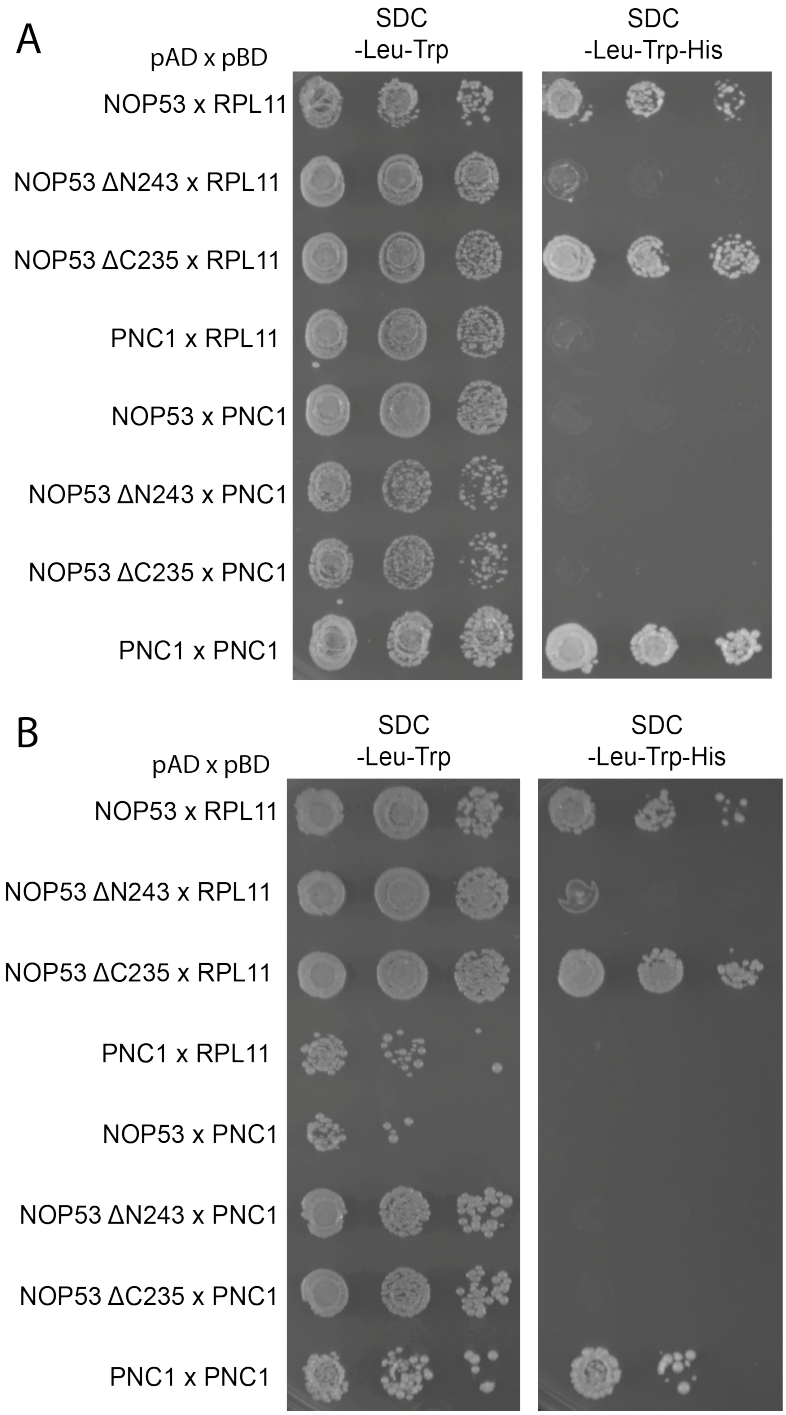


Figure 8.3: Yeast-two-hybrid analysis of NOP53 ΔN243 and NOP53 ΔC235 with RPL11. Yeast-two-hybrid dot plates for NOP53ΔN243 and NOP53 ΔC235 with RPL11 grown on SDC-Leu-Trp and SDC–Leu-Trp-His.

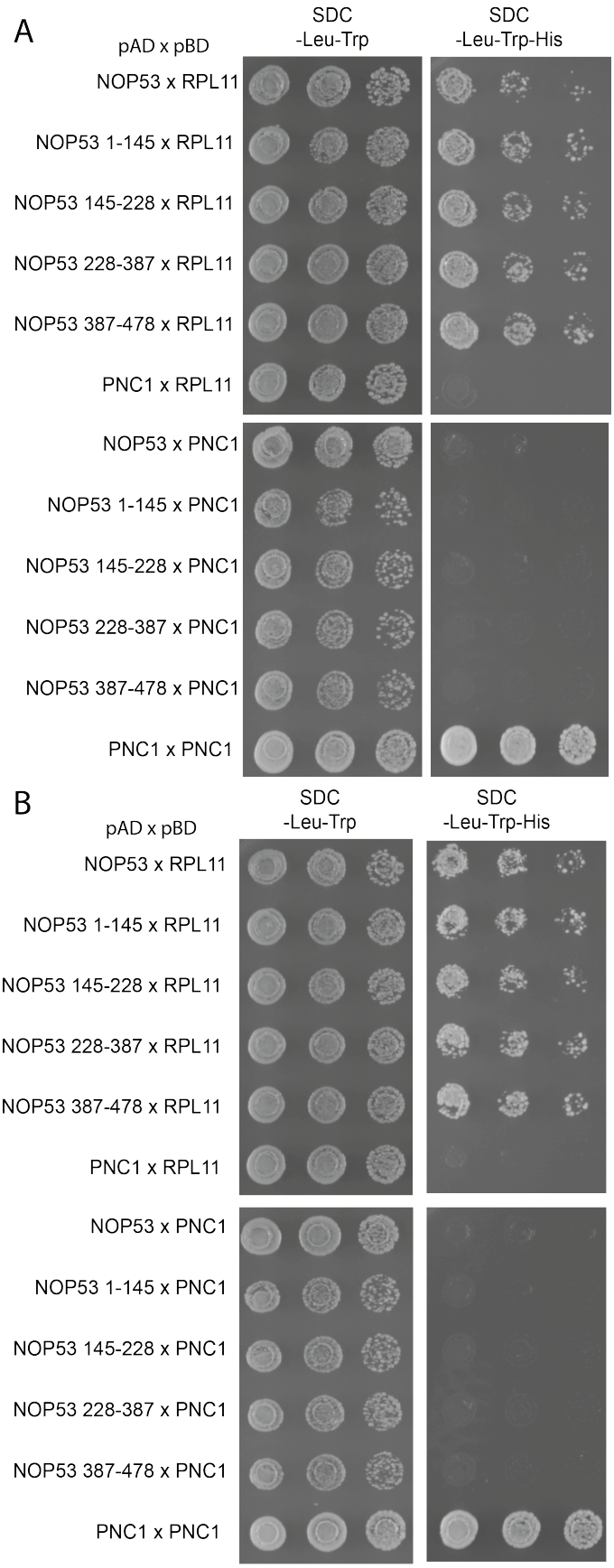


Figure 8.4: Yeast-two-hybrid analysis of NOP53 constructs; 1-145, 146-228, 229-387 and 388-478 with RPL11. Yeast-two-hybrid dot plates for duplicate NOP53 transformants; 1-145, 146-228, 229-387 and 388-478 with RPL11 grown on SDC-Leu-Trp and SDC–Leu-Trp-His.

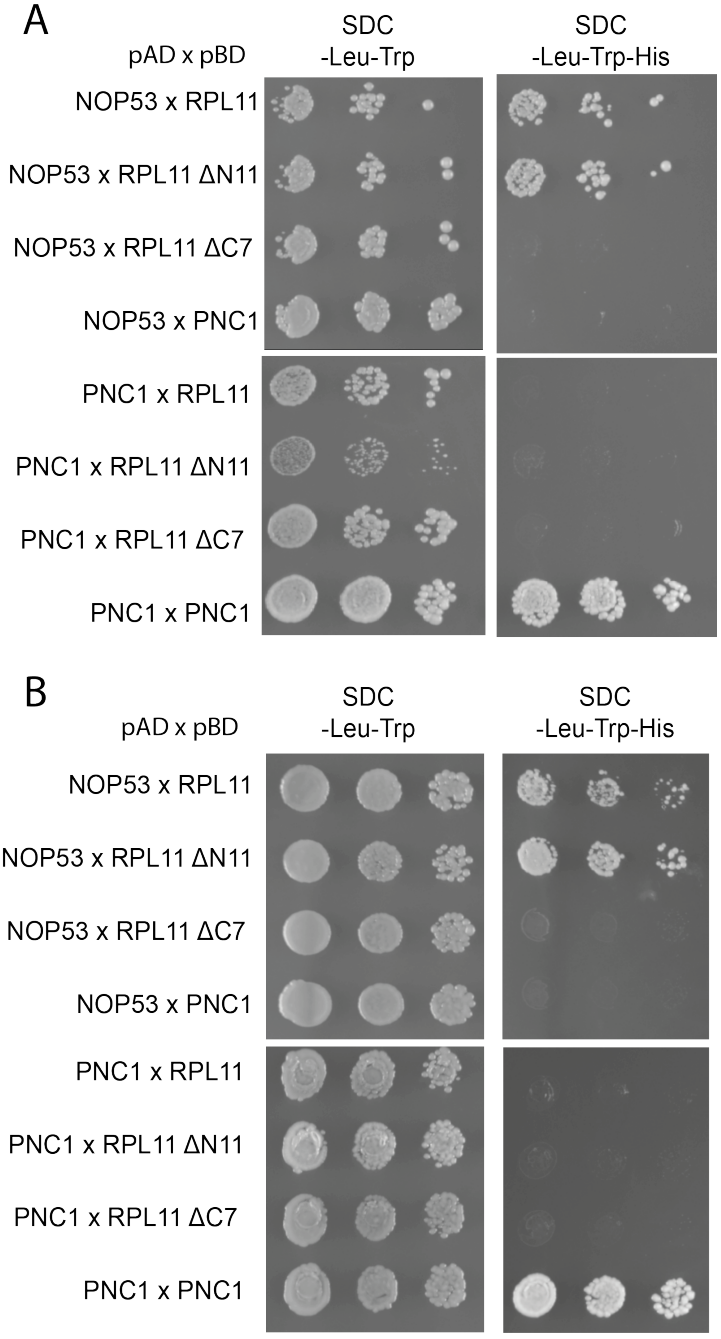


Figure 8.5: Yeast-two-hybrid analysis of NOP53 with RPL11 ΔN11 and ΔC7. Yeast-two-hybrid dot plates for duplicate NOP53 transformants with RPL11 ΔN11 and RPL11 ΔC7 grown on SDC-Leu-Trp and SDC–Leu-Trp-His.

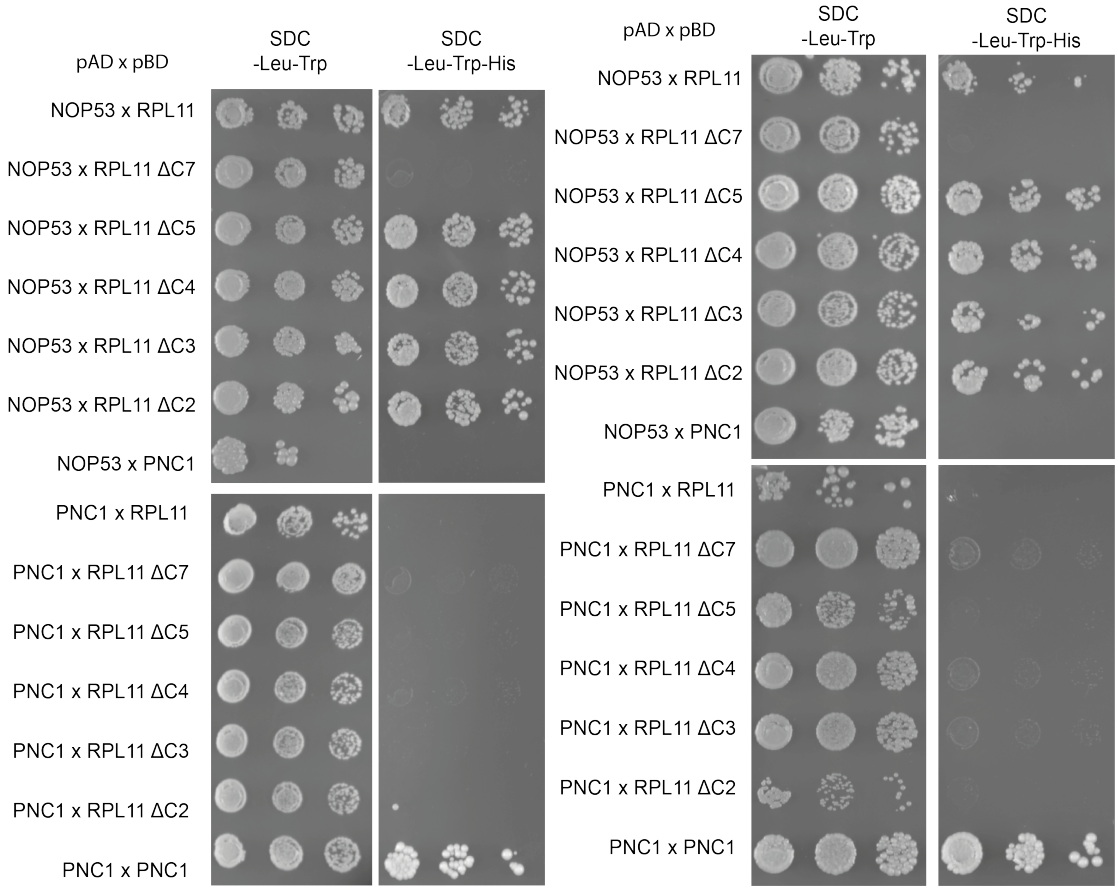


Figure 8.6: Yeast-two-hybrid analysis of NOP53 with RPL11 ΔC7, RPL11 ΔC5, RPL11 ΔC4, RPL11 ΔC3 and RPL11 ΔC2. Yeast-two-hybrid dot plates for NOP53 transformants with RPL11 ΔC7, RPL11 ΔC5, RPL11 ΔC4, RPL11 ΔC3 and RPL11 ΔC2 grown on SDC-Leu-Trp and SDC–Leu-Trp-His.

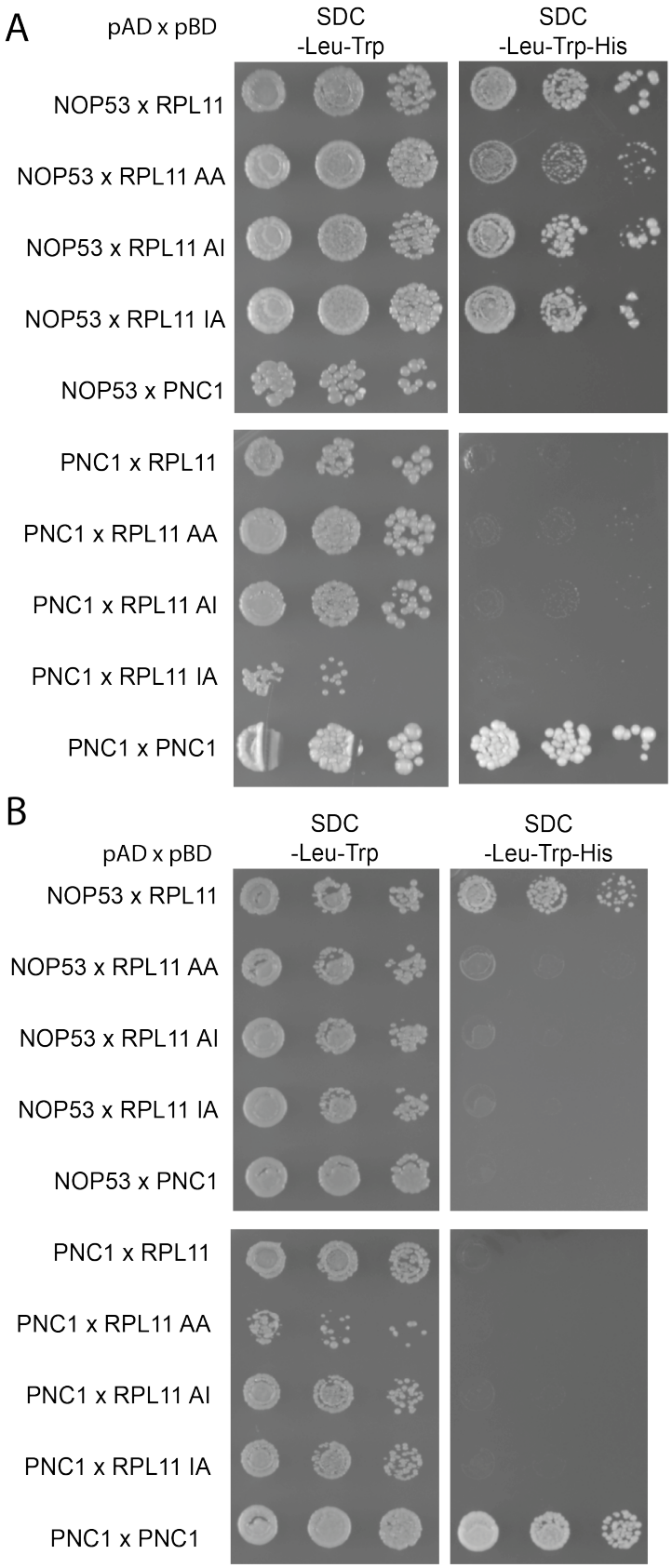


Figure 8.7: Yeast-two-hybrid analysis of NOP53 with RPL11 AA, RPL11 AI and RPL11 IA. Yeast-two-hybrid dot plates for duplicate NOP53 transformants with with RPL11 AA, RPL11 AI and RPL11 IA grown on SDC-Leu-Trp and SDC–Leu-Trp-His.